

AD 742 127

JANAIR Report 711107

STI Technical Report 183-2

**PILOT EXPERIMENTS FOR
A THEORY OF INTEGRATED DISPLAY FORMAT**

(Final Report)

*Warren F. Clement
R. Wade Allen
Dunstan Graham*

**SYSTEMS TECHNOLOGY, INC.
Hawthorne, California 90250**

October 1971

Jointly sponsored by
**OFFICE OF NAVAL RESEARCH
NAVAL AIR SYSTEMS COMMAND
ARMY ELECTRONICS COMMAND**
Under
Contract N00014-68-C-0443, NR 213-044

DOCUMENT CONTROL DATA - R & D

(Security classification of title, body of abstract and indexing annotation must be entered when the overall report is classified)

1. ORIGINATING ACTIVITY (Corporate author)

Systems Technology, Inc.
13766 S. Hawthorne Blvd.
Hawthorne, Calif. 90250

20. REPORT SECURITY CLASSIFICATION

Unclassified

20. GROUP

N/A

2. REPORT TITLE

Pilot Experiments for a Theory of Integrated Display Format

4. DESCRIPTIVE NOTES (Type of report and inclusive dates)

Final Report

8. AUTHOR(S) (First name, middle initial, last name)

Clement, Warren F.
Allen, R. Wade
Graham, Dunstan

9. REPORT DATE

October 1971

70. TOTAL NO. OF PAGES

203

70. NO. OF REFS

35

9a. CONTRACT OR GRANT NO.

N00014-68-C-0443

9b. ORIGINATOR'S REPORT NUMBER(S)

TR-183-2

b. PROJECT NO.

NR-213-044

9c. OTHER REPORT NO(S) (Any other numbers that may be assigned this report)

JANAIR Report 711107

10. DISTRIBUTION STATEMENT

This document has been approved for public release and sale; its distribution is unlimited.

11. SUPPLEMENTARY NOTES

Joint Army Navy Aircraft
Instrumentation Research Program
(JANAIR)

13. SPONSORING MILITARY ACTIVITY

Office of Naval Research, Code 461
Department of the Navy
Washington, D. C.

15. ABSTRACT

In support of a theory for manual control displays, and, in particular, for integrated displays, a series of two pilot experiments were performed to enlarge the data base for the theory. A single-axis tracking experiment was performed with two different controlled elements and four different display formats. The effects of display format were separately evaluated from task difficulty and task performance with a particular view toward quantification of the pilots' parafoveal perceptual ability. In the second experiment four different integrated displays were tested in a precision tracking task with a view toward quantifying the effect of integration in the display. Different forms of integration of the display were found to strongly influence the pilots' excess control capacity which is the complement of workload. Describing functions, remnant, eye-movements, and pilot opinion data were also recorded in these experiments. Interpretation and the conclusions to be drawn from all these data are presented in the report.

Unclassified

Security Classification

KEY WORDS	LINK A		LINK B		LINK C	
	ROLE	WT	ROLE	WT	ROLE	WT
Manual control Control displays Integrated displays Single-axis tracking experiment						

NOTICE

Change of Address

Organizations receiving JANAIR Reports on the initial distribution list should confirm correct address. This list is located at the end of the report. Any change in address or distribution list be conveyed to the Office of Naval Research, Code 461, Arlington, Virginia 22217, ATTN: JANAIR Chairman.

Disposition

Destroy this report when it is no longer needed. Do not return to the originator or the monitoring office.

Disclaimer

The findings in the report are not to be construed as an official Department of Defense of Military Department position unless so designated by other official documents.

FOREWORD

This report presents work which was performed under the Joint Army Navy Aircraft Instrumentation Research (JANAIR) Program, a research and exploratory development program directed by the United States Navy, Office of Naval Research. Special guidance is provided to the program for the Army Electronics Command, the Naval Air Systems Command, and the Office of Naval Research through an organization known as the JANAIR Working Group. The Working Group is currently composed of representatives from the following offices:

U. S. Navy, Office of Naval Research, Aeronautics, Code 461
Washington, D. C.

- Aircraft Instrumentation and Control Program Area

U. S. Navy, Naval Air Systems Command, Washington, D. C.

- Avionics Division, Navigation Instrumentation and Display Branch (NAVAIR 5337)
- Crew Systems Division, Cockpit/Cabin Requirements and Standards Branch (NAVAIR 5313)

U. S. Army, Army Electronics Command, Avionics Laboratory,
Fort Monmouth, New Jersey

- Instrumentation Technical Area (AMSEL-VI-I)

The Joint Army Navy Aircraft Instrumentation Research Program objective is: To conduct applied research using analytical and experimental investigations for identifying, defining and validating advanced concepts which may be applied to future, improved Naval and Army aircraft instrumentation systems. This includes sensing elements, data processors, displays, controls and man/machine interfaces for fixed and rotary wing aircraft for all flight regimes.

ABSTRACT

In support of a theory for manual control displays, and, in particular, for integrated displays, a series of two pilot experiments were performed to enlarge the data base for the theory. A single-axis tracking experiment was performed with two different controlled elements and four different display formats. The effects of display format were separately evaluated from task difficulty and task performance with a particular view toward quantification of the pilots' parafoveal perceptual ability. In the second experiment four different integrated displays were tested in a precision tracking task with a view toward quantifying the effect of integration in the display. Different forms of integration of the display were found to strongly influence the pilots' excess control capacity which is the complement of workload. Describing functions, remnant, eye-movements, and pilot opinion data were also recorded in these experiments. Interpretation and the conclusions to be drawn from all these data are presented in the report.

ACKNOWLEDGEMENTS

The authors gratefully acknowledge the sponsorship whose recognition of the continuing value of applied research made possible these applications of a systematic theory for manual control displays. This work was sponsored by the Office of Naval Research, Department of the Navy, under Contract No. N00014-68-C-0447, as part of the Joint Army Navy Aircraft Instrumentation Research (JAN AIR) Program. For their guidance, encouragement and criticism, we are particularly grateful to the Scientific Officers, the late Lt. Cdr. Francis A. Cundari, Lt. Cdr. H. Lyon, and the Project Monitors, Mr. David S. Siegel and Lt. Cdr. John Hamrack.

The authors wish also to acknowledge the sustaining technical direction provided by Mr. D. T. McFuer, the helpful suggestions of their colleagues, and their appreciation for the painstaking work of the Systems Technology, Inc. staff in the production of the report.

CONTENTS

	<u>Page</u>
I. INTRODUCTION	1
II. MATHEMATICAL MODELS AND DEFINITIONS	8
A. MODELS FOR HUMAN PILOT DYNAMICS	8
B. MULTIAXIS SCANNING BEHAVIOR	12
1. Scanning Phenomena to be Described	12
2. Describing Function and Remnant Phenomena Accompanying Scanning	16
3. Multiaxis Scanning Models for Control Tasks	22
C. DISPLAY DEFINITIONS	35
III. THE SINGLE-AXIS EXPERIMENT	39
A. PURPOSE OF THE SINGLE-AXIS EXPERIMENT	39
B. SCENARIO	42
C. SIMULATION	42
1. Cockpit	42
2. Displays and Viewing Conditions	43
3. Controlled Element Dynamics and Input	44
4. The Describing Function Analyzer	44
5. Eye-Point-of-Regard (EPR)	44
D. MEASUREMENTS	46
E. SUBJECTS	47
F. IMPORTANT RESULTS OF THE SINGLE-AXIS EXPERIMENTS WITH DIFFERENT DISPLAY FORMATS	48
IV. AN EXPLORATORY MULTIAXIS INTEGRATED DISPLAY EXPERIMENT	53
A. PURPOSE OF THE MULTIAXIS EXPERIMENTS WITH DIFFERENT DISPLAY FORMATS	53
B. SCENARIO	53
C. SIMULATION	55
1. Control Tasks and Dynamics	55
2. Displays	63
D. MEASUREMENTS AND PROCEDURES	65
1. Performance and Describing Function Measurements	67
2. Eye-Point-of-Regard (EPR)	67

	<u>Page</u>
3. Pilot Opinion Ratings	68
4. Cross Adaptive Excess Control Capacity Measurement	68
E. SUBJECTS	68
F. TRAINING AND TEST AGENDAS	70
G. ORGANIZATION OF THE RESULTS	70
H. TRACKING ERRORS, COHERENCE, CONTROL AND MOTION VARIABLES	74
I. DESCRIBING FUNCTIONS	78
1. Observations on the Open-Loop Crossover Model Parameters for $Y_p Y_c$ with $Y_c = K/s$	83
2. Observations on the Open-Loop Crossover Model Parameters for $Y_p Y_c$ with $Y_c = K/s^2$	83
J. EYE-POINT-OF-REGARD MEASUREMENTS	85
1. Concise Summary of EPR Observations from Figures IV-16 through 20	87
2. Discussion of EPR Results	94
K. THE CROSS ADAPTIVE MEASURE OF EXCESS CONTROL CAPACITY AND SUBJECTIVE RATINGS OF DISPLAY QUALITY	98
7. CONCLUSIONS AND RECOMMENDATIONS	100
A. CONCLUSIONS FROM THE RESEARCH AND IMPLICATIONS FOR A THEORY OF INTEGRATED DISPLAY FORMAT	100
B. RECOMMENDATIONS FOR FORMAL INTEGRATED DISPLAY EXPERIMENTS	103
REFERENCES	106
GLOSSARY OF SOME TECHNICAL TERMS USED IN THIS REPORT	109
APPENDIX A Systematic Manual Control Display Design	A-1
APPENDIX B Summary of Predicted Pilot Loop Closures for the Multiaxis Experiment with CH-53 Airframe Dynamics	B-1
APPENDIX C Derivation of Rating Scales for Display Evaluation	C-1

FIGURES

		<u>Page</u>
I-1.	Scope of Manual Control Display Theory	2
II-1.	Block Diagram for the Compensatory Quasi-Linear Pilot Model	9
II-2.	Horizontal EPR Time Traces on Two Pilots for Various Experimental Conditions	13
II-3.	Predicted and Measured Dwell Fractions and Transition Link Probabilities for Manual ILS Approach	21
II-4.	Assumed Form of Pilot Models	24
II-5.	"Switched Gain" Multiaxis Scanning Model for Compensatory Multiaxis Tracking with One Among Several Displays	28
II-6.	Simplified Equivalent "Switched Gain" Multiaxis Scanning and Tracking Model for Compensatory Tasks	29
II-7.	Basic Features of Finite Dwell Sampling and Reconstruction	33
II-8.	"Reconstruction Hold" Multiaxis Scanning Model for Compensatory Multiaxis Tracking with one Among Several Displays	36
II-9.	Simplified Equivalent "Reconstruction-Hold" Multiaxis Scanning and Tracking Model for Compensatory Tasks	37
III-1.	The Formats for the Single-Axis Experiments	40
III-2.	Tracking Tasks, Data Measurements and Analysis	45
III-3.	Summary of Crossover Model Effective Time Delay for Different Single-Display Formats	49
III-4.	Summary of Parafoveal to Foveal Crossover Gain Ratio for Different Single-Display Formats	50
III-5.	Summary of Normalized Error Coherence for Different Single-Display Formats	51
IV-1.	Simulation Block Diagram for the Longitudinal Control Task	56
IV-2.	The Tasks for the Multiaxis Experiment	58
IV-3.	Longitudinal Control Task Dynamics	59

FIGURES (CONT'D)

	<u>Page</u>
IV-4. Secondary Control Tasks	63
IV-5. Cross Adaptive Workload Task	64
IV-6. Cockpit Display Panel Configuration, Primary Task CRT Display Formats and Scaling	66
IV-7. Velocity Error Performance with Velocity AFCS	75
IV-8. Velocity Error Performance with Pitch AFCS	77
IV-9. Selected Runs Showing Mean Errors and Root-Mean-Squared Errors for Primary Task Motion Variables with Velocity AFCS	79
IV-10. Selected Runs at High Workload Showing Mean Errors and Root-Mean-Squared Errors for Primary Task Motion Variables with Pitch AFCS	80
IV-11. Selected Runs Showing Mean Errors and Root-Mean-Squared Errors for Secondary Task Displayed Motion Variables	81
IV-12. Crossover Describing Function Parameters with Velocity AFCS	82
IV-13. Crossover Describing Function Parameters with Pitch AFCS	84
IV-14. Pilot's Contributions to Effective Lead Equalization with Pitch AFCS $Y_c = K/s^2$	86
IV-15. Pilot's Contributions to Effective Time Delay with Pitch AFCS $Y_c = K/s^2$	86
IV-16. Horizontal EPR Time Traces on Two Pilots for Various Experimental Conditions	88
IV-17. EPR Dwell Times and Scanning Intervals on Two Pilots for Various Experimental Conditions	89
IV-18. More Demanding Side Tasks: Summary of Scanning Behavior	90
IV-19. Less Demanding Side Tasks: Summary of Scanning Behavior	91
IV-20. Partition of EPR Dwell Times on the Primary Display Between Flight Director and Displacement Error Symbols	93
IV-21. Scanning Frequency Parameter as a Function of Display Configuration	96
IV-22. Display Qualities Ratings	99

FIGURES CONCLUDED

		<u>Page</u>
A-1.	Typical Eye Fixation Transition Link Vectors and Dwell Fractions Measured in Simulated Jet Transport Instrument Approaches	A-1
A-2.	Simulated Glide Slope Beam-Following Performance Under Manual Control with Various Inputs	A-2
A-3.	Predicted and Measured Dwell Fractions and Transition Link Probabilities for Manual ILS Approach	A-4
A-4.	Single-Loop Primary Task with Secondary Cross-Coupled Loading Task	A-6
A-5.	Subjective Pilot Rating Versus First-Order Cross-Coupled Instability Score	A-7
A-6.	Integrated Display Arrangement with Examples of Format Tested for Excess Control Capacity	A-7
A-7.	Cross Adaptive Task Measure of Excess Control Capacity	A-8
A-8.	Inverse Effective Time Delay as a Function of the Order of Lead Equalization Required of the Pilot	A-8
A-9.	Effective Time Delay as a Function of Average Neuromuscular Tension	A-8
B-1.	Human Pilot Loop Closure Configuration	B-2
B-2.	Detailed Implementation of Augmented Airframe Dynamics	B-3
B-3.	Root Loci for $x \rightarrow \theta_c$ Loop Closure with K_x as the Variable Gain and the Effective Time Delay $\tau_\theta = 0.33$ sec	B-8
B-4.	Root Loci for $h \rightarrow \delta_c$ Loop Closure with K_h as the Parameter and Using a Free Collective Stick	B-17
B-5.	A Graph for Predicting Single-Axis Excess Control Capacity and Attentional Workload Based on the Pilot's Lead Equalization	B-23
B-6.	Predicted Link Values for the Multiaxis Experiment	B-31
B-7.	Open-Loop Bode Diagram for Manually Controlled Inner and Outer Loops	B-34

TABLES

		<u>Page</u>
II-1.	Axis Scanning Phenomena for Pilots' Visual Modalities	17
II-2.	Sampling Remnant Power Spectral Density	30
II-3.	Processing Noise Power Spectral Density	34
III-1.	Experimental Design for Single-Axis Display Format Experiments	41
III-2.	Pilot Background	47
IV-1.	Outline of Experimental Test Plan for Multiaxis Experiments	54
IV-2.	Command Velocity Input	50
IV-3.	Helicopter Simulation Equations of Motion	61
IV-4.	Pilot Opinion Rating Scales	69
IV-5.	Pilot Background and Experience	70
IV-6.	Run Log for the First Format Experimental Session with the Velocity AFCS Controlled Element	71
IV-7.	Run Log for the Second Format Experimental Session with the Pitch AFCS Controlled Element	72
A-I.	Procedure for Predicting Multiaxis Scanning Behavior on a Preliminary Control Display Design	A-5
B-I.	Augmented Longitudinal Transfer Functions Resulting from AFCS Implementation in Fig. B-2 (Ref. 2)	B-4
B-II.	Predicted Forms for the Human Pilot Describing Functions in Fig. B-1 with Changes in Display Format	B-6
B-III.	Open-Loop Frequency Response $ x/x_e $	B-9
B-IV.	Summary of Parameter Choices for Maximum Phase Margin in the Outer Longitudinal Separation Loop Closure	B-13
B-V.	Open-Loop Frequency Response $ h/\delta_c $	B-19
B-VI.	Summary of Parameter Choices for Maximum Phase Margin in the Attitude Regulation Closure	B-21
B-VII.	Predicted Average Display Scanning Statistics for the Pilot Experiment	B-29

TABLES CONCLUDED

	<u>Page</u>
B-VIII. Open-Loop Transfer Functions and Closed-Loop Roots, Spectra and Variances for Manually Controlled Inner Pitch Attitude and Outer Longitudinal Separation Loops with a State Display and Longitudinal Gust Disturbances	B-35
B-IX. Closed-Loop Spectra and Variances for Manually Controlled Inner Pitch Attitude and Outer Longitudinal Separation Loops with a State Display and Remnant Disturbances.	B-39
C-I. Sematic Relationship of Display Rating Phrases	C-4

SYMBOLS

a_d	Displayed error of item a among several displayed quantities
AFCS	Automatic Flight Control System
ATT	Attitude display
A_i	Amplitude of the i^{th} sinusoidal component in the quasi-random command velocity input
b_d	Displayed error of item b among several displayed quantities
B_1	Longitudinal cyclic pitching moment control displacement in rad (see also δ_b, δ_e)
c	Pilot's control action
c_a	Pilot's control action in response to displayed error of item a
c_b	Pilot's control action in response to displayed error of item b
CRT	Cathode Ray Tube
$C(s)$	Laplace transform of control displacement
d_c	Glide slope displacement guidance beam command
D	Director display format without any confidence-inspiring situation information
DF	Describing function
DFA	Describing function analyzer
e	Displayed error signal; also Napierian base 2.71828...
$\overline{e^2}$	Mean-squared error or time variance of error
$(\bar{e})^2$	Square of the mean error or square of the time-averaged error
e_c	Error criterion
e_d	Displayed error
eff	Effective value

EPR	Eye-Point-of-Regard
e_s	Scanned and sampled (displayed) error
$E, E(s)$	Laplace transform of displayed error signal
FD	Flight Director
\bar{f}_s	Mean fixation (scanning) frequency in Hz.
$\bar{f}_{u_{as}}$	Mean fixation frequency on the displayed airspeed signal
g	Gravitational acceleration
GSD	Glide Slope Deviation display
h	Altitude
\dot{h}	Vertical velocity
h_e	Altitude error
HSI	Horizontal Situation Indicator
Hz	Abbreviation for Hertz, a unit of frequency measure equivalent to one cycle per sec.
i	Command input signal or forcing function symbol; summation index
$I, I(s)$	Laplace transform of command input
IAS	Indicated Air Speed
IE	Time integral of error
IE^2	Time integral of error-squared
IFR	Instrument Flight Rules
ILS	Instrument Landing System
Im	Imaginary part of ...
IVSI	Instantaneous Vertical Speed Indicator
I_y	Pitching moment of inertia of controlled element in slug-ft ²
j	$\sqrt{-1}$; summation index

$j\omega$	Operational argument of the Fourier transform; also imaginary part of the complex argument of the Laplace transform
k	Summation index
K	Gain of a transfer function or of a describing function
K_e	Controlled element gain in the roll axis
K_c	Controlled element gain in the collective axis
K/s	Velocity controlled element transfer function; an integrator of control input with gain K
K/s^2	Acceleration controlled element transfer function; a double integrator of control input with gain K
K_f	Pilot's foveal describing function gain
K_h	Pilot's perceptual gain or attenuation factor
K_m	Pilot's gain in response to motion cues, used for lead equalization $\sim T_L$
K_p	Pilot's adaptive gain in general; parafoveal gain
K_{pe}	Pilot's compensatory gain
K_{le}	Pilot's gain in response to the displayed longitudinal error signal
K_{δ_e}	Longitudinal cyclic pitch control stick gain
K_θ	Pilot's or flight director gain in response to pitch attitude deviations from trimmed attitude
K_ϕ	Pilot's gain in response to roll attitude deviations from trimmed attitude
m	Controlled element state variables or output motion signals; mass of the helicopter in slugs
M	Pitching moment applied to controlled element; integer
$M(s)$	Laplace transform of controlled element motion
M_{B_1}	$(1/I_y)(\partial M/\partial B_1)$ in sec^{-2}

M_q	$(1/I_y)(\partial M/\partial q)$ in sec^{-1}
M_s	Scanning workload margin
M_u	$(1/I_y)(\partial M/\partial u)$ in $\text{ft}^{-1}\text{sec}^{-1}$
n_a	Equivalent "observation" remnant associated with displayed error of item a
n_b	Equivalent "observation" remnant associated with displayed error of item b
n_c	Pilot's remnant associated with control action, c
n_p	"Processing" remnant, <u>i.e.</u> , portion of pilot's remnant dependent on error level
n_r	Constant residual level of pilot's remnant
n_s	"Scanning" remnant, a special type of processing remnant, n_p
N	Integer
P_c	Crossover period, $2\pi/\omega_c$, in sec
q	Pitching angular velocity in rad/sec
q_{ij}, q_{ji}	Fixation transition probabilities (link values) in the direction $i \rightarrow j$ and $j \rightarrow i$, respectively ; $i \neq j$
R	Pilot's perceptual rate weighting coefficient
$\text{Re} \dots$	Real part of ...
rms, RMS	Root-Mean-Squared value
s	Complex argument of the Laplace transform
S	"State" display format without rate (no longitudinal error rate symbol); also a dimensionless scanning frequency ratio, $\omega_s/\omega_c(1 - \eta) = P_c/T_\Delta$
$\frac{S}{N}$	Signal-to-noise power ratio
$S + R$	"State and Rate" display format (longitudinal error rate symbol added to S)

t	Time
T_d	Eye fixation dwell interval in sec
\bar{T}_d	Mean value of fixation dwell interval in sec
\bar{T}_{CRT}	Mean fixation dwell interval on cathode ray tube display
T_D	Effective display lag time constant in sec
T_{d_e}	Human operator's effective internal dwell interval given by product $\eta_e \bar{T}_s$
\bar{T}_{d_e}	Effective average dwell interval in sec
$\bar{T}_{h, \dot{h}}$	Mean fixation dwell interval on altitude and vertical speed displays
T_I	Lag equalization time constant in sec
T_L	Lead equalization time constant in sec
T_{L_x}	Value of T_L adopted for longitudinal (x-) position regulation in sec
T_N	Effective neuromuscular lag time constant in sec
T_O	Lower bound on the domain of T_s in sec
T_R	Rolling subsidence time constant for the helicopter
T_B	Fixation (scanning) interval in sec
\bar{T}_B	Mean fixation (scanning or sampling) interval in sec
$T_{\Delta}, \bar{T}_{\Delta}$	Mean fixation interrupt interval, $T_B - \bar{T}_d$
u	Deviation in the longitudinal component of inertial velocity from trimmed value in ft/sec
u_c	Command velocity in ft/sec
u_e	Velocity error in ft/sec

u_g	Random longitudinal gust velocity in ft/sec
VFR	Visual Flight Rules
w_g	Random normal (vertical) gust velocity in ft/sec
x_e, X_e	Displayed position error in ft
X	Longitudinal force applied to the controlled element
X_{B_1}	$(1/m)(\partial X/\partial B_1)$ in ft/sec ²
X_q	$(1/m)(\partial X/\partial q)$ in ft/sec
X_u	$(1/m)(\partial X/\partial u)$ in sec ⁻¹
$Y_c, Y_c(j\omega)$	Controlled element describing function
Y_d	Display describing function
$Y_h, Y_H, Y_H(j\omega)$	Pilot's perceptual describing function, representing operations such as observation, scanning, sampling and reconstruction
$Y_{OL}, Y_{OL}(j\omega)$	Open loop frequency response function
$Y_p, Y_p(j\omega)$	Pilot's adaptive describing function, representing operations such as equalization and summing
Y_{Pa}	Pilot's describing function in operating on displayed error of item a
Y_{Pb}	Pilot's describing function in operating on displayed error of item b
$Y_{Pc}, Y_{Pe}(j\omega)$	Pilot's compensatory describing function in general
$Y_{p\theta}$	Pilot's pitch attitude describing function
$Y_{p\phi}$	Pilot's roll attitude describing function
$1 - \eta$	Mean fixation interrupt fraction
$1 - \eta_e$	Mean effective interrupt fraction
$1 - \bar{\eta}_f$	Mean foveal interrupt fraction

α	Effective low frequency phase coefficient in the extended crossover model; $\alpha = \sum_{i=1}^M \left(\frac{1}{T_L} - \frac{1}{T_I} \right)_i$; M, an integer which reflects the number of lower frequency leads and lags
α_c	Value of α computed near unit-gain crossover from describing function measurements
δ	Normalized lower bound on the domain of T_s , $T_o/\sqrt{T_s}$
δ_a	Lateral cyclic rolling moment control displacement in rad
δ_b	Same as δ_e
δ_c	Collective lift control displacement in rad
δ_e	Longitudinal cyclic pitching moment control displacement in rad
$\Delta\alpha$	Incremental low frequency phase coefficient, e.g., such as that caused by parafoveal perception
$\Delta\tau(\dots)$	Incremental time delay which is a function of (...)
$\Delta\tau_s$	Pilot's incremental time delay caused by scanning, sampling and reconstruction
$\Delta\tau_f$	Pilot's incremental time delay caused by low frequency lead equalization
ζ	Damping ratio of a second order dynamic system
ζ_I	Damping ratio of a second order lag
ζ_L	Damping ratio of a second order lead
$\eta, \bar{\eta}$	Mean fixation dwell fraction, \bar{T}_d/\bar{T}_s , fractional scanning workload, probability of fixation
η_{CRT}	Value of η for CRT display
$\eta_e, \bar{\eta}_e$	Mean effective dwell fraction = \bar{T}_{de}/\bar{T}_s
$\eta_f, \bar{\eta}_f$	Mean foveal dwell fraction

η_{FD}	Mean fixation dwell fraction on flight director
$\eta_{h, h}$	Mean fixation dwell fraction on altitude and vertical speed displays
$\eta_{u, AS}$	Mean fixation dwell fraction on airspeed display
θ	Pitch attitude angle
θ_c	Pitch attitude command
θ_e	Pitch attitude error
λ	Inverse time constant of the first order divergence in the controlled element of the (unstable) subcritical tracking task
λ_c	Critical limiting value of λ
λ_{CA}, λ_s	Cross-adaptive or subcritical value of λ , when the subcritical tracking task is employed to measure excess control capacity by adapting λ as a function of primary task error
λ_h, μ_h	Altitude divergence parameter
λ_φ	Roll attitude (spiral) divergence parameter
μ_h, λ_h	Altitude divergence parameter
v	Fixation or look fraction
v_{CRT}	Fixation or look fraction on Cathode Ray Tube display
$v_{h, h}$	Fixation or look fraction on altitude and vertical speed displays
$v_{u, AS}$	Fixation or look fraction on airspeed display
π	3.14159...; also used for look fraction in some of the original literature
ρ_E^2	Error coherence, $\sigma_{e_1}^2 / \sigma_e^2$
$\rho_{u_e}^2$	Velocity error coherence
σ^2	Signal variance in time

σ_v	Standard deviation (RMS value) of the command velocity input in ft/sec
σ_v^2	Time variance of the command velocity input in (ft/sec) ²
σ_{a_c}	Standard deviation (RMS value) of beam command in ft
$\sigma_{e'}^2$ $\sigma_{e''}^2$	Time variances of the (displayed error) displacement and its first derivative to which the human operator is responding
$\sigma_{e_i}^2$	Input-correlated error variance
$\sigma_{e_f}^2$	Uncorrelated error variance (caused by remnant)
$\sigma_{u_i}^2$	Command input or forcing function variance
σ_{T_d}	Human operator's RMS fixation dwell interval or standard deviation in T_d
σ_{T_s}	Human operator's RMS fixation scanning or sampling interval or standard deviation in T_s
$\sigma_{v_e}^2$	Velocity error variance
$\sigma_{u_i}^2$	Command velocity input variance
σ_{u_g}	Standard deviation (RMS value) of longitudinal gust velocity in ft/sec
σ_{v_g}	Standard deviation (RMS value) of normal (vertical) gust velocity in ft/sec
τ	Pilot's time delay, sec, due to latencies in perception, neural conduction, and coding
τ_e	Effective time delay in the crossover model, $\tau_e = \tau + T_D + T_N + \sum_{j=1}^M (T_{I_j} - T_{L_j}) + \sum_{k=1}^N \left(\frac{2\zeta_{I_k}}{\omega_{I_k}} - \frac{2\zeta_{L_k}}{\omega_{L_k}} \right) k ;$
	M, N, are integers which reflect the number of higher frequency lead and lag contributions from the display, pilot, and controlled element

τ_{e_c}	Value of τ_e computed near unit-gain crossover from describing function measurements
τ_e	Effective time delay for response to motion cues
τ_0	Value τ_e for zero forcing function bandwidth ($\omega_1 = 0$)
φ	Roll attitude angle
φ_e	Roll attitude error
φ_i	Phase angle of the i^{th} sinusoidal component in the quasi-random command velocity input; also used for probability of fixation in some of the original literature
Φ_M	Phase margin
Φ_{M_c}	Computed value of the phase margin at unit-gain crossover from describing function measurements
$\Phi, \Phi(\omega)$	Power spectral density in (units) ² per rad/sec
$\Phi_{cc}, \Phi_{cc}(\omega)$	Total control output power spectral density in (units) ² per rad/sec
$\Phi_{ee}, \Phi_{ee}(\omega)$	Error power spectral density in (units) ² per rad/sec
Φ_{ee1}	Portion of Φ_{ee} which is input-correlated
Φ_{ee2}	Portion of Φ_{ee} which is uncorrelated with input
$\Phi_{ii}, \Phi_{ii}(\omega)$	Input power spectral density in (units) ² per rad/sec
Φ_{nna}	Power spectral density of aural tracking remnant in (units) ² per rad/sec
$\Phi_{nne}, \Phi_{nne}(\omega)$	Remnant power spectral density referred to the operator's input
Φ'_{nne}	Normalized power spectral density of processing remnant, $\Phi_{nna}/\sigma_e^2 = \Phi_{nne}/\sigma_e^2$

ϕ_{nnm}	Power spectral density of motion cue remnant in (units) ² per rad/sec
ϕ_{nno}	Power spectral density of residual remnant in (units) ² per rad/sec
ϕ_{nnp}	Power spectral density of processing remnant in (units) ² per rad/sec
ϕ_{nns}	Power spectral density of scanning or sampling remnant in (units) ² per rad/sec
ϕ_{nns}^i	Normalized power spectral density of scanning or sampling remnant, ϕ_{nns}/σ_e^2
ω	Circular frequency in rad/sec
ω_c	Unit-gain crossover frequency; crossover gain
ω_{cc}	Computed value of ω_c from describing function measurements
ω_{cf}	Crossover frequency with continuous foveal attention
ω_{cp}	Crossover frequency with continuous peripheral attention
ω_1	Forcing function bandwidth in rad/sec; also circular frequency of the 1 st sinusoidal component in the quasi-random command velocity input
ω_I	Undamped natural frequency of a second order lag in rad/sec
ω_L	Undamped natural frequency of a second order lead in rad/sec
ω_u	Unstable frequency in rad/sec
ω_{uc}	Computed value of ω_u
ω_s	Circular fixation (scanning) frequency in rad/sec
ω_{sFD}	Fixation scanning frequency on the flight director in rad/sec

Ω Effective parafoveal-to-foveal gain ratio,

$$K_p/K_f = \frac{\eta_e - \eta}{1 - \eta}$$

Mathematical Symbols

<	Less than
>	Greater than
\leq	Less than or equal to
\geq	Greater than or equal to
\ll	Much less than
\gg	Much greater than
\neq	Not equal to
\approx	Approaches; approximately equal to
\equiv	Identically equal to
\rightarrow	Red to; approaches
\Rightarrow	Identified with
$\bar{}$	(raised bar) average value
$\dot{}$	(raised period) d/dt
d	Differential operator
∂	Partial differential operator
\int	Integration operator
Σ	Summation operator
o	Location of a transfer function zero in the complex s-plane
x	Location of a transfer function pole in the complex s-plane
+	Addition operator
-	(hyphen) subtraction operator; negative value prefix

SECTION I

INTRODUCTION

The ability to describe in a predictive model the various ways in which a human pilot can function as a controller and instrument monitor will achieve direct and important savings in the design and evaluation of displays. Figure 1-1 shows a framework for such a description. The entire display-pilot-control-vehicle combination is considered as a multiloop feedback control system. One or more controlled elements correspond to the dynamics of vehicle response to control. Controlled elements are subjected to environmental and internal disturbances, d , such as wind gusts and hydraulic power supply fluctuations. A human operator will pilot the controlled elements through control actions, c , by perceiving several loop closure possibilities. These possibilities may be both directly-controlled outputs, m , and displayed inputs, commands, or implicit environmental functions, i , such as intruding aircraft or terrain height along the intended flight path (pursuit displays); or the possibilities for display may represent only differences between i and m called errors (compensatory displays).

The display/control system for the vehicle is to be synthesized so as to improve piloted system performance to a point where a set (or subset) of mission requirements can be satisfied. In system engineering terms, the improvement of performance implies greater frequency bandwidths and correspondingly reduced closed-loop system lags and errors in following commands and suppressing disturbances. In terms of pilot behavior, the improvement of performance implies reduced effective time delay, reduced pilot-generated noise; increased allowable range of pilot-gain variation consistent with closed-loop system stability; and reduced workload to a level where he is efficiently and gainfully occupied, yet able to cope to a prescribed degree with the unexpected while he obtains and maintains the system performance required by the task.

In previous reports in this series (Refs. 1 and 2) it was shown, in connection with both fixed wing and rotary wing aircraft, how a display/control system might be synthesized for the conventional case of separated instruments. In particular, calculations were made of.

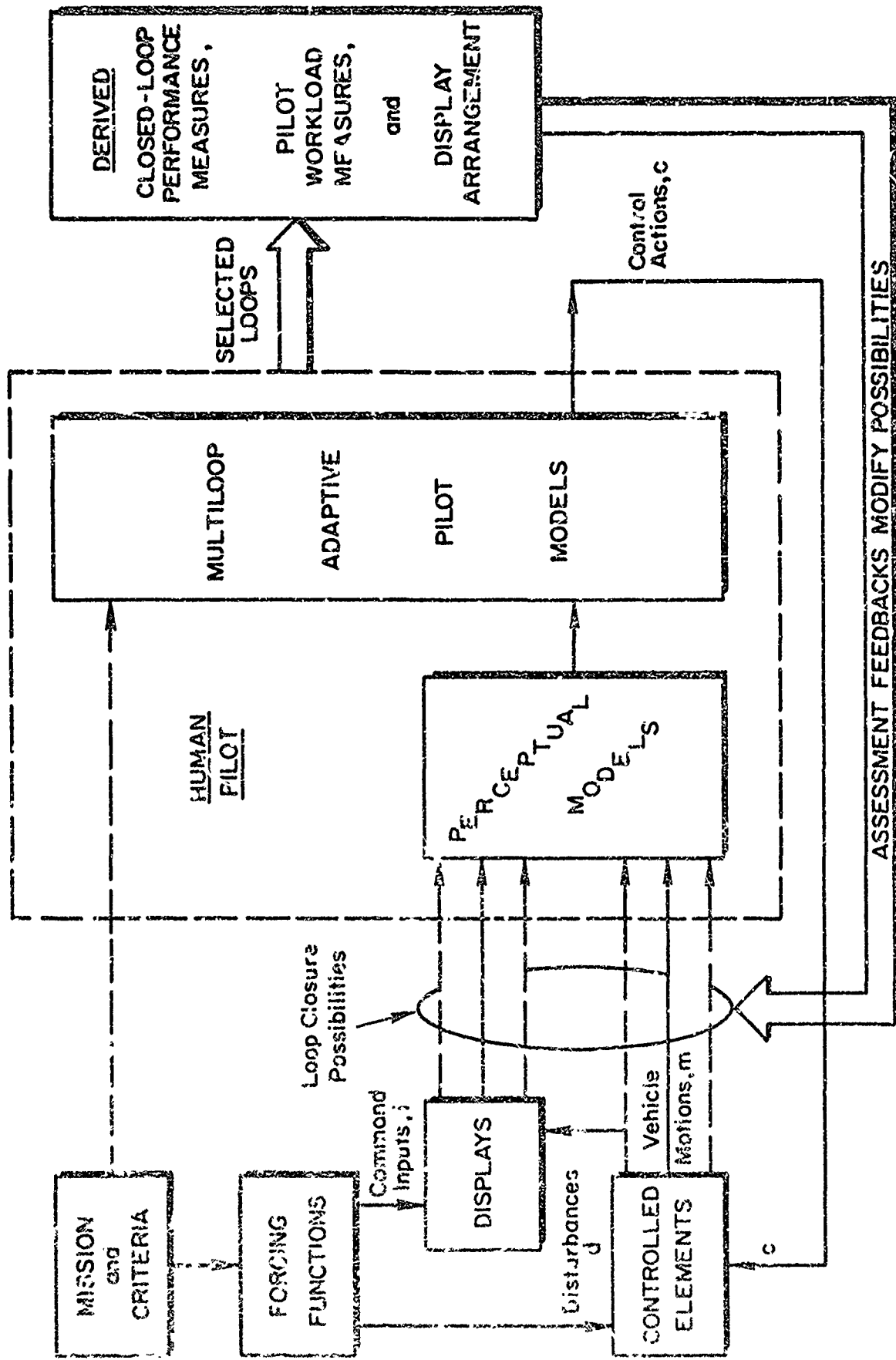


Figure 1. Scope of Manual Control Display Theory

- the quantities which, of necessity, had to be displayed to enable the specified mission phase (instrument approach) to be performed
- the pilot's appropriate dynamic behavior in acting on the displayed quantities
- system performance measures, such as rms errors and pilot workload data including fixation times and frequencies on each instrument
- the preferred arrangement of displays

Considering the relatively undeveloped state of theoretical knowledge on which the calculations were predicated, the dwell fractions and link probabilities resemble later measurements in the case in which there has been a direct comparison to be made between the predictions and the results of experiment. (See, for example, Fig. 3, Ref. 3 which is incorporated here as Appendix A.)

The prediction of system performance, workload, and preferred display arrangement for separated displays does not, however, address a contemporary question of practical interest. There exists a conviction, supported by both theoretical and experimental evidence, that for high precision tracking, such as in landing approach under instrument flight rules (IFR), it is necessary to combine or "integrate" displays. While the conviction is commonly held, there does not seem to be any commonly understood definition of an integrated display, nor any accepted answer to the question: "How is the display properly integrated?" A brief survey (Ref. 4) shows a tremendous variety of "integrated" displays even for the single mission phase of instrument low approach. This tremendous variety is very likely, in part, the result of a technique in experimental display research. For example, system performance measures such as mean square tracking errors and pilot workload measures such as mean square control deflections are often used to evaluate the relative merit of displays. Yet these same measures do not necessarily vary appreciably with large variations in the qualities of the display. On the other hand, there may be at the same time a strong preference on the part of the subjects of an experiment for one form of display over another. An analogy to the field of aircraft handling qualities research strongly suggests that such changes in pilot preference or opinion are correlated with changes in behavior required to maintain the specified performance by working to control in spite of variations in difficulty. Quite apparently we should look for such changes

in the pilot's behavior when using variations in the information which is displayed.

Curiously, perhaps, in view of the large amount of experimental work on displays, our ability to postulate perceptual behavioral models far exceeds our ability to generate believable experimental evidence which would tend to validate them. This incongruity is for the reason, described above, that very often the only measurements which are made concern mean squared tracking errors and control displacements. Such measurements are, of course, necessary (but not sufficient) for determining whether a particular system is, in fact, satisfactory. Mean squared error and control measurements alone leave much to be desired in determining the causes of and corrections for difficulties, except by ad hoc adjustments which may in themselves be influenced by some artificial characteristics of the simulation. Therefore, no improvement in the display design process, nor indeed in the more general problem of cockpit layout, is to be expected until we have in hand a validated theory for cause and effect in perceptual behavior in particular, and workload in general.

Such a theory of perceptual behavior, if it existed, would never completely replace experimentation in display design, development and evaluation, but it would enhance the efficacy of these processes by helping one to:

- Predict experimental possibilities which, in turn, help one to:
 - (1) suggest relatively critical experiments
 - (2) guide the experimental design
- Interpret experimental findings
- Discover limitations on experimental results by identifying task variables which would change the results
- Provide a basis for extrapolating experimental findings to different applications

It was to the elaboration of such a theory of the effects of format and content on perceptual behavior in using "integrated" displays and to the acquisition of a suitable data base that the research reported here was addressed.

In particular, it was hoped to:

- Answer four questions posed by the JANAIR Committee in 1966 when research on the theory of manual control displays was first initiated, viz.,
 - (1) What is an integrated display?
 - (2) How may the proper signals for manual control of a task be predicted and verified?
 - (3) How is the display properly integrated?
 - (4) How can the display be evaluated?
- Separate the controllability and precision of the task from the attentional workload in using the display by using special measures, such as:
 - (1) pilot's describing function gain
 - (2) effective time delay
 - (3) error coherence (relative remnant)
 - (4) excess control capacity
 - (5) display ratings
 - (6) eye-point-of-regard
- Quantify measures of attentional workload as functions of:
 - (1) display size, subtended field of view, and density of symbols
 - (2) form of the symbols
 - (3) display content (e.g. "quickered" command, situation, etc.)
- Codify the empirical results in a theory having predictive value for new tasks and integrated display designs.

More specifically, we note that in performing precise compensatory tracking tasks such as, for example, in landing approach under instrument flight rules (IFR), pilots should be provided with preferably only one but not more than two distinctly separate displays for the purpose of flight control. It has been shown by theoretical reasoning (Refs. 1 and 5) and experimental measurement (Refs. 6, 7 and 8) that in a landing approach under IFR there is sufficient time to fixate on not more than two separate displays with sufficient probability or dwell fraction to suitably suppress scanning remnant. More than one symbolic signal may, however, be presented on each of two displays to take advantage of pilots' parafoveal perceptual ability. Each display may then be called a "combined" or "integrated" display. Integrated displays have necessarily evolved from the pilot's inner control loop displays, such as the gyro horizon and compass, because the pilot must monitor a half-dozen or more multiloop situation variables even to maintain

confidence in using a two-axis flight director display. In reality, of course, especially in V/STOL approaches, there are three axes which require precision control, viz , longitudinal, as well as vertical and lateral, so that an integrated display for precise approach control under IFR is then most essential to maintaining a tolerably unsaturated level of pilot workload. Provided that it does not become "cluttered", the combined presentation of signals in a single display will allow the pilot to increase his effective dwell fraction on any particular displayed signal by using parafoveal perception. By helping the pilot to increase his effective dwell fraction, integrated displays can have a profound influence in reducing pilots' monitoring workload, and this may possibly be measured in terms of a reduction in the task-related scanning remnant.

Reference 9 shows that relative scanning remnant power or relative incoherent error power is directly proportional to the effective fraction of time between "looks" at the given displayed error. It is desirable to keep the tracking error coherence as high as possible (or to keep the error incoherence as low as possible) to achieve the best task performance within the constraint of attentional workload, of which scanning workload is one measure. One way is to increase the foveal dwell fraction on each object of fixation, but this is limited by the physical upper bound on scanning workload, which cannot exceed unity. The other way for a pilot to increase tracking error coherence is to increase his average parafoveal tracking gain up to a level where the closed-loop remnant is not amplified. This can be successful if the display format allows the pilot to maintain an average parafoveal tracking gain which is a large fraction of his foveal gain.

It was with a view toward a better understanding of interactions among parafoveal perception, error coherence, display format and attentional workload that the experiments reported here were conducted.

The balance of the report is divided into three technical sections.

The first of these reviews the tentative mathematical models and some new definitions of terms which provide the framework within which the experiments were planned and performed. Here the reader, perhaps unfamiliar with the previous results of research sponsored by the Joint Army Navy

Aircraft Instrumentation Research (JANAR) Program at Systems Technology, Inc. (STI), may acquire a knowledge both of the state-of-the-art perceptual models for integrated displays as well as the older models for motor response.

The models are summarized in compact analytical form for the reader who is already acquainted with pilot models for single-axis compensatory tracking control tasks. The review of mathematical models in Section II is not intended as a substitute for the more thorough description and validation of the models presented in Ref. 9--14, to which the dedicated practitioner and interested reader should refer.

An exposition of the complete array of models required for control display analysis is given in Ref. 1, and a narrative of the systematic control display design procedure including the multi-axis scanning models (Ref. 5) is included herein as Appendix A. Terms which are used in the balance of this report, especially the ones which are used to describe the measurements which were made and the results which were obtained, are defined in Section II and in the Glossary of Technical Terms.

As will be pointed out subsequently, two sets of experiments were performed. The first set of experiments, which is the subject of Section III, were concerned with single-axis tracking with the use of parafoveal viewing of displays. The second set of experiments, were concerned with the effects of display content and format in an integrated display. The latter experiments themselves and the results obtained are described in Section IV.

A brief final Section summarizes the report and presents the conclusions to be drawn from the research results.

We have already mentioned the first appendix which narrates the possibilities for systematic manual control display design. A second appendix presents the pre-experimental analyses for the set of experiments which addressed the effects of display content and format in an integrated display. A third appendix presents the derivation of some new subjective rating scales proposed for use in the experimental evaluation of control displays.

SECTION II

MATHEMATICAL MODELS AND DEFINITIONS

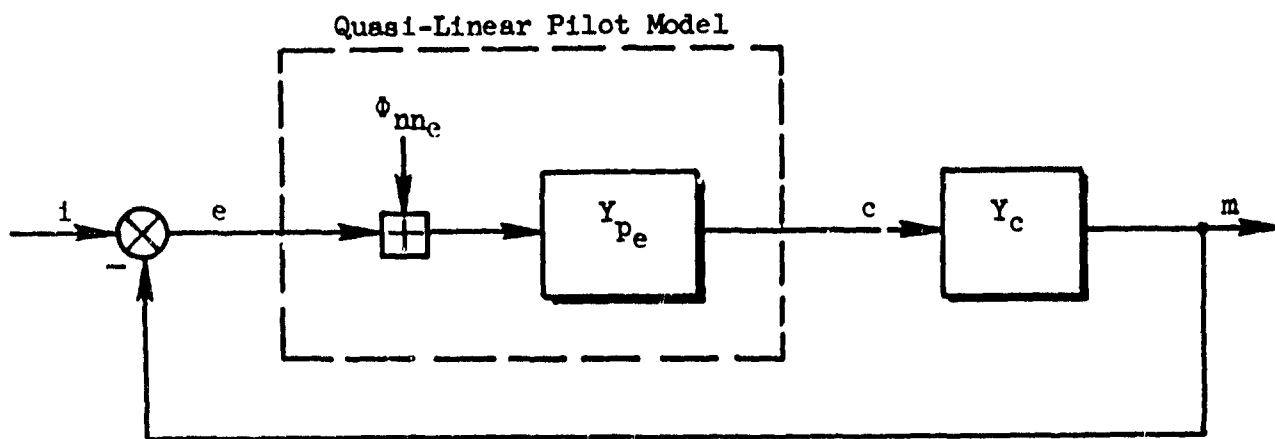
A. MODELS FOR HUMAN PILOT DYNAMICS

The human attributes of perception, response, judgment, and adaptability lead to a great number of possible loop structures for a given control task. To cope with this variety of possibilities in advance of any experiment, the theory of manual control displays (Ref. 1) first postulates possible interpretations and organizations of the input data available to the pilot. Then the theory postulates that the pilot will establish appropriate organization and adaptation of his behavior so that the data may be used for effective control.

In preliminary design, manual control display theory can serve as a tool for the pilot-vehicle system analyst by providing the set of rules for selecting the mathematical pilot model appropriate to a particular situation. However, in the application which concerns us here, the theory is being tested for its ability to predict and explain attributes of human behavior observed in controlled experiments. As a result of these tests, we may be able to extend or improve the characterization of a sample of pilot behavior in terms of task variables, operator-centered variables, and/or procedural variables in these specific experiments.

Manual control theory characterizes human behavior in terms of 1) mathematical models which express the dynamic motor response of the pilot to various sensory stimuli and 2) verbal-analytical models which express the adaptation of the pilot population to the task variables. Not all of these models, however, are based on sufficient experimental data to be definitive. This does not mean that these models lack usefulness. In all cases, the models are sufficiently developed to permit relative dynamic performance and workload estimates to be made. In these experiments, we are simply trying to characterize more definitely the dependence (or independence) of pilot behavior on properties of display format. Pilot models are described and reviewed in Refs. 1, 10, 11, 12 and 13. Only a synopsis of the simplest of models for compensatory single-loop control will be given here so as to introduce the reader to the form of the models and to some of the terminology used in describing the models.

In a closed-loop compensatory control task (Fig. II-1) the pilot responds to the displayed error, e , between a desired command input, i , and the comparable vehicle output motion, m , and produces a control action, c . The control servo actuator, vehicle, motion sensor, and display dynamics are combined and represented by the "controlled element" transfer function, $Y_C(s)$, which expresses the Laplace transform $M(s)$ in terms of $C(s)$. Compensatory single-loop pilot models comprise both a describing function*, $Y_{pe}(j\omega)$, and an additive "remnant" power spectral density, ϕ_{nn_e} , as shown in Fig. II-1. The portion of the pilot's control action which is linearly correlated with the input is represented by the quasi-linear describing function $Y_{pe}(j\omega)$ operating on the error signal, e . It also includes the effects of the control manipulator "feel" characteristics. The remnant is defined as the portion of the pilot's control output power which is not linearly correlated with the system input. As shown in Fig. II-1, the remnant can be represented by an additive noise, characterized by a power spectral density, ϕ_{nn_e} , in the quasi-linear pilot model. The total control output power spectral density, $\phi_{cc}(\omega)$, is thus the sum of two linearly uncorrelated



ϕ_{nn_e} is the power spectral density of the remnant referred to the operator's input

Figure II-1. Block Diagram for the Compensatory Quasi-Linear Pilot Model

*The term describing function is applied to emphasize that this is not a "human transfer function". The remnant must be added to complete the model, and the describing function is appropriate only for continuous random-appearing signals of relatively low bandwidth. It is strictly valid only in the frequency domain and should not be used, without appropriate modification, to compute the system response to a deterministic input.

power spectral densities:

$$\phi_{cc}(\omega) = \left[\frac{Y_{pe}}{1 + Y_{pe}Y_c} \right]^2 \left[\phi_{11}(\omega) + \phi_{rme}(\omega) \right]$$

where

ϕ_{11} = the input power spectral density

ϕ_{rme} = the remnant power spectral density referred to the operator's input

The remnant has been measured as a continuous and smooth power spectrum in tracking experiments of a time duration sufficient to define the operator's describing function over a broad frequency band. Sources of remnant may not be uniquely determined using only two-terminal measurements. However, one can infer the dominant sources of remnant from contrived experiments with particular task variables such as continuous attention, scanned and sampled attention, displayed signal thresholds and quantization, low-frequency lead equalization, unstable controlled elements, and non-stationary analog pilots. Inferred sources of the remnant in ascending order of importance for single-axis tasks are believed to be: pure noise injection, nonlinear action, and non-steady operator behavior.

For examples of pure noise injection, Ref. 30 suggests two models for generating low frequency lead equalization within the human operator which inherently produce noise, although the subject may appear to devote continuous attention to his single-axis tracking task. In some multi-axis tasks, as we shall subsequently discuss, pure noise injection caused by scanned and sampled attention can become dominant.

A model for the remnant can satisfactorily be taken to be a signal with a power spectral density which is a function of the pilot's lead equalization, the error variance, and the "difficulty" of the controlled element. Reference 32 has shown that the power spectral density of the human operator's remnant for certain (single-axis) tracking situations can be represented simply by injecting white noise processes at the operator's input where each state variable is perceived. The power spectral density of each injected white noise process is proportional to the variance of the (error) signal being perceived. As explained in Ref. 33 a number of quasi-random sampling, reconstruction, and derived-rate processes as well as Weber-Law errors in tracking control action all lead to wide-band remnant whose power spectral density is uniform at low frequencies and proportional to the variance of the error

signal displayed to the human operator. Therefore, the most consistent results seem to be obtained if the remnant is taken to be injected at the pilot's input (see Fig. II-1), although in special cases discussed next it is preferable to inject the remnant at the pilot's output.

If all sources of remnant power were proportional to the displayed error variance, the remnant should disappear when no external input (and, hence, no input-correlated error) is present. However, the experiments reported in Ref. 51 show that some output remnant is present in the absence of any external input. The cause is the cumulative effect of the "residual" sources described in Ref. 19. Hence, the name "residual remnant" is given to that noise which is present in the human operator's control output even without any external input and without the need for low-frequency lead equalization. It is preferable to model the residual remnant by injecting a noise process at the pilot's output. (Vide Ref. 19.)

The describing function comprises two parts:

- (1) a generalized mathematical operational form
- (2) a set of rules which specify how to select the parameters in the generalized form so that it becomes an appropriate, albeit approximate, model of human behavior for the particular task of interest.

The linear theory of servomechanisms suggests that, for reasons explained in Ref. 12, the describing function of the pilot ought to be adjusted in such a way that the open-loop frequency response function, $Y_{OL}(j\omega)$, of the single-loop compensatory system in Fig. II-1 will be

$$Y_{OL}(j\omega) = Y_{p_e}(j\omega)Y_c(j\omega) \doteq \frac{\omega_c}{j\omega} e^{-j(\tau_e \omega + \frac{\alpha}{\omega})}; \quad \omega \text{ near } \omega_c$$

This is called the "extended crossover model" (See Refs. 10, 11, 12 and 13). The unit-gain crossover frequency, ω_c , is equivalent to the loop gain product $K_{p_e}K_c$. τ_e is the effective time delay, and α is the effective low frequency phase coefficient, all in the open-loop describing function $Y_{p_e}Y_c$ (See Fig II-1). The difference between 180° and the phase angle of the (complex) describing function at the crossover frequency, ω_c , is the phase margin, ϕ_M . The frequency,

ω_u , at which the phase angle of the describing function is -180° , is called the unstable frequency. When the controlled element demands lead equalization by the pilot below the crossover frequency, $\alpha \approx 1/T_L$, where T_L is the lead equalization time constant. Otherwise, α represents the influence near the crossover frequency of very-low frequency lead-lag dynamics with amplitude ratio break points which are below the measurement bandwidth in many experiments.

The display designer will rarely need a model more precise than the extended crossover model, even for analyzing multiloop tasks. With the extended crossover model and the set of rules for adjusting its parameters, the designer can make valid forecasts of pilot equalization, effective time delay, crossover frequency, stability margins, tracking performance, and pilot opinion rating, in manual, compensatory, single-loop tracking tasks. Before we proceed to show how the extended crossover model can be applied in multiloop control tasks, we shall digress for a moment to define some new terminology which arises to describe the pilot's visual scanning and sampling behavior among the various sources of displayed inputs required in a typical multi-axis control task.

B. MULTIAxis SCANNING BEHAVIOR

1. Scanning Phenomena to be Described

Several examples of pilots' scanning phenomena are shown on the eye-point-of-regard time traces in Fig. II-2 for various experimental conditions to be discussed subsequently. Each trace records a pilot's eye saccade between the central cathode ray tube attitude director display (CRT) and the altitude display (left of center), or the airspeed display (right of center). After a saccade, denoted by the abrupt steps in each trace, the eye fixates or dwells on the display of concern for a brief interval before the next saccade. We often speak of the pattern of saccades and fixations as generating a pattern of scanning "traffic" or fixation transitions among instruments or displays. The circled enlargements of portions of the traces show that secondary fixation transitions also occur between symbols within

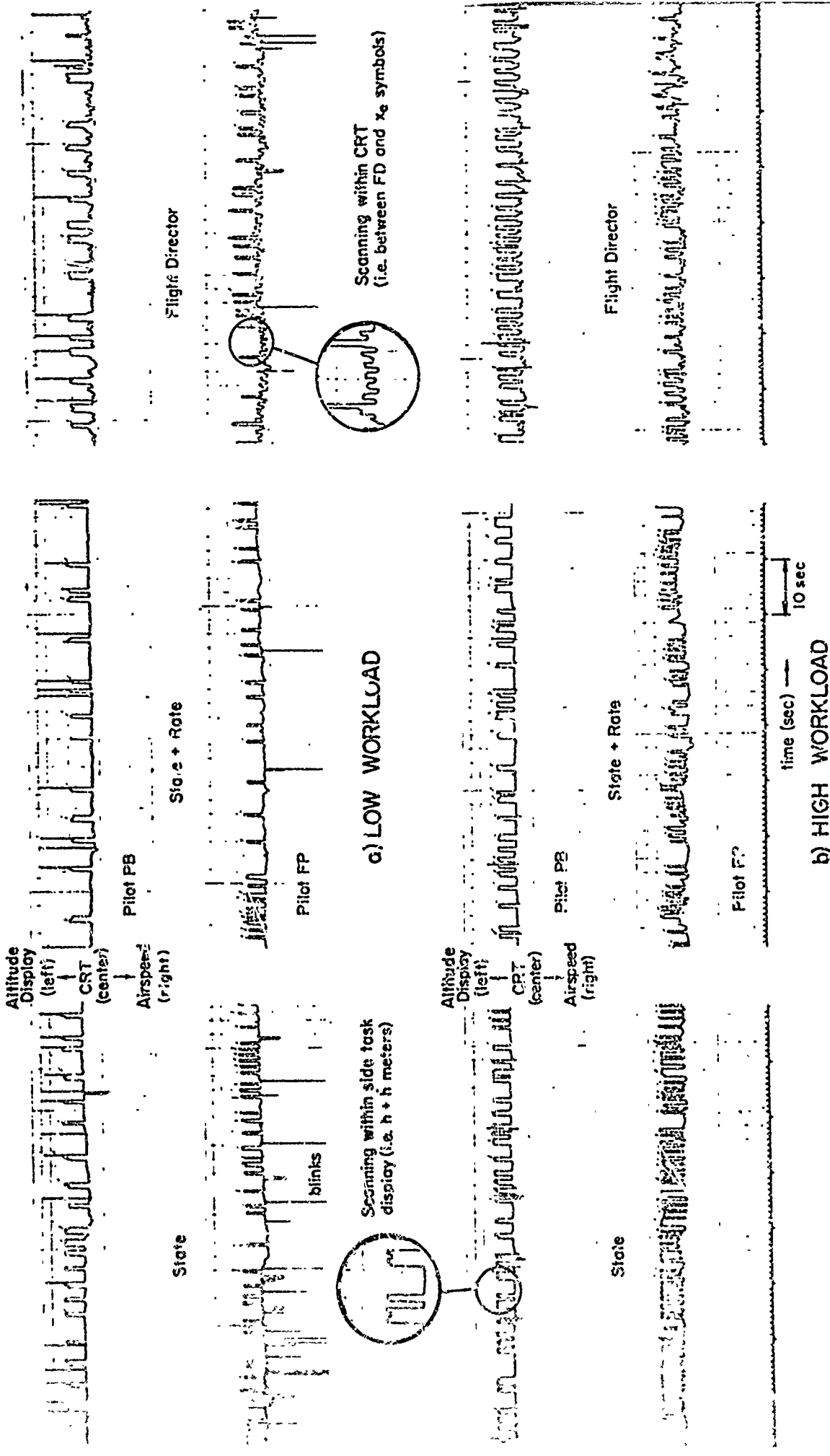


Figure II-2. Horizontal EPR Time Traces on Two Pilots for Various Experimental Conditions

the central, integrated CRT and between the altitude and altitude rate meters left of center. Reference 3 also presents several examples of pilot's scanning patterns on different panel arrangements. Obviously, however, one must speak of a foveal scanning pattern among "symbols" in the case of an integrated display, rather than among "instruments" as we shall do in most of what follows.

Furthermore, an observable foveal* scanning pattern may be accompanied by a parafoveal scanning pattern which is not directly observable by measuring eye movements. However, the presence of parafoveal awareness is indirectly observable by its influence on the pilot's describing function. We shall return to discuss this effect subsequently.

Although we shall be speaking primarily about the visual modality, the pilot can also choose to use or ignore motion and aural cues. While this is not quite like sampling, the more or less continuous use of the vestibular or aural modality is akin to a process of selection when these cues reinforce the visual modality.

Scanning of an instrument panel permits the displayed information to be sampled foveally during a variable foveal fixation dwell time interval on the order of one-half second or more. Between fixations the information may perhaps be observed parafoveally. Each saccade in Fig. II-2 describes the direction of a foveal fixation transition between two instruments, after which the visual axis of fixation will pause or dwell on an informative part of the instrument (e.g., the tip of a pointer) before beginning the next transition. Measurements have shown variability in the time interval which elapses between successive fixations on the same instrument. This time interval is called the scan interval or sampling interval. It will, in general, exhibit a different ensemble average value for each instrument.

Besides instrument to instrument scans, scanning occurs among the elements of combined displays. For instance, secondary fixation transitions within the two-axis attitude director on various symbols, indices, and scales have been observed, but not yet analyzed, in the experiments of Ref. 6.

*Foveal perception is "seeing where you are fixating." Colloquially, parafoveal perception is "seeing without looking," but more formally, it is "seeing without fixating."

Thus, the addition of a third axis to a flight director for direct lift control which requires a separate foveal fixation may deprive the pilot of time which would otherwise be spent monitoring the situation information, unless a three-axis director presentation can be contrived to convey three commands in one fixation through foveal and parafoveal channels of awareness.

The average number of fixations in a unit of time which fall upon a particular instrument is called the average fixation frequency, scan rate, or sampling frequency. The arithmetic average scan rate will be reciprocally related to the harmonic mean scan interval.

The proportion of the total number of fixations which fall upon a particular instrument is called the average look fraction for the instrument. Its upper bound is one-half, which implies that every other fixation or look is on the instrument with a look fraction equal to one-half.

The proportion of the total time during which fixations dwell on a particular instrument is called the average dwell fraction for that instrument. Since the cumulative sum of all dwell fractions, including blinks and distractions, must equal unity, by definition, the dwell fraction is also termed "fractional scanning workload" or "probability of fixation".

The proportion of all fixation transitions which go in the same direction between a pair of instruments is called the "one-way link-value" in the specified direction. The sum of the two one-way link values between a pair of instruments is called the "two-way" link value.

Since the scanning statistics are quite stationary over measurement intervals as short as 100 sec, different one-way link values between the same pair of instruments would be indicative of determinism in scan patterns. The results in Ref. 6 show no evidence of determinism in one-way link values. Thus, it seems that pilots' scanning behavior can be characterized as a zero-order Markovian process, i.e., that, given a fixation on one instrument, the conditional probability of transition to a particular different instrument is independent of the present (and past) fixation. This simplification proves useful in making predictions of scanning behavior.

A summary of properties of foveal and parafoveal scanning behavior, most of which we have just discussed and some of which are not yet observable, except in contrived experiments, is presented in Table II-1. Symbols, nomenclature, and some of the interrelationships which follow by definition are also given in Table II-1, together with a qualitative indication of ways in which scanning affects the pilot's multiloop describing function.

2. Describing Function and Remnant Phenomena Accompanying Scanning.

As far as we can tell currently, we have not discovered a unique relationship between observable foveal scanning statistics and the accompanying pilot's describing function and remnant. Instead, as we shall describe in the next topic, two different limiting forms have been discovered for multiloop pilot models in control tasks (Refs. 1 and 14).

In experiments in Refs. 9 and 14 the foveal input information samples are obtained from a finite dwell period, with an average minimum dwell time of about 0.4 sec. The pilot's effective time delays in closing several loops increase only slightly (on the order of 0.05 to 0.15 sec) because of the necessity for scanning, although the pilot gains are reduced from those that would be expected on a single-loop basis. This is not what one would obtain with a simple zero-order-hold sampled-data system, so the sampling and scanning theory required to describe the pilot's eye movements has been quite elaborate.

On the other hand, among flight test results from Gemini X during retro-fire in Ref. 15, the pilot is controlling the attitude of the vehicle about three axes; and the measured yaw axis describing function exhibits the rather large time delay predicted in Ref. 1 from an intersample "reconstruction-hold" model.

With the empirical facts as starting points, two likely mental processes have been proposed, called the "switched gain" model (Ref. 14) and the "reconstruction-hold" model (Ref. 1). For the switched gain process the quasi-linear describing functions in the several loops incur no time delay because of the scanning and sampling processes, although the gain switching (multiplexing) from loop to loop reduces the effective gain in each. In the reconstruction-hold model a sampling delay is incurred, but may be largely offset by lead equalization as part of the signal reconstruction process.

TABLE II-1. MULTIAxis SCANNING PHENOMENA FOR PILOTS' PERCEPTUAL MODALITIES

Modality/Channel	Qualitative Properties	Observable Measures	Symbol for Mean Value	$\sigma_{(s)}$ for Standard Deviation	Formulae	Alternative Nomenclature
Visual/Foveal Fixation	Primary channel under IFR; can be voluntarily switched, but sometimes serves as only a stabilizing fixation for parafoveal perception in "stare mode" High photopic acuity in form, displacement, rate and contrast perception No scotopic acuity	Number of fixations/unit time Scan interval (between fixations on the same point) Fixation dwell time Dwell fraction Look fraction (1 = number of different fixation points) Cumulative dwell fraction (1 = number of different fixation points) Scanning workload margin Link value	\bar{T}_f, Δ	--	$1/\bar{T}_f$	Fixation frequency, scan frequency, scanning rate
			σ_{T_f}, sec	σ_{T_f}, sec	$1/\bar{T}_f$	Fixation interval, look interval, sampling interval
Visual/Parafoveal	Secondary multiple parallel channels under IFR, but may have primary elements under VFR; can be involuntarily inhibited under stress by foveal "visual vision"; uniformly very low photopic acuity in form, displacement and contrast; progressively higher rate thresholds with increasing angle off visual axis; only source of scotopic acuity	Displacement Gains Rate-weighting coefficient Rate-to-displacement gain ratio Effective time delay Low frequency phase coefficient Power spectral density of residual remnant, θ_{mp} , scanning remnant, θ_{ms} , and processing remnant, θ_{mp}	\bar{T}_d, sec	σ_{T_d}, sec	$1/\bar{T}_d$	Dwell time, foveal dwell time
			η	--	\bar{T}_d/\bar{T}_f	Fractional scanning workload; probability of scanning
			ν	--	$\bar{T}_d/\sum \bar{T}_{d_i}$	Fixation fraction (upper bound is 0.5)
			$\sum \eta_i$	--	$\sum \eta_i$	Scanning workload (upper bound is 1.0)
			η_k	--	$1 - \sum \eta_i$	
			η_{ij}, η_{ji}	--	$\eta_{ij} + \eta_{ji} = 2\eta_{ij}/(1 - \sum \eta_k^2)$; $i \neq j$; $k = \text{intermediate index}$	
			K_T	--	$K_T = \begin{cases} \eta, & \text{if parafoveal perception is inhibited} \\ \eta_k, & \text{if parafoveal gain is significant} \end{cases}$	
			R	--	$R = \eta_k$; R is a theoretical construct proportional to η_k	
			η_c, sec	--	η_c is observable as the pilot's lead equalization time constant	
			τ_c, sec	--	$\tau_c (Y_c, \eta_c, R, \bar{T}_f, \eta) = \tau_c(Y_c) - \Delta t(\eta_c) + \Delta t(R, \bar{T}_f, \eta)$	
			$\alpha, \text{rad/sec}$	--	$\tau_c = \text{controlled element transfer function}$	
			$\theta_{mp}, \theta_{ms}, \theta_{mp}$	--	$\alpha = \text{forcing function bandwidth}$	
			$\theta_{mp}, \theta_{ms}, \theta_{mp}$	--	Formula not yet identified for θ_{ms} . See below for θ_{mp}, θ_{mp}	
Visual/Parafoveal	Effective Dwell Fraction Parafoveal-to-Foveal Gain Ratio Low frequency phase coefficient Effective Gain Effective Fix Delay Power spectral density of residual remnant, θ_{mp} , scanning remnant, θ_{ms} , and processing remnant, θ_{mp}	Describing Function Observation, Scanning, Equalization Remnant	η_c	--	$\eta_c = \eta + \alpha(1-\eta)$; $(1-\eta)$ is the foveal interrupt fraction	
			α	--	$\alpha = \frac{\eta_c \eta}{1-\eta}$	η_c is a theoretical constant η_c and η are observable separately, but not simultaneously.
			α	--	$\alpha = \frac{\eta_c \eta}{1-\eta}$	
			K_T	--	See foveal effective time delay	
			$\Delta t(R, \bar{T}_f, \eta), \text{sec}$	--	$\theta_{mp} = \frac{\sigma_{T_d}^2(1-\eta_c)\eta_c^2}{\pi \left[1 + \left(\frac{\alpha}{\eta_c} \right)^2 \right]} \left(\frac{\text{units}^2}{\text{rad/sec}} \right)$	θ_{mp}, θ_{ms} are displayed error, error rate
			$\theta_{mp}, \theta_{ms}, \theta_{mp}$	--	$\theta_{mp} = \frac{\sigma_{T_d}^2(1-\eta_c) \left(\sigma_{T_d}^2 + \eta_c^2 \right)}{\pi \left(1 + \frac{\alpha^2}{\eta_c^2} \right)} \left(\frac{\text{units}^2}{\text{rad/sec}} \right)$	variance; $\sigma^2 = \int_{-\infty}^{\infty} f(\omega) d\omega$ η_c is lead equalization time constant in sec.

Reproduced from best available copy.

TABLE II-1 CONCLUDED

Modality Channel	Qualitative Properties	Observable Measures	Symbol for Meas Value	Symbol for Standard Deviation	Formulas	Alternative Nomenclature
Vestibular Aural	Can be used effectively if cues in either visual case; can be voluntarily inhibited	Gain	K_g		K_g used for lead equalization ~ $\frac{1}{s}$ 0.2 sec (semicircular canals); 0.5 sec (utricle)	Formulas have not been identified; however, they probably contain residual and processing elements.
		Effective Time Delay	T_d			
Tactile	Multiple parallel channels with force, form and displacement acuity; can be voluntarily switched by touch	Power spectral densities	$\phi_{v_{1n}}$ $\phi_{v_{2n}}$			
		Discrete events				
		Continuous element				

The principal performance penalty caused by the scanning, sampling, and reconstruction (or switching) behavior is an increased "remnant." This remnant depends on the sampling frequency, fixation dwell time, and sampling frequency variations, as well as the signal variance. The remnant acts like an injected noise, and is the real cause of saturation in multi-instrument displays. So, as we said at the outset, measurement of eye fixation is certainly connected with pilot inputs and workload but the connection is by no means simple.

Remnant is so important in both scanning and workload considerations and has so many different sources that, before presenting analytical models of data for simplified situations, we shall summarize below the diverse physical sources of remnant. First off, remnant sources in general are those items which contribute, under varying circumstances, to pilot control movements which are not linearly correlated (via the describing function) with the externally imposed forcing functions. The remnant sources are:

Observation Remnant due to poor coupling between the displayed signal and the eye. Resolution, retinal rate thresholds, saturation levels, and refractory delay are of key relevance to instrument design.

Scanning Remnant due to scanning and sampling of multiple instrument displays or symbols. To the extent that parafoveal information can be used for nonfixated instruments in an array or for symbols within a display, the parafoveal display perception is of interest because it can reduce scanning remnant.

Equalization Remnant due to asynchronous, discrete mental data processing to derive rate (lead equalization), time and amplitude variations in gain, and intentional dither. Except in properly designed flight directors, these are dominant remnant sources, and can affect the remnant resulting from use of a given instrument design (e.g., if low frequency lead generation is required, the instrument must provide smooth data in the low frequency range).

Motion-Cue Remnant due to vestibular feedback noise.

Crosstalk Remnant due to neuromuscular commands for other axes in a given control action (e.g., some aileron control showing up in elevator control inputs).

Neuromuscular Remnant due to neural and muscular nonlinearities and tension (gain) variations. An important remnant source is residual neural noise and tremor which remain even when no command is being followed.

In a particular two-terminal man-machine measurement it is impossible to separate out most of these sources of remnant because they do not have narrowband spectral "signatures," and any distinct waveform effects are blurred by the limited neuromuscular response. Furthermore, the central-limit-theorem principle, coupled with the feedback around the loop, acts to blend the diverse remnant contributions into a fairly wideband stationary random process. This has the important implication that a simple power spectral representation is well suited to represent most remnant (dither excepted), while attempts to model it with an ensemble of nonlinear, time-varying deterministic elements will never be efficient; however, "analog" models may be useful to check out complex aspects of power spectral models.

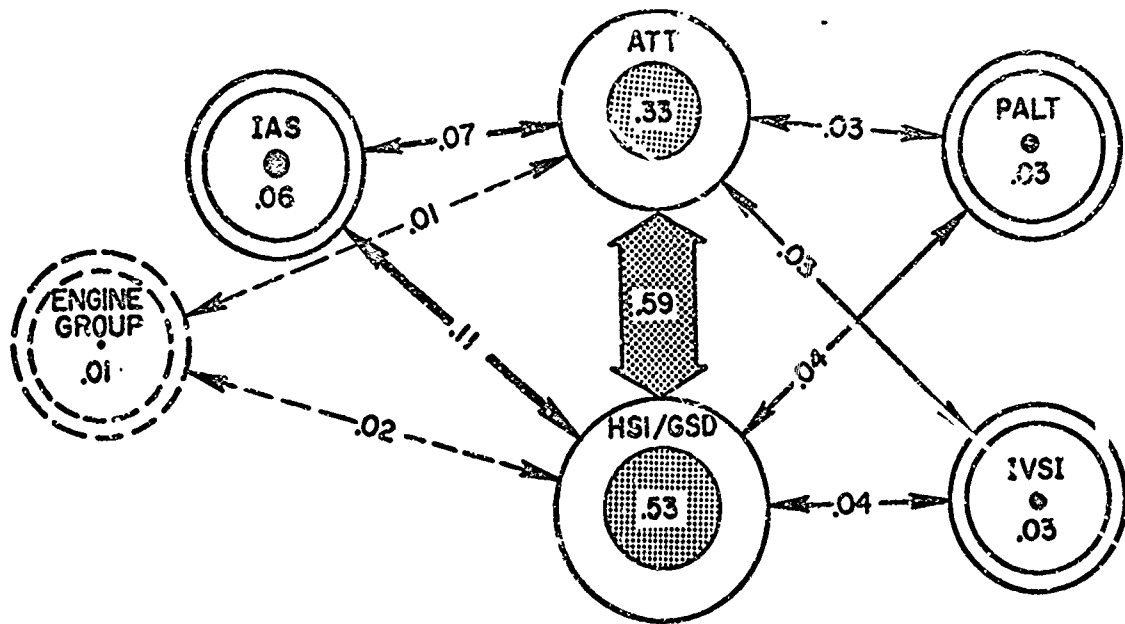
Rather than attempt a detailed buildup of remnant contributions from each of the sources listed above, we will take a more practical approach. Recent analyses have suggested that the observed remnant in the error signal is fairly smooth, broadband, and can be considered as resulting from an injected error-remnant source (Φ_{nn_e}). In turn, the measured injected error spectra are remarkably similar for a given-order controlled element. Φ_{nn_e} seems to consist of two basic components: a "residual remnant," Φ_{nn_0} , which exists and forces the system even without external forcing functions, and a "processing remnant," $\Phi_{nn_p} = \sigma_e^2 \Phi_{nn'_e}$, which scales with the displayed error variance. Thus:

$$\Phi_{nn_e} = \Phi_{nn_0} + \Phi_{nn_p} = \Phi_{nn_0} + \sigma_e^2 \Phi_{nn'_e}$$

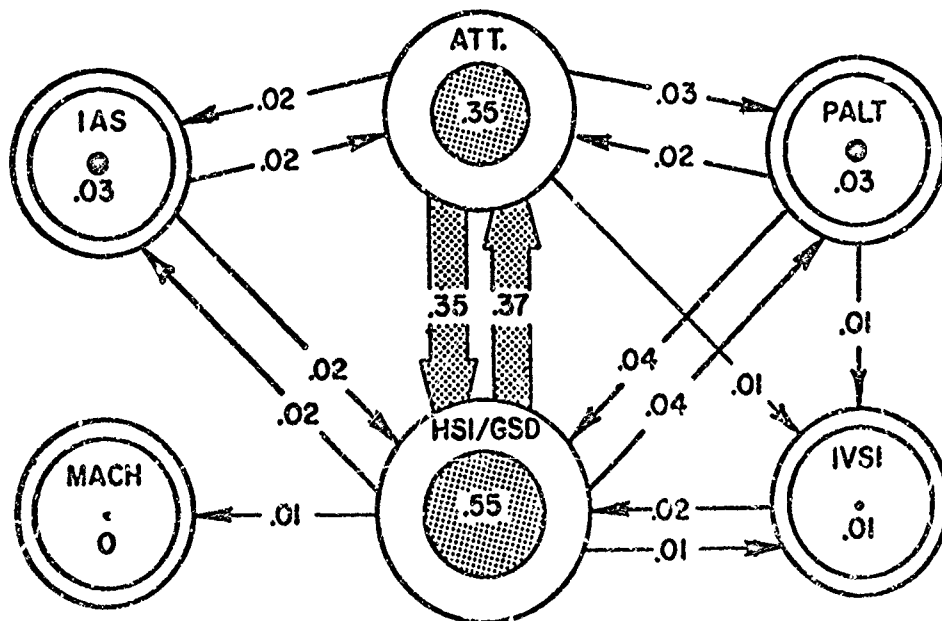
where $\Phi_{nn'_e}$ is defined as that part of Φ_{nn_e} which can be normalized by the displayed error variance. (See Fig. II-1.)

Scanning remnant is a particular form of processing remnant. It is given the symbol Φ_{nn_s} to distinguish its unique spectral bandwidth, which depends on the effective fixation dwell interval rather than the lead equalization time constant (See Table II-1.)

As it now stands, the theory of multiaxis scanning can be used to estimate fixation probabilities and instrument-to-instrument link probabilities fairly accurately. As an example, Fig. II-3 shows some predictions made with the reconstruction-held version of the theory (Ref. 1)



a) Predicted



b) Measured

Figure II-3. Predicted and Measured Dwell Fractions and Transition Link Probabilities for Manual ILS Approach

for a landing approach using Boeing 707 aircraft dynamics, as compared with measurements (Ref. 6) made using the DC-8 landing approach simulator at the Ames Research Center. The resemblance is quite good, especially considering the infant state of the theory at the time.

This concludes a review of the inspirations for eye movement studies in flight control and monitoring tasks, a description of scanning phenomena, and a summary of the relationship to pilot describing functions and remnant. In the next topic we shall discuss two limiting forms of multi-axis scanning models.

3. Multi-axis Scanning Models for Control Tasks

In this subarticle we first review the basic concepts of scanning during multiloop control tasks and then give an overview of two limiting forms of our model for the scanning, sampling, and perceptual reconstruction process.

a. Review

- 1) Scanning During Multiloop Control Tasks. We are concerned with the class of pilot/vehicle situations characterized by a closed-loop piloted multiloop regulation or tracking task, having more than one display, and requiring manipulation of one or more controls. The pilot's selection of preferred display feedbacks from the presented array has been found to be governed by a set of "Multiloop Feedback Selection Rules" which have been evolved previously and verified experimentally for integrated displays (Vide Refs. 1, 11, among others).

Past work shows that in the process of extracting the feedback information from the displays: 1) a fairly stationary scanning and sampling strategy evolves for a given task and instrument array, and 2) the control motions are much more continuous than the discrete sampling would seem to imply from a pure stimulus-response sequence. Furthermore, most of the information used in aircraft maneuvering is of an analog nature, displayed as the motion of a moving pointer or scale. These facts indicate that a form of sampled data feedback theory is appropriate to model this process. The facts further imply that the

display feedbacks ultimately selected would be affected not only by vehicle and task criteria (as with the integrated display case), but also by penalties from the required scanning and sampling operations.

Before proceeding let us clarify some terms that are used frequently below:

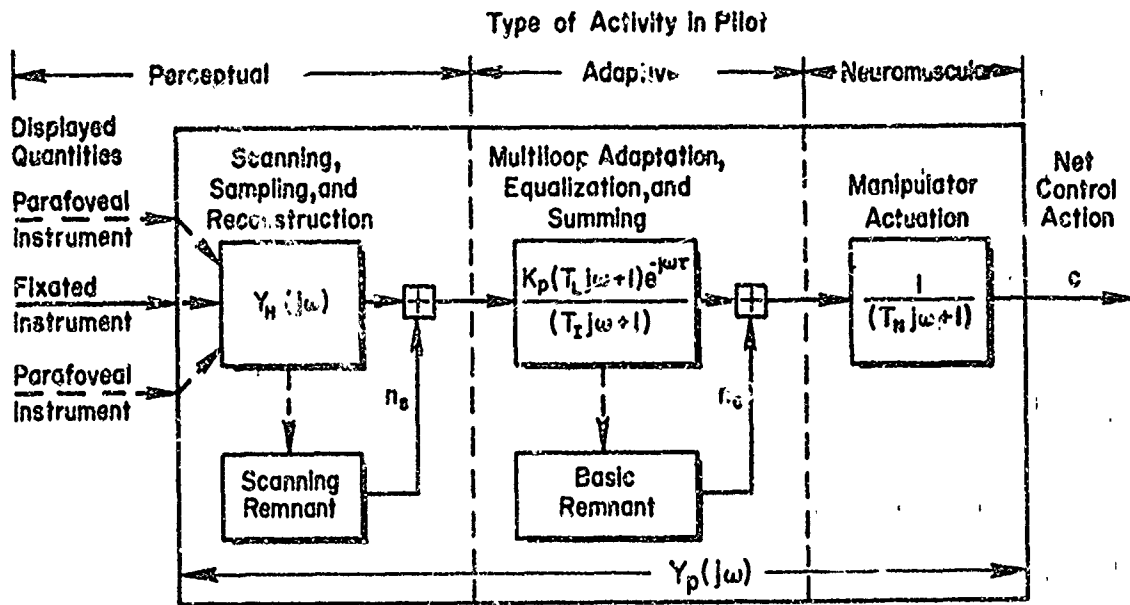
Scanning is defined here as the process of selecting and fixating each instrument in an array of, or specific portions of, a complex display field. For the manual control tasks a "scanning traffic pattern" is evolved, causing a given instrument to be examined from time to time.

Sampling covers the perceptual acts of: focusing on a display; interpreting this as an appropriate command or error signal; and perceiving its displacement, rate (or direction), and, possibly, acceleration during a sequence of fixations. In the present context, the sampling does not have to be impulsive or periodic.

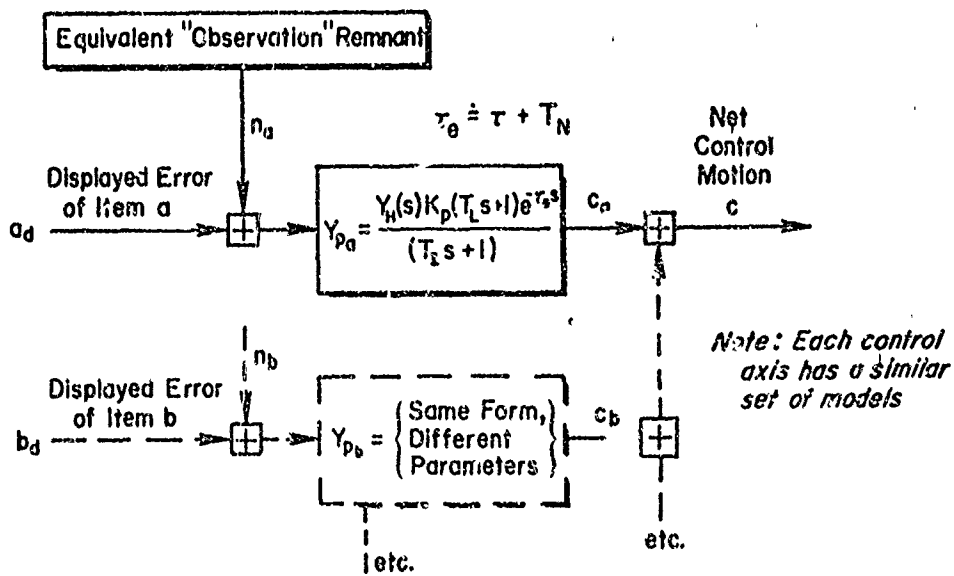
Reconstruction covers the process of extrapolating a hypothetical continuous signal using the series of samples available from each display, plus parafoveal (nonfixated) information which may be perceived between samples. Reconstruction provides the mental signal upon which the subsequent pilot equalization operations are assumed to operate.

- 2) Description of the Model. The development of a display scanning and sampling model for multiloop manual control tasks is reported in Ref. 1. Basically, it treats the complex processes involved in scanning, selecting, sampling, and reconstructing internal signals from an array of dials as an added "perceptual" functional block in a quasi-linear description of the pilot. Figure II-4a shows the assumed basic model and Fig. II-4b its simplified equivalent. The latter represents the simplest form that can be measured from inputs and outputs external to the human operator.

Let us review the key elements in the basic model before presenting its two limiting forms. The human display control behavior is represented by a series of functional blocks, loosely labeled "Perceptual," "Adaptive," and "Neuromuscular" in Fig. II-4a.



a) Assumed Basic Model (Sequential Scanning)



b) Equivalent Simplified Model (Parallel, continuous)

Figure II-4. Assumed Form of Pilot Models

The signals shown connecting the blocks are unmeasurable practically (being located in the central nervous system), and, in fact, the functions may overlap. It is useful to consider the perceptual block as an additional serial element, and to define the scanning and sampling effects as the ratio between behavior under continuous, full-foveal tracking and the actual sampled tracking, in each of the multiple loops. We will not dwell further on the adaptive block (feedback selection, equalization, summing, etc.) or neuromuscular block (manipulator interfacing and actuation). These have been well documented in recent years (e.g., Refs. 1, and 10 through 13).

At this time the conceptual model is still quite general, and any of several mathematical or physical models could be used to describe the above processes. Because of our interest in the overall closed-loop performance of display-pilot-vehicle systems, we need a form of analytical model compatible with feedback analysis. After much investigation (much of it based on the background information reviewed previously), we have made the following assumptions and choices of model form, and have accepted certain limitations in consequence:

- The basic analytical models are extensions of the quasi-linear descriptions presently used for non-scanned multi-loop cases (i.e., adjustable, random-input describing functions, plus a remnant for the incoherent effects). Although the fine-grain scanning and sampling processes are difficult to model this way, the resulting pilot output is sufficiently continuous so that describing functions can still account for the major closed-loop effects.
- It is assumed that the pilot's learning process has stabilized so that scanning behavior is stationary (in the statistical sense). Sampling of a given display is assumed to be "almost periodic," with appreciable statistical fluctuations which randomize the data. The model then treats the average properties of this scanning during typical task intervals. Although sampling effects on loop closures and scanning statistics are well represented this way, it is not possible to account for the particular order in which the displays are scanned.

- The detailed high frequency effects of the scanning, sampling, and reconstruction are circulated around the closed-loop system, giving rise to a broadband "sampling" remnant. This is modeled as an injected noise at the pilot's input (i.e., "observation noise"). The sampling remnant is a function of the scanning, sampling, and reconstruction processes, and may strongly affect which physical loops are closed, the choice of equalization, and closed-loop performance.
- The resulting model for scanning, sampling, and reconstruction comprises:
 - a) A quasi-linear, random-input "perceptual describing function," denoted as $Y_h(j\omega)$ which multiplies the human operator's continuous describing function, and
 - b) A broadband sampling remnant, n_s , which adds to the basic remnant, and is described as a spectrum Φ_{nn_s} of wideband observation noise injected at the pilot's perceptual input.

Examples of two limiting forms of these sampling and reconstruction models will be introduced for compensatory tracking loops. Either limiting form of the multi-axis scanning model is compatible with the existing multiloop pilot model for integrated displays. For clarity in presentation we shall use the modified crossover model ($Y_d Y_h Y_p Y_c$), to represent the display describing function (Y_d), the perceptual describing function (Y_h), the pilot's describing function (Y_{p_a}, Y_{p_b}, \dots) from Fig. II-4b, and the controlled element describing function (Y_c). We shall ask the reader to visualize without benefit of repetitious illustration the several additional (sometimes coupled) loops among which the pilot must scan his attention in the relevant modalities.

We shall now illustrate one of the limiting forms of the multi-axis scanning model by incorporating a single-axis model in each of two (among several) sensory channels: a foveal channel and a parafoveal channel.

b. A "Switched-Gain" Model for Multiaxis Scanning. This form of the model is termed "switched-gain" because it incorporates a quasi-random finite dwell sampling or switching process between the pilot's foveal gain and his effective parafoveal gain on each of the several displays involved. Figure II-5 illustrates the model with a block diagram. The foveal path is closed during the foveal dwell interval, and the parafoveal path is closed during the foveal interrupt interval. Each of these paths will, in general, exhibit different gains, equalization and effective time delays before the paths are combined in the higher neural centers to send a signal to the actuation describing function.

The conceptual block diagram in Fig. II-5 can be remarkably simplified by recalling (Ref. 16) that any quasi-randomly sampled and processed signal can be modelled by 1) replacing the sampling or switching process by a continuous transmission path and 2) adding an uncorrelated wide band noise process whose power spectral density is proportional to the variance of the (displayed) signal before sampling. Since the quasi-random sampling process has a finite foveal dwell interval, the wide band noise process will exhibit a low-pass power spectrum with a first-order break frequency which is inversely proportional to the average foveal dwell interval (Ref. 9). The power spectral density of this foveal-parafoveal switched-gain sampling remnant is described in Table II-2. Measurements of this switched-gain remnant in Ref. 9 have shown that it so predominates over the other sources of remnant that the other sources cannot even be identified. This makes for great simplification of the remnant in the equivalent switched-gain model shown in Fig. II-6.

Representation of the pilot's describing function in the switched-gain model can also be greatly simplified. The foveal gain exceeds the parafoveal gain in all measurements which have been made (Refs. 9, 14 and 17). This is probably because of the large displacement and increased rate thresholds in parafoveal perception by comparison with foveal perception. The switched-gain model is represented simply by multiplying the ratio (α) of parafoveal gain to foveal gain by the interrupt fraction ($1 - \eta$) and adding the product to the dwell fraction (η) to obtain the effective dwell fraction, viz.,

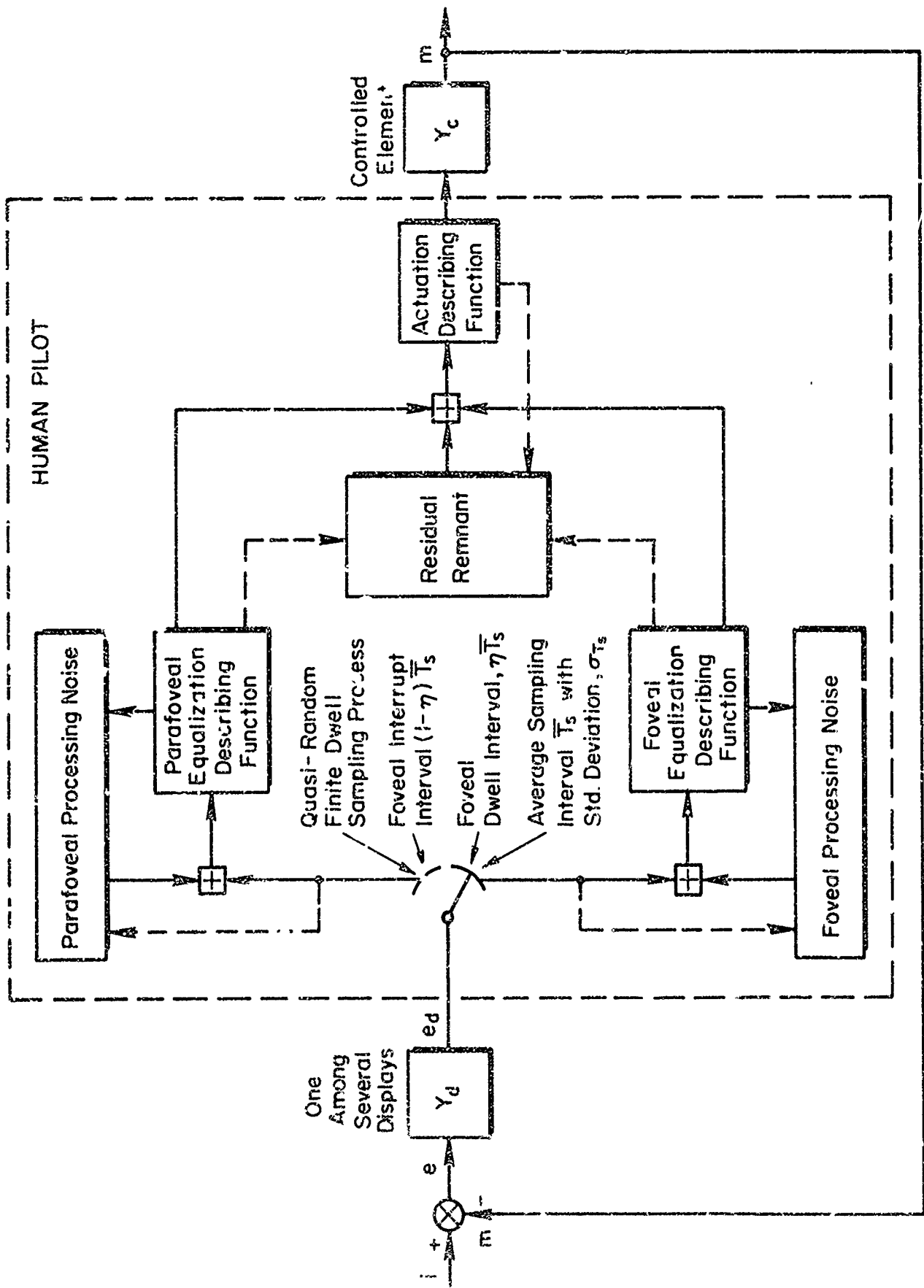
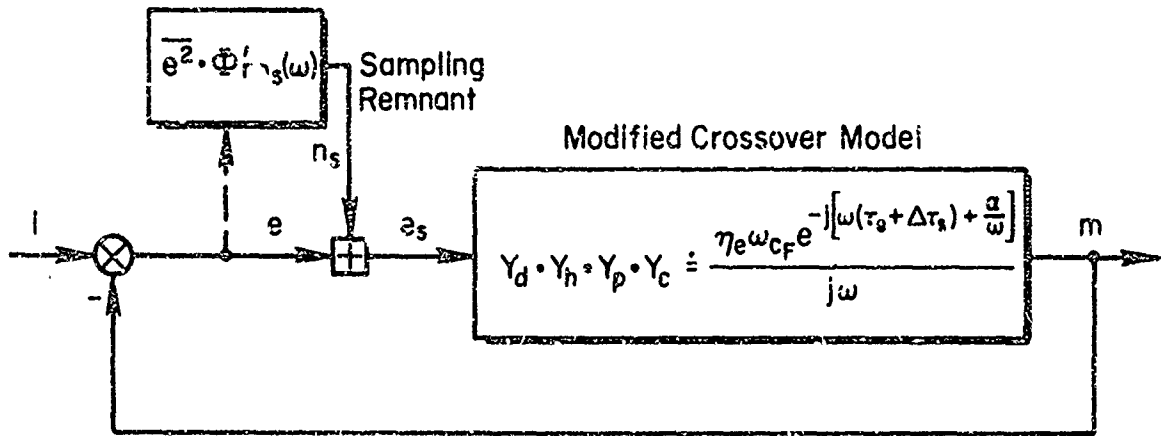


Figure II-5. "Switched Gain" Multiaxis Scanning Model for Compensatory Multiaxis Tracking with One Among Several Displays



Normalized Power Spectral Density of Sampling Remnant,

$$\Phi_{nn_s}(\omega) = \frac{\sigma_{T_s}(1 - \eta_e)}{\pi[1 + (\omega T_{de}/2)^2]} \frac{\text{units}^2}{\text{rad/sec}}$$

Standard Deviation of Scanning Interval $\sigma_{T_s} \doteq 0.5 \bar{T}_s$

Mean Scanning Interval \bar{T}_s , sec

Effective Dwell Interval $\bar{T}_{de} = \eta_e \bar{T}_s$, sec

Effective Dwell Fraction $\eta_e = \eta + \Omega(1 - \eta)$

where $\Omega = \omega_{c_f}/\omega_{c_p}$ = ratio of crossover gains for continuous parafoveal relative to continuous foveal tracking ($0 \leq \Omega < 1$)

η = foveal dwell fraction

$\Delta\tau_s$ = incremental effective scanning time delay, normally negligible, except if $\Omega \rightarrow 0$, $0.05 \leq \Delta\tau < 0.15$ sec

Y_d = display describing function

Y_h = perceptual describing function ($Y_h = \eta_e e^{-j\omega\Delta\tau_s}$)

Y_p = pilot's describing function

Y_c = controlled element describing function

ω_c = crossover gain

τ_e = effective time delay

α = low frequency phase approximation parameter

Figure II-6. Simplified Equivalent "Switched-Gain" Multi-axis Scanning and Tracking Model for Compensatory Tasks

TABLE II-2
 SAMPLING REMNANT POWER SPECTRAL DENSITY

$$\sigma^2 = \int_0^{\infty} \phi(\omega) d\omega$$

Definition of sampling remnant power spectral density:

$$\phi_{nn_s}(\omega) = \frac{\bar{T}_s(1-\bar{\eta}_e)(1-\delta)\sigma^2}{\pi \left[1 + \left(\frac{\omega\bar{T}_{de}}{2} \right)^2 \right]} \left(\frac{\text{units}^2}{\text{rad/sec}} \right)$$

where σ^2 is mean-squared signal to be sampled

\bar{T}_s is mean sampling interval

$\bar{\eta}_e$ is effective dwell fraction = \bar{T}_{de}/\bar{T}_s

\bar{T}_{de} is effective dwell interval

δ is normalized lower bound on the domain of T_s : T_0/\bar{T}_s

$(1-\delta)$ is approximately σ_{T_s}/\bar{T}_s , the sampling variability ratio

σ_{T_s} is standard deviation in T_s

Assume sampling variability ratio $(\sigma_{T_s}/\bar{T}_s) \leq 0.5$ for skilled pilots.

Effective dwell fraction is related to foveal dwell fraction, η_f , if parafoveal perception is possible during interrupt fraction, $1-\bar{\eta}_f$, by the expression

$$\bar{\eta}_e = \bar{\eta}_f + (1-\bar{\eta}_f) \frac{\omega_{cp}}{\omega_{cf}} = \eta_f + (1-\eta_f)\Omega$$

where ω_{cp} is crossover frequency with continuous parafoveal attention and

ω_{cf} is crossover frequency with continuous foveal attention

$$\Omega = \omega_{cp}/\omega_{cf}$$

Typically, $\frac{\omega_{cp}}{\omega_{cf}} \leq \frac{1}{2}$ for K/s controlled element with separated displays

(Refer to Ref. 18 for complete theory of sampling remnant applied to crossover model of human operator tracking.)

$$\eta_e = \eta + \Omega(1 - \eta)$$

where $\Omega = \omega_{c_p}/\omega_{c_f}$ = ratio of crossover gains for continuous parafoveal tracking relative to continuous foveal tracking. ($0 \leq \Omega < 1$)

The effective crossover gain for the equivalent switched-gain model in Fig. II-6 is $\eta_e \omega_{c_f}$, where ω_{c_f} is the foveal crossover gain in continuous single-axis tracking of the same display and controlled element constrained by the same task variables. The low frequency phase approximation parameter, α , will, in general, account for differences between foveal and parafoveal equalization. There are no apparent phase penalties associated with switched-gain scanning as long as parafoveal perception is not completely inhibited. Inhibition can occur either by requiring a multitude of different widely separated fixations with a time constraint or by inducing "tunnel vision" on one or two displays. Even so, measurements reported in Ref. 9, where parafoveal perception was inhibited by blanking the parafoveally viewed display, show only small effective time delay increments ($\Delta\tau_g$) on the order of 0.05 to 0.15 sec attributable to scanning as the parafoveal-to-foveal gain ratio (Ω) approached zero.

The switched-gain model has been quite successful in modeling behavior on a main task in laboratory experiments with induced natural scanning between a primary tracking task and a secondary subcritical tracking task (Ref. 9), and on foveal and parafoveally viewed displays (Refs. 14 and 17).

c. A "Reconstruction-Hold" Model for Multiaxis Scanning. Consider next an alternate form of the model for the effects of perception in scanning and sampling. The notion of intersample extrapolation or reconstruction of the displayed signals and their rates of change from primarily foveally-derived samples (still with possible help from parafoveal vision) is emphasized in this model. Scanning and sampling remains a quasi-random finite-dwell process with the additional hypothesis that somewhere in the mental processing of perceived signals during the foveal interrupt fraction there is an intersample extrapolation process acting on retained foveal samples. The extrapolation process serves to attenuate the scanning remnant at the expense of a small incremental time delay.

One unique feature of the "reconstruction-hold" model is that it can account for much larger effective time delays than can the "switched-gain" model. These delays, still compatible with scanning behavior, arise in connection with extrapolation of samples of displayed error. The "reconstruction-hold" model incorporates first-order extrapolation based on weighted displayed error rate which may largely offset the effective incremental time delay accompanying a zero-order-hold. The effective incremental scanning time delay for the zero-order-hold is equal to $(\bar{T}_S - \bar{T}_D)/2$, or one-half the average foveal interrupt interval on the particular display of concern. In contrast, the effective incremental scanning time delay for the first-order extrapolation process with a partial rate-weighting coefficient, R , ($0 < R < 1$) is equal to $(1 - R)(\bar{T}_S - \bar{T}_D)/2$, which can be made very small as $R \rightarrow 1$. Since R cannot be measured directly, there is only inferential evidence that the pilot may increase his foveal dwell interval above 0.4 sec in some direct proportion to the desired partial rate-weighting coefficient for reconstruction between foveal fixations (Refs. 1 and 9).

Another unique feature of the "reconstruction-hold" model for multiloop scanning is that it can explain a greatly reduced sampling remnant level below the one appropriate for the "switched-gain" model. This fact is portrayed graphically for a single sinusoidal component in Fig. II-7 (from Ref. 9). This shows the relative remnant contributions by the shaded differences between the original and reconstructed sinusoids. In the case of purely finite dwell sampling shown in part c of Fig. II-7, there is no intersample reconstruction, no incremental scanning time delay, and the remnant is the largest as we would expect. The gain is low as is evidenced by the small amplitude of the describing function approximation sinusoid. With the zero-order-hold (part d), remnant is reduced, an incremental time delay, $\Delta\tau_S$, is incurred, and gain is increased. Remnant is further reduced and gain is further increased by a first-order-hold, and the incremental time delay is reduced (part e). The remnant here is called processing noise. The observed half-power frequency of the normalized processing noise referred to the operator's input will be inversely proportional to the ratio of rate-to-displacement gain in the first-order

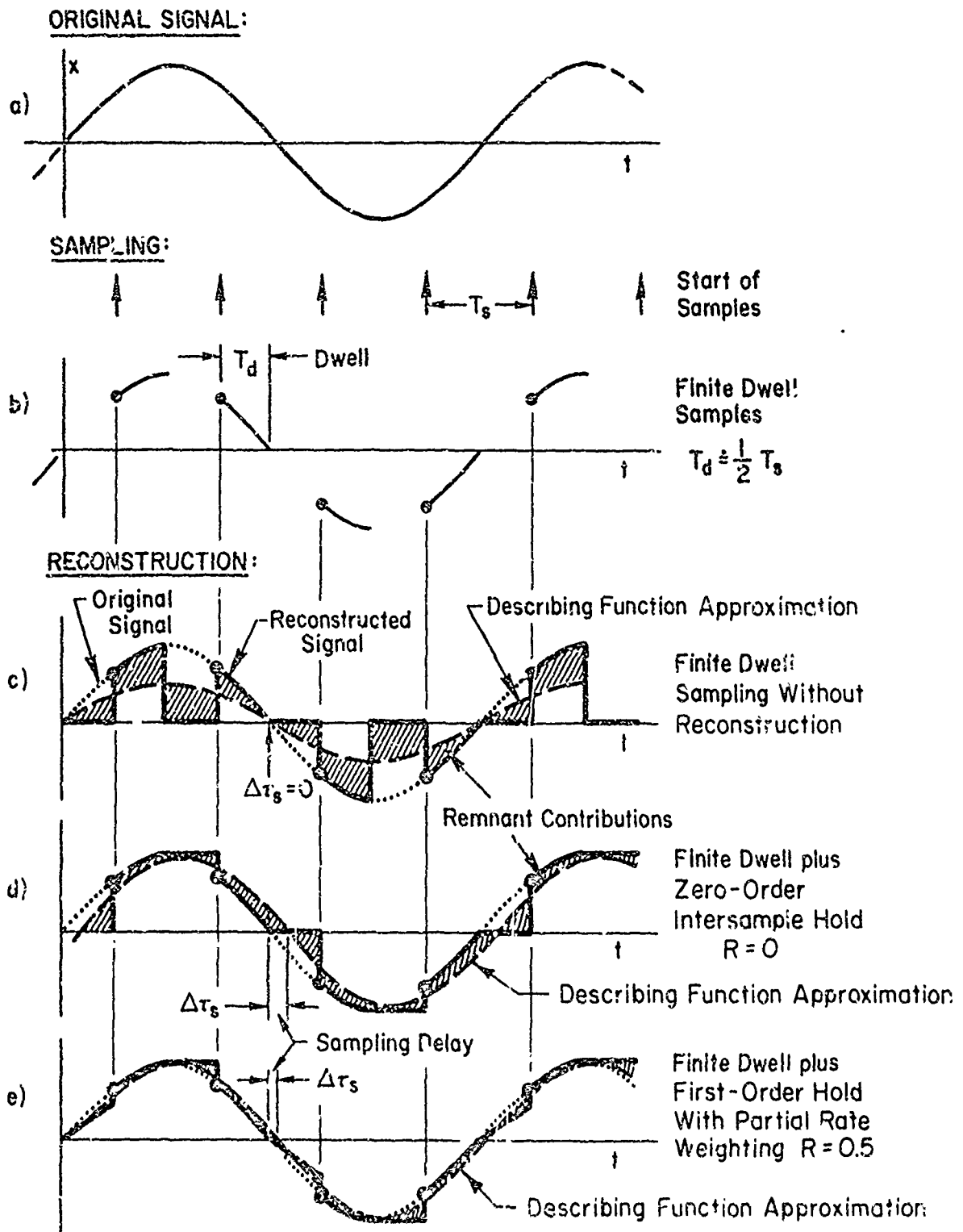


Figure II-7. Basic Features of Finite Dwell Sampling and Reconstruction

extrapolator. The rate-to-displacement gain ratio is the human operator's lead equalization time constant, T_L . The power spectral density of processing noise can be represented as shown in Table II-3.

Table II-3

PROCESSING NOISE POWER SPECTRAL DENSITY

$$\sigma^2 = \int_0^{\infty} \Phi(\omega) d\omega$$

Definition of processing remnant power spectral density for single-axis compensatory tracking:

$$\Phi_{nne}(\omega) = \frac{\sigma_{T_s}(1-\eta_e) (\sigma_e^2 + T_L^2 \sigma_{\dot{e}}^2) (\text{units})^2}{\pi (1 + T_L^2 \omega^2) \text{ rad/sec}^2}$$

where

σ_{T_s} is the square root of the operator's sampling interval variance. It is about 0.1 sec

η_e is the human operator's effective dwell fraction on the order of 0.1 or 0.2 in single-loop tracking tasks

σ_e^2 and $\sigma_{\dot{e}}^2$ are the variances of the (displayed error) displacement and its first derivative to which the human operator is responding

T_L is the lead equalization time constant in sec

A limiting form of the "reconstruction-hold" model for multiloop scanning is shown in Fig. II-8 for the case without a parafoveal input. In Fig. II-8, the quasi-random finite-dwell foveal sampling process is replaced by its continuous equivalent plus additive sampling and/or processing noise whose power spectral density scales with displayed error variance. A simplified equivalent modified crossover model is shown in the accompanying Fig. II-9. In both figures an additional "residual" remnant is also shown. The sampling-and-reconstruction describing function (Y_h) precedes the pilot's equalization-and-actuation describing function (Y_p) in Fig. II-9. Y_h consists merely of an attenuation factor, K_h and an effective incremental sampling-and-reconstruction time delay $\Delta\tau_s$:

$$Y_h(j\omega) \cong K_h e^{-j\omega \Delta\tau_s}$$

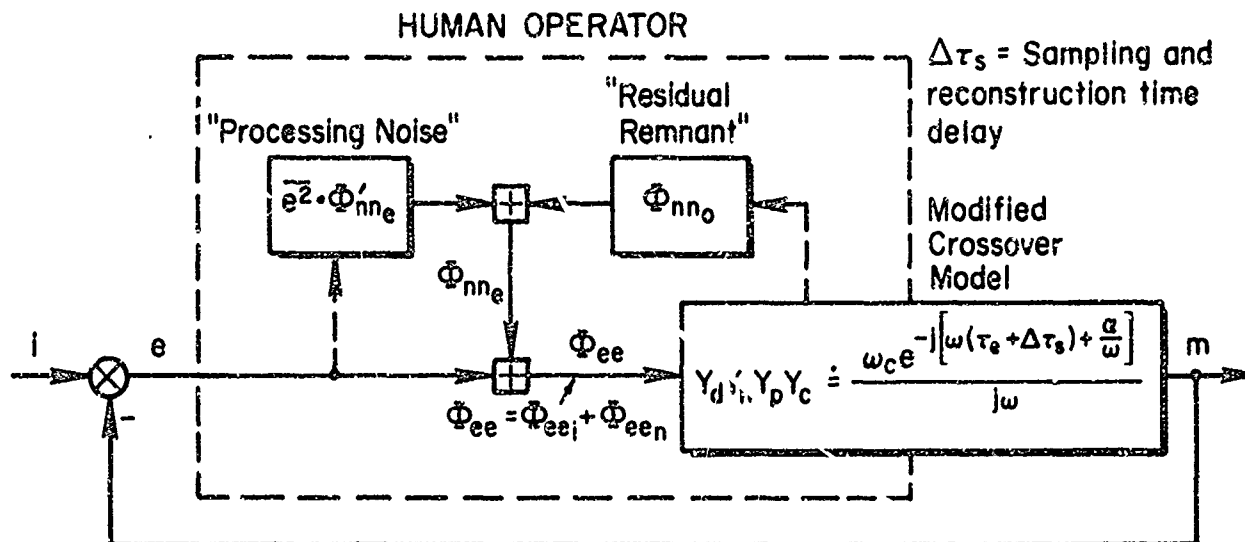
The values of K_h and $\Delta\tau_s$ depend on the average scanning interval, \bar{T}_s , the foveal dwell fraction, η , the rate-weighting coefficient, R , and the type of intersample reconstruction weighting function.

The "reconstruction-hold" model was used in early 1967 to make the predictions (shown in Fig. II-3) of scanning behavior for a precision instrument approach in a jet transport (Ref. 1). Although some evidence for this model is offered in Refs. 15 and 35, this model remains to be more fully validated.

This concludes the discussion of the two limiting forms of a multi-axis scanning model for the tracking control-display tasks.

C. DISPLAY DEFINITIONS

In addition to the background in the mathematical models which has been presented in the previous subsections, it is necessary for an understanding of the subsequent sections for us to offer some new definitions. Thus, we wish to define the elements of a display, the display content, and the display format.



Injected Remnant Φ_{nne} : Primarily residual and processing noise in Table II-3 by virtue of intersample reconstruction which suppresses sampling remnant.

Figure II-9. Simplified Equivalent "Reconstruction-Hold" Multi-axis Scanning and Tracking Model for Compensatory Tasks.

The elements of a display (not all of which are necessarily presented) comprise:

- forcing functions or command-input signals, i
- controlled element state variables or output motion signals, m
- error signals, $e = (i - m)$
- references or background

The display content represents the specific elements which are present and which are either required for guidance and control of a task or are required for monitoring task performance.

The display format is the symbolic code by which each member of the content can be identified. It can be characterized by describing the display in such terms as separate or integrated, symbolic or pictorial, quickened or "deadened", as a flight director and so forth. It can also be characterized by describing the number, size, type, color, contrast and separation of the symbols.

It was with the primary intent of investigating the most prominent effects of display format in integrated displays that the experiments described in the next two Sections were performed.

SECTION III

THE SINGLE-AXIS EXPERIMENT

A. PURPOSE OF THE SINGLE-AXIS EXPERIMENT

The purpose of this set of "pilot experiments" was to establish baseline describing functions and levels of remnant and intern attentional workload under foveal and parafoveal viewing conditions for each of four different practical tracking display formats appearing individually in a single-display single-axis cockpit scenario. A plan of the experimental design is presented in Table III-1.

Four display formats were used in the first set of vertical speed tracking experiments. The four formats were 1) a thin moving luminous line with a fixed scale on a cathode-ray tube (CRT), 2) continuous moving vertical bar with a fixed scale on the CRT, 3) quantized vertically moving bar with fixed scale on the CRT, 4) moving pointer, rotary dial flight instrument. In presenting results here, we shall abbreviate reference to each format as Line (L), Bar (B), Quantized (Q), and Dial (D), respectively. The four formats are illustrated in Fig. III-1. The display formats were selected from the survey in Ref. 4 to include stereotypes from past, present and proposed examples of instruments and integrated displays.

The influence of display quantization was investigated with the RMS error comparable to the displayed quantum. The influence of parafoveal viewing angle was investigated with all four formats. Two parafoveal viewing angles, 10 and 20 deg, were employed during the training sessions with the two pilot subjects. Eye-point-of-regard measurements were taken to insure that the subjects maintained parafoveal viewing angles of 10 deg and 20 deg. These two angles were representative of conditions under which a pilot might view an integrated display format.

The controlled element, $K/s(s+2)$ was selected for the extensive investigations of format because its baseline attentional workload is reasonably high; hence, either increases or decreases should be measurable without extreme overloading or underloading in the experiments, and

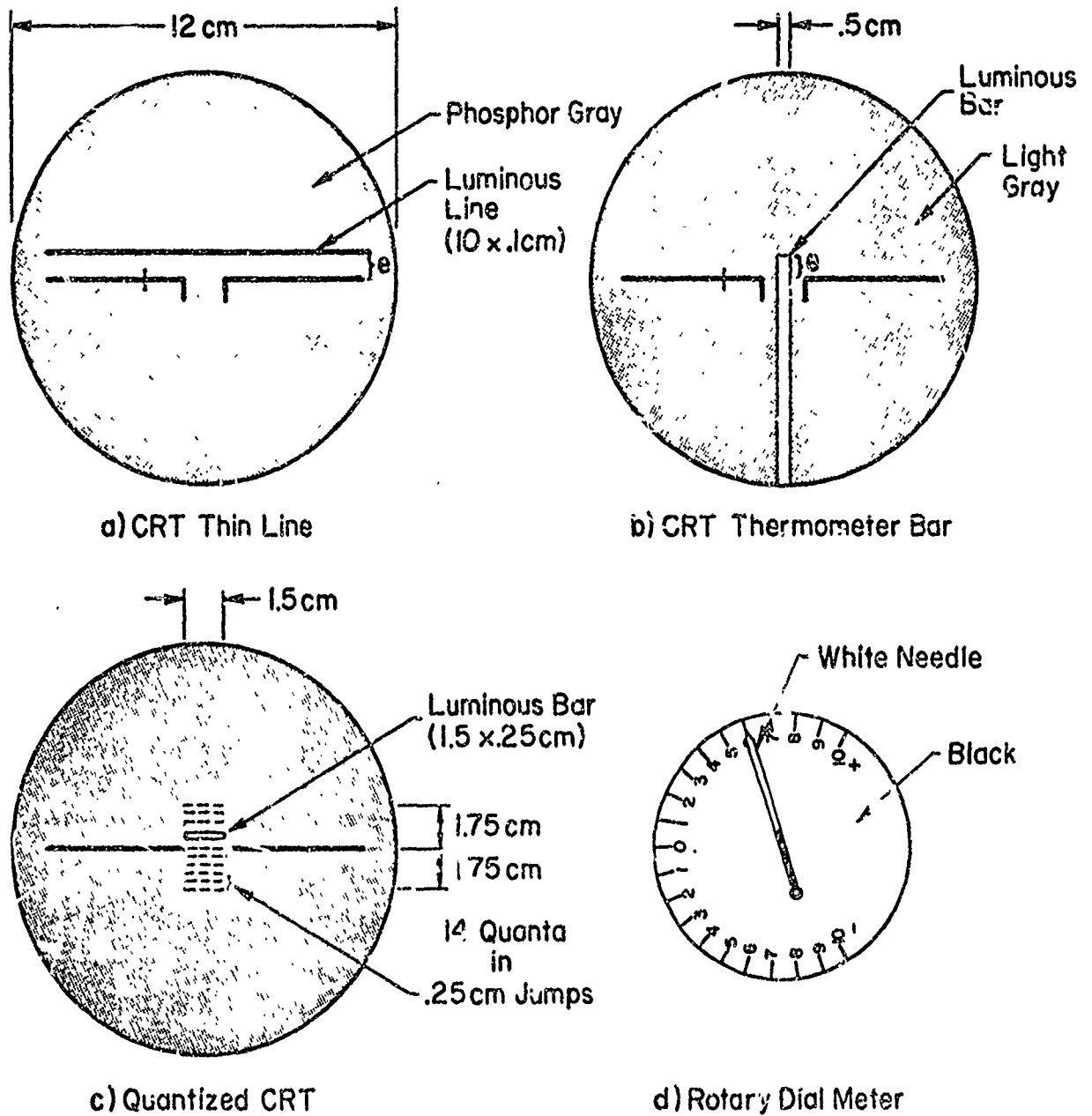


Figure III-1. The Formats for the Single-Axis Experiments

TABLE III-1

EXPERIMENTAL DESIGN FOR SINGLE-AXIS DISPLAY FORMAT EXPERIMENTS

Independent Variables	Viewing Angle		
	0° Foveal	Parafoveal	
		10°	20°
"LINE" CRT Line (Standard)	✓	✓	✓
"BAR" Vertical Bar	✓	✓	✓
"DIAL" Rotary Dial-Pointer	✓	✓	✓
"QUANT" Quantized (14-Bars) with displayed quantum on the order of RMS displayed error.	✓	✓	✓

In Each Tested Cell:

- 2 Replications
- 2 Pilot Subjects

TRACKING TASK SCENARIO - vide Fig. III-2 (p. 45)

MEASUREMENTS:

- Pilot Describing Functions (e.g., gain, effective time delay, equalization)
- Serial Segment Remnant Power Spectra
- Error Coherence and Signal/Noise Ratio in Error
- Error and Error Rate Variance
- Mean Error

SPECIAL MEASUREMENT APPARATUS:

- Describing Function Analyzer (STI/NASA Mark II)
- Eye-Point-of-Regard Instrumentation (STI/NASA Mark I)

because it induces pilot lead qualization at 2 rad/sec, which is well within the spectrum of remnant power measurement.

Since the first set of experiments was planned and executed jointly with an experimental investigation for the U. S. Air Force Aerospace Medical Research Laboratory (AMRL) of the effect of single display format on the character of single-axis tracking remnant, the reader interested in the full details of the experimental design may refer to Ref. 19. We shall summarize here only those results which have a bearing upon a theory for integrated display format.

B. SCENARIO

A single-axis tracking task was both necessary and desirable in order to keep the experiment simple and economical, but we wanted to create an aircraft piloting scenario having more face validity than the usual laboratory tracking task in an arm chair. To achieve some degree of validity, we employed actual experienced pilots as subjects in a fixed-base aircraft cockpit with a center stick for pitch-axis tracking.

C. SIMULATION

The apparatus included:

1. A modified fighter aircraft cockpit, with center stick and instrument panel.
2. An analog computer to provide the controlled element dynamics, display signal processing, and some performance measurement capability.
3. A Describing Function Analyzer that provided the input disturbance to the simulation while simultaneously processing data from which dynamic response and remnant measurements were obtained.
4. The Eye-Point-Of-Regard measurement apparatus.

These are described in more detail below.

1. Cockpit

The STI fixed-base fighter cockpit facility was used. It included the standard seat and center stick and a special-purpose instrument panel, described later. The stick had negligible friction and viscous damping, and a force gradient of approximately 15 Newtons/cm (8.6 lb/in.). The

instrument panel was approximately 57 cm (23 in.) from the pilot's eye, so that 1 cm of display travel on the panel equalled 1 deg of visual arc. The stick grip center position was 17 cm aft of the instrument panel plane and 25 cm below the pilot's horizontal line of sight.

2. Displays and Viewing Conditions

Two basic display devices were used: (a) a low persistence 5 in. CRT, and (b) a rotary dial meter. The CRT was used to present the three vertical movement display formats shown in Fig. III-1. These included:

- a. A thin horizontal LINE, 10 cm in length and 0.1 cm thick. There were no dynamic lags in this display.
- b. A VERTICAL BAR format 0.5 cm in width extending from the bottom edge of the CRT as shown in Fig. III-1b. The height of the bar relative to the CRT reference line represented the tracking error.
- c. A QUANTIZED format consisting of a luminous horizontal bar 1.5 cm long and 0.25 cm thick that moved in 0.25 cm vertical steps. Fourteen segments (seven above and below null) were available but were seldom used. The quantization logic for this display was mechanized using comparators with millisecond switching times.

To eliminate subjective brightness of the various formats as a confounding experimental variable, each pilot was asked to adjust the CRT brightness control such that a particular CRT format gave the same "apparent brightness" as the adjacent rotary dial's mechanical pointer.

The CRT display/stick relationship was such that moving the stick forward caused the CRT mark to move up. This relationship is consistent with aircraft gunnery tracking and with conventional artificial horizon instruments ("inside out" view).

The rotary DIAL meter shown in Fig. III-1d was an aircraft instrument quality voltmeter (galvanometric movement drive). The pointer was 3 cm in length and 0.25 cm thick. The basic response of the meter was second-order with a natural frequency of 1 Hz and a damping ratio of 0.35. This response was too sluggish for the purposes of this experiment, so the meter was compensated to provide a flat response over the input bandwidth. For small angles, the meter sensitivity was scaled to give arc length

deflections at the needle point equal to vertical deflections on the CRT for corresponding error signals.

3. Controlled Element Dynamics and Input

The controlled element dynamics, $K/s(\tau + 2)$ were selected as being intermediate in lead equalization required of the pilot ($T_L \dot{=} 0.5$ to 1.0 sec). The dynamics were mechanized on an EAI 231R computer.

The input was a sum of five randomly phased sine waves with amplitudes inversely proportional to frequency. To produce roughly equal RMS displayed signals, the input RMS amplitude was set at 0.75 cm. This resulted in RMS errors on the order of 0.3-0.5 cm. The input frequencies were approximately equally spaced logarithmically and span the frequency range important for human operator dynamic response measurements (i.e., 0.5-10 rad/sec). The sine waves were generated by the Describing Function Analyzer. The input spectral shaping and frequency spread was designed to give display motions subjectively equivalent to gust disturbances in an airplane, to allow accurate measurement of pilot dynamic response and remnant behavior, and to avoid excessively high displayed signal peaks during adverse display viewing conditions.

4. The Describing Function Analyzer

An electromechanical Fourier analyzer, STI/NASA Mk II Describing Function Analyzer (DFA), was used to obtain dynamic response measurements. A thorough description of the measurement technique and functional mechanization is given in Ref. 20. Basically, the analyzer generates a sum-of-sinusoids input which is provided to the tracking loop as shown in Fig. III-2, and computes the Fourier transform of the system error signal at each of the input sine wave frequencies, referred to each component sinusoid.

5. Eye-Point-of-Regard (EPR)

The EPR equipment consisted of three units: 1) spectacle frame-mounted transducers and associated electronics for measuring eye angle with respect to the head; 2) a goniometer gripped in the mouth for measuring head angles with respect to the display panel; 3) a special purpose analog computer for combining the head and eye angles to give voltage signals proportional to

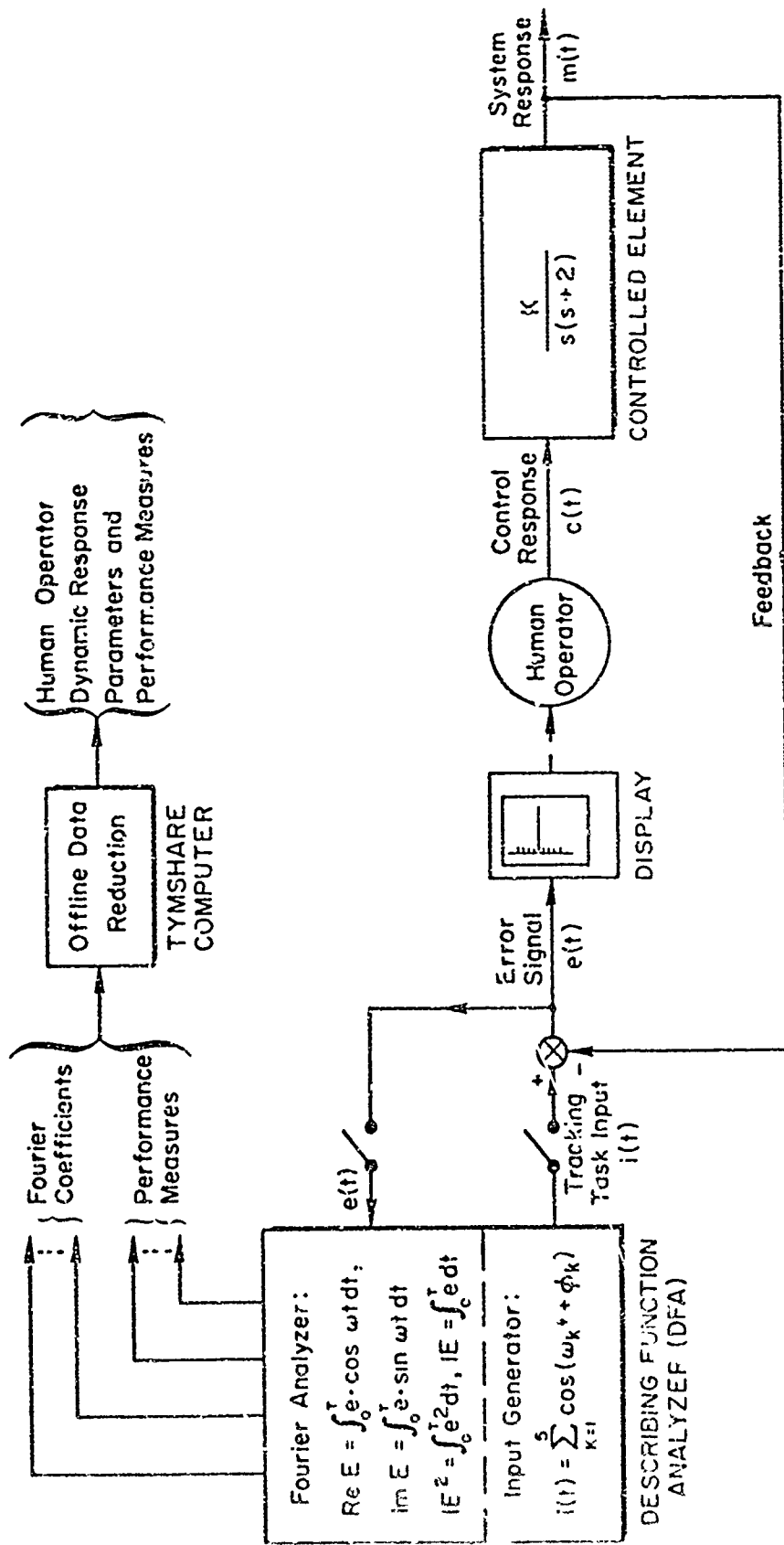


Figure III-2. Tracking Tasks, Data Measurements and Analysis

the eye-point-of-regard on the display panel. This system is more fully described in Ref. 21.

D. MEASUREMENTS

The fashion in which the performance measures and describing function parameters were obtained is illustrated in Fig. III-2. The describing function analyzer generates a sum of sine waves which is the input to the tracking loop. From the loop tracking error signal, it computes the Fourier coefficients at each frequency present in the input. The corresponding input-referenced Fourier transform of the input is known a priori, so that the error-to-input transform ratio or describing function, $E(j\omega)/I(j\omega)$, can be computed. Given this describing function, it is a simple matter to compute the open-loop and closed-loop describing functions using the vector relationships:

$$\frac{M(j\omega)}{E(j\omega)} = \left[\frac{E(j\omega)}{I(j\omega)} \right]^{-1} - 1 \quad (\text{open-loop DF})$$

$$\frac{M(j\omega)}{I(j\omega)} = 1 - \frac{E(j\omega)}{I(j\omega)} \quad (\text{closed-loop DF})$$

Since the controlled element, $Y_c(j\omega)$, is known (and calibrated), the pilot describing function can be computed as well:

$$Y_p(j\omega) = \frac{M(j\omega)}{E(j\omega)} \cdot Y_c^{-1}(j\omega)$$

A time shared computer system (Tymshare) was used to reduce the analyzer data. In addition to describing function and performance measure calculations, the program also included interpolation and curve fitting routines to interpolate (between adjacent frequency points) the extended crossover model properties such as open-loop gain and phase crossover frequencies (ω_{c_c} , ω_{u_c}), phase margin (ϕ_{m_c}), and equivalent operator time delay (τ_{e_c}). See Ref. 19, Appendix B, for the mathematical details. The other important parameter, the parafoveal to foveal gain ratio, Ω , was computed from the describing function parameters as described above in Section II.

In addition to $E(j\omega)$ the DFA computes the integral squared value of system error and the mean value of error. These data were used to calculate

the variance of error, $\sigma_e^2 = \overline{e^2} - (\bar{e})^2$. Most relevant to tracking tests is the normalized tracking error, σ_e^2/σ_i^2 . Error rate variance was also measured. The DFA further yielded data giving the input-coherent error variance, $\sigma_{e_i}^2$, and this permitted computation of the important remnant error power, $\sigma_{e_n}^2 = \sigma_e^2 - \sigma_{e_i}^2$. A final measure of overall error performance was the error coherence, ρ_E^2 , which is the ratio of input-coherent error variance to total error variance. The various relationships of interest here are:

$$\text{Error coherence: } \rho_E^2 = \sigma_{e_i}^2/\sigma_e^2$$

$$\text{Relative remnant power fraction in error: } \sigma_{e_n}^2/\sigma_e^2 = 1 - \rho_E^2$$

$$\text{Signal/noise ratio in error signal: } \left. \frac{S}{N} \right|_e = \frac{\sigma_{e_i}^2}{\sigma_{e_n}^2} = \frac{\rho_E^2}{1 - \rho_E^2}$$

E. SUBJECTS

Two pilots were selected to participate in this study. Both pilots had extensive flight experience. A resume of their experience is given in Table III-2.

TABLE III-2

PILOT BACKGROUND

	Pilot 1 (RH) ⊙	Pilot 2 (DH) □
Aeronautical Ratings	Airline transport pilot Flight instructor	Military transport pilot
Total Flight Hours	3150	2180
Hours By Duty	Student, 150 First Pilot, 1000 Instructor, 2000	Student, 260 Copilot, 570 First Pilot, 1260 Instructor, 90
Hours By Aircraft	2650 Single Engine; 500 Multi-Engine (All Light Aircraft)	550 High Perf. Jet; 920 Piston Engine Transport, 71 Misc.
Instrument Hours	200	275

F. IMPORTANT RESULTS OF THE SINGLE-AXIS EXPERIMENTS WITH DIFFERENT DISPLAY FORMATS

The principal reduced experimental results are summarized concisely in Figs. III-3, 4 and 5. Each graph presents foveal results on the left side and parafoveal results in the center and on the right side. Each figure includes results for the Line, Bar, Dial and Quant(ized) format in that order from left to right. The results for each pilot's tracking run are coded symbolically in the legend on each figure. Replications are tagged. The 20 deg parafoveal results are training data.

In Fig. III-3 both pilot-subjects in these single-axis experiments exhibited an incremental effective time delay with the Quantized format on the order of $1/10$ sec more than that delay (about $1/4$ sec) with the other formats under foveal viewing conditions. Since quantization alone will not produce the increase in delay, whereas internal reconstruction or extrapolation and smoothing among quanta to derive rates of change can produce the observed increase in delay, the effect would seem to be perceptual. This result is relevant for raster-scanned displays.

Smaller average increases in effective time delay on the order of $1/20$ sec resulted for the Line, Bar and Dial formats between foveal and parafoveal viewing. This small time delay increment is consistent with values observed while tracking with the Line format in previous experiments. It may be "explained" by association with the differential difference extrapolation model for higher frequency lead generation (Ref. 22). One pilot subject exhibited a further increment in time delay of between 0.15 and 0.20 sec under 20° parafoveal viewing conditions.

The results under parafoveal viewing conditions are particularly relevant to a theory of integrated display format. Those formats which induce marked changes in behavioral properties, coherence, or error scores between foveal and parafoveal viewing conditions would seem to be inferior candidates for an integrated display application with respect to those formats which induce few and/or lesser changes.

These single-axis baseline results offer no clear distinction in measures

Pilots : ○ = RH , □ = DH ; Replications = Tagged

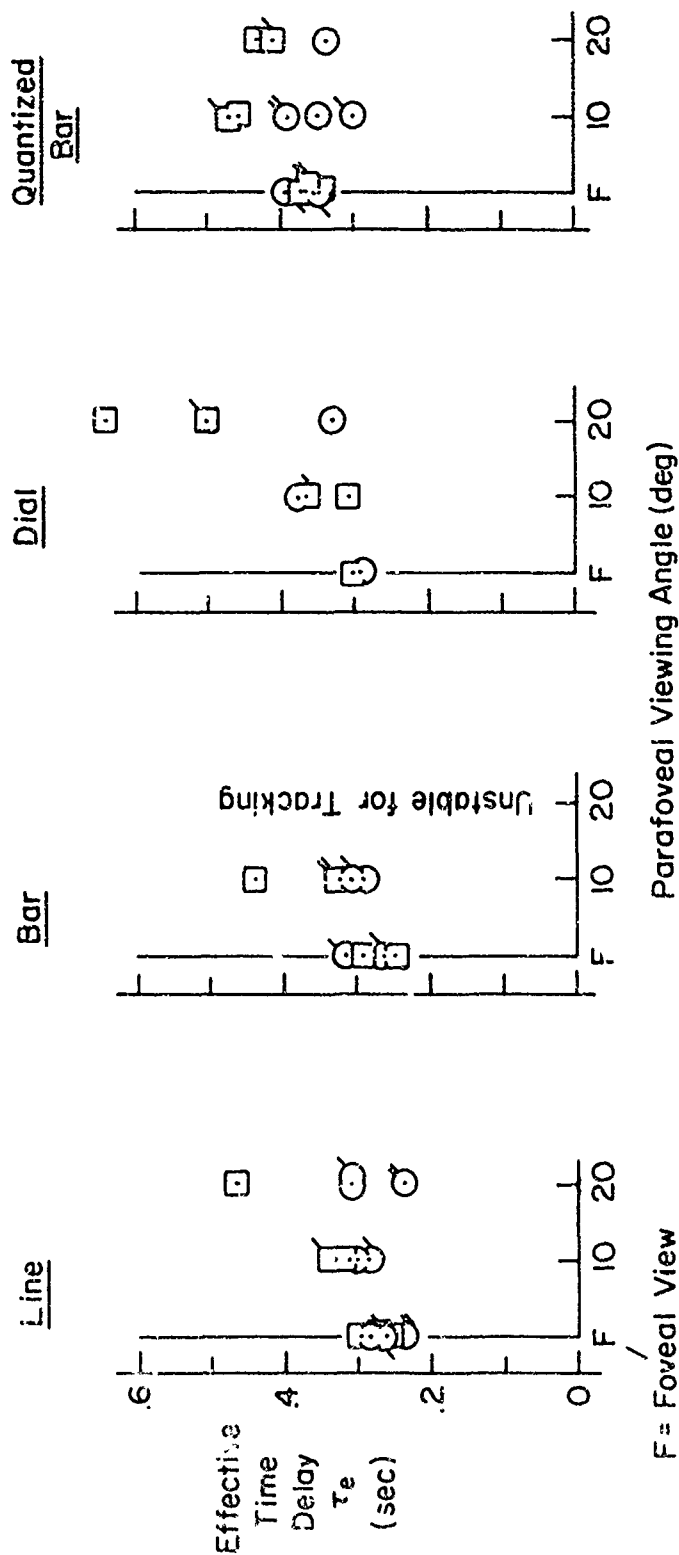


Figure III-3. Summary of Crossover Model Effective Time Delay for Different Single-Display Formats Computer-Fitted to Two Frequencies Nearest Crossover

$$\text{Controlled Element } Y_c = \frac{K}{s(s+2)}$$

Pilots : ○ = RH, □ = DH ; Replications = Tagged

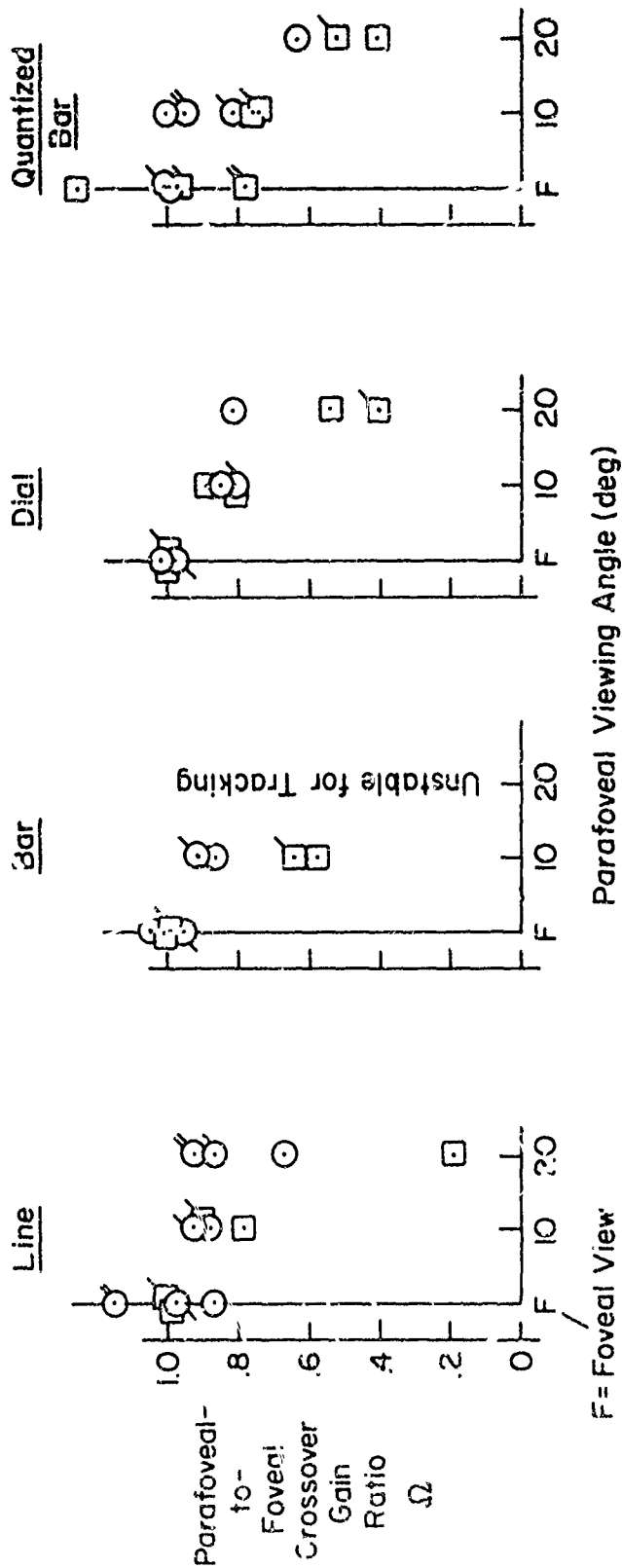


Figure III-4. Summary of Parafoveal to Foveal Crossover Gain Ratio for Different Single-Display Formats Computer-Fitted to Two Frequencies Nearest Crossover

$$\text{Controlled Element } Y_c = \frac{K}{s(s + 2)}$$

Pilots: ○ = RH, □ = DH ; Replications = Tagged

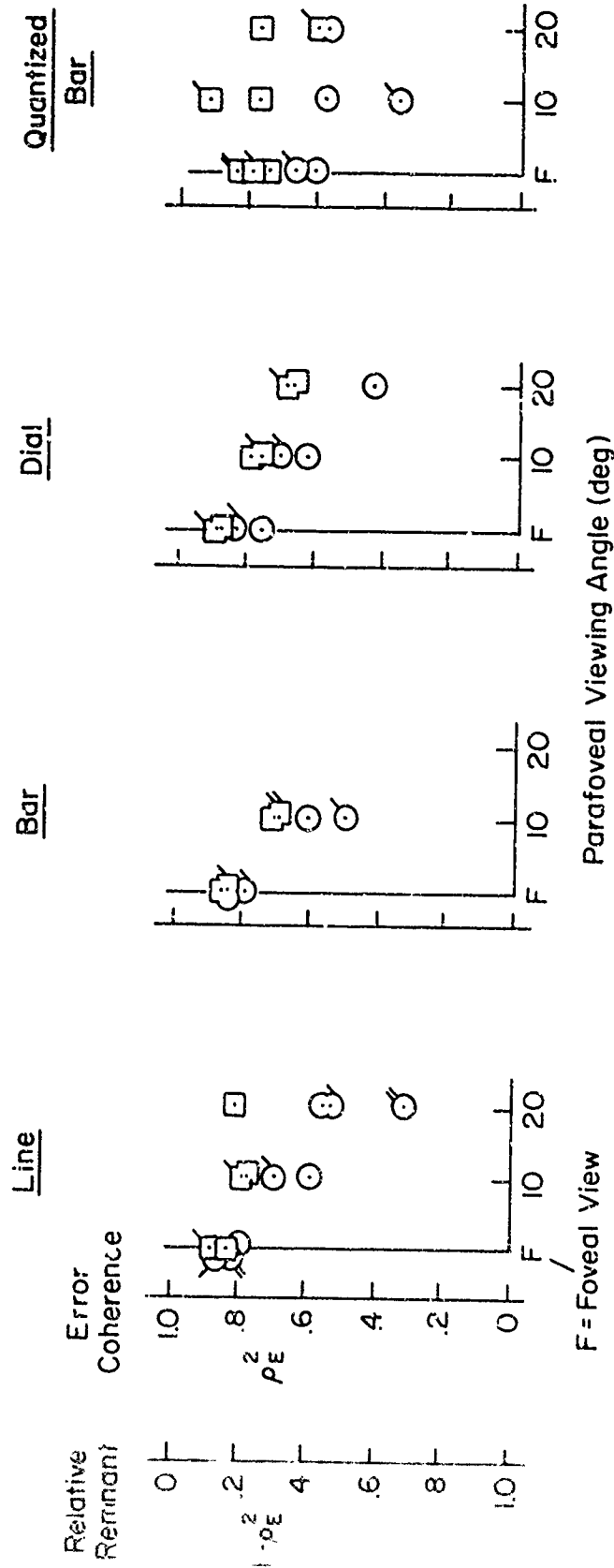


Figure III-5. Summary of Normalized Error Coherence for Different Single-Display Formats
 Controlled Element $Y_c = \frac{K}{s(s+2)}$

of behavior, coherence, or error scores between foveal and parafoveal tracking with the Line and Dial formats. With both Line and Dial formats, however, measures of behavior, coherence and error scores deteriorated relatively more at 20 deg than at a 10 deg parafoveal viewing angle. For example, a display designer might be impelled to increase the field of view of an integrated display format to improve the pilot's basis for monitoring the situation. Alternatively, the designer might want to increase the displayed field of view to reduce foveal clutter among symbols in a dense format, if the content must be preserved and the field of view scaling does not otherwise have to be in the ratio 1:1 with the real world. However, the results of the single-axis experiment imply that increasing the field of view of an integrated display format greater than about 10 deg will produce diminishing returns through the relatively greater deterioration of parafoveal tracking ability.

The only format for which the single-axis baseline results offer consistent evidence of inferior suitability is the Bar. This is exemplified by a rather large reduction in average parafoveal gain at 10 deg in Fig. III-4 and by consistent increases in relative and absolute remnant power and total error variance. The results for relative remnant and error coherence are shown in Fig. III-5. The Bar format was found to be unusable for tracking at a 20 deg parafoveal viewing angle. It should be emphasized that these preliminary results suggest inferiority of the Bar format under parafoveal viewing conditions only in a closed-loop tracking context.

Qualitative analysis of these single-axis experiments and several past experiments shows that many of the parafoveal viewing effects (e.g., relatively greater higher frequency gain, relatively less low frequency phase lag, increased normalized injected remnant power, etc. could be "explained" by an increase in the displacement perception threshold relative to the rate perception threshold under parafoveal viewing conditions. A model of this effect, however, remains to be validated.

SECTION IV

AN EXPLORATORY MULTIAXIS INTEGRATED DISPLAY EXPERIMENT

A. PURPOSE OF THE MULTIAXIS EXPERIMENTS WITH DIFFERENT DISPLAY FORMATS

As indicated in Appendix A, the arrangement of information displayed to a pilot can have major effects on the pilot-vehicle system performance (in terms of dynamic response and injected noise) and on pilot workload, in terms of the pilot's excess available capacity for handling other tasks such as emergency situations as well as the psychological stress level associated with the task. The preliminary experiment discussed here is an attempt to develop and test a variety of quantitative techniques for measuring the above effects in conjunction with integrated display formats. In addition, we hoped to quantify some of the characteristics of display integration to guide future display research, development and design. We wished to quantify a definition for an "integrated" display in terms of measurable (and predictable) properties of format and content, which are related to the pilot's workload in a realistic cockpit scenario. Table IV-1 outlines the experimental design. The plan and procedure for the multiaxis experiment will be presented next. This is followed by a discussion of the results which were obtained.

B. SCENARIO

In this experiment, we attempted to set up as simple a simulation as possible and yet achieve an operational relevance that would be motivating to pilots and which would provide results that could be extrapolated to more complex simulations and operational situations. A helicopter formation flying task was chosen that required both cyclic and collective control. The pilot's primary task was to control the longitudinal displacement errors of his ship from a commanded position behind a maneuvering lead aircraft. It was in this task that the different display formats described below were evaluated.

The lateral cyclic and collective control tasks were somewhat abstract in that they were uncoupled from each other and the primary task (so as to simplify the measurement of describing functions). The vehicle response to control inputs, however, was judged to be realistic. The lateral task was

TABLE IV-1. OUTLINE OF EXPERIMENTAL TEST PLAN FOR MULTIAxis EXPERIMENTS

Independent Variables

CONTROLLED ELEMENTS		Situation Display Format				Flight Director Display Format		Pitch Attitude Command K_p/K_{θ} (ft)
		Without Explicit Longitudinal Velocity Error Abbreviated as "State, (S)"	With Explicit Longitudinal Velocity Error Scaling Proportional to T_L Abbreviated as "State + Rate, (S + R)"	With Longitudinal Velocity Error Proportional to T_L Abbreviated as "Flight Director, (FD)"	Without Longitudinal Displacement Error (Laboratory Tracking Anchor Point, Abbreviated as "Director, (D)")			
Longitudinal	Altitude Divergence λ_e (rad/sec)	Roll Divergence λ_{ϕ} (rad/sec)	Workload Rating	$T_L = 1.5$ sec (Near-Optimum)	$T_L = 3.0$ sec (Off-Optimum)	$T_L = 1.5$ sec (Near-Optimum)	$T_L = 3.0$ sec (Off-Optimum)	
CB-53 Helicopter with Velocity FCS ($T_C = K_v/s$)	0.1	0.1	"Low" for Error Variance Measurement "High" for Error Variance and Excess Control Capacity Measurement	✓		✓		0
				Cross-Adaptive	✓	✓	✓	0
CB-53 Helicopter with Pitch FCS ($T_C = K_p/s^2$)	0.1	0.1	Low	$T_L = 1.0$ sec (Off-Optimum)	$T_L = 3.0$ sec (Near-Optimum)	$T_L = 1.0$ sec (Off-Optimum)	$T_L = 3.0$ sec (Near-Optimum)	
				0.2	High	✓	✓	✓
				✓	✓	✓	✓	50
				✓	✓	✓	✓	100

In each Checkered Cell Block: 2 Replications
2 Pilot Subjects

Dependent Variables (i.e., measurements)
Pilot describing functions (e.g., gain, effective time delay, equalizations)
Serial segment remnant power spectra
Velocity error coherence and variance
Longitudinal separation error variance
Mean longitudinal separation error
State variables (e.g., pitch attitude, pitch rate, roll attitude, altitude error)

Dependent Variables (Cont'd)
Longitudinal control displacement variance
Eye-Point-of-Regard Statistics
Excess control capacity
Subjective display rating (e.g., controllability and precision) status utility; clutter, and attentional demand)

Special Measurement Apparatus
Describing Function Analyzer (SFI/NASA W-11)
Eye-Point-of-Regard Instrumentation (SFI/USC W-1)
Cross-adaptive suboptimal tracking task for excess control capacity

to maintain a level roll attitude with slightly unstable roll response, and the collective task was to maintain a command altitude, again with slightly divergent dynamics.

The lateral and collective control tasks were used to represent the combined workload a pilot might encounter in an operational situation when combined with the longitudinal task. The lateral cyclic and collective control tasks might be viewed in the terms of experimental psychology as classical subsidiary or secondary tasks. See Knowles (Ref. 23). Then the workload demand is a direct function of the level of instability of the dynamics (Ref. 24). This technique has been used very successfully in the past (Refs. 9, 25). It is relevant to vehicle control simulations which mainly involve continuous control tasks.

C. SIMULATION

The simulation consisted of a cockpit with display panel and control together with an analog computer which was used to mechanize the control task dynamics. Additional measurement equipment included a Describing Function Analyzer (DFA) which was used for dynamic response measurements, and an Eye-Point-of-Regard (EPP) system for measuring the pilot's eye movements.

1. Control Tasks and Dynamics

a. Primary Task. The pilot-subjects' primary task was to control longitudinal position deviations of his aircraft from a commanded position behind a maneuvering lead aircraft. A compensatory display was used so that the pilot was aware only of his deviation from the commanded position. The simulated formation was moving at an average forward speed of 60 knots, which set the flight condition for the longitudinal control dynamics, but random commanded speed variations occurred in the control loop because of the presumed maneuvering of the lead aircraft.

A block diagram of the above described task is shown in Fig. IV-1. The Describing Function Analyzer (DFA)* was used to generate the commanded velocity (u_c)

*An Electromechanical Fourier Analyzer developed for the NASA-Ames Research Center. The measurement theory upon which this device is based is given in Ref. 20.

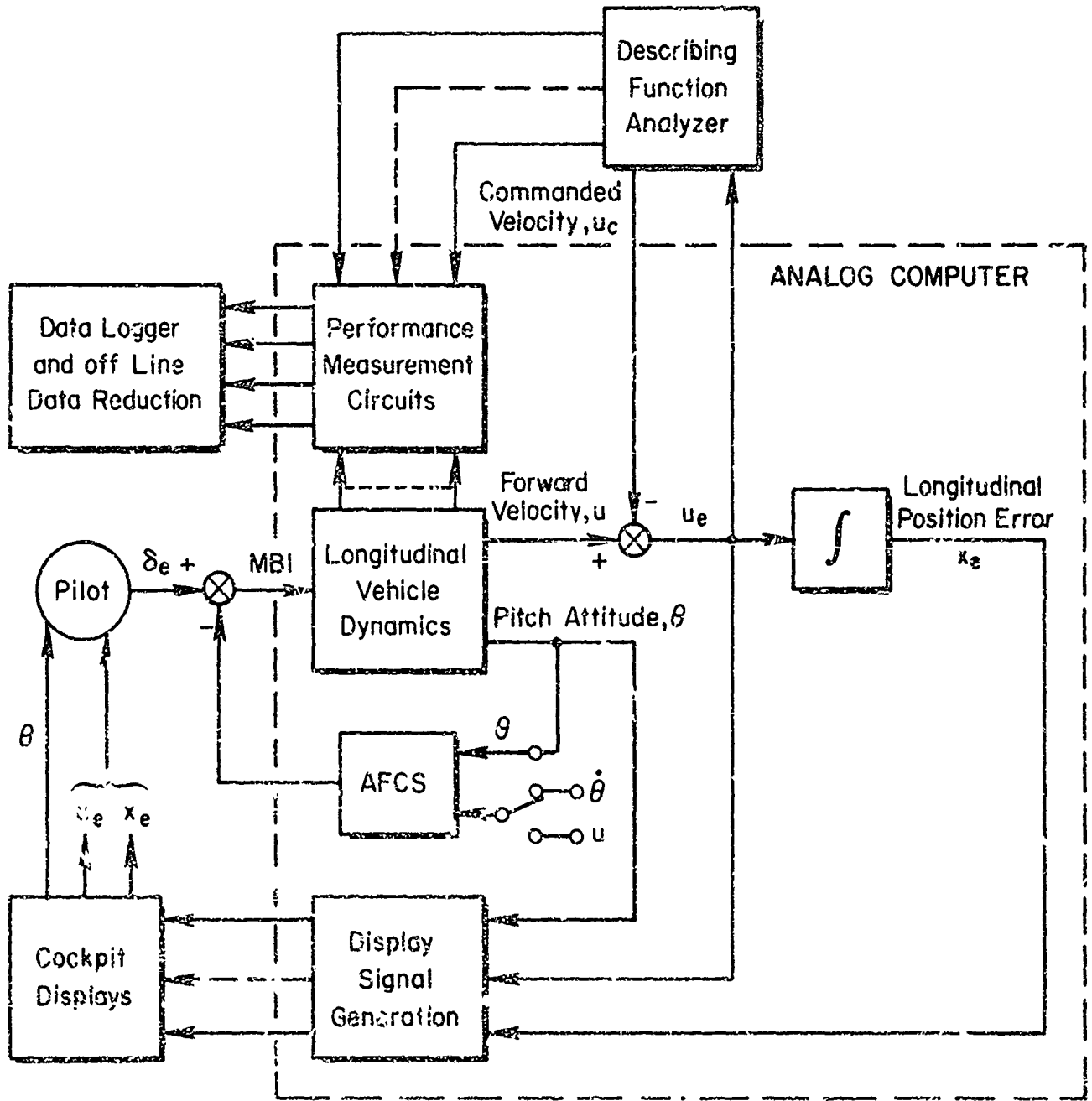


Figure IV-1. Simulation Block Diagram for the Longitudinal Control Task

input to the control loop, as well as to analyze the resulting velocity error (u_e) so as to give measures of system stability and bandwidth.

The command velocity input was a sum of sinusoids as described in Table IV-2. The input appeared random to the pilot and allowed dynamic response measurements to be made at each of the input frequencies which spanned the range from 0.2 to 6.3 rad/sec.

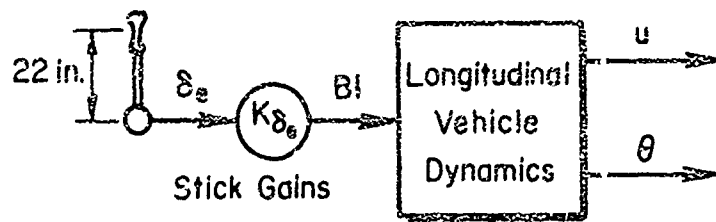
The pilot was displayed information on pitch attitude and combinations of position and velocity error (x_e, u_e) as explained below in connection with the description of the actual display formats which were employed in the experiments.

The pilot controlled longitudinal vehicle motions by commanding pitch attitude changes with fore-aft motions of a center-mounted cyclic stick. The displacement and force gradients are described in Figure IV-2. The longitudinal control dynamics were mechanized as a linear, two degree of freedom set of motion equations given in Table IV-3. Stability derivatives which were used corresponded to the dynamics of the CH-53 single rotor helicopter as analyzed in Ref. 2. The basic vehicle dynamics are unstable, and a simulated automatic flight control system (AFCS) was provided to stabilize vehicle attitude.

The AFCS was employed in two different modes so as to give the two sets of dynamics shown in Fig. IV-3. In the first case, velocity feedback was employed in addition to pitch attitude. In the frequency range below 1 rad/sec, pitch attitude response was approximately the derivative of the stick input, and longitudinal position response was approximately the integral of stick inputs. These dynamics amount to the rate dynamics used in classical tracking research (Ref. 26). Appropriate pilot behavior in this case (as shown in Ref. 10) is to make control deflections proportional to displayed position errors (x_e). Some lead equalization might be helpful for these dynamics in the neighborhood of one rad/sec but no low frequency lead is required within the practical closed-loop bandwidth of the system (less than 1 rad/sec).

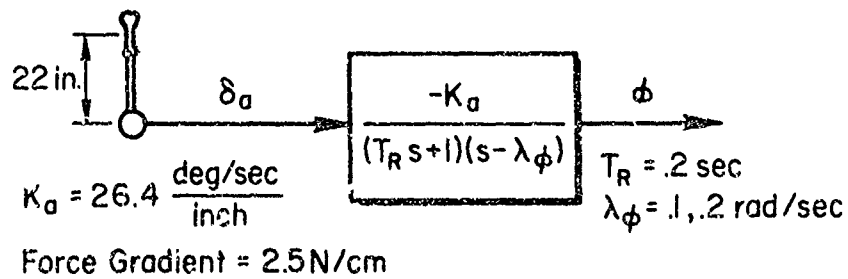
The second AFCS mode included pitch rate along with pitch attitude feedback. This is equivalent to the CH-53 operational configuration. This system gives a pitch response comparable to a first order lag (low pass filter) with a break frequency at about 2 rad/sec. It amounts to a "pitch command" system where

PRIMARY LONGITUDINAL



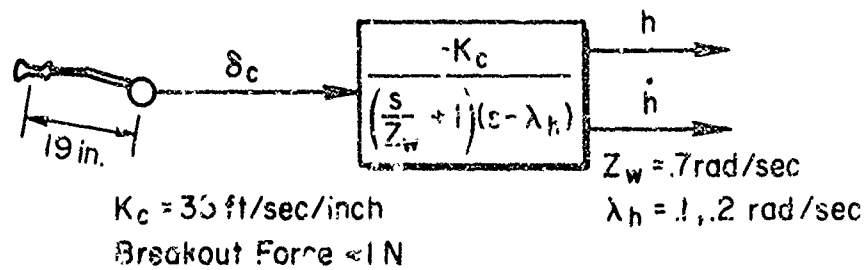
u Feedback $K_{\delta_e} = .28 \text{ rad (BI) / inch}$
 θ Feedback $K_{\delta_e} = .056 \text{ rad (BI) / inch}$
 Force Gradient = 2.5 N/cm

SECONDARY LATERAL



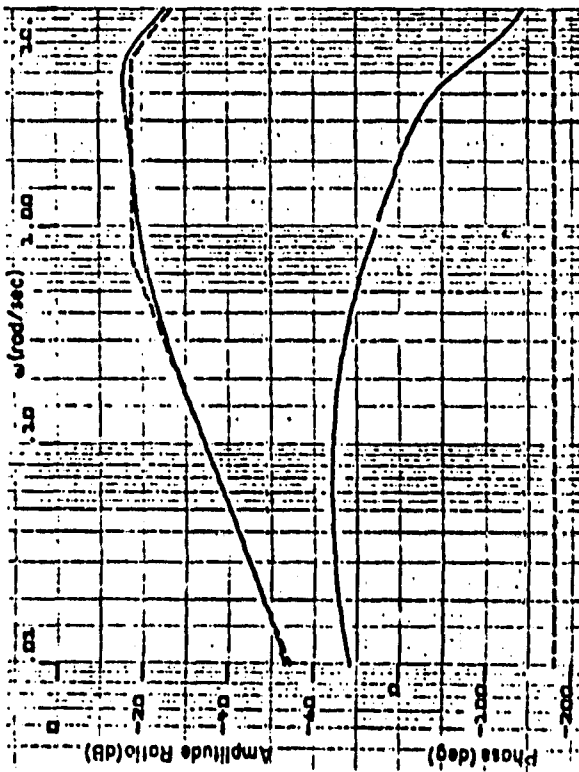
$K_a = 26.4 \frac{\text{deg/sec}}{\text{inch}}$
 Force Gradient = 2.5 N/cm
 $T_R = .2 \text{ sec}$
 $\lambda_\phi = .1, .2 \text{ rad/sec}$

SECONDARY COLLECTIVE

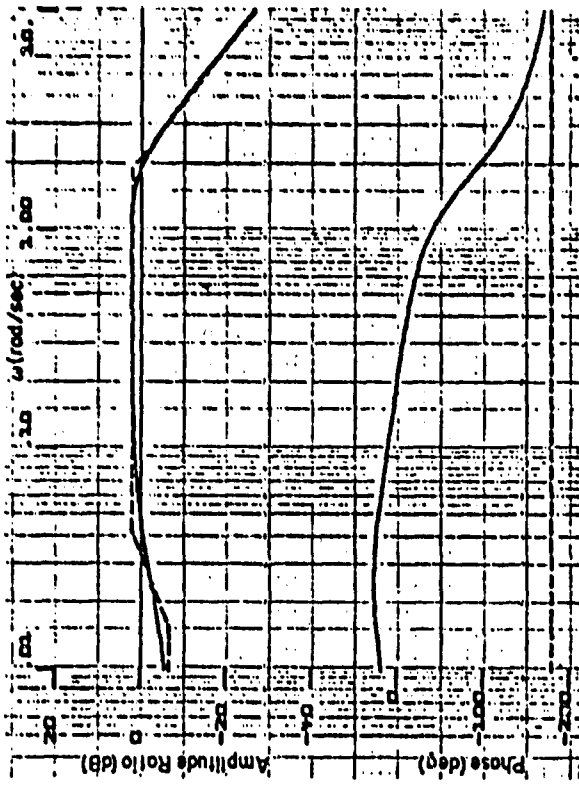


$K_c = 35 \text{ ft/sec/inch}$
 Breakout Force $\ll 1 \text{ N}$
 $Z_w = .7 \text{ rad/sec}$
 $\lambda_h = .1, .2 \text{ rad/sec}$

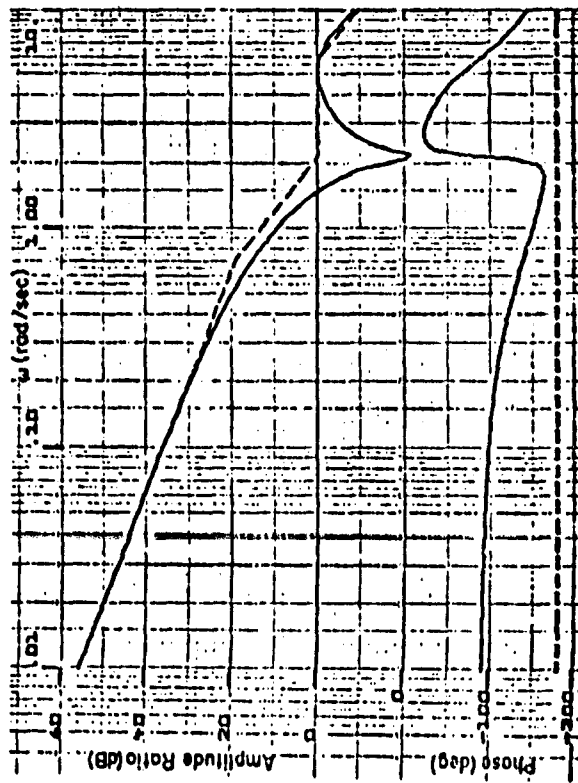
Figure IV-1. The Tasks for the Multiaxis Experiment



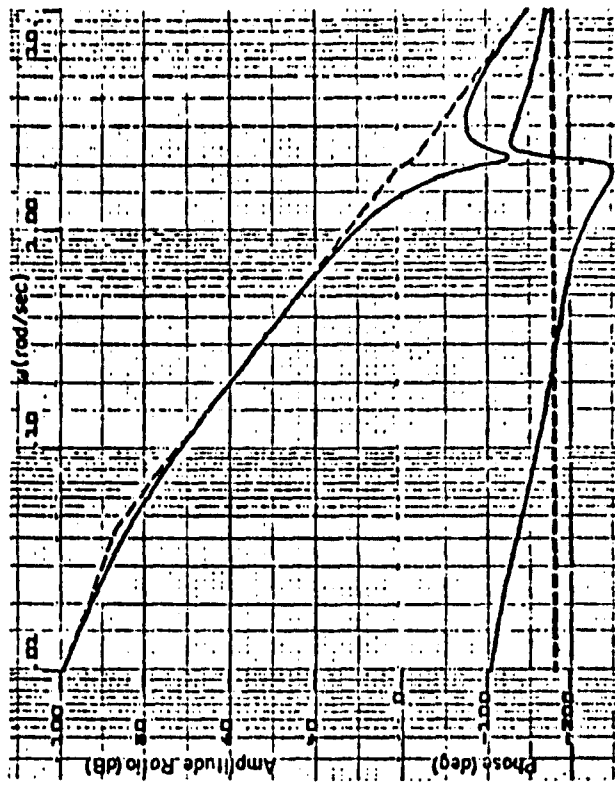
Pitch Attitude Response



Longitudinal Position Response



a) Velocity Feedback Dynamics



b) Pitch Rate Feedback AFCS

Figure IV-3. Longitudinal Control Task Dynamics.

TABLE IV-2. COMMAND VELOCITY INPUT

$$u_c = \sum_{i=1}^5 A_i \sin(\omega_i t + \phi_i)$$

	ω_i	A_i
Sinusoid	Frequency (rad/sec)	Amplitude (ft/sec)
1	0.188	0.5
2	0.503	0.2
3	1.26	0.1
4	3.02	0.033
5	6.28	0.033

$$\sigma_c = 0.389 \text{ ft/sec}$$

ϕ_i randomly phased from run to run

TABLE IV-3. HELICOPTER SIMULATION EQUATIONS OF MOTION

Matrix

$$\begin{bmatrix} s - X_u & -X_q s + g \\ -M_u & s^2 - M_q + M_{B_1} \end{bmatrix} \begin{bmatrix} u \\ \theta \end{bmatrix} = \begin{bmatrix} X_{B_1} \\ M_{B_1} \end{bmatrix} B_1$$

Stability Derivatives

$$\begin{aligned} X_u &= -.037 \text{ sec}^{-1} \\ X_q &= 2.85 \text{ ft/sec} \\ X_{B_1} &= 32.3 \text{ ft/sec}^2 \\ g &= 32.2 \text{ ft/sec}^2 \end{aligned}$$

$$\begin{aligned} M_u &= .003 \text{ ft}^{-1} \text{ sec}^{-1} \\ M_q &= -.562 \text{ sec}^{-1} \\ M_{B_1} &= -4.55 \text{ sec}^{-2} \end{aligned}$$

pitch attitude is proportional to stick deflection. The resulting position response to stick inputs is equivalent to acceleration dynamics used in classical tracking research (Ref. 26). They require the pilot to make stick deflections proportional to the derivative or rate of change of the displayed position error (x_e). (Vide Ref. 10.) In this case it was very helpful to provide displayed lead equalization such as with a flight director, or to display velocity error (u_e) explicitly.

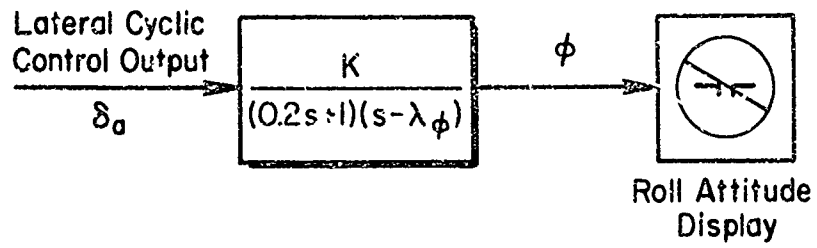
b. Secondary Tasks. The pilot was required to maintain a level roll attitude and a commanded altitude with the dynamics shown in Fig. IV-4 as secondary tasks. The roll dynamics included a roll time constant T_R of 0.2 sec and a small spiral divergence or instability. The collective control was used to maintain a commanded altitude through dynamics which included a flight path response time constant of 1.4 sec and a slow divergence. Both altitude error (from the commanded altitude) and rate of climb were displayed to the pilot on vertical meter movements placed side by side.

Pilot induced noise or remnant was sufficient to excite the unstable dynamics, so disturbance inputs were not required for the secondary tasks. The level of instability was used to control the attentional demand or workload on the pilot. As shown in Fig. IV-3 two levels of instability were selected which respectively corresponded to low and high workload demands on the basis of the pilot's subjective opinions. Previous research (Refs. 23, 27, and 28) has shown that high workload demands on the pilot tend to accentuate observable effects of differences in primary task variables. This was also found to be the case in the present research and the phenomenon was used very effectively in evaluating different display formats.

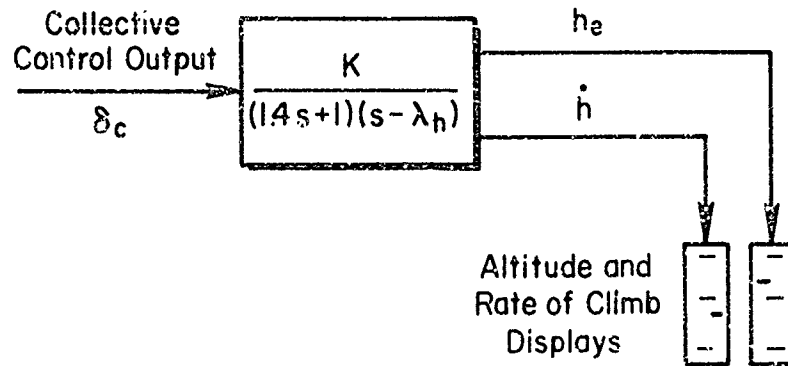
c. Cross adaptive Workload Task. A scheme employed by McDonnell (Ref. 25) was used here to quantify the workload demands of various display formats. This technique involved a variation of the above described tasks where the pilot was only controlling the longitudinal axis and stabilizing roll attitude. The variation was such that the divergence time constant of the roll axis dynamics was adaptively adjusted as a function of primary task performance. The adaptive adjustment scheme is shown in Fig. IV-5.

The performance measure was the absolute value of the sum of position and velocity errors (x_e , u_e). When this measure exceeds the error criterion, the

ROLL CONTROL TASK



ALTITUDE CONTROL TASK



Workload	Instability Level (rad/sec)	
	λ_ϕ	λ_h
Low	0.1	0.1
High	0.2	0.25

Figure IV-4. Secondary Control Tasks

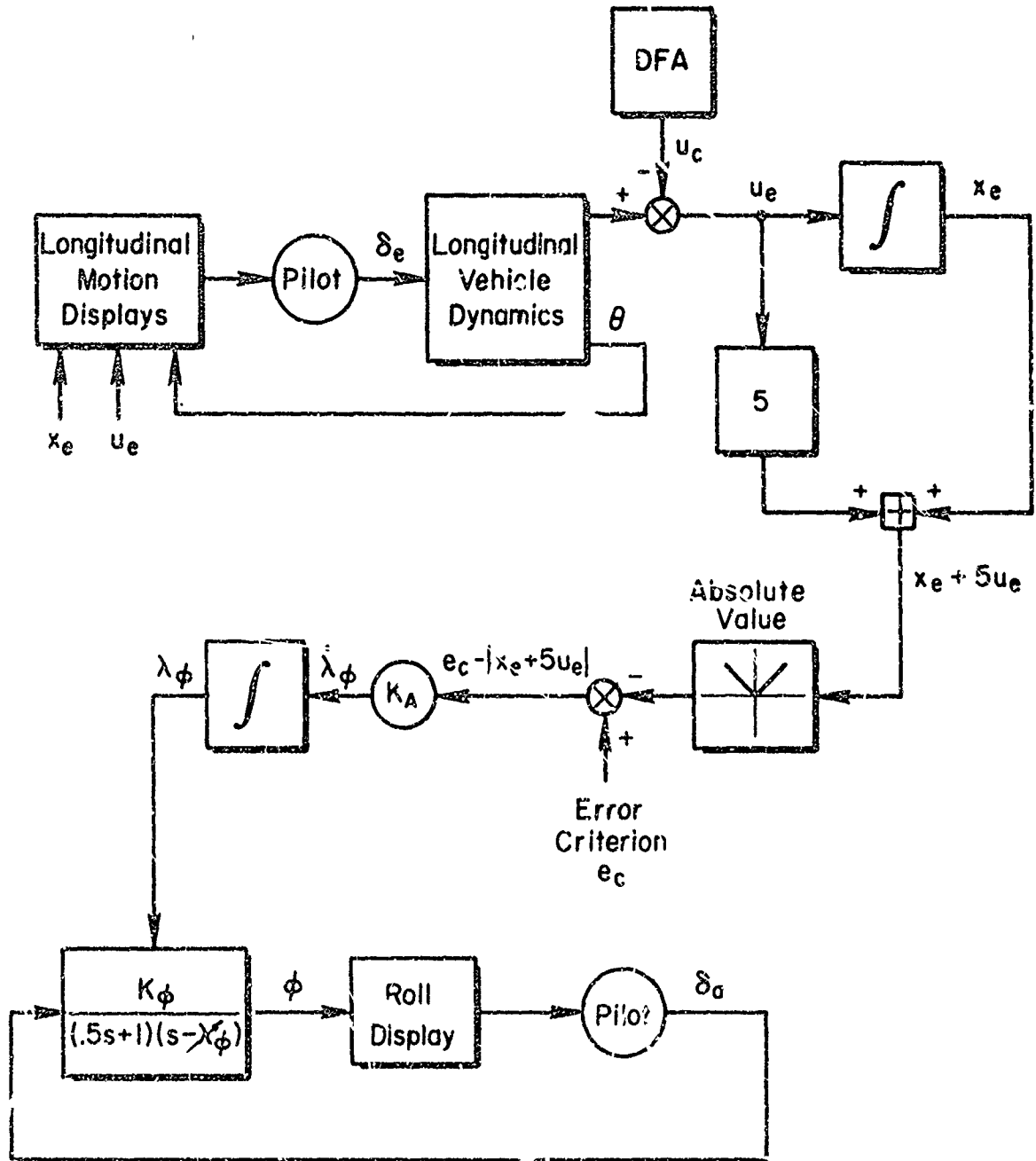


Figure IV-5. Cross Adaptive Workload Task

roll task divergence decreases, and when the performance is below the criterion value the divergence increases. The error criterion was adjusted to be nominally 25% above the performance achieved during a preceding period of steady state tracking. (The same DFA input was used in both cases.)

The amount by which the roll divergence parameter, λ_{ϕ} , increases over the steady state trial is directly related to the increased workload which the pilot can tolerate on the side task for a 25% increase in error on the primary task. Presumably this increased workload will vary according to the experimental condition in the main task, such as, for example, the display format. Thus, the adapted λ_{ϕ} will give a quantitative measure of the allowable excess workload a pilot can tolerate for a given display format. The optimum display format is the one which yields the most excess capacity.

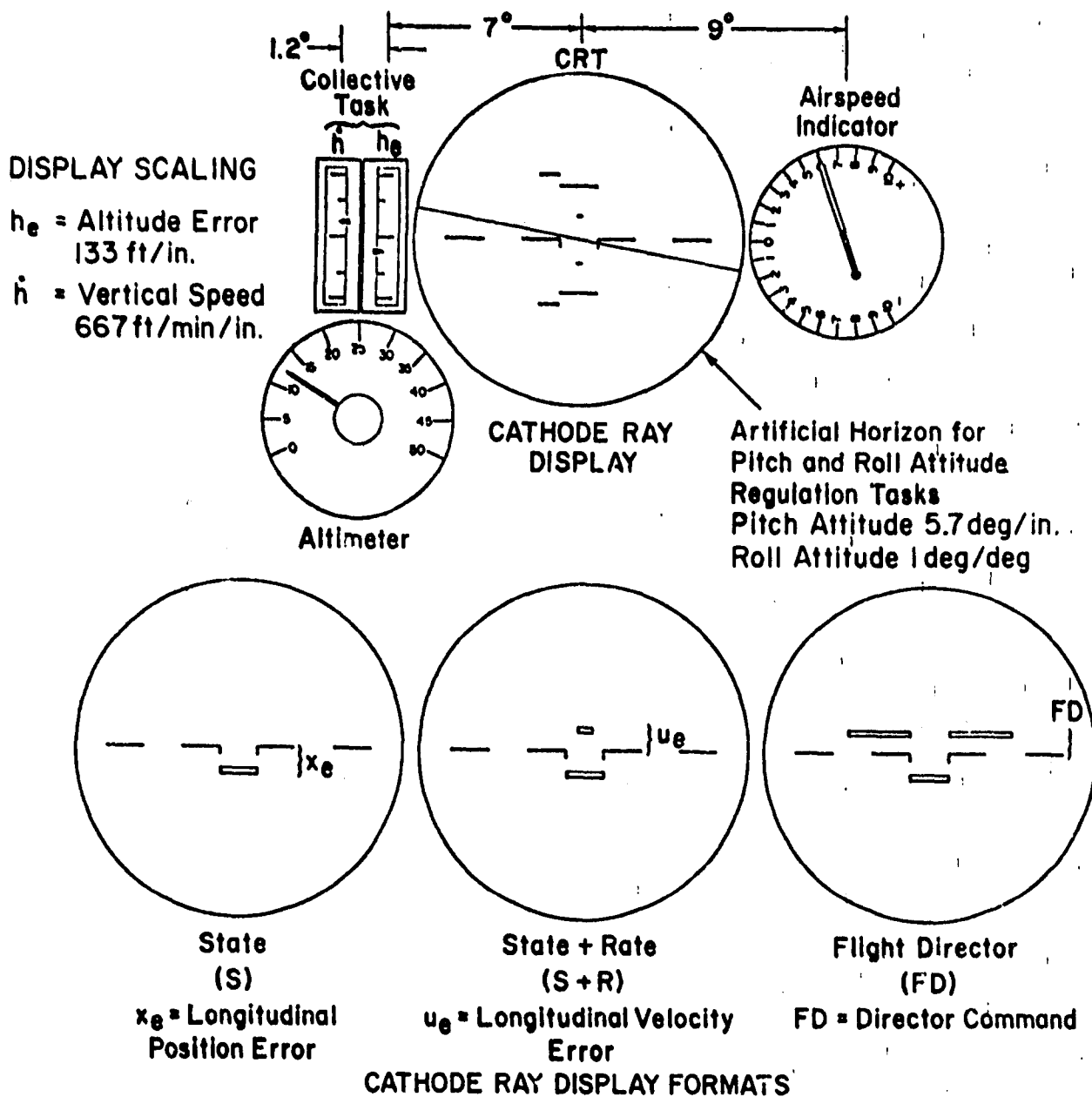
2. Displays

The configuration of the cockpit display panel is shown in Fig. IV-5. The viewing distance to the panel was approximately 31 in. The CRT presented an artificial horizon for pitch and roll attitude information as well as the longitudinal display formats described below. The collective control (altitude hold) task utilized the two vertical edge meters mounted to the left of the CRT. The altimeter and airspeed indicator were provided for status information, but they did not provide useful control information because of their relatively insensitive scaling.

The primary task display formats presented on the CRT are shown in Fig. IV-6. The state format gave longitudinal position error only. Velocity error information was added in the state + rate format so as to aid in the rate or lead equalization required of the pilot in the primary task. As noted in Fig. IV-6 the u_e scaling was proportioned to the lead required. Finally, the flight director configuration gave a stick command signal which the pilot could track with stick deflections proportional to display deflections. The flight director equation took into account the equalization required for the longitudinal dynamics. Figure IV-6 gives the display gains which were used including the various flight director equations tested.

D. MEASUREMENTS AND PROCEDURES

A variety of measurements were performed both to investigate various



Display	Scaling	Flight Director Equations	
		Velocity AFCS	FD = $.25(x_e + T_L u_e)$ ft/in.
Position Error, x_e 4 ft/in.	Velocity Error, u_e $4T_L$ ft/in.	Pitch Rate and Attitude AFCS	FD = $.125(x_e + T_L u_e + 200)$ ft/in.
			FD1 = $.025(x_e + T_L u_e + 1000)$ ft/in.
			FD2 = $.025(x_e + T_L u_e + 500)$ ft/in.

Figure IV-6. Cockpit Display Panel Configuration, Primary Task CRT Display Formats and Scaling

techniques for evaluating displays, as well as to obtain comprehensive data on a range of display formats. The measurements are divided into performance and describing function measures obtained during steady tracking tasks, eye-point-of-regard obtained during these same tasks, pilot opinion ratings obtained at the end of the tracking runs, and excess workload capacity as measured by the instability score obtained during the cross adaptive task.

1. Performance and Describing Function Measurements

During the steady state tracking tasks the pilots were instructed to minimize longitudinal position deviations caused by the command velocity generated by the DFA (Fig. IV - 1). After a warm up period to allow the pilot to reach steady state, data were measured over a 100 second period. Mean and mean-squared measures of a variety of variables associated with both the primary and secondary tasks were obtained on the analog computer. These data were then further reduced off line to give RMS values. The DFA computed Fourier coefficients and additional performance measures during the measurement period, and these data were also further reduced off line to yield the pilots' describing functions, remnant, and describing function fitting parameters related to primary task bandwidth. (These were crossover frequency, ω_c , and stability in the sense of the phase margin, Φ_m .)

2. Eye-Point-of-Regard (EPR)

The display arrangement (Fig. IV - 6) required scanning between the CRT and the collective control task displays. It was desired to measure the amount of time spent viewing each display and the rate of scanning between displays as well as to see if the different longitudinal display formats caused differences in these statistics. It was also desired to see if the different display formats might cause scanning among the elements of the display on the CRT.

The EPR equipment consisted of three units: 1) spectacle frame-mounted transducers and associated electronics for measuring eye angle with respect to the head; 2) a goniometer gripped in the mouth for measuring head angles with respect to the display panel; 3) a special purpose analog computer for combining the head and eye angles to give voltage signals proportional to the eye-point-of-regard on the display panel. This system is more fully

described in Ref. 31. In the experiment described here we only measured horizontal eye movements. This was because we were primarily interested in scanning between the collective side task displays and the CRT.

3. Pilot Opinion Ratings

At the end of each tracking run the pilot was asked to record his subjective opinion of various display qualities on the questionnaires given in Table IV-4. The pilot recorded his opinion by making a mark on the right hand edge of the scale assuming it to be a continuum.

The scales were designed according to recent ideas on psychophysical scaling of aircraft handling qualities. (Vide Appendix C and Ref. 25.) The scales were designed to measure a broader range of effects than were tested in these multi-axis experiments. The approach here was to partition display factors into several dimensions, in order to obtain a more comprehensive measure of display acceptability than might have been obtained from a single rating.

4. Cross Adaptive Excess Control Capacity Measurement

The cross adaptive task described above was performed on each display format after the steady tracking run. The roll divergence parameter (λ_ϕ) was started at 0.1 rad/sec and was held steady at the beginning of the run to obtain a steady state measure of performance. The error criterion was then reset 25% greater and the adaptive adjustment of λ_ϕ commenced. The adaptive rate K_A (see Fig. IV-5) was set to obtain a rapid, stable adaptation. The run was allowed to continue either until the pilot lost control or until λ_ϕ settled out at a stable level. The λ_ϕ occurring at loss of control or the final, stable level were then recorded as a measure of the pilot's excess control capacity for a given display format.

E. SUBJECTS

Two experienced Air Force test pilots, one with considerable helicopter experience, were employed as subjects. Their background and flying experience are summarized in Table IV-5.

TABLE IV-4. PILOT OPINION RATING SCALES

Rating Scale for Utility of Status Information

Criteria	Descriptive Phrase	Rating
Sufficiency of the information supplied, on the specified display unit, on the vehicle status - type and of the relevant flight parameters such as: altitude, speed, heading attitudes, path errors, etc. Successful with respect to the mission phase, task criteria and operator's sense of need for safety.	All desired states presented with adequate resolution and readability	S1
	Many of desired states presented, with a few deficiencies in scaling, resolution or readability	S2
	Some desired states presented, and/or some problems with scaling, resolution or readability	S3
	Inadequate number of states, or serious deficiencies in scaling, resolution or readability	S4
	No direct status information or unusable	S5

Rating Scale for Task Controllability and Precision

Category	Descriptive Phrase	Rating
Controllable/Precise?	Very easy to control, with good precision	C1
	Easy to control, with fair precision	C2
Yes	Controllable, with inadequate precision	C3
	Marginally controllable	C4
No	Uncontrollable	C5

Rating Scale for Clutter

Criteria	Descriptive Phrase	Rating
Degree of subjective symbol - background clutter on specified display unit	Completely uncluttered - e.g. only one pair of elements	K1
	Mostly uncluttered - no confusing or distracting elements	K2
	Some clutter - multiple elements competing for attention	K3
	Quite cluttered - difficult to keep track of desired quantities among competitors	K4
	Completely cluttered - nearly impossible to tell desired elements or quantities due to competing elements	K5

Rating Scale for Display Attentional Workload

Criteria	Descriptive Phrase	Rating
Demands on the operator attention, skill, or effort	Completely undemanding and relaxed	D1
	Mostly undemanding	D2
	Mildly demanding	D3
	Quite demanding	D4
	Completely demanding	D5

Table IV-5. Pilot Background and Experience

Pilot and Age	Background	Flight Time		
		Total	Instruments	V/STOL
PB 38 Yr.	Experimental Helicopter Flight Test; Opinion Rating of Flying Qualities	5900	650	4000
FP 32 Yr.	Aerospace Research and Experimental Flight Test; Opinion Rating of Flying Qualities	3600	300	100

F. TRAINING AND TEST AGENDAS

Both pilot subjects were given a preliminary orientation session in which they were told the background and objectives of the research and allowed to familiarize themselves with the simulator and tasks. This was followed by a training session during which preliminary data were collected. The formal data collection then occurred during two further sessions. The first session involved working with the velocity AFCS longitudinal task dynamics, and included cross adaptive workload measurements. During the second test session, the pitch rate feedback AFCS was employed, and the side task instabilities were varied as indicated in Fig. IV-4 to give both low and high workload conditions for the EPR measurements. The run logs for the formal data sessions are given in Tables IV-6 and IV-7.

Each test session was conducted over an 8 hour period with the pilots taking turns in the simulator at nominally 1 to 1 1/2 hour intervals. As mentioned previously the test sessions were conducted on a shoot-look-shoot basis and do not reflect formal experimental design practice. The order of presentation, however, was randomized. The main emphasis was on obtaining data that were valid from both the experimenters' and pilots' points of view, and that would demonstrate the usefulness of the various measurement techniques employed here for display evaluation.

G. ORGANIZATION OF THE RESULTS

In the previous subsection, we discussed four different classes of

TABLE IV-6. RUN LOG FOR THE FIRST FORMAL EXPERIMENTAL SESSION
WITH THE VELOCITY AFCS CONTROLLED ELEMENT

Pilot	Main Task Display	Lead Time Constant, T_L (sec)
PB	State	-0-
	State + Rate	1.5
	Flight Director	1.5
FP	State + Rate	1.5
	State	-0-

Lunch

PB	State + Rate	3.0
	State	-0-
	Flight Director	1.5
	State + Rate	1.5
	Flt. Dir. (no State)	1.5
FP	Flight Director	3.0
	State + Rate	1.5
	State	-0-
	Flt. Dir. (no state)	1.5
	Flight Director	1.5
	State + Rate	3.0

TABLE IV-7. RUN LOG FOR THE SECOND FORMAL EXPERIMENTAL SESSION WITH THE PITCH AFCS CONTROLLED ELEMENT

Pilot	Main Task Display	Lead Time Constant, T_L (sec)	EPR Measurements	Side Task Workload
PB	State	-0-	No	Low
	State	-0-		
	State + Rate	3.0		
	State + Rate	1.0		
FP	Flt. Dir., FD*	1.0	Yes	
PB	Flt. Dir., FD	1.0		
Lunch				
PB	Flt. Dir., FD	3.0		
FP	Flt. Dir., FD2	3.0		
	Flt. Dir., FD2	3.0		
	State	-0-		
	State + Rate	3.0		
PB	State + Rate	3.0		High
	State	-0-		
	Flt. Dir., FD1	3.0		
FP	Flt. Dir., FD1	3.0		
PB	Flt. Dir., FD1	3.0	No	
	State	-0-		
	State + Rate	3.0		
FP	State + Rate	3.0		
	State	-0-		
	Flt. Dir., FD1	3.0		
	Flt. Dir., FD1	1.0		
PB	Flt. Dir., FD1	1.0		

*Flight Director equations given in Figure IV-6.

measurements which were made during the course of these pilot experiments for a theory of integrated display format. These four classes of measurements are repeated below with a list of the specific forms in which the results of each class of measurement will be discussed.

1. Performance and Describing Functions
 - a. Tracking errors, coherence, relative remnant, control and motion variables
 - b. Describing Functions
2. Eye-Point-of-Regard (EPR)
3. Cross Adaptive Excess Control Capacity
4. Pilot Opinion Ratings

Because of the extraordinary volume of results which has been obtained from these experiments, we have chosen to call attention to specific observations about each type of measurement in a terse illustrated review rather than to attempt to present all the results in detail. Following each review, we shall endeavor to relate key results to the pre-experiment analysis which was performed and to the theory of manual control displays.

Since we have also six display configurations and two controlled elements to discuss, we have abbreviated the notation for each in the following ways. The primary display configurations are denoted by alphabetical letters and by a number which represents the lead equalization time constant, T_L (sec), used to scale the error rate display or the error rate signal in the flight director. These primary display configuration codes are repeated below with their definitions.

S	"State" without rate (no longitudinal error rate symbol)
S + R	"State-and-Rate" (longitudinal error rate symbol added to S) with T_L specified in sec.
FD	"Flight Director" with T_L specified in sec for $Y_c = K/s$ and including pitch attitude feedback scaled at $K_\theta/K_{x_e} = -20$ ft for $Y_c = K/s^2$
FD ¹	"Flight Director" with T_L specified in sec and $K_\theta/K_{x_e} = -100$ ft for $Y_c = K/s^2$
FD ²	"Flight Director" with T_L specified in sec and $K_\theta/K_{x_e} = -50$ ft for $Y_c = K/s^2$
D	"Director" display without longitudinal error symbol and with T_L specified in sec for $Y_c = K/s$.

The primary controlled element with a velocity AFCS is denoted by $Y_c = K/s$. Similarly, with a pitch AFCS, the primary controlled element is denoted by $Y_c = K/s^2$.

H. TRACKING ERRORS, COHERENCE, CONTROL AND MOTION VARIABLES

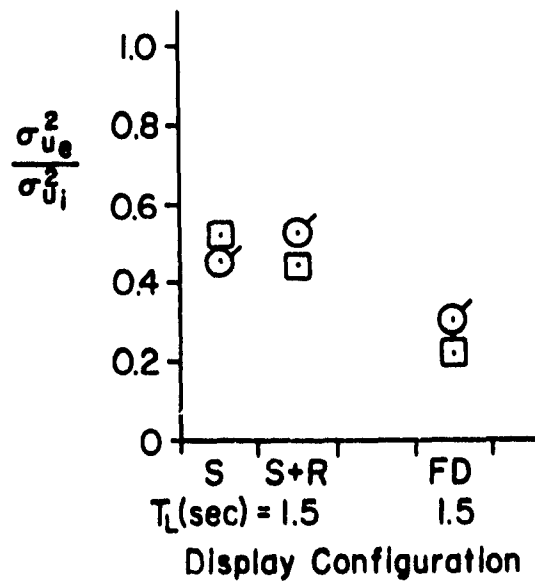
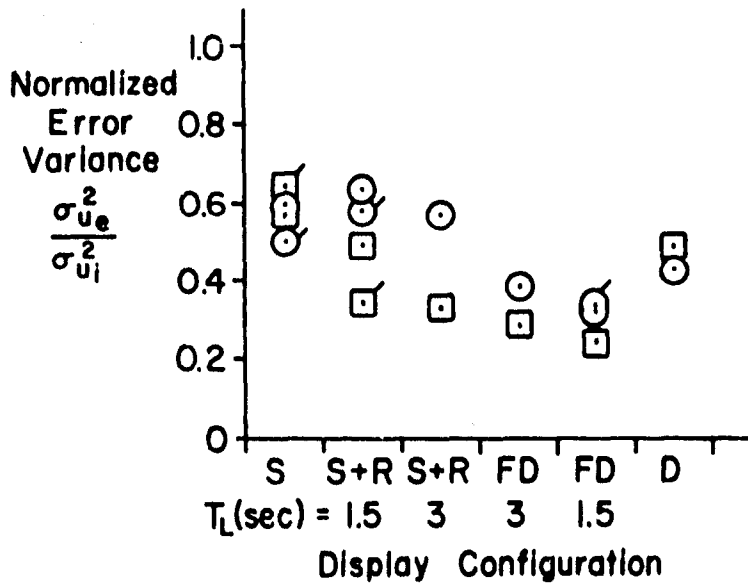
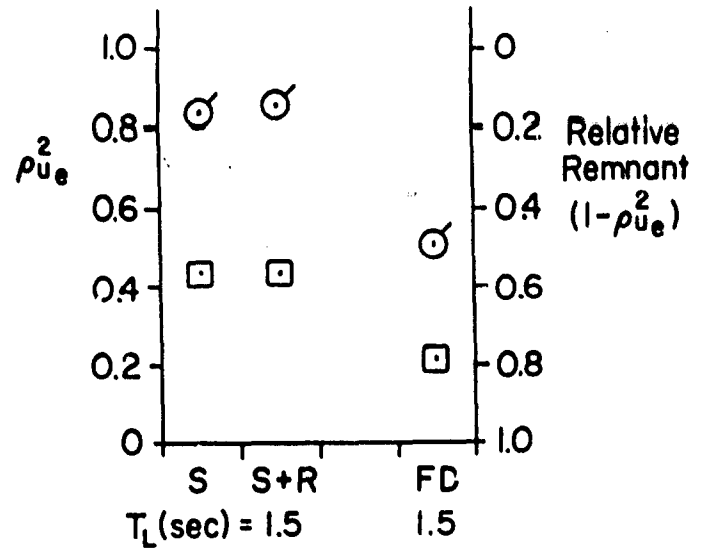
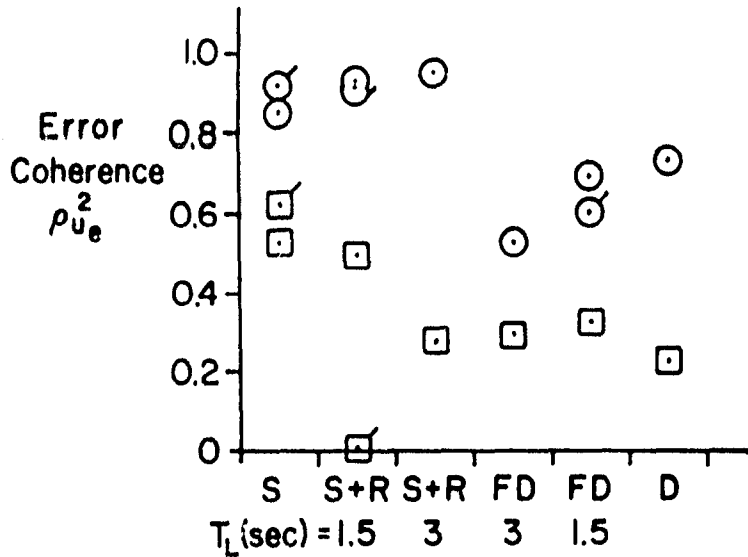
This class of measurements is often termed "performance", because it describes the pilots' control activity and vehicle motions as well as the task error. Three types of error measurements were obtained in these experiments 1) average errors and 2) mean-squared errors (variances) over each 100 sec run length, and 3) error-to-input describing functions at each of the five input frequencies. Both coherent and incoherent error spectra were computed at the five input frequencies by our on-line serial segment technique (Ref. 29). These spectra revealed that the signal-to-remnant power ratio at each of the measurement frequencies was on the order of 10:1, even though the average coherence might have been only about 0.5. This was because all of the input power was concentrated at the five frequencies.

The ratio of the incoherent error variance to the total error variance is called the relative remnant over each 100 sec run length. Since the computed remnant error spectra have offered no new insight for display evaluation based on the frequency distribution of uncorrelated error power, we shall not illustrate the remnant error spectra here. Instead, we shall show some effects of display configuration on the more compact average metric: relative remnant.

Figure IV-7 shows the velocity error coherence, $\rho_{u_e}^2$, the relative remnant, $1 - \rho_{u_e}^2$, and the variance ratio, $\sigma_{u_e}^2/\sigma_{u_1}^2$, as a function of display configuration with $Y_c = K/s$. The variance ratio is normalized with respect to the leader's (input) variance, $\sigma_{u_1}^2$. The results for each run by each subject are presented at the left when averaged over the entire 100 sec run duration. Selected runs are presented at the right when averaged over the 100 sec run duration in four serial segments of 25 sec each. Differences between the coherence and variance averaged in these two ways for the same run by each subject are indicative of non-stationarity in pilot tracking behavior. There are evidences of slight differences in this regard in Fig. IV-7, primarily with the flight director display.

Both subjects' velocity error coherence was less in using the flight

Pilots: \odot PB, \square FP ; Replications Tagged ; $Y_c = K/s$; (710527)



Averaged over the entire 100 sec run duration

Selected runs averaged over the 100 sec run in serial segments of 25 sec

Figure IV-7. Velocity Error Performance with Velocity AFCS

director with $Y_c = K/s$, and both subjects achieved lower velocity error variance with the flight director (Fig. IV-7), because both adopted higher gain equalization with the flight director.

Subject FP's velocity error coherence was always less than subject PB's coherence with $Y_c = K/s$ (Fig. IV-7), because of FP's higher gain equalization technique. (Recall that subject FP had the much smaller amount of helicopter time.)

Figure IV-8 shows the corresponding velocity coherence and variance ratio with the controlled element $Y_c = K/s^2$. At least for the three runs analyzed in serial segments, there is strong evidence for non-stationarity in FP's coherence with the S and S + R formats. PB's coherence tended to increase slightly on the state-and-rate format and on the better director format ($T_L = 3$ sec) with $Y_c = K/s^2$. His coherence dropped markedly on the off-design director format ($T_L = 1$ sec) with $Y_c = K/s^2$ and on the off-design director format ($T_L = 3$ sec) with $Y_c = K/s$.

For corresponding display configurations, the normalized velocity error variance is always greater with $Y_c = K/s^2$ (Fig. IV-8) than with $Y_c = K/s$ (Fig. IV-7). Furthermore, both subjects amplified the leader's velocity variance with the S format and $Y_c = K/s^2$ (Fig. IV-2).

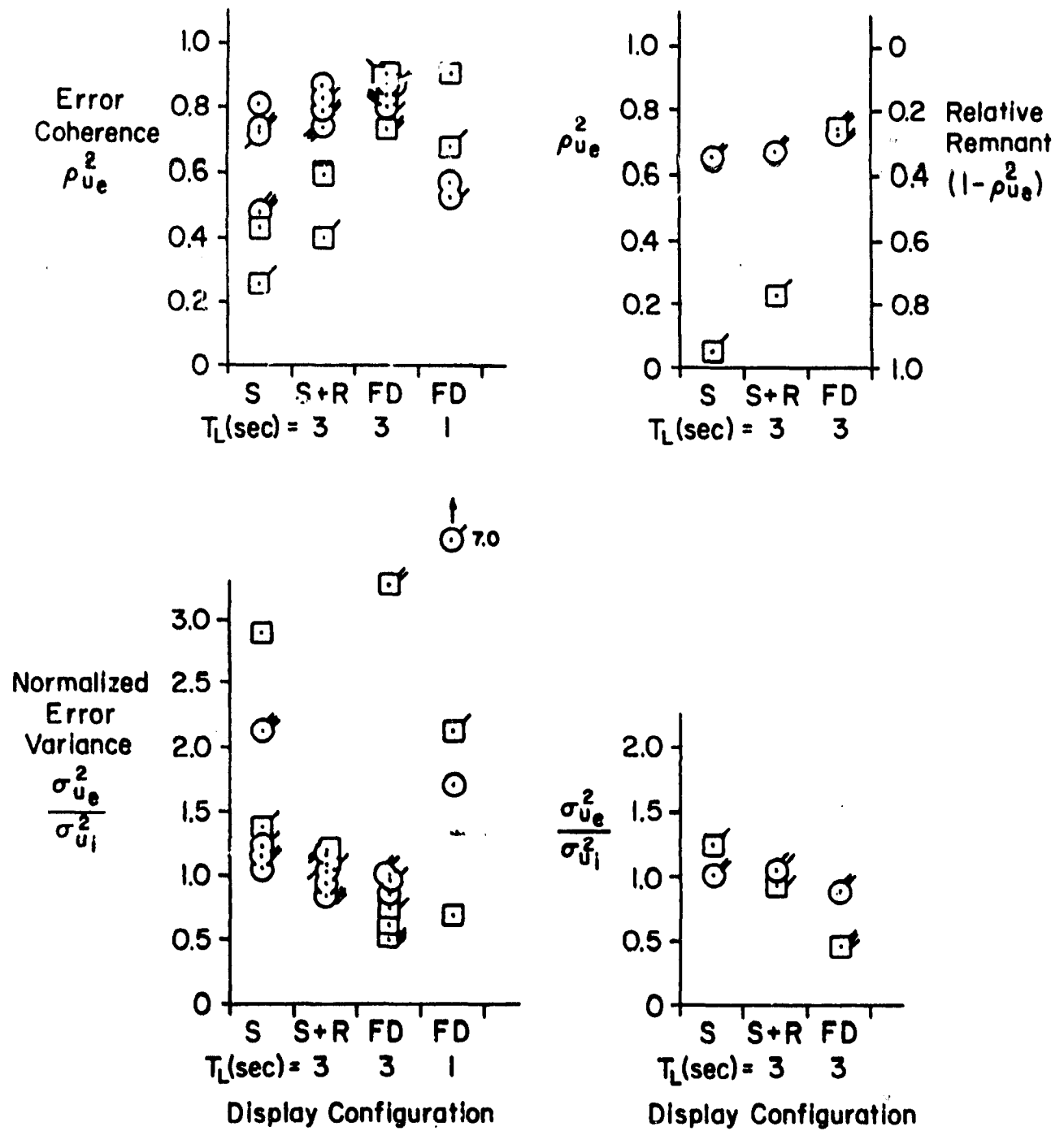
There is no consistent evidence of the influence of low and high side task workload on subject PB's velocity error coherence and variance with $Y_c = K/s^2$ (Fig. IV-8).

Likewise, there is no consistent evidence of the influence of low and high side task workload on subject FP's velocity error variance with $Y_c = K/s^2$ (Fig. IV-8). With the exception, however, of the preferred flight director ($T_L = 3$ sec) configuration, FP's velocity error coherence was about 0.2 point lower in replications of the primary task with the higher secondary task workload.

Subject FP's tracking error variance and coherence (or relative remnant) are more sensitive to display configuration with controlled element $Y_c = K/s^2$ (Fig. IV-8) than with $Y_c = K/s$ (Fig. IV-7).

Relative remnant, although sensitive to display content with $Y_c = K/s^2$ (Fig. IV-8) where lead equalization is required, is more sensitive to change in the pilots' gain equalization technique than to display format (Figs. IV-7, 8).

Pilots: ○ PB, □ FP ; Replications Tagged ; $Y_c = K/s^2$; (710528)



Averaged over the entire 100sec run duration

Selected runs averaged over the 100sec run in serial segments of 25sec

Figure IV-8. Velocity Error Performance with Pitch AFCS

The lowest tracking error variance and the lowest relative remnant with $Y_C = K/s^2$ were achieved with a properly equalized flight director having $T_L = 3$ sec (Fig. IV-8). This value of T_L agreed closely with the predicted best value, $T_L = 3.3$ sec.

The lowest tracking error variance with $Y_C = K/s$ was achieved with a flight director display by both subjects (Fig. IV-7); however, the lowest relative remnant with $Y_C = K/s$ was achieved without a flight director by subject PB, because his describing function shows that he chose to adopt a lower gain equalization technique with S and S + R. (Fig. IV-12).

The mean errors and root-mean-square errors from trimmed values of other motion variables and control displacements, shown for selected runs in Figs. IV-9 and 10, are more sensitive to piloting technique than to display configuration. The FD, however, does help to achieve the lowest RMS longitudinal displacement error.

The secondary task errors shown for selected runs in Fig. IV-11 are not sensitive to primary display configuration with either controlled element.

Since most of the trends in the measures of performance presented here can be "explained" by the trends in the subjects' adopted describing function gains, we shall defer the discussion of performance until the describing functions themselves have been presented.

I. DESCRIBING FUNCTIONS

The amplitude and phase angle of both open-and closed-loop describing functions were computed from the measurements by the Fourier analyzer (DFA) at each of the five input frequencies. The extended crossover model (Ref. 10) provided a good representation of the open-loop describing functions ($Y_p Y_c$) in the neighborhood of the unit-gain crossover frequency ω_c . This parameter determines the effective closed-loop tracking bandwidth. Therefore, we have used an automatic computer-interpolation program to select appropriate values of the effective time delay, τ_{e_c} , and the low frequency lead-lag phase coefficient, α_c , for fitting the extended crossover model to the two measurements nearest ω_c . We believe that the extended crossover model parameters (ω_c ; τ_{e_c} ; α_c ; ϕ_M , and ω_u), fitted in this simple way adequately represent the dominant describing function properties for the purposes of display evaluation.

Pilots: \odot PB., \square FP ; Replications Tagged ; $Y_c = K/s$; (710527)

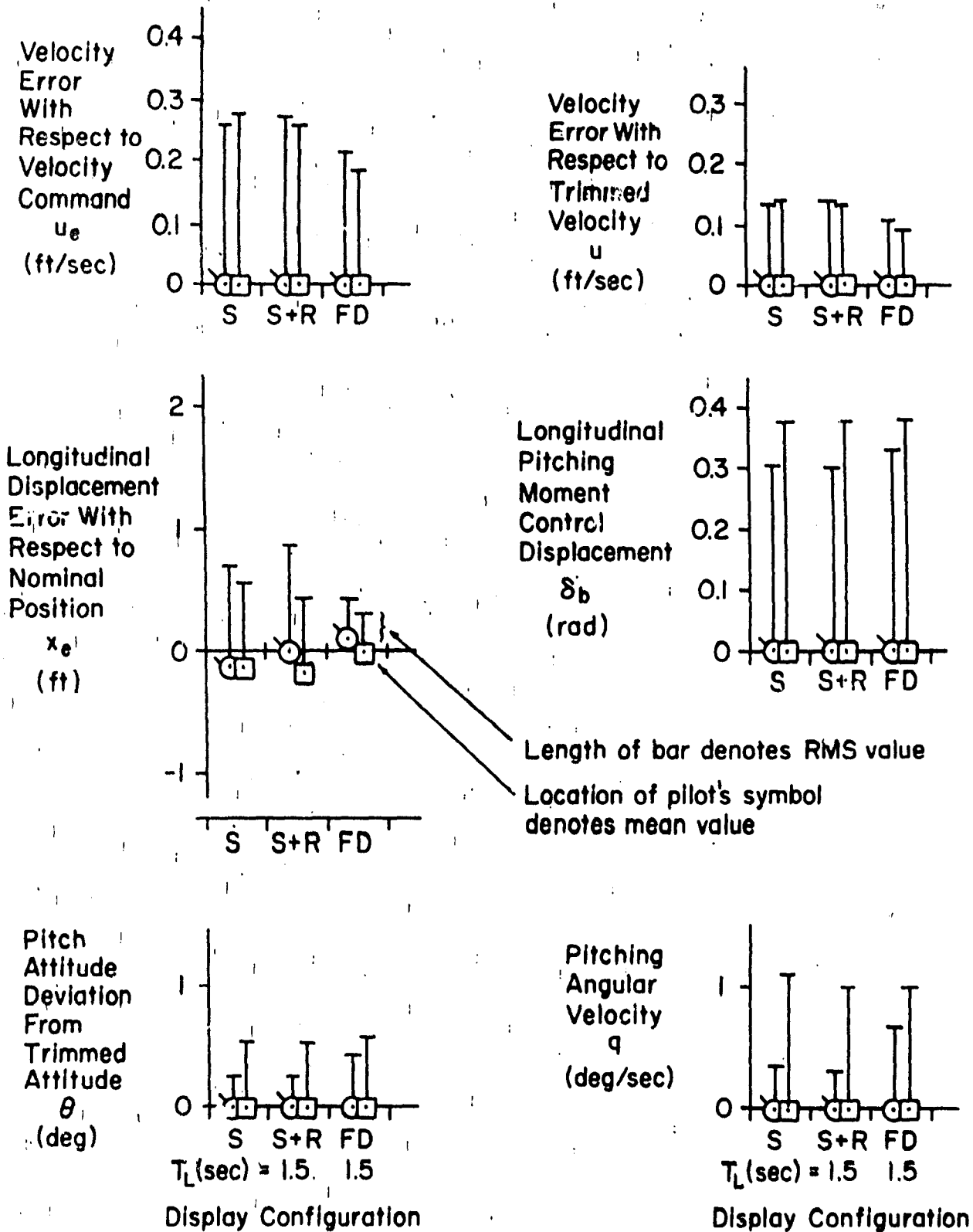


Figure IV-9. Selected Runs Showing Mean Errors and Root-Mean-Squared Errors for Primary Task Motion Variables with Velocity AFCS

Pilots: \odot PB, \square FP ; Replications Tagged ; $Y_c = K/s^2$; (710528)

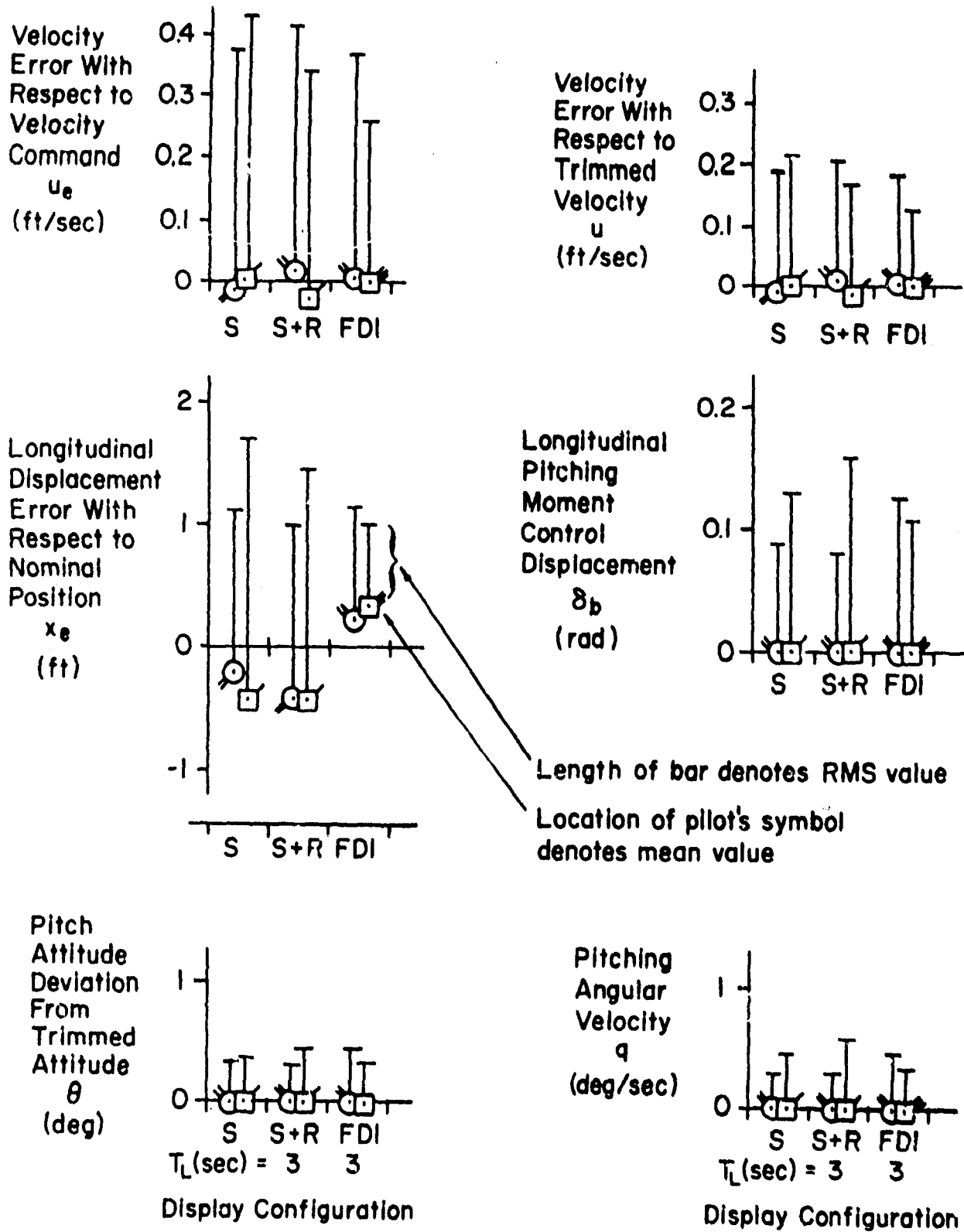
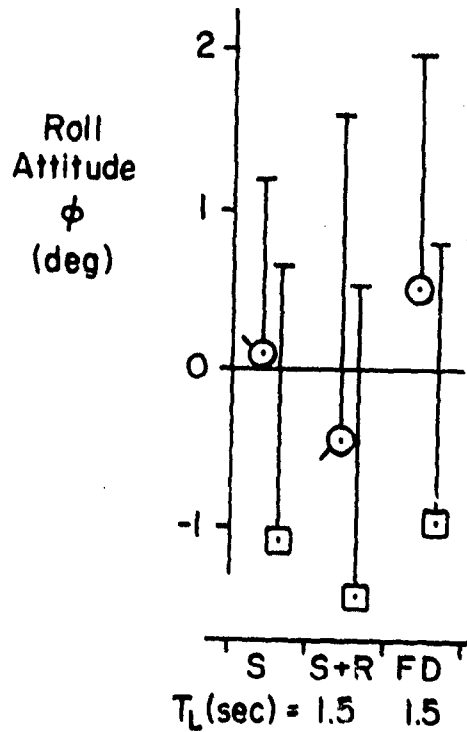
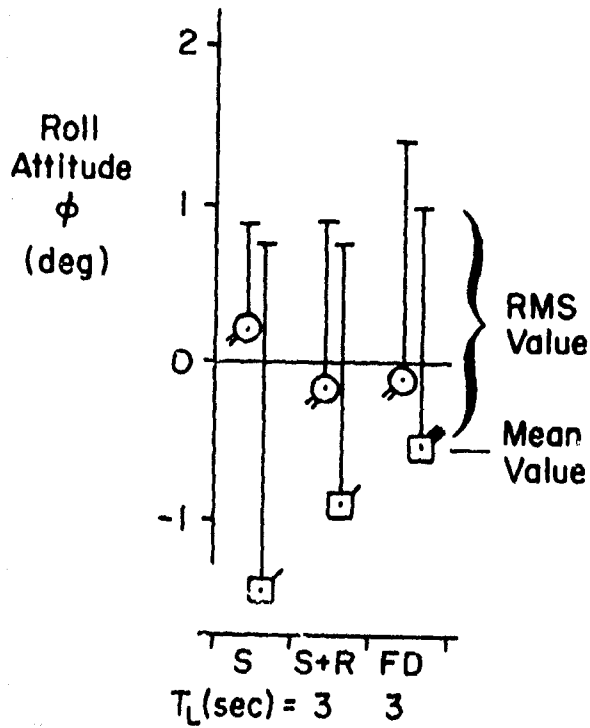
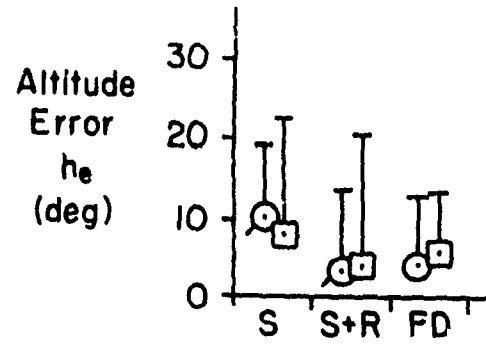
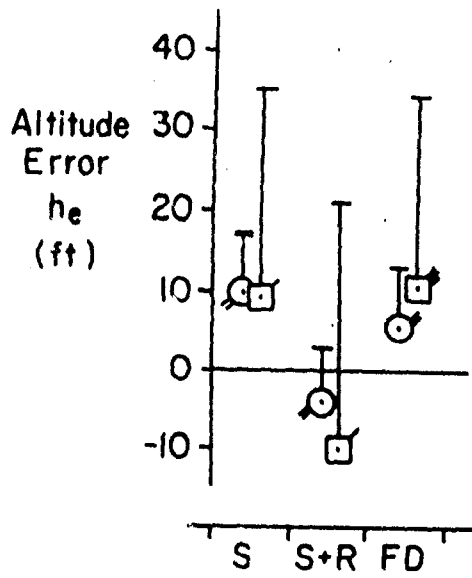


Figure IV-10. Selected Runs at High Workload Showing Mean Errors and Root-Mean-Squared Errors for Primary Task Motion Variables with Pitch AFCS

Pilots: ○ PB, □ FP ; Replications Tagged



Primary Display Configuration
 Primary $Y_c = K/s^2$
 (710528)

Primary Display Configuration
 Primary $Y_c = K/s$
 (710527)

Figure IV-11. Selected Runs Showing Mean Errors and Root-Mean-Squared Errors for Secondary Task Displayed Motion Variables

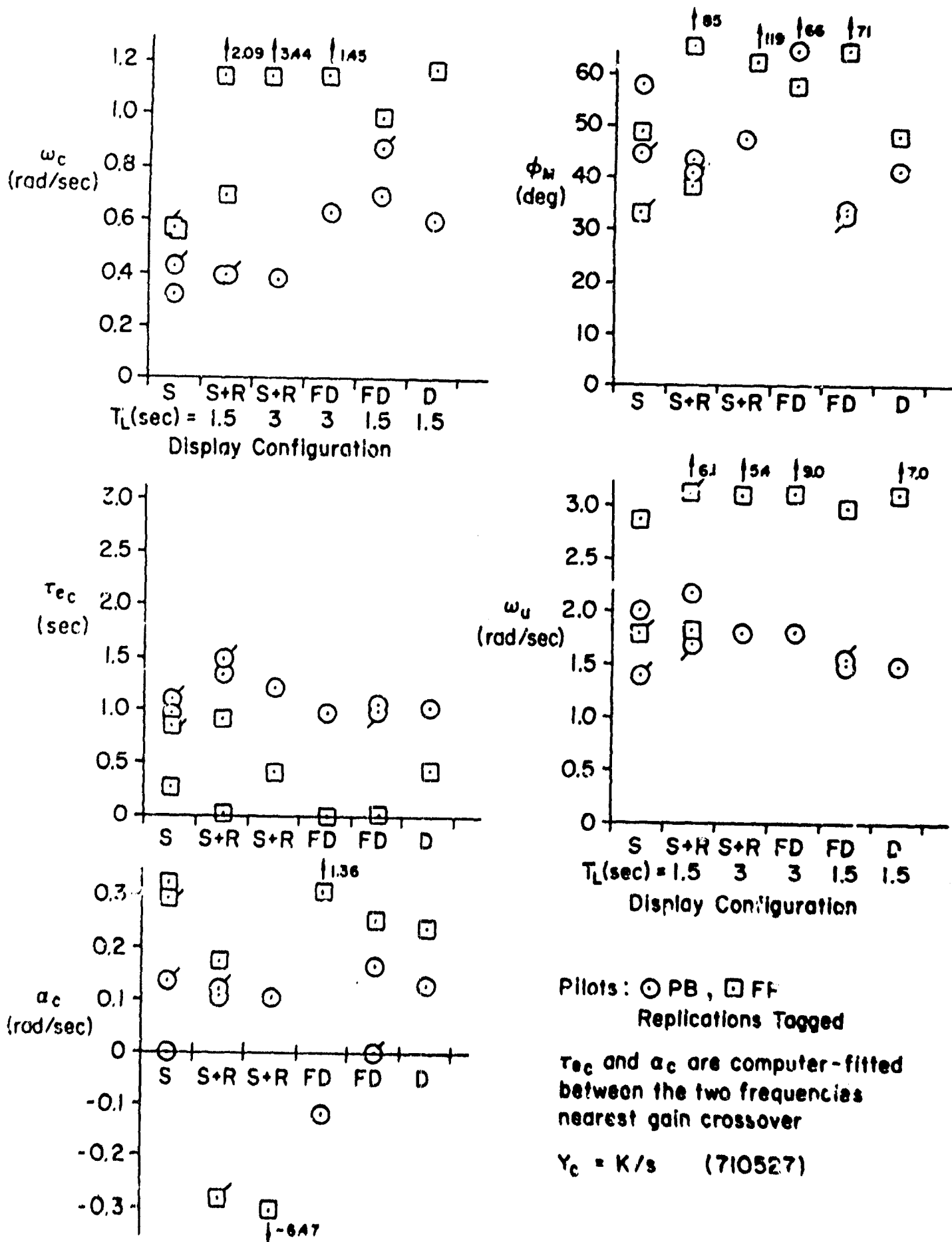


Figure IV-12. Crossover Describing Function Parameters with Velocity AFCA

1. Observations on the Open-Loop Crossover Model Parameters for $Y_p Y_c$ with $Y_c = K/s$.

The computed parameters are shown as a function of the primary display configuration in Fig. IV-12. The measured range of adopted crossover frequencies with the S format and $Y_c = \frac{K}{s}$ was $0.32 \leq \omega_c \leq 0.57 \frac{\text{rad}}{\text{sec}}$. The predicted value was $0.4 \frac{\text{rad}}{\text{sec}}$.

The measured range of adopted crossover frequencies with the preferred director ($T_L = 1.5 \text{ sec}$) for $Y_c = \frac{K}{s}$ was $0.7 \leq \omega_c \leq 1.0 \frac{\text{rad}}{\text{sec}}$. This higher gain explains the lower velocity error coherence and normalized variance with $FD(T_L = 1.5 \text{ sec})$ in Fig. IV-7.

Subject PB's piloting technique was more consistent than FP's technique. Subject FP adopted very high crossover frequencies with the error rate display configurations (S + R, FD) by taking advantage of the higher frequency (circa $2 \frac{\text{rad}}{\text{sec}}$) second order lead equalization inherently provided by this controlled element. FP's technique is reflected in lower effective time delays, higher phase margins, and higher unstable frequencies than those recorded for PB.

The trends in adopted crossover frequency among display configurations and between subjects "explain" the comparable trends in normalized error variance and coherence shown previously in Figs. IV-7 and 8.

2. Observations on the Open-Loop Crossover Model Parameters for $Y_p Y_c$ with $Y_c = K/s^2$.

The computed parameters are shown as a function of the primary display configuration in Fig. IV-13. The measured range of adopted crossover frequencies with the S format and $Y_c = \frac{K}{s^2}$ was $0.32 \leq \omega_c \leq 0.43 \frac{\text{rad}}{\text{sec}}$. This agreed well with the predicted value of $0.4 \frac{\text{rad}}{\text{sec}}$.

The measured range of adopted crossover frequencies with the preferred director ($T_L = 3 \text{ sec}$) for $Y_c = \frac{K}{s^2}$ was $0.43 \leq \omega_c \leq 0.58 \frac{\text{rad}}{\text{sec}}$. This agreed well with the predicted value of $0.5 \frac{\text{rad}}{\text{sec}}$.

The measured range of adopted crossover frequencies with the S + R format and $Y_c = \frac{K}{s^2}$ was $0.35 \leq \omega_c \leq 0.62 \frac{\text{rad}}{\text{sec}}$.

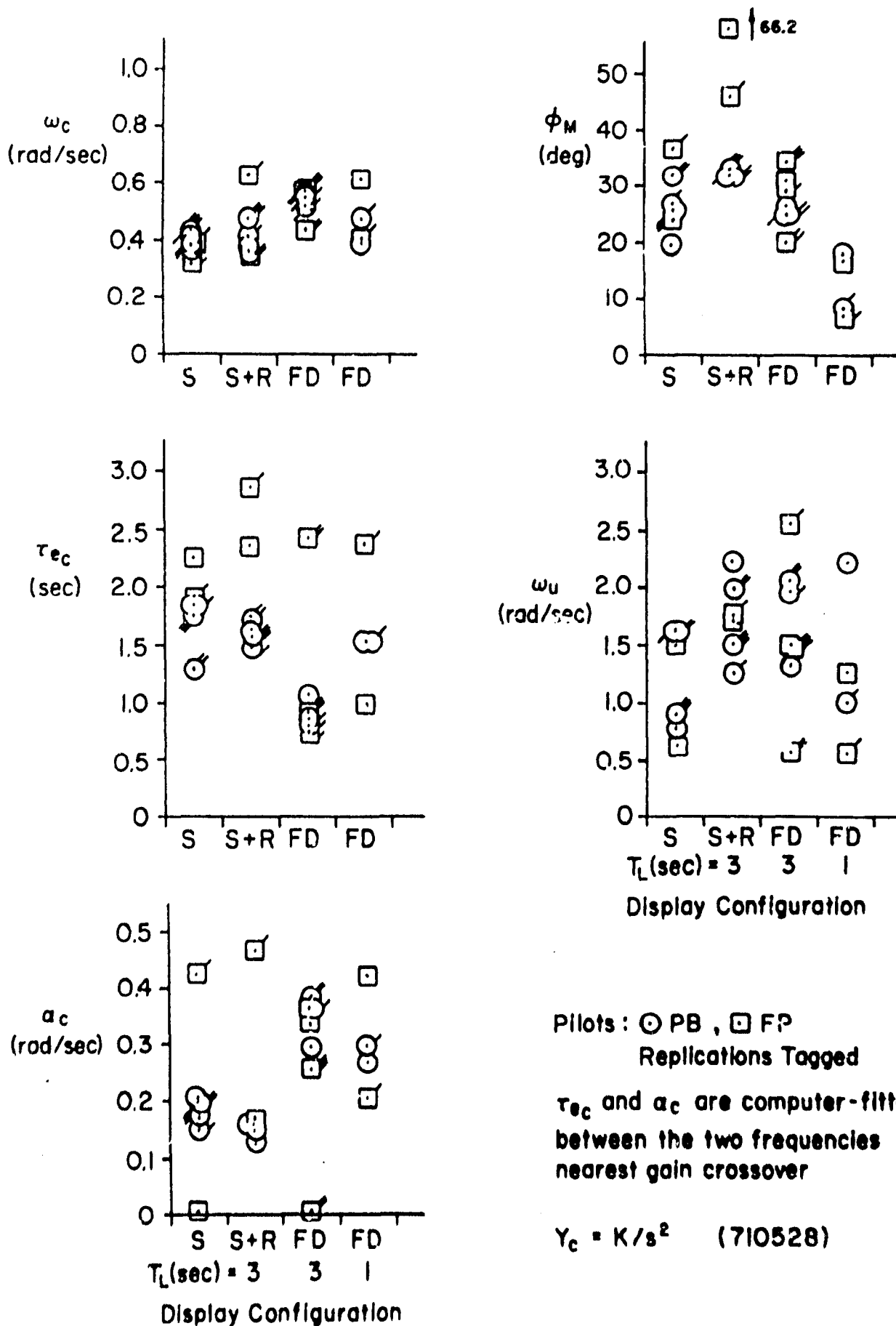


Figure IV-13. Crossover Describing Function Parameters with Pitch AFCS

The measured phase margins were between 20 and 36 deg for the S and FD($T_L = 3$ sec) formats. Predicted crossover frequencies were based on phase margins of 36 deg for the state format and 35 deg for the director. The measured phase margins were greatest with the state-and-rate format ($31^\circ \leq \phi_m < 66^\circ$).

The effective time delays for subject FP were greater than for subject PB except with display FD($T_L = 3$ sec). The effective time delays were roughly comparable between the S and the S + R formats and appreciably lower with the preferred FD($T_L = 3$ sec) format. The result with the preferred director would be expected, since Fig. IV-14 shows that the pilots did not have to adopt low frequency lead equalization with its consequent incremental time delay to get the results displayed in Fig. IV-9. The results for the state-and-rate format suggest that explicit presentation of the rate symbol integrated with the position error symbol did not reduce the effective time delay accompanying the adoption of lead equalization by the pilots, although it did reduce the scanning workload required for monitoring speed variations, as the EPR measurements will show. An hypothesis for the state-and-rate result is advanced in Ref. 4.

The effective low frequency phase approximator coefficients, G_c , for pilot PB are less variable than for pilot FP. Those for PB are roughly comparable between the state and the state-and-rate formats and appreciably higher with the best director. This result reflects the difference between the lead-lag equalization supplied by the pilot with the state and the state-and-rate formats and the similar type of equalization supplied by the effective controlled element with the preferred flight director display. The preferred range of pitch attitude feedback gains to the flight director shown in Figs. IV-14 and 15 was chosen by the pilots based on the relatively low rate of director null axis-crossing required to maintain tight pitch attitude control while performing the primary task. The preferred range of K_θ/K_{x_e} includes the value -62.5 ft, which was predicted.

The measured phase crossover (unstable) frequencies showed great variability among all display configurations, subjects and replications. Their range was lowest with the state format (Figs. IV-6 and 7).

J. EYE-POINT-OF-REGARD MEASUREMENTS

All of the EPR data were obtained with $Y_c = \frac{K}{s^2}$ for the longitudinal

Pilots: ○ PB, □ FP; Replications Tagged

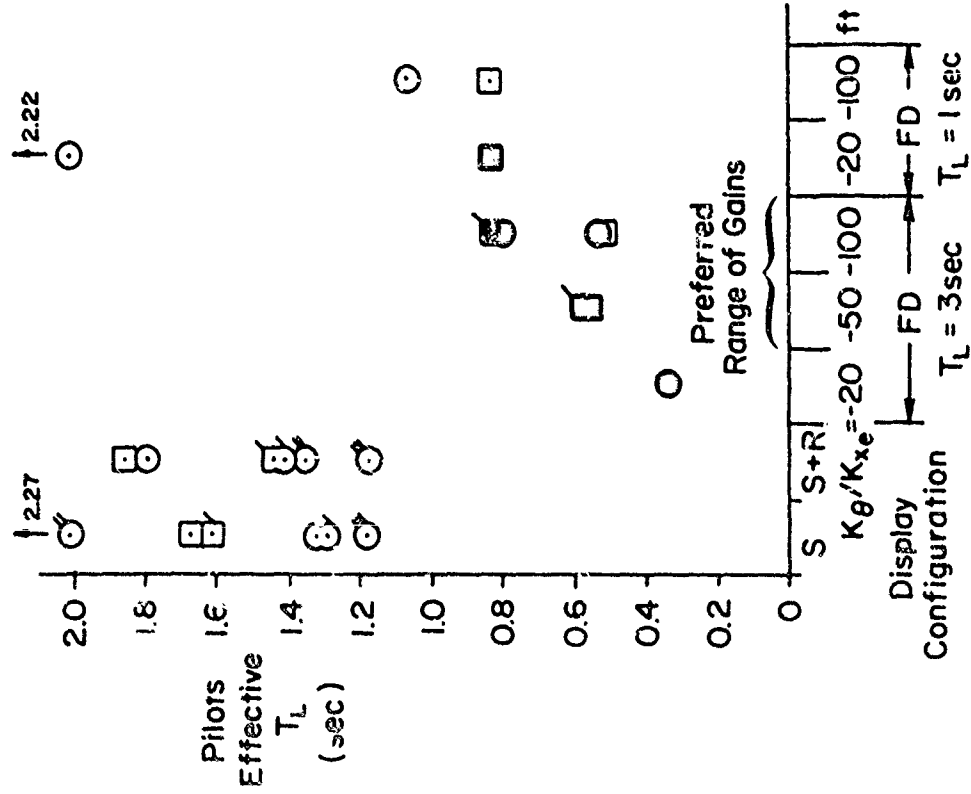


Figure IV-14. Pilots' Contributions to Effective Lead Equalization with Pitch AFCS $Y_C = K/s^2$

○ - First Order Lead
 □ - Second Order Lead

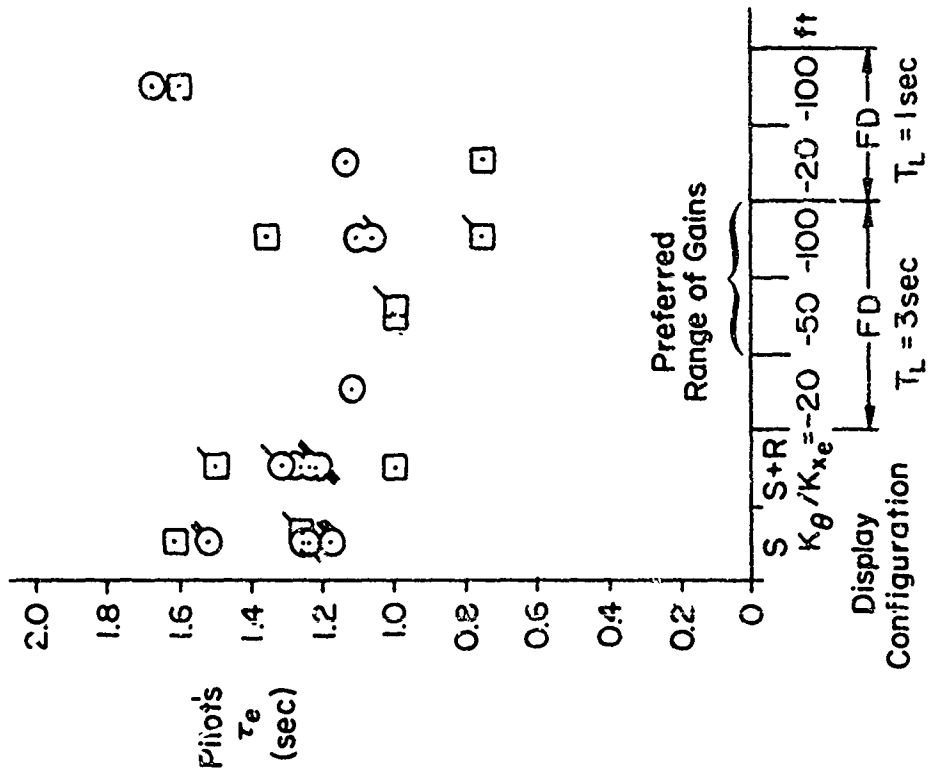


Figure IV-15. Pilots' Contributions to Effective Time Delay with Pitch AFCS $Y_C = K/s^2$

station-keeping task. However, two levels of workload were established for the altitude-keeping task in order to determine the effects of a more and a less demanding secondary task on the EPR measurements and pilot ratings. Some effects of secondary task workload, subjects, and display configuration on the EPR are illustrated in Figs. IV-16 and 17.

Figure IV-16 presents examples of the time histories of the EPR on each display format for both subjects at the two levels of secondary workload. Figure IV-17 compares some of the average fixation sampling intervals and dwell times which have been estimated from the EPR data at the two levels of workload. A complete summary of average scanning properties with high workload is presented in Fig. IV-18 and with lower workload, in Figs. IV-19 and 20.

Before we discuss and interpret some of the EPR data in the light of pre-experimental predictions, we shall offer a concise summary of observations from the EPR data presented in Figs. IV-17 through 20 in terms of the most notable effects of workload, subject pilots, and display configurations.

1. Concise Summary of EPR Observations from Figures IV-16 through 20

a. Workload -

- More blinking (spikes in traces) with the lower workload condition (Fig. IV-16)
- Higher, more regular scan rate for the higher workload condition (Figs. IV-16 and 18)
- Monitoring workload margins were measurably reduced by the state-and-rate and director formats for the lower workload condition (Fig. IV-19)

b. Pilots -

- PB has a lower scan rate, a higher side task dwell, and a more regular scan pattern than FP (Figs. IV-17, 18 and 19)
- FP did more monitoring than PB (Fig. IV-19)

c. Displays -

- Definite scanning within the CRT for flight director display (Fig. IV-16) (looking between FD and x_e symbols) with about equally partitioned dwells of about 0.5 sec for the lower workload condition. (Fig. IV-20)

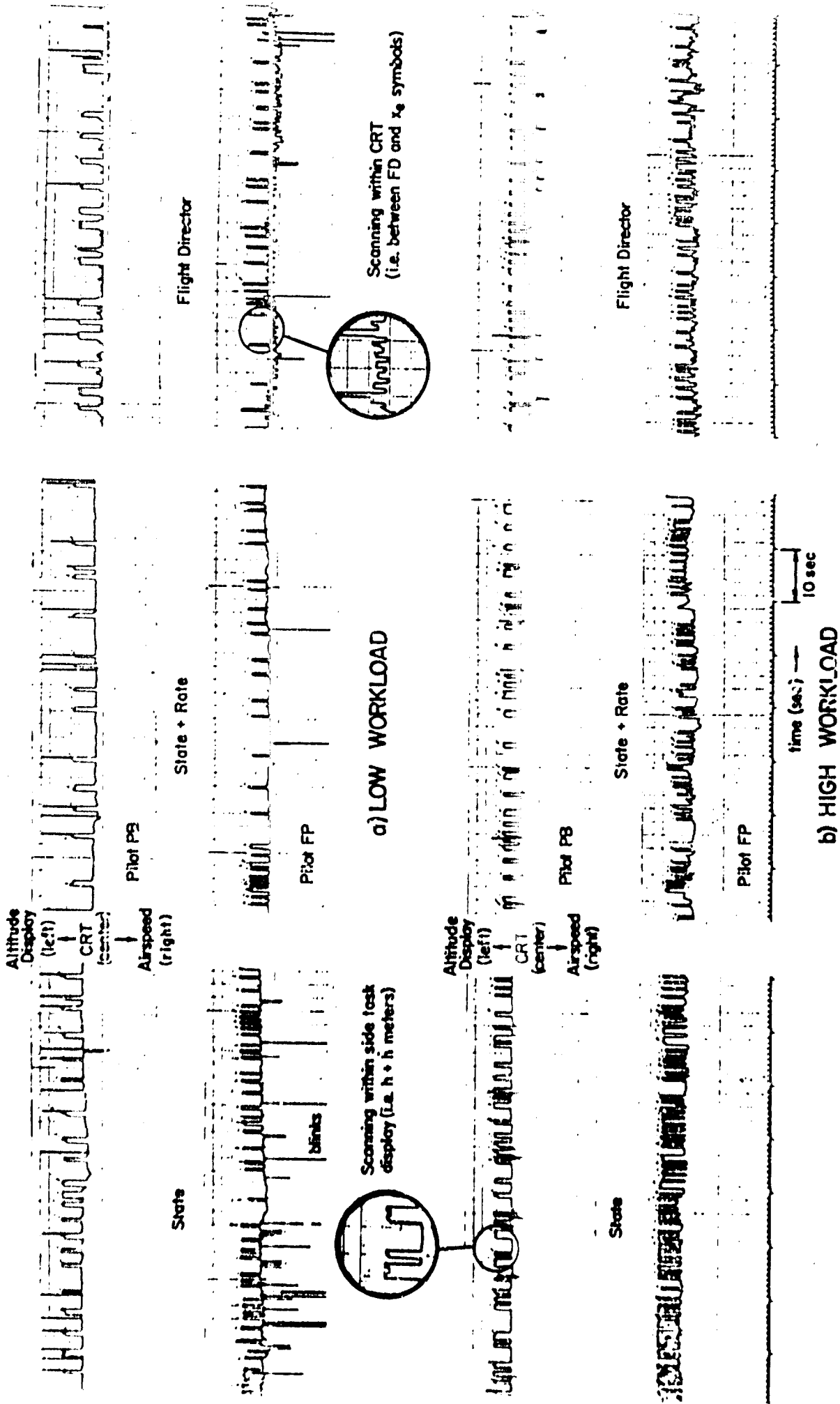


Figure IV-16. Horizontal EPR Time Traces on Two Pilots for Various Experimental Conditions

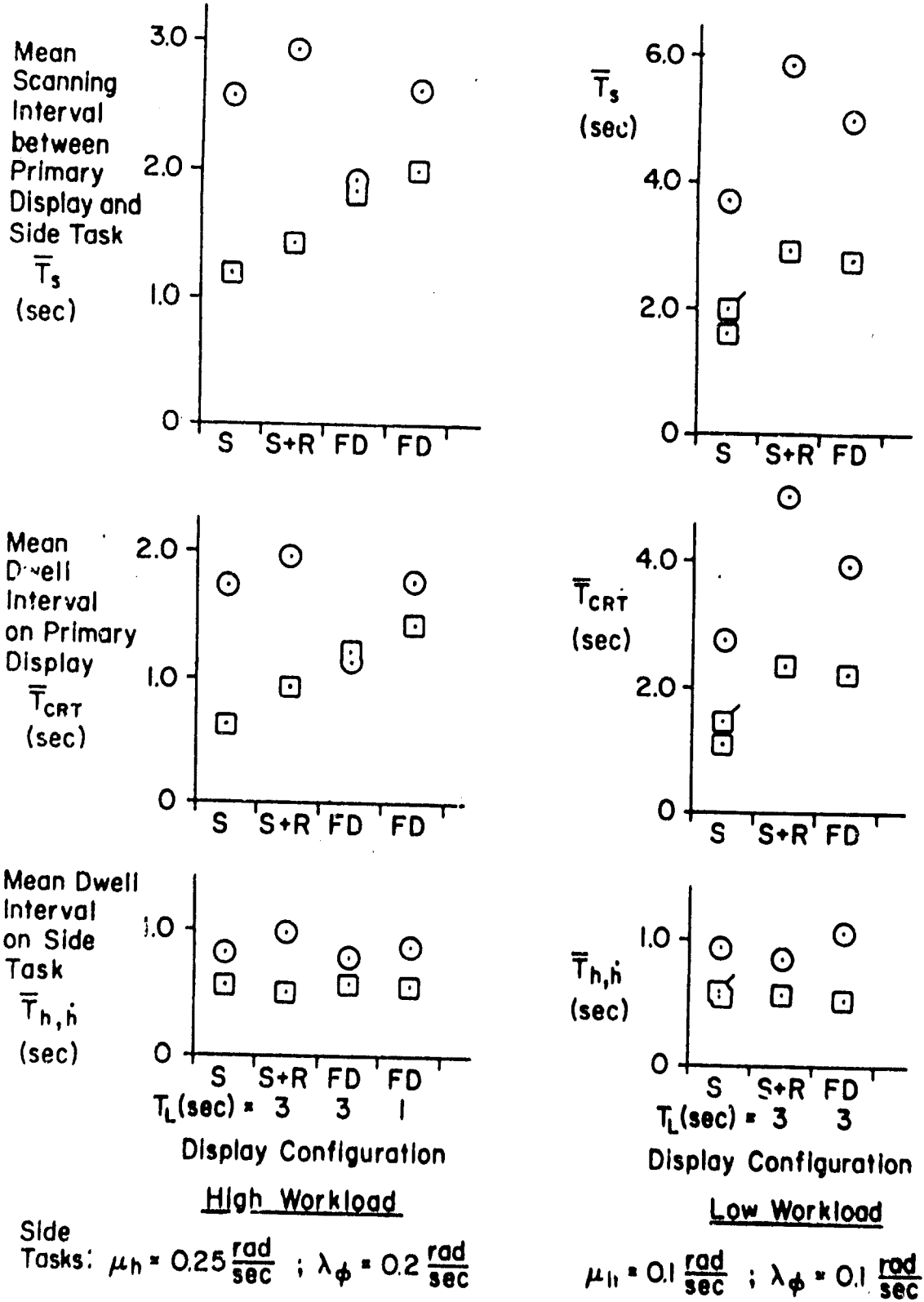
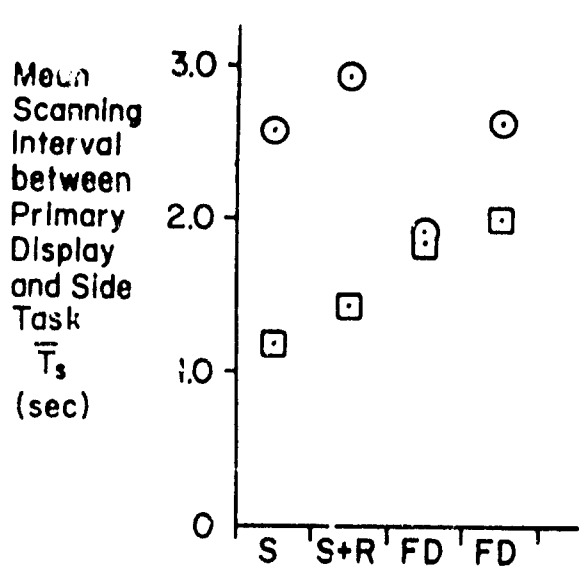
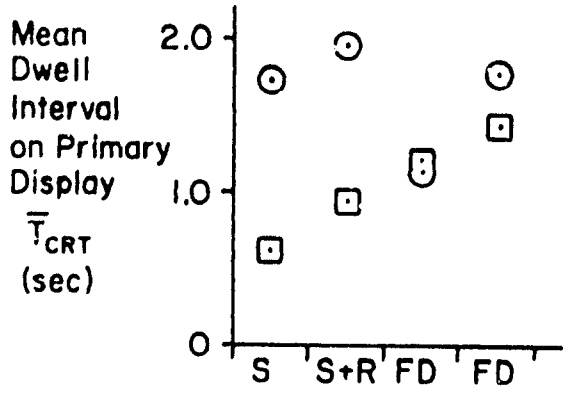
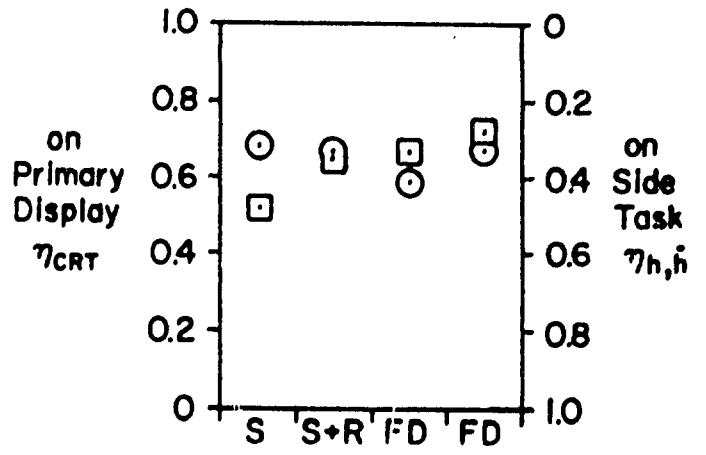


Figure IV-17. EPR Dwell Times and Scanning Intervals on Two Pilots for Various Experimental Conditions



Look Fractions $\nu_{CRT} = \nu_{h,h} = 0.5$
 Dwell Fractions $\eta_{CRT} = 1 - \eta_{h,h}$



Airspeed was not monitored by either pilot during each 100sec run for record

Pilots : \odot PB, \square FP

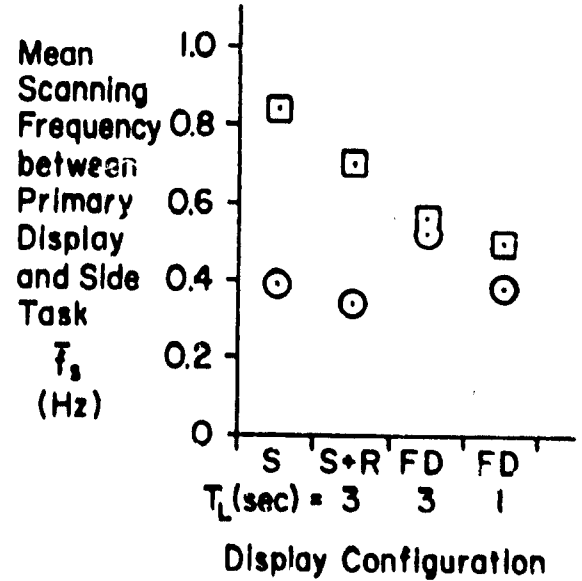
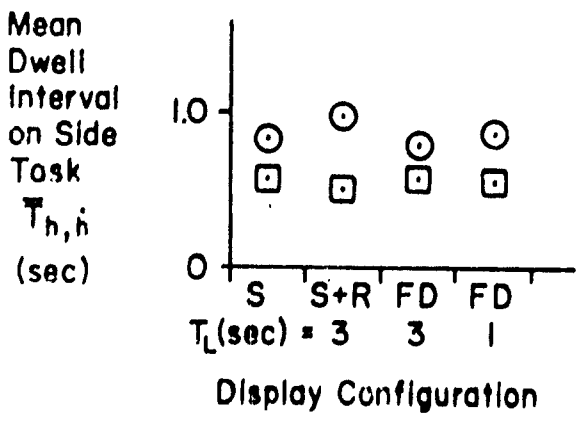
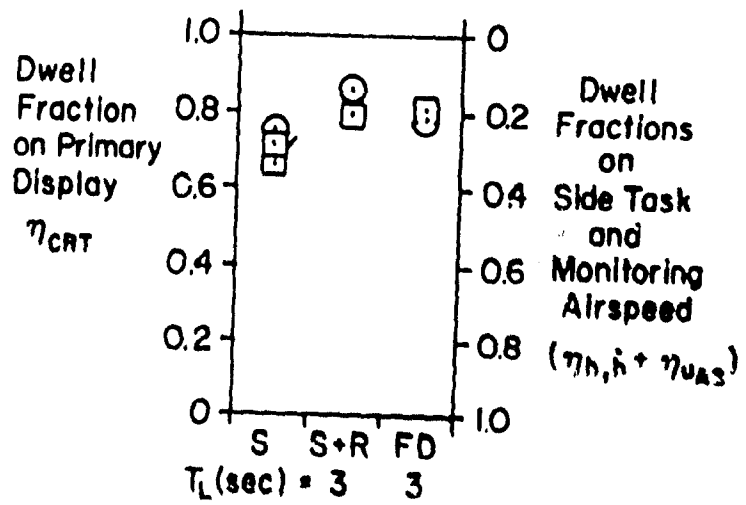
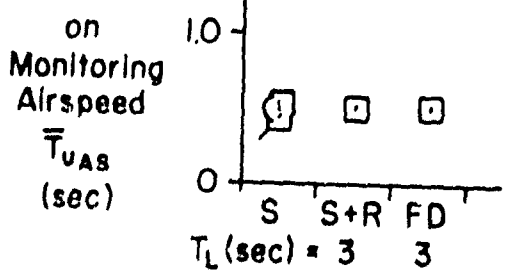
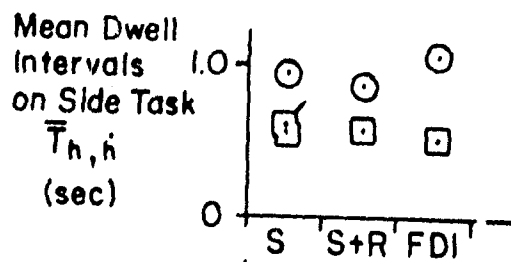
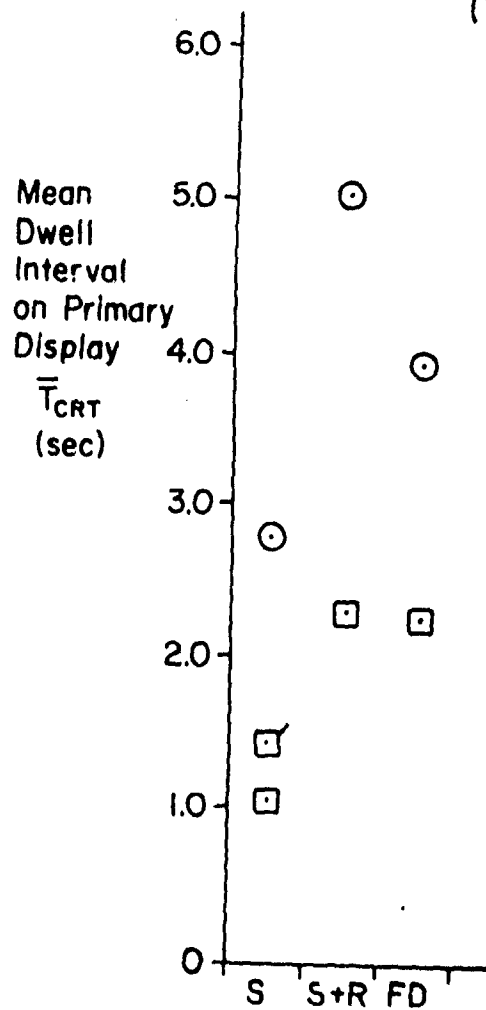
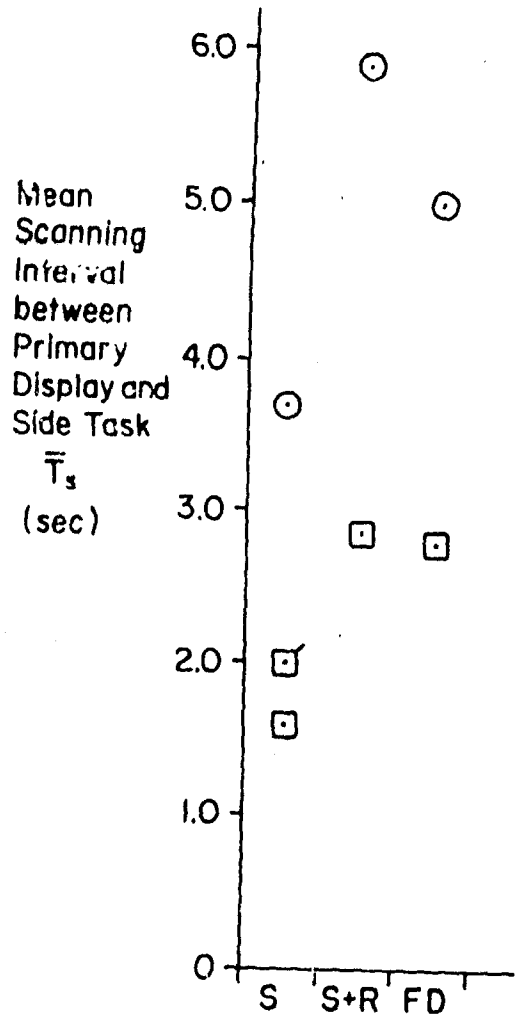


Figure IV-18. More Demanding Side Tasks:
 $\mu_h = 0.25$ rad/sec; $\lambda_p = 0.2$ rad/sec
 Summary of Average Scanning Behavior
 with Pitch APCS
 $\gamma_c = K/s^2$ (710528)

Pilots: \odot PB, \square FP ; Replications Tagged

$Y_c = K/s^2$
(710528)



Display Configuration

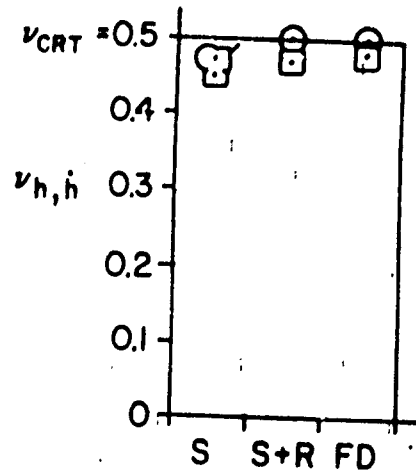
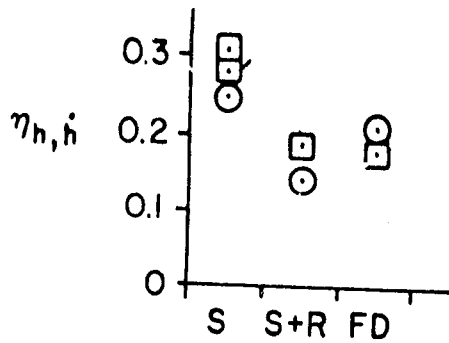
Display Configuration

Figure IV-19. Less Demanding Side Tasks:
 $\mu_n = 0.1$ rad/sec; $\lambda_p = 0.1$ rad/sec
Summary of Average Scanning Behavior
with Pitch AFCS

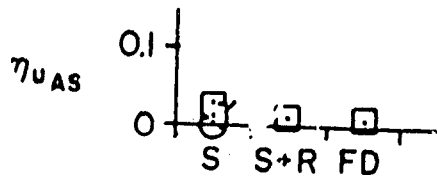
Pilots: ○ PB, □ FP;
Replications Tagged

Look Fractions
on Primary Display
and Side Task

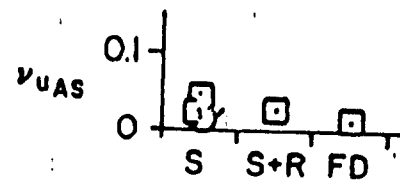
Dwell Fraction
on Side Task



Dwell Fraction
on Monitoring Airspeed

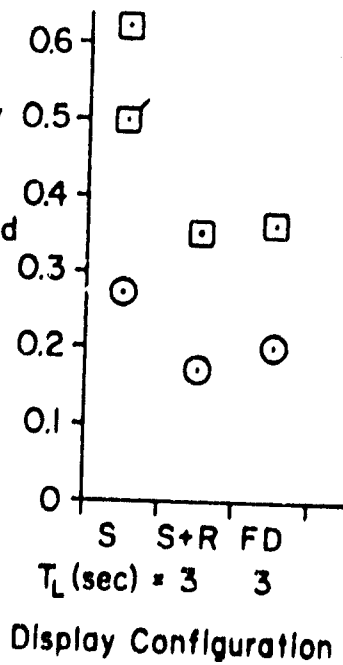


Look Fraction
on Monitoring Airspeed



Mean Scanning
Frequency
between
Primary
Display and
Side Task

\bar{f}_s
(Hz)



Mean Scanning Frequency
on Monitoring Airspeed

\bar{f}_{UAS}
(Hz)

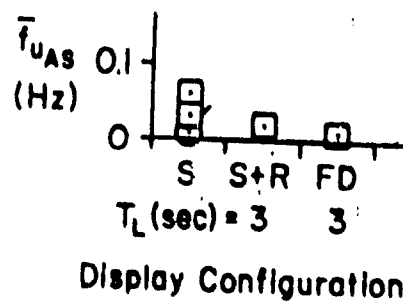


Figure IV-19 Concluded

Run No. 710528-	-9	-14
Pilot	□ FP	○ PB
Average Internal Scanning Frequency on CRT (Hz)	1.11	1.07
Average Internal Scanning Interval on CRT (sec)	0.9	0.935
Average Internal Dwell Interval on FD Symbol (sec)	0.487	0.455
Average Internal Dwell Interval on X _e Symbol (sec)	0.413	0.48

Less Demanding Side Tasks

$$\mu_h = 0.1 \frac{\text{rad}}{\text{sec}} ; \lambda_\phi = 0.1 \frac{\text{rad}}{\text{sec}}$$

$$(Y_{c, \text{eff}} = K/s) \quad Y_c = K/s^2$$

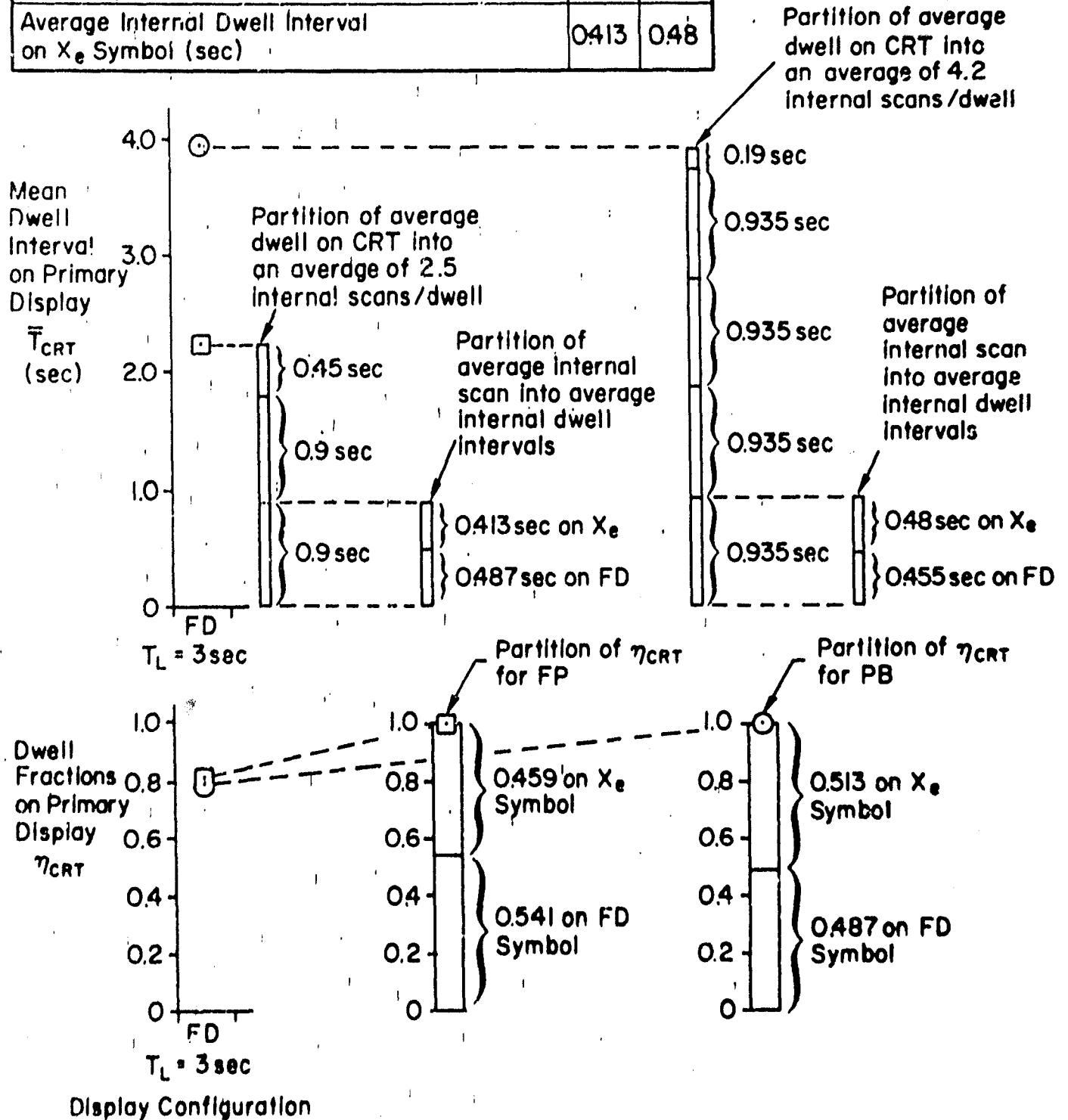


Figure IV-20. Partition of EPR Dwell Times on the Primary Display Between Flight Director and Displacement Error Symbols

- Definite scanning between h_e and h displays (Fig. IV-16)
- Scanning Behavior similar between pilots for low workload condition (Figs. IV-17, 19 and 20)
- CRT dwell time trends quite different between pilots under high workload (Fig. IV-17)
- Fairly constant side task dwell times over all display and workload conditions (as noted in previous research, e.g. Ref. 9) (Fig. IV-17)

2. Discussion of EPR Results

The airspeed indicator was not monitored by either subject with the more demanding altitude-keeping task. However, even with the less demanding side task (Fig. IV-19), the lock fractions on the CRT and the side task are nearly 0.5 each, so that very little monitoring of the circular airspeed indicator and altimeter occurred with the state format. (More monitoring fractions were predicted than occurred.) The monitoring fractions were reduced further with the state-and-rate and director formats. Monitoring dwell intervals and side task dwell intervals were seldom less than 0.5 sec.

The altitude control side task dwell fraction agreed well with the predicted value 0.57 under conditions of high workload in Fig. IV-18. Dwell fractions on the CRT under conditions of high side task workload were slightly greater than the predicted value (0.57) by the amount (0.06) predicted for monitoring airspeed and altitude.

Under conditions of high workload in Fig. IV-18, subject PB's scanning frequency on the CRT for the state format (0.39 Hz) agreed well with the predicted value (0.4 Hz). FP's scanning frequency, however, on the same format (0.84 Hz) was over twice the predicted value.

In an effort to coalesce the effects of the several scanning variables, we have computed a unifying parameter combination which appears in several derivations for finite-dwell sampling and is termed the "Scanning Frequency Parameter" S : (Ref. 9 and 18)

$$S = \frac{\omega_B}{\omega_C(1 - \eta)}$$

where: ω_B/ω_C = ratio of scanning-to-crossover frequencies

$\eta = \frac{T_d}{T_B}$ = dwell fraction

If we denote the average nonfixated period by $\bar{T}_\Delta = \bar{T}_s - \bar{T}_c$, and the crossover period as $P_c = 2\pi/\omega_c$, algebraic manipulation of the above expression gives the simpler expression: $S = P_c/\bar{T}_\Delta$. This suggests a simple physical meaning for S, as the ratio of the crossover period relative to the time-away from the display. This ratio should be large to minimize scanning remnant effects. The results of this computation of S are shown in Fig. IV-21. Subject PB's normalized scanning frequency parameter, S, was closely bounded ($14 < S < 18$) for all display configurations at high workload, whereas FP's measured values of S ranged between 19 and 35, when the dwell fraction on the CRT, n_{CRT} , was used in the computation of S.

Scanning among symbols on the CRT (called "internal CRT scanning," for short, in Fig. IV-20), however, is evident with both low and high side task workload. [Winblade (Ref. 28) also noted scanning among CRT symbols on an integrated vertical situation display in previous research.] When scanning among CRT symbols with lower workload is accounted for by using manual control theory together with the simplest of describing function measurements (exemplified by the crossover model, the partitioned scanning frequency parameter, S, for the preferred flight director ($T_L = 3$ sec) with $Y_c = K/s^2$ becomes very nearly the same value for both subjects, whereas S exhibits a two-fold difference if otherwise based on CRT scanning as a whole (Fig. IV-21). This finding is consistent with the close agreement between coherence (Fig. IV-8) and crossover frequency (Fig. IV-13) for both subjects with the same flight director and $Y_c = K/s^2$.

Velocity error coherence of subject FP (≤ 0.43) in Fig. IV-8 was much lower than predicted (0.75) with $Y_c = K/s^2$ for the state format. Since the normalized eye scanning measurements ($S = 35$) for subject FP with the state format agreed quite well with predictions ($S = 39$), another significant source of remnant such as non-stationarity may have been present. The difference between whole run length average coherence and serial segment average coherence would tend to conform the presence of non-stationarity. Pilot FP's coherence increased about two-fold on the state-and-rate format and increased to a level comparable with PB's coherence ($0.8 \leq \rho_{U_e}^2 < 0.9$) on the better director format (FD: $T_L = 3$ sec).

Velocity error coherence of subject PB was about equal to that predicted (0.75) for the state format with $Y_c = K/s^2$. However, EPR measurements (summarized separately) for subject PB with the state format showed a consistently

Pilots: \odot PB, \square FP ; Replications Tagged

$\omega_s = 2\pi \bar{f}_s =$ Scanning frequency on primary display

$\omega_c =$ Crossover frequency for longitudinal separation control loop

$(1-\eta_{CRT}) =$ Scan interrupt fraction on primary display

$(1-\eta_{FD}) =$ Scan interrupt fraction on flight director within primary display.

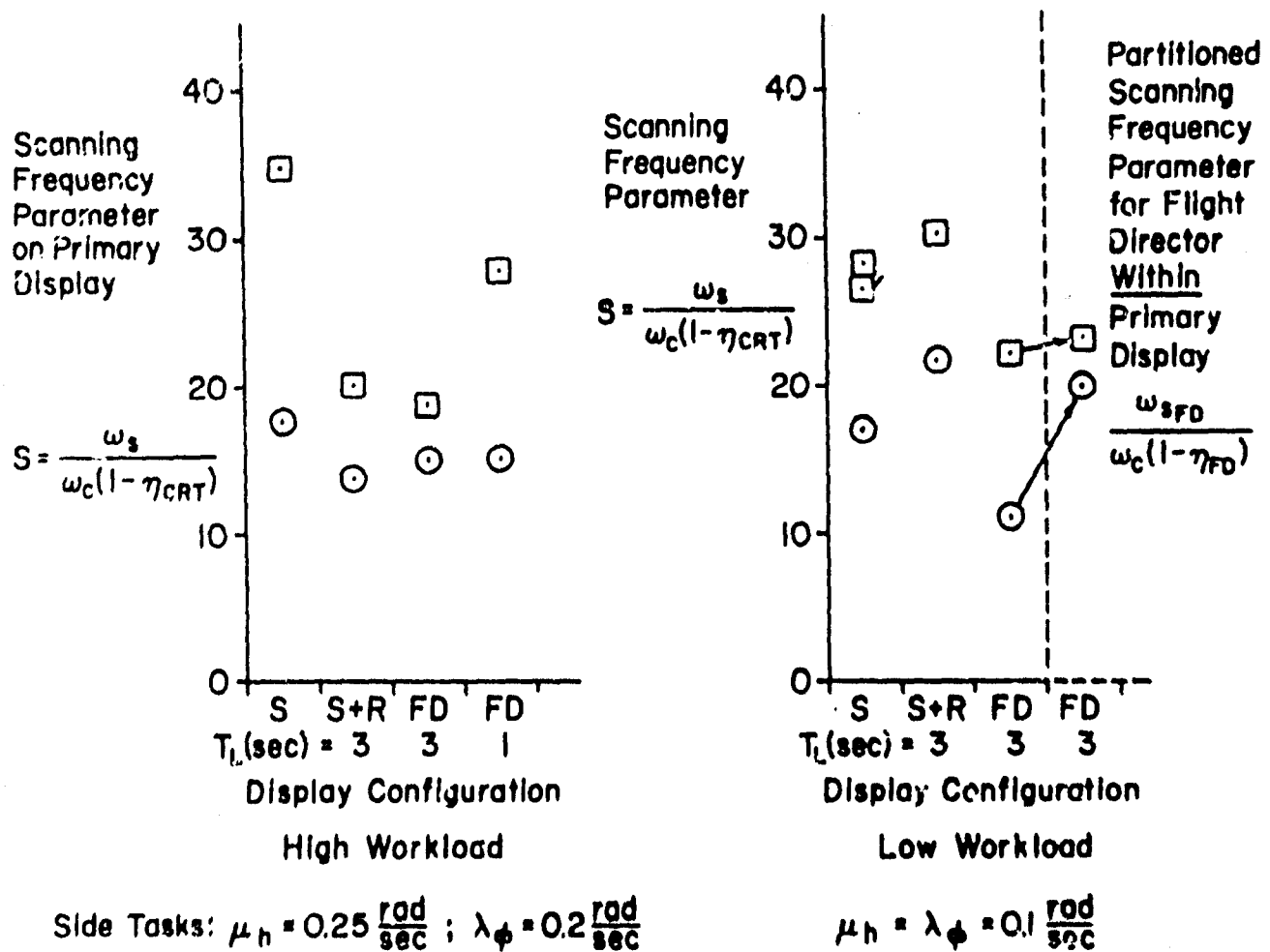


Figure IV-21. Scanning Frequency Parameter as a Function of Display Configuration

lower foveal scanning frequency parameter ($S_f \leq 18$) than the effective value predicted ($S_e = 39$) to achieve the coherence of 0.75. This roughly two-fold difference in S can be attributed to the two-fold difference between the measured (foveal) and predicted (effective) interrupt fractions on the primary display (CRT). (Measured $1 - \eta_{CRT} = 0.32$; predicted $1 - \eta_e = 0.16$ to achieve coherence of 0.75 which actually approximately agreed with the measured coherence.) This difference is quite consistent with that attributable to the effects of parafoveal viewing. In fact, an estimate of PB's average parafoveal-to-foveal gain ratio, Ω , can be inferred from the relationship (Ref. 2) between Ω and the two interrupt fractions

$$\Omega = \frac{\eta_e - \eta_f}{1 - \eta_f} = 1 - \frac{(1 - \eta_e)}{(1 - \eta_f)} = 0.5$$

This example shows how coherence (relative remnant), EPR, and crossover frequency measurements can be gainfully combined with manual control display theory to infer the effectiveness of a pilot's parafoveal visual ability which cannot be directly observed!

EPR measurements alone are not sufficient to serve as a measure of the quality of an integrated display. However, EPR measurements are a necessary adjunct in concert with coherence, describing function, and excess control capacity measurements to help in discovering the rationale for pilots' adopted tracking control behavior when confronted with an integrated display. Within the constraints of a precision flight control task involving high attentional workload, the integration of the displayed variables required for control and monitoring can help the pilot in two ways. First, the integration may relieve a saturated (or potentially over saturated) scanning condition. Second, the integration may help to increase the controlling scanning workload fraction by reducing the monitoring scanning workload fraction, which is, of necessity, small anyway. In either or both of these ways the integration may effect a reduction in the whole-task remnant and effective time delay with a consequent measurable increase in excess control capacity for coping with unexpected workload.

K. THE CROSS ADAPTIVE MEASURE OF EXCESS CONTROL CAPACITY AND SUBJECTIVE RATINGS OF DISPLAY QUALITY

In our first application of the cross-coupled secondary subcritical task for display evaluation, secondary scores reflecting a measure of excess control capacity have been obtained with $Y_c = \frac{K}{s}$. This is believed to be a fairly sensitive test of the cross-adaptive task for the purpose of display evaluation for two reasons. First, the controlled element did not require low frequency lead equalization with its concomitant incremental effective time delay which is known to reduce the cross adaptive measure of excess control capacity. (Vide Appendix A.) Second, the subjective pilot ratings of attentional demand in Fig. IV-22 were not sensitive to display configuration with $Y_c = \frac{K}{s}$, whereas the same ratings were more sensitive to display configuration with $Y_c = \frac{K}{s^2}$, which does require low frequency lead equalization.

The secondary scores obtained on the several primary display configurations are shown in Appendix A, Fig. 7 and described in the accompanying text of Appendix A. The results for both pilots show that the cross adaptive measure of excess control capacity appears to be a more unique measure of display quality than does relative remnant on scanning workload fraction and a more sensitive measure than subjective opinion with $Y_c = \frac{K}{s}$.

Among the other subjective display quality ratings in Fig. IV-16, the off-design flight directors ($T_L = 3$ sec with $Y_c = \frac{K}{s}$ and $T_L = 1$ sec with $Y_c = \frac{K}{s^2}$) were down rated for controllability and precision by both subjects, and the director format (D) without task error was down rated for status utility as expected. Pilot PB also recognized correctly that he had no basis for rating "precision" of the task with format D. As noted previously, attentional demand ratings were sensitive to primary display configuration with $Y_c = \frac{K}{s^2}$ and to the workload on the altitude-keeping task in predictable senses. The following table compares predicted and measured ratings for "controllability-and-precision" and "attentional demand". Other ratings by the pilots did not show distinct or unique trends with display configuration.

	State Format S		Director Format FD	
Predicted Ratings	C3	D4	C2	D3
Measured Ratings	C3 to C1	D4 to D3	C3 to C1	D3 to D2

Pilots: ○ PB, □ FP ; Replications Tagged

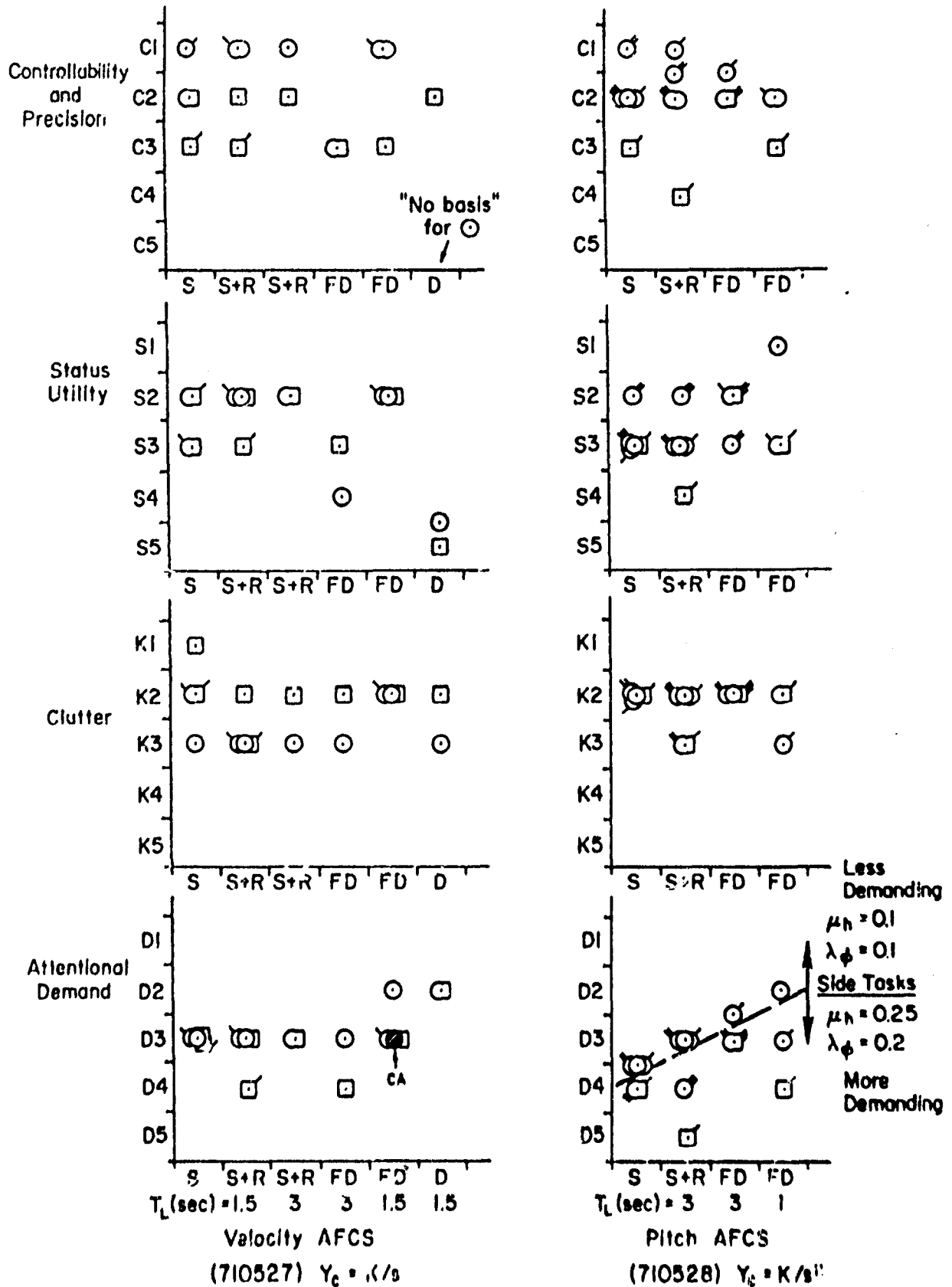


Figure IV-22. Display Qualities Ratings.

SECTION V

CONCLUSIONS AND RECOMMENDATIONS

A. CONCLUSIONS FROM THE RESEARCH AND IMPLICATIONS FOR A THEORY OF INTEGRATED DISPLAY FORMAT

The first (single-axis) experiment gave results which led to the following conclusions with respect to the various formats which were tested. The quantized format, at least with the comparatively coarse quantization which was employed in the experiments, caused an incremental effective time delay of approximately 0.1 sec under both foveal and parafoveal viewing conditions. For this reason, this type of display is not to be recommended for precision tracking tasks. Use of the vertical bar format (thermometer type) caused notably degraded performance, and the format should preferably not be employed in closed-loop tracking tasks. There were no distinctive differences in measures of pilot behavior, coherence or error scores between foveal and parafoveal tracking with the line and dial formats as long as the parafoveal viewing angle was 10 deg. At a 20 deg parafoveal viewing angle, however, these measures deteriorated. For example, a display designer might be impelled to increase the field of view of an integrated display format to improve the pilot's basis for monitoring the situation. Alternatively, the designer might want to increase the displayed field of view to reduce foveal clutter among symbols in a dense format, if the content must be preserved and the field of view scaling does not otherwise have to be in the ratio 1:1 with the real world. However, the results of the single-axis experiment imply that increasing the field of view of an integrated display format greater than about 10 deg will produce diminishing returns through the relatively greater deterioration of parafoveal tracking ability.

In connection with integrated displays for multi-axis tracking tasks (the second experiment) the theory of manual control displays has been successfully employed in designing display evaluation experiments so as to isolate the effects of the controlled element, the effects of individual pilot behavior and the difficulty of the task from the effects of the display itself. Use of the secondary cross-adaptive sub-critical tracking task, by separately identifying a measure of tracking precision from a measure of

excess control capacity, can enable one to understand some of the heretofore confounding effects caused by employing difficult controlled elements without proper equalization in display evaluation experiments. The secondary cross-adaptive measure of excess control capacity on the pilot's primary task discriminates among examples of display format and content in a sense which is predictable, because the cross-adaptive task can guarantee that the pilot will be fully occupied with relevant tracking control tasks during the workload measurement interval.

Although eye scanning patterns are relevant to workload (e.g. Vide Appendix A), the relationship is not a simple one. Since there is a minimum dwell time of about 0.4 sec for monitoring each instrument or symbol under IFR conditions, it is possible to contrive saturated conditions where the control task demands fixations by the pilot on too many instruments too often in order to maintain control. However, even without driving the pilot to his controllability limit, the interpretation of eye-point-of-regard data alone will sometimes be ambiguous if one is looking for a measure of excess control capacity. The ambiguity will arise in the interpretation of the partition of scanning workload between displays for controlling the task and for monitoring the situation. This partition of scanning workload is not uniquely related to excess control capacity because of the constraint imposed by "Parkinson's Law" for the eyeball (vide Appendix A). The partition of eye-point-of-regard statistics alone may not reflect the partition afforded by excess control capacity between the pilot's subjective confidence level in the situation and the pilot's subjective impression of the difficulty of maintaining the required performance on the task.

Measures of the pilot's remnant, although sensitive to display content where lead equalization is required, are more sensitive to changes in the pilots' gain equalization technique than to changes in display format. The cross-adaptive measure of excess control capacity appears to be a more unique and, therefore, more useful measure of display quality than does either the pilots' remnant or the eye-point-of-regard by itself.

The theory of manual control displays already embraces the ingredients for a valid theory of integrated display format founded on the comprehensive behavioral measurement techniques (coherence, describing function,

eye-point-of-regard, and excess control capacity) applied in these pilot experiments. In particular, the theory offers a new technique for discovering the suspected correlation among display format, a pilot's parafoveal visual ability, and attentional workload in whole cockpit precision flying tasks. There were four questions about an "integrated" display which were posed to us by the JANAIR Committee in 1966 when research on the theory of manual control displays was first initiated. We believe now that we have answers to these questions. The questions themselves and our proposed answers are as follows:

What is an integrated display?

It is a combined presentation to the pilot of the proper signals for controlling as well as monitoring the performance of a task. Reference 3, which is included herein as Appendix A, discusses the basis for this answer in terms of the flight director (vide pp. A-1, -2 herein). In the multiaxis tracking experiment reported in Section IV, the highest measure of excess control capacity was obtained on the properly equalized integrated flight director format, a result which also supports the proposed answer to the first question.

How may the proper signals for manual control of a task be predicted and verified?

This should be done by a combination of systems analysis theory of displays, simulation and flight test. References 1, 2, 3 and 3⁴ address the answer to the question of prediction. Reference 3, which is included herein as Appendix A, also addresses the question of verification with an example.

How is the display properly integrated?

This is done 1) by providing the pilot with sufficient excess control capacity in a multiloop display, i.e., an equalized display or a flight director, 2) by minimizing the scanning workload for monitoring the task and 3) by choosing a content allowing the pilot to satisfy all task performance requirements. This answer is also supported by results in Appendix A and by the results of excess control capacity and eye-point-of-regard measurements in the multiaxis tracking experiment reported in Section IV.

How can the display be evaluated?

This is best done by means of the secondary cross-adaptive subcritical tracking task. This task measures excess control capacity, including the effects of scanning workload and whole-task effective time delay, while the pilot maintains the required task performance. The basis for this contention is described in Appendix A.

Four simple pilot rating scales for use in research on and evaluation of manual control displays were derived and used in the pilot experiments reported on here. The scales are of interval-scale quality and will permit averaging and other standard parametric statistical analyses. The use of four trait categories: 1) task controllability-and-precision, 2) status utility, 3) clutter, and 4) attentional demand should help to separate subjective identification of these often confounded effects.

An "integrated" display does not necessarily eliminate eye scanning between symbols and improve tracking coherence, but it may very well increase the pilot's excess control capacity for coping with the unexpected. This hypothesis deserves further investigation, test, and quantification as a basis for measuring the quality of an "integrated" display, as well as a whole display panel arrangement, in a sense having practical value to problems of military and naval instrument flying.

B. RECOMMENDATIONS FOR FORMAL INTEGRATED DISPLAY EXPERIMENTS

Since it has now become clear that the systems analysis theory of manual control displays already embraces the ingredients for a valid theory of integrated display format, we recommend that the experimental data base for integrated display design calculations be increased and related to a practical common basis for evaluation, viz., excess control capacity. To this end we recommend further development and practical application of the cross-adaptive measure of excess control capacity described in Section IV and Appendix A for the purpose of formal display evaluation by employing a weighted sum of more than one "primary" task error variance. We also recommend that the subjective display quality rating scales, used in the pilot experiments reported herein, be employed in future display-related simulations to provide the data base needed to refine the scales and to provide a basis for separating the identification of the "status utility" and "clutter index" of a display as they relate to excess control capacity.

We continue to recommend with increasing confidence that anyone contemplating control-display evaluation or related research should apply the systems analysis theory of manual control displays first to establish the content, arrangement, scaling and resolution (as well as automatic

stability augmentation) for reducing scanning and lead equalization workload in the visual modality before attempting to evaluate the effects of the format, i.e., the relative number, size, type, color, contrast, and separation of symbolic elements in the displayed field of view.

A multiloop (equalized or flight director) format is recommended to provide superior excess control capacity over the "state-and-rate" format for closed-loop tracking. However, the scaling and symbolism of the "state-and-rate" format should be investigated for the acquisition of a guidance-and-control tracking reference, because the excess control capacity of the state-and-rate format for monitoring the acquisition may be relatively greater than in pure tracking.

The subtended angular field of view of the display for controlling and monitoring the primary task(s) should not exceed about ten degrees in order to take advantage of pilots' parafoveal visual ability in tracking. Within this field of view continue to use cathode ray tube line symbols for the primary task(s); limit the use of the bar format to monitoring; avoid alpha-numeric-, discrete-, or raster-quantization on the order of rms tracking signals; and avoid moving scale formats without a "command" bug for tracking. Outside this primary ten-degree field of view fixed vertical scale displays for monitoring the situation tend to reduce scanning workload by virtue of their compact width, but circular dials provide better resolution and scale length within the same vertical (diametric) dimension.

After taking into account all of the foregoing conclusions and recommendations, we further recommend the following plan for applying formal integrated display experiments to a problem of immediate operational relevance.

- Adopt recommendations for formal experiments based on the reported "pilot" experiments re:
 - (1) content for reducing scanning and lead equalization workload the visual modality
 - (2) effects of scaling, resolution, field of view and quantization.
 - (3) effects of symbol and scale format

- Use a cockpit scenario such as helicopter IFR approach with:
 - (1) three-control multiloop task
 - (2) three-color integrated display with selectable line symbols for IFR
 - (3) describing function analyzer for forcing functions, gain, phase and coherence measurements
 - (4) cross-adaptive sub-critical task for measuring the level of attentional workload
 - (5) eye-point-of-regard system for measuring foveal fixation statistics
- Investigate symbol color, contrast and clutter effects of display-related remnant
- Expected results are: definition of an integrated display for helicopter IFR approach with acceptable workload and sufficient excess control capacity.

REFERENCES

1. McRuer, D. T., H. R. Jex, W. F. Clement and D. Graham, Development of a Systems Analysis Theory of Manual Control Displays, Systems Technology, Inc., Tech. Rept. 163-1, Oct. 1967.
2. Clement, W. F. and L. G. Hofmann, A Systems Analysis of Manual Control Techniques and Display Arrangements for Instrument Landing Approaches in Helicopters Vol. I: Speed and Height Regulation, Systems Technology, Inc., Tech. Rept. 183-1, July 1969.
3. Clement, W. F., D. T. McRuer and R. H. Klein, Systematic Manual Control Display Design, Systems Technology, Inc., Paper 113, Oct. 1971.
4. Clement, W. F., Some Contemporary Examples of "Integrated" Displays for Precision Flight Control, Systems Technology, Inc., WP 183-11, June 1971.
5. Clement, W. F., "A Theory for the Human Operator's Remnant in Multiloop Display-Control Tasks," presented at Fifth Annual NASA-University Conference on Manual Control, NASA SP-215, Cambridge, Mass., March 27-29, 1969, pp. 637-654.
6. Weir, D. H., and R. H. Klein, The Measurement and Analysis of Pilot Scanning and Control Behavior During Simulated Instrument Approaches, NASA CR-1535, June 1970.
7. Dunham, R. E., Jr., R. W. Sommer, Evaluation of a Moving-Graph Instrument Display for Landing Approaches with a Helicopter, NASA TN D-6025, Oct. 1970.
8. Garren, J. R., Jr., J. R. Kelly, R. W. Sommer and D. J. DiCarlo, Flight Investigation of VTOL Control and Display Concept for Performing Decelerating Approaches to an Instrument Hover, NASA TN D-6108, Feb. 1971.
9. Allen, R. W., W. F. Clement, and H. R. Jex, Research on Display Scanning, Sampling, and Reconstruction Using Separate Main and Secondary Tracking Tasks, NASA CR-1569, July 1970.
10. McRuer, D. T., D. Graham, E. Krendel and W. Reischer, Jr., Human Pilot Dynamics in Compensatory Systems, AFFDL-TR-65-15, July 1965.
11. McRuer, D. T., D. Graham and E. S. Krendel, "Manual Control of Single-Loop Systems: Part I, and Manual Control of Single-Loop Systems: Part II," J. Franklin Inst., Vol. 283, No. 1, Jan. 1967, and No. 2, Feb. 1967.
12. McRuer, D. T., H. R. Jex, "A Review of Quasi-Linear Pilot Models," Trans. IEEE, Vol. HFE-8, No. 3, Sept. 1967, pp. 231-249.

13. McRuer, D. T. and D. H. Weir, "Theory of Manual Vehicular Control." Trans. IEEE, Vol. MMS-10, No. 4, Dec. 1969, pp. 257-291, also Ergonomics, Vol. 12, No. 4, 1969, pp. 599-633.
14. Levison, W. H. and J. I. Elkind, Studies of Multivariable Manual Control Systems: Two-Axis Compensatory Systems with Separated Displays and Controls, NASA CR-875, Oct. 1967.
15. Wingrove, R. C. and F. G. Edwards, "Measurement of Pilot Describing Functions from Flight Test Data with an Example from Gemini X," IEEE Trans. MMS-9, No. 3, Sept. 1968, pp. 49-55.
16. Bergen, A. R., "On the Statistical Design of Linear Random Sampling Systems," Automatic and Remote Control (Proc. 1st International Cong. IFAC), J. F. Coales, et al, eds., Washington, D. C., Butterworth, 1961, pp. 430-436.
17. Levison, W. H., and J. I. Elkind, Studies of Multivariable Manual Control Systems: Four-Axis Compensatory Systems with Separated Displays and Controls, Bolt Beranek and Newman, Inc., Rept. No. 1965, 14 March 1969.
18. Clement, W. F., Random Sampling Remnant Theory Applied to Manual Control, Systems Technology, Inc., Tech Memorandum 183-A, March 1969.
19. Jex, H. R., R. W. Allen and R. E. Magdaleno, Display Format Effects on Precision Tracking Performance, Describing Functions, and Remnant, Systems Technology, Inc., Tech. Rept. 191-1, 1971.
20. Allen, R. Wade and Henry R. Jex, "A Simple Fourier Analysis Technique for Measuring the Dynamic Response of Manual Control Systems," Sixth Annual Conference on Manual Control, Air Force Institute of Technology, Wright-Patterson Air Force Base, Ohio, April 1970, pp. 785-801.
21. Klein, R. H. and H. R. Jex, An Eye-Point-of-Regard System for Use in Scanning and Display Research, Systems Technology, Inc., Paper 99, Sept. 1970.
22. Clement, W. F., Successive Approximations to a Model for Remnant in Visual Tracking Tasks with Continuous Visual Attention on a Single Display, Systems Technology, Inc., WP 153-8, May 1970.
23. Knowles, W. B., "Operator Loading Tasks", Human Factors, Vol. 5, 1963, pp. 163-168.
24. Jex, H. R., "Two Applications of the Critical Instability Task to Secondary Workload Research", IEEE Trans., Vol. HFE-8, No. 4, Dec. 1967, pp. 279-282.
25. McDonnell, J. D., Pilot Rating Techniques for the Estimation and Evaluation of Handling Qualities, AFFDL-TR-68-76, Dec. 1968.

26. Birmingham, H. P., and F. V. Taylor, A Human Engineering Approach to the Design of Man-Operated Continuous Control Systems, Naval Research Lab., Rept. 4333, 7 April 1954.
27. Dougherty, D. J., J. H. Emery, and J. G. Curtin, Comparison of Perceptual Work Load in Flying Standard Instrumentation and the Contact Analog Vertical Display, Bell Helicopter Co. JANAIR Tech. Rept. No. D228-421-019, Dec. 1964.
28. Winblade, R. L., Current Research on Advanced Cockpit Display Systems, NATO, AGARD Rept. 491, Oct. 1964.
29. Magdaleno, R. E., "Serial Segments Method for Measuring Remnant", Presented at the 7th Annual University Conference on Manual Control, June 1971, NASA SP forthcoming.
30. McRuer, D. T., and etal., New Approaches to Human-Pilot/Vehicle Dynamic Analysis, AFFDL-TR-67-150, Feb. 1968.
31. McDonnell, J. D., and H. R. Jex, A "Critical" Tracking Task for Man-Machine Research Related to the Operator's Effective Delay Time, Part II. Experimental Effects of System Input Spectra, Control Stick Stiffness, and Controlled Element Order, NASA CR-674, Jan. 1967.
32. Levison, W. H., S. Baron and D. L. Kleinman, "A Model for Human Controller Remnant," Trans. IEEE, Vol. MMS-10, No. 4, Dec. 1969, pp. 101-108.
33. Jex, H. R., and R. E. Magdaleno, "Corroborative Data on Normalization of Human Operator Remnant," Trans. IEEE, Vol. MMS-10, No. 4, Dec. 1969, pp. 137-140.
34. Weir, D. H., R. H. Klein, and D. T. McRuer, Principles for the Design of Advanced Flight Director Systems Based on the Theory of Manual Control Displays, NASA CR-1748, March 1971.
35. Anderson, R. O., "Application of Pilot Models to Display Design; Some Basic Experiments", Fifth Annual NASA--University Conference on Manual Control, NASA SP-215, March 27-29, 1969, pp. 655-659.

GLOSSARY OF SOME TECHNICAL TERMS
USED IN THIS REPORT

- Axis (Axes) of Control - The manipulated variable(s) or control variable(s) acted upon by the controller in a tracking task; the control point(s) in a system.
- Coherent Error Spectrum - The power spectral density of that portion of an error signal which is correlated with the forcing function or command input to the system.
- Controlled Element - That part of a system to be controlled whose parameters are usually unalterable by the display designer; the "plant".
- Controller - That part of a system which implements a control law.
- Critical Tracking Task - When the rate of divergence of an unstable controlled element is gradually increased until control is lost on the subcritical tracking task, the task is said to be at its "critical" limit of divergence, or "critical", for brevity.
- Cross-Adaptive (Subcritical) Tracking Task - A subcritical tracking task which includes means to measure functions of one or more variables in a separate but simultaneous task and which uses such measurements to adjust the rate of divergence of the subcritical controlled element; also called cross-coupled subcritical task.
- Crossover Frequency, ω_c - The frequency at which the decreasing amplitude of the open-loop frequency response becomes equal to unity with increasing frequency. The name "crossover" derives from the connotation that the desirably large but decreasing amplitude of the open-loop frequency response "crosses over" unity to very small values at this frequency. The characteristics of the open-loop frequency response in the neighborhood of the crossover frequency are of fundamental importance in the analysis of closed-loop manual--as well as automatic--control tasks.
- Crossover Model - An approximate representation of the open-loop frequency response which is valid in the neighborhood of the crossover frequency.
- Describing Function - An operational (mathematical) description of that part of a non-linear controller's output which is linearly correlated with the input to the controller.
- Display Content - The specific elements of display which are actually present and which are required for guidance and control of a task or are required for monitoring task performance and decision-making.
- Display Format - The symbolic code by which each member of the display content can be identified.

- Display Ratings - Subjective pilot opinion ratings of a manual control display based on psychometric scales of "controllability and precision," "status utility," "clutter," and "attentional demand".
- Dither - In the context of tracking control, a voluntary quivering of the manipulator by the pilot at 1 to 3 Hz. (Cf. Tremor.)
- Dwell Fraction, Effective - The foveal dwell fraction increased by the cumulative effect of parafoveal perception.
- Dwell Fraction, Foveal - The proportion of all available time spent looking at a particular object of fixation; probability of fixation.
- Dwell Interval - The time duration of a particular foveal fixation.
- Effective Low Frequency Phase Coefficient, α - The effective low frequency phase coefficient in the extended crossover model represents the influence near the crossover frequency of very low frequency lead-lag dynamics with amplitude ratio break points which are below the measurement bandwidth in many experiments.
- Effective Time Delay, τ_e - The algebraic sum of the pure reaction transport delay and high frequency neuromuscular dynamics, equalization characteristics, and (sometimes) controlled element dynamics which are sufficiently high in relation to the unit-amplitude crossover frequency that each contribution can be represented by a pure delay near the crossover frequency.
- Elements of Display - Forcing Functions or Command-Input Signals, i
 Controlled Element State Variables or
 Output Motion Signals, m
 Error Signals, $e = (i - m)$
 References or Background
- Ensemble Average Value - The arithmetic mean of a collection of discrete numerical values.
- Equalization - Purposeful alteration of an open-loop frequency response to achieve the best compromise (in the crossover frequency region) between high gain over the input bandwidth and low gain beyond the input bandwidth.
- Equalization Remnant - A form of remnant attributable to the generation of low-frequency lead equalization by the human operator.
- Error Coherence - The ratio of the mean-squared input-correlated error power to the total mean-squared error power. It is the complement of relative remnant referred to the error.
- Feedback Selection - The technique of equalization whereby "inner" loops which are subsidiary to the "outer" or task loops are introduced.

Feed-Forward Control - A control law specified in terms of only forcing functions or command-input signals; pursuit control.

Foveal Perception - "Seeing where you are looking"; seeing that upon which one is fixating; or seeing the (object of the) eye-point-of-regard (EPR).

Gain - The low or high frequency asymptotic amplitude of a frequency response to an input; if unqualified, usually means low frequency asymptote except in the case of a washout.

Loop Gain - The low or high frequency asymptotic amplitude of an open-loop frequency response; if unqualified, usually means low frequency asymptote.

Incoherent Error Spectrum - The power spectral density of that portion of an error signal which is uncorrelated with the forcing function or command input to the system; the frequency distribution of uncorrelated error power.

Injected Error-Remnant Source - When mean-squared values of signals within control loops are of prime interest, the remnant can be satisfactorily represented by a signal source having a specified power spectral density injected into the closed-loop system. When considered as an injected signal, the point of application of the remnant can be transferred from the pilot's output to the pilot's input or error signal as long as no nonlinear elements are passed in the process of transfer. At low frequencies the remnant data for a wide variety of controlled elements coalesce best when all of the remnant is injected at the pilot's input or error signal. (Cf. Observation Remnant.)

Integrated Display - A complete combined, connected or collective presentation to the pilot of the proper signals for controlling as well as monitoring the performance of a task. The adjective "proper" applies to equalization, scaling, codification, and consonance in ways hypothesized by the theory of manual control displays.

Interrupt Fraction - The complement of the dwell fraction.

Link Values - (Transition Link Probabilities) - The proportion of the number of all possible fixation transitions which occur between pairs of objects of fixation; link values may be one-way (in one direction) or two-way (the sum of both one-way values between a pair of objects.)

Look Fraction - The proportion of the number of all possible fixations which are directed to a particular object.

Loop Closure (or Feedback Control Loop) - A control law specified in terms of controlled element state variables or output motion signals, which are compared with input signals in such a way that the difference signal can be used in the controller; compensatory control.

Loop Gain - The low or high frequency asymptotic amplitude of an open-loop frequency response; if unqualified, usually means low frequency asymptote.

Gain - The low or high frequency asymptotic amplitude of a frequency response to an input; if unqualified, usually means low frequency asymptote except in the case of a washout.

Theory of Manual Control Displays - A verbal-analytical theory for predicting the displayed variables, controller behavior and control technique, and measures of performance and workload for pilots of manually controlled vehicles. The theory is based on the notion that display design is fundamentally a guidance and control problem which has interactions with our knowledge of human psychomotor activity.

Observation Remnant - Noise caused by poor coupling between the displayed signal and the eye. Observation remnant includes scanning remnant in multidisplay control tasks. (Cf. Injected Error-Remnant.)

Parafoveal Perception - "Seeing without looking"; seeing that upon which one is not fixating; or seeing that which is outside the eye-point-of-regard (EPR).

Power Spectral Density - The frequency distribution of the square of the amplitude of (a) the (complex) Fourier coefficients of a periodic function or (b) the Fourier transform (if it exists) of a non-periodic function. The power spectral density of a random process is the mathematical expectation of the power spectral densities of the individual functions comprising the process.

Quasi-Linear Pilot Model - A verbal-analytical describing function of a class of human pilot behavior with remnant.

Reaction Time Delay - A pure transport delay due to sensor excitation (the retina in the visual modality; the semicircular canals and utricles in the vestibular modality, for examples), nerve conduction, computational lags, and other processing activities in the central nervous system. It is closely related to, but not identical with certain kinds of classical reaction times.

Reconstruction (from the Sampled-Data) - The extrapolation of a continuous signal from discontinuous observations or samples of data.

Relative Remnant (referred to the Error) - The ratio of the mean-squared uncorrelated error power to the total mean-squared error power. It is the complement of the error coherence. If so designed, relative remnant can also be referred to a control point.

Remnant - That part of a non-linear controller's output which is not linearly correlated with the input to the controller.

Remnant Error Spectrum - The power spectral density of an injected error-remnant source.

Injected Error-Remnant Source - When mean-squared values of signals within control loops are of prime interest, the remnant can be satisfactorily represented by a signal source having a specified power spectral density injected into the closed-loop system. When considered as an injected signal, the point of application of the remnant can be transferred from the pilot's output to the pilot's input or error signal as long as no nonlinear elements are passed in the process of transferral. At low frequencies the remnant data for a wide variety of controlled elements coalesce best when all of the remnant is injected at the pilot's input or error signal. (cf. Observation Remnant)

Saccade - The quick movement of the eye by which the gaze is transferred from one fixation point to another.

Sampled Data System - A system in which at least one signal is observed discontinuously at random or systematically.

Scanning Interval (Look Interval) - The elapsed time between the start of successive foveal fixations on a particular object.

Scanning Remnant - A form of remnant attributable to foveal scanning by the human operator.

Separated Displays - A multipartite collection or arrangement of distinct individual or disparate displays or instruments having at least a task or controlled element in common.

Subcritical Tracking Task - An unstable controlled element which can be stabilized by a loop closure.

Symbol Density - The relative proportion of the total displayed field of view which is occupied by members of the symbolic format exclusive of the background element.

System - A collection of interconnected physical devices or mathematical operations.

Tremor - In the context of tracking control, the involuntary quivering of the manipulator contributed by the neuromuscular system at 10 to 15 Hz. (Cf. Dither.)

Washout - A dynamic frequency response function having no response whatsoever to a static input.

Weber-Law Errors - Deviations from the linearity of stimulus-response relationships in accord with the Weber-Fechner law. The law asserts that equal increments of sensation are associated with equal increments of the logarithm of the stimulus.

Zero-Order Hold - A type of continuous signal reconstruction from samples of data whereby the value of each observation is held constant until the next sample is taken.

APPENDIX A

SYSTEMATIC MANUAL CONTROL DISPLAY DESIGN

W. F. Clement, D. T. Wehrer and R. H. Klein
Systems Technology, Inc.
Beverly Hills, California 90230

SUMMARY

A theory of displays, together with validated techniques for analyzing closed-loop pilot-vehicle dynamic performance, provides a systematic procedure for improving the guidance and control display design process. Central to this theory is the notion that display design is fundamentally a guidance and control problem which has interactions with our knowledge of human psychomotor activity.

In outlining the principles of this analytic approach to display design, we review the inspirations for eye movement studies in flight control and monitoring tasks and summarize the relationship of eye scanning phenomena to pilot describing functions and workload. Several measures of pilot workload in control tasks are discussed. One measure, in particular, has great promise in quantifying a practical definition of workload. This is excess control capacity. It is a major workload connector with pilot opinion rating and whole-task effective time delay. We conclude by illustrating the further connections with load equalization, scanning workload, physiological measures of neurovascular tension, and the effects of additional modalities on visual workload.

INTRODUCTION

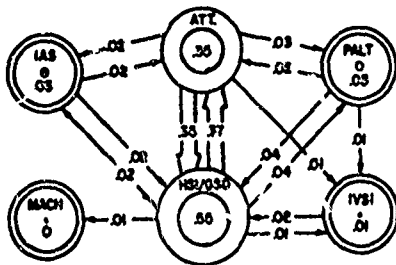
The design of guidance and control displays which properly interface with the pilot and the control system of a new aircraft or spacecraft is often based on intuition and tradition backed by a qualitative understanding of the potentially useful control information. Instrument arrangements, integrated display formats, and flight director systems are selected using this background and experience and are then subjected to exhaustive and often expensive development and comparison in simulators and, ultimately, in flight. The simulation process usually reveals shortcomings in the preconceived display systems which are overcome by progressive modification, retesting, reevaluation and reassessment. This procedure is often time-consuming and costly. Until recently, however, it has been entirely necessary for selection of the best compromise display system.

A theory for guidance and control displays (e.g. Ref. 1 and 2) together with validated techniques for analyzing closed-loop pilot-vehicle dynamic performance (e.g., Ref. 3 and 4) now provides the means for considerably improving the display design process. A first step in the application of the theory is to translate the verbally understood purposes of a guidance and control display system into more specific engineering terms. For the display designer, this first step has been most difficult. Although he may assume that human unreliability is related to workload, he can only verbally qualify workload, because he does not presently have a quantifiable expression of the penalties associated with human errors in performance which is commensurate with the customary performance metrics of mission success.

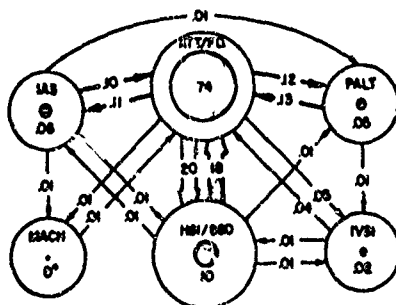
PURPOSE OF A GUIDANCE AND CONTROL DISPLAY SYSTEM

Stated broadly, the purpose of a new guidance and control display system should be to improve piloted system performance to a point where at least a subset or even the whole set of mission requirements can be satisfied. In system engineering terms, the improvement of performance implies greater frequency bandwidths and correspondingly reduced closed-loop system lags and errors in following commands. It also implies improved suppression of the effects of external disturbances. In terms of pilot behavior the improvement of performance implies reduced effective time delay; reduced pilot-induced noise insertion (unwanted control action); increased allowable range of pilot-gain variation consistent with closed-loop system stability; and reduced workload to a level where he is efficiently and gainfully occupied, yet able to cope to a prescribed degree with the unexpected.

For example, the prototype Zero Reader[®] flight director, like its counterpart, the automatic pilot, inspired awe rather than confidence in professional pilots, because it failed to display the confidence-inspiring situation or status information to which pilots have always been accustomed. Since the pilot still went to his separate displays for status information, use of the prototype flight director for guidance and control seemed to be an extra task. Many experiments (Ref. 5-8) have proved that the contemporary integrated flight director can and does improve over-all system performance. However, even without significant performance improvement (sometimes difficult to measure experimentally) the flight director system should always make the pilot's job easier. That is, it should reduce his workload from that required to perform the task using normal cockpit instrumentation. This includes both the scanning workload and the perceptual workload required, e.g., for pilot generation of low frequency equalization. The result of such reductions is improved pilot rating through increased confidence in the display and increased excess control capacity



Manual H.S. Configuration, C1



Flight Director Configuration, E1

Figure 1. Typical Eye Fixation Transition Link Vectors and Dwell Fractions Measured in Simulated Jet Transport Instrument Approaches

for coping with unexpected workload.

An example of the reduction in scanning workload [exemplified by transition link vectors to and from and dwell fraction on the Horizontal Situation Indicator/Glide Slope Display (HSI/GSD)] obtained with a flight director presentation can be found in Ref. 6. Figure 1 (from Ref. 6) is included here to show the changes in scanning workload (the fraction of total time spent on each instrument is indicated thereon) is going from a manual ILS task (top figure) to a flight director configuration (lower figure). This conventional flight director configuration was also used in preliminary simulation studies performed at STI utilizing the results of the advanced flight director design program of Ref. 9. In the advanced director system derived from the study, a pilot lead equalization (as predicted, and measured in the simulator by pilot describing functions) was required. The simulation results showed an improvement in pilot rating of 1 to 1 1/2 points (from 3 1/2 to 2 on the Cooper Scale) and improved glideslope beam-following performance for various inputs as indicated in Fig. 2.

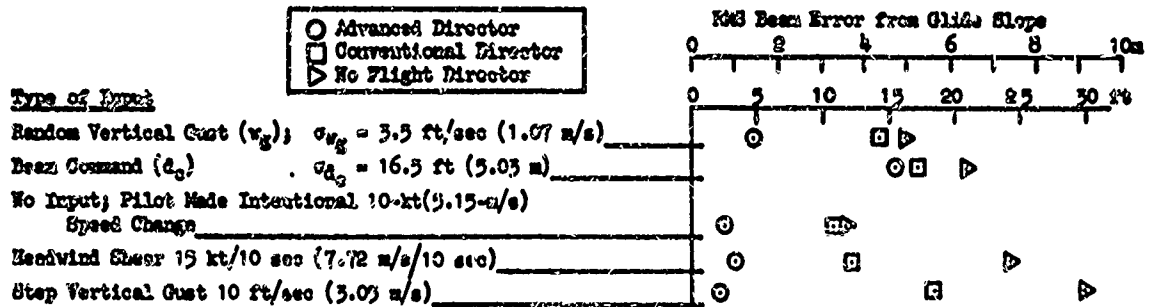


Figure 2. Simulated Glideslope Beam-Following Performance Under Manual Control with Various Inputs.

With regard to its impact on closed-loop system performance, and pilot workload, a good flight director system is competitive with an automatic flight control system. In fact, for approach in CAT I and II conditions flight directors offer less weight, volume, and power penalties and are more reliable and less costly at a given level of redundancy than their automatic equivalents. Also, flight director system performance can be nearly equal to that of automatic systems for beam command following and disturbance suppression. For certain other inputs, such as overflights, the flight director/pilot system performance may be superior to that of a fully automatic system. Furthermore, the flight director permits better utilization of the pilot and copilot in their normal roles as active controllers and monitors of the situation. In this way they are kept in the loop in case of aircraft or system failures. However, assuming an automatic flight control system is installed and used, an additional purpose of the flight director is to provide an overall monitor on the automatic system's performance both to instill confidence in the pilot and to permit him to take over in case of system malfunction.

The extent to which the above purposes are actually accomplished defines the "goodness" of an integrated flight director system as an example of a guidance and control display. Having expressed the purposes of display design in systems engineering terms, we can apply an analytical design approach such as that illustrated in Refs. 2, 7 and 10. In what follows, we shall only be able to summarize the principles of this approach to display design. By means of this analytical approach we can achieve a quantitative understanding of the interactions among the pilot, the display system and the vehicle. Putting this understanding to work will then achieve direct and important savings in the display design and evaluation process.

PRINCIPLES OF GUIDANCE AND CONTROL DISPLAY DESIGN

Display design, in our view, is fundamentally part of a guidance and control problem which has interactions with our knowledge of human psychomotor activity. Our treatment of the display-pilot-aircraft system rests on three fundamental hypotheses:

1. To accomplish guidance and control functions, such as flying a desired track in the presence of disturbances, maintaining precision control (as in formations or refueling), flying intercepts or approaches, etc., the human pilot sets up a variety of closed-loops about the aircraft which, by itself, could not otherwise accomplish these tasks. In control systems engineering terms his control actions are functions of desired and actual aircraft motions.
2. To be satisfactory these closed-loop systems, comprising both animate and inanimate components, must share certain of the qualitative dynamic features of "good" closed-loop systems of a solely inanimate nature. As the adaptive means to accomplish this end, the pilot must make up for any dynamic deficiencies of the aircraft by appropriate adjustments of his dynamic properties. (Here the "aircraft" includes the display and controls).
3. There is a cost to this adjustment--in workload-induced stress, in concentration of pilot faculties, and in reduced potential for coping with the unexpected. This cost can also be traded for the cost of automatic controls. In making this trade-off, one may allocate part of the task to manual and part to automatic control.

To apply closed-loop theory one must have some kind of model to describe pilot behavior. Our models have evolved from simple single-loop, fixed base situations to represent multiloop fixed and moving base scenarios. They are very useful in predicting potential handling quality problems for new and unexplored areas and for flight control system/airplane combinations which are not of the "classical" variety. They can also be used to analyze and explain simulator results after the fact. This usefulness has increased over the years and is today far more concrete. Over a decade of research and application (see the Bibliography in Ref. 4), in both America and Europe, has resulted in models of pilot behavior that are much more sophisticated and which can be used to treat very complex manual flight control problems. Models of pilot

ynamics now exist which can be used to predict:

1. The displayed variables and control display associations required for the task from the likely loops closed by the pilot to accomplish a given task (i.e., instruments used in IFR, visual cues in VFR);
2. The dynamic behavior required of the pilot (e.g., describing functions), and hence the piloting techniques exhibited in the given tasks for fixed-base operations;
3. Effects of certain motions on the pilot dynamic behavior including cues likely to be utilized or ignored;
4. Closed-loop system performance;
5. Pilot commentary and ratings;
6. Excess manual control capacity, i.e., measures of task workload or additional workload that could be accomplished; preferred combinations of displayed variables which are compatible with the physical scanning workload constraint.
7. Scan patterns (for IFR) including proportions of time spent on each instrument and link probabilities from instrument to instrument.

This is a very impressive list, but we should note, of course, that not every item on it can be predicted with equal confidence, largely because of the differences in the underlying empirical bases. Consequently, while estimates can be made for everything listed, the degree of precision in these estimates will vary. Nonetheless, the point we wish to make is that all of these things can be, and have been, done. They are very useful for preliminary design analysis, for prediction of key problems in novel situations, for experimental planning and guidance, and for the interpretation of experimental results.

Remarkably, the theory is, generally speaking, far more advanced than the usual measurements practiced in experimental simulation. These are normally based on a state of art appreciation which is at least a decade behind the appreciation afforded by dedicated closed-loop analyses. Often the only measures taken are system performance and pilot rating. Such measurements can at best give only a gross smoothed-over view. They are, of course, enormously useful in determining whether a particular system is satisfactory, but they leave much to be desired in determining the causes and corrections for difficulties except by ad hoc adjustments which may be unduly influenced by "artificial" simulation characteristics. We believe that many of the complexities which devolve from the human pilot's presence are now a proper and useful subject of engineering analysis. This view is amply supported by the reports and papers listed in the Bibliography in Ref. 4.

We shall now turn to a brief discussion of some principles at the fringe or low-confidence side of the theory. These are display sampling and scanning, and workload assessments.

INSPIRATIONS FOR EYE MOVEMENT STUDIES IN FLIGHT CONTROL AND MONITORING TASKS

The measurement of pilots' eye fixations and movements about the instrument panel within the cockpit has attracted research for over a quarter of a century (e.g., in Ref. 10, see Ref. 67-77, 82-85, 93, and 96). Not surprisingly, the motivation for the earliest available results seems to have been to compare pilot fatigue under instrument flight rules induced by differences in "scanning workload" among instruments between the Standard (circa 1944) Army Air Force and Royal Air Force instrument panels. To explain statistically significant different experimental results on the two different panel arrangements, an embryonic display arrangement hypothesis was set forth in 1944: "Differences between the time spent on the various instruments in the two panel arrangements may be explained by the hypothesis that pilots tend to spend more time on the centrally located instruments, and particularly on the instrument located in the top center position. While not definite, this finding suggests that instrument panel designs should place the most important instrument for instrument flight in the top center position of the panel, and the next most important instrument in the lower center position." (From Ref. 67 in Ref. 10)

Other early studies of eye movements of flight personnel were concerned with open-loop signal detection, for example, searching for targets on radar scopes, monitoring multi-engine performance for threshold-exceedence, and establishing minimum visual angles external to the cockpit under visual flight rules.

However, the inspiration for much of this eye movement work was founded on the belief that the cues used by the pilot in controlling flight would be revealed by noting the (separated) instruments upon which the focus of the eye was fixating inside the cockpit under instrument flight rules, and by correlating the directions of fixations external to the cockpit with significant ground-based cues in landing approaches under visual flight rules. Information about the useful instrument flight control cues was believed to be fundamental to an understanding of the function served by flight instruments. It was expected that this understanding would, in turn, form a basis for improving the design of aircraft instruments, increasing the efficiency of instrument flight training, and simplifying the task of instrument flying.

Today we are still working to fulfill this expectation, because the premise on which it was founded twenty years ago has been shown to be only a partial truth for several reasons. Pilots develop an ability to operate effectively on parafoveally and peripherally perceived information (Ref. 11), albeit with some limitations (Ref. 12), and, of course, on reinforcing (i.e., nonconflicting) motion and aural cues. Further, there is considerable indirect evidence (e.g., Ref. 13) that in "stare mode" circumstances fixing the eye-point-of-regard serves merely to stabilize the eyeball for good parafoveal viewing, so that the fixation point may be unconnected with the information actually used, or even perceived, by the pilot. We cannot say that what is being fixated necessarily corresponds to an input.

The inspiration for the earliest pilots' eye movement studies--that scan patterns might be useful for workload measures--was revived more recently in Ref. 14. While scan patterns are indeed relevant to workload, the connection is not simple. The eye requires fixation to keep the eyeball stable, so there is a kind of Parkinson's Law for the eyeball--the sum of the fixation dwell times on the instruments expands or contracts to equal the time available (neglecting saccadic times). There is, of course, a minimum dwell time of about 0.4 sec per instrument, so it is possible to contrive saturated conditions where the control task demands pilot fixations on too many instruments too often in order to maintain control. But the interpretation of such results would often be ambiguous if one is looking for the pilot's inputs.

The early eye movement studies referenced above considered fixations as a function of the overall pilot-instrument system task, such as landing approach, but completely apart from the controlled element dynamics.

To get at the total "piloteability" problem we proposed some years ago that pilot-aircraft system dynamic techniques be applied to the display area. Under coordinated NASA-ARC and JAAIR sponsorship we have in the last four years developed, refined, and elaborated a theory (Refs. 2, 10 and 15) applied it to a number of interesting situations (Refs. 2, 15 and 16), and have supported and augmented the theoretical development in crucial areas with experimental efforts (Refs. 6, 16 and 17).

SCANNING PHENOMENA TO BE DESCRIBED

Besides instrument-to-instrument scans, scanning occurs between elements within combined or integrated symbolic and pictorial displays. For example, secondary fixation transitions within the two-axis attitude director on various symbols, indices and scales have been observed in the experiments of Ref. 6. Among several pictorial examples of pilot's scanning patterns on different instrument panel arrangements in Ref. 15, there is shown an internal pattern on an integrated contact analog display. Obviously, one must speak of a foveal scanning pattern among "symbols" in the case of the contact analog or some other integrated display, rather than among "instruments" as we shall do in most of what follows.

Furthermore, an observable foveal scanning pattern may be accompanied by a parafoveal scanning pattern of awareness which is not directly observable by measuring eye movements. However, the presence of parafoveal awareness is indirectly observable by its influence on the pilot's describing function.

Although we shall be speaking primarily about the visual modality, the pilot can also choose to use or ignore motion and aural cues. While this is not quite like sampling, the more or less continuous use of the vestibular or aural modality is akin to a process of selection when these cues reinforce the visual modality.

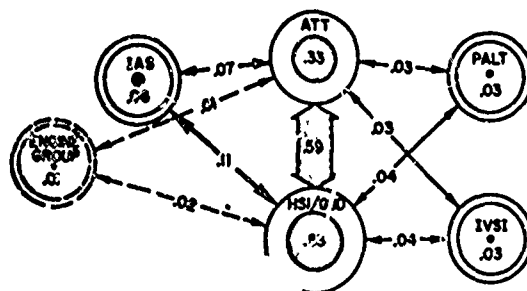
The proportion of the total number of fixations which fall upon a particular instrument is called the average look fraction for that instrument. Its upper bound is one-half, which implies that every other fixation or look is on that instrument having a look fraction equal to one-half.

The proportion of the total time during which fixations dwell on a particular instrument is called the average dwell fraction for that instrument. Since the cumulative sum of all dwell fractions, including blinks and distractions, must equal unity, by definition, the dwell fraction is also termed "fractional scanning workload" or "probability of fixation."

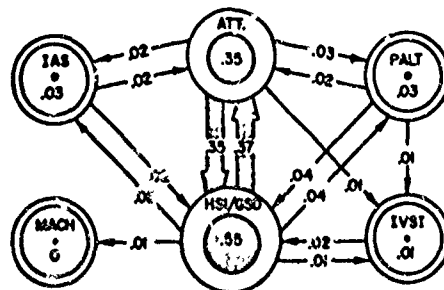
The proportion of all fixation transitions which go in the same direction between a pair of instruments (arrows in Fig. 1) is called the "one-way link-value" in the specified direction. The sum of the two one-way link-values between a pair of instruments is called the "two way" link value. In 1950, new research extended the display arrangement hypothesis of 1944 to suggest that the pattern of link values between instruments is indicative of the goodness of different panel arrangements. Since, in point of fact, the scanning statistics are quite stationary over measurement intervals as short as 100 sec, different one way link values between the same pair of instruments are also indicative of determinism in scan patterns. The results in Ref. 6 show no evidence of circulatory determinism in scanning traffic. This simplification proves useful in making predictions of scanning behavior.

MULTILOOP SCANNING MODELS FOR DESCRIBING FUNCTION AND REMNANT PHENOMENA ACCOMPANYING SCANNING

As far as we can tell currently, we have not discovered a unique relationship between observable foveal scanning statistics and the accompanying pilot's describing function and remnant. Instead, we have two different limiting forms for multiloop pilot models in control tasks. In experiments in Refs. 11 and 17, the pilot's describing function dynamics in closing the several loops are not much degraded with additional time delays because of the scan, although the pilot gains are reduced from those that would be expected on a single-loop basis, and the foveal input information samples are obtained from a finite dwell period with an average minimum dwell time of about 0.4 sec. This is not what one would obtain with a simple zero-order-hold sampled-data system, so the sampling and scanning theory required to describe the pilot's eye movements has been quite elaborate.



a) Predicted



b) Measured

Figure 3. Predicted and Measured Dwell Fractions and Stochastic Link Probabilities for Manual IIS Experiment

With these empirical facts as starting points, two likely mental processes have been proposed (Ref. 17), called the "switched gain" model and the "reconstruction-hold" model. For the switched gain process the quasi-linear describing functions in the several loops incur no time delay because of the scanning and sampling processes, although the gain switching (multiplexing) from loop to loop reduces the effective gain in each. In the reconstruction-hold model a sampling delay is incurred, but may be largely offset by lead equalization as part of the signal reconstruction process, which tends also to restore part of the average loop gain lost in the sampling process.

The principal cost of the scanning, sampling, and reconstruction (or switching) behavior is an increased "remnant." This depends on the sampling frequency, fixation dwell time, and sampling frequency variations, as well as the signal variance. Since the hypothetical signal reconstruction process attenuates sampling remnant, the switched-gain model will produce relatively more remnant, if other variables are equal. The remnant represents pilot control movements which are incoherent, i.e., not linearly correlated (via the describing function) with the externally imposed forcing functions. The remnant acts like an injected noise, and is the real cause of saturation in multi-instrument displays. So, as we said at the outset, measurement of eye fixation is certainly connected with pilot inputs and workload but the connection is by no means simple.

As it now stands, the theory of multi-axis scanning can be used to estimate fixation probabilities and instrument-to-instrument link probabilities fairly accurately. As an example, Fig. 3 shows some predictions made with the reconstruction-hold version of the theory (Ref. 10) for a landing approach using Boeing 707 aircraft dynamics, as compared with measurements (Ref. 6) made using the DC-8 landing approach simulator at Ames Research Center. The resemblance is quite good, especially considering the infant state of the theory at the time.

This concludes a review of the inspirations for eye movement studies in flight control and monitoring tasks, a description of scanning phenomena, and a summary of this relationship to pilot describing functions and remnant. Before discussing some other measures of workload in control tasks, we shall summarize the procedure for applying the multi-axis scanning models to a display design problem and relate key steps in the systematic procedure to predictable display design characteristics.

A SYSTEMATIC GUIDANCE AND CONTROL DISPLAY DESIGN PROCEDURE

The principal steps in the procedure for predicting multi-axis scanning behavior during preliminary control display design are ordered numerically in Table I. The required information which serves as a starting point for predicting scanning behavior is developed in step 4. The general principles of closed-loop system synthesis and the required analytical techniques which help to complete steps 1 through 4 have been described in Refs. 1, 2, 3, 4, 10 and 18. The results of step 4 will include a quantified block diagram for one or more manual control technique(s) appropriate for the task and closed-loop frequency responses for all of the displayed variables required for controlling and monitoring the task in response to all command inputs, disturbance inputs, and to models for remnant. These remnant models make it practical to consider the observed remnant as resulting from equivalent injected noise sources at the pilot's perception and control points in the multiloop structure.

In step 5 the effective dwell fraction and scanning frequency for each required point of fixation (instrument or displayed symbol) are predicted in a way which minimizes the total error variance vector. This prediction must be subject, of course, to the time-available constraint on the cumulative foveal dwell fraction, which will be ultimately verified in step 10. Two different techniques exist for performing steps 5 through 10: one, based on the physical insight afforded by classical feedback control theory, is described and applied in Refs. 2, 15 and 19; the other, based on optimal control theory, is described and applied in Ref. 20.

The coherence determinant in step 6 governs multiloop stability in the mean-square sense; therefore, it must be greater than zero. A value for the determinant which is much less than unity means that incoherent error power due to sampling remnant will be much greater than the coherent error power due to inputs and disturbances. If the coherence determinant approaches unity (its upper bound), the error power will become increasingly coherent.

The coherence determinant depends on the display scanning statistics as well as the closed-loop frequency responses to models for sources of remnant. Therefore, it is desirable to obtain the coherence determinant in analytic form first, so that the average scanning statistics can be estimated in conjunction with their influence on scanning workload (cumulative dwell fraction) in step 10 and mean-squared errors in steps 7 and 8.

TABLE I. PROCEDURE FOR PREDICTING MULTI-AXIS SCANNING BEHAVIOR ON A PRELIMINARY CONTROL DISPLAY DESIGN		
STEP NUMBER AND PURPOSE	PREDICTABLE RESULTS FOR DISPLAY DESIGN	RESULTS USED NEXT IN STEPS
1. Define the Control Problem and Task	Forcing Functions, Task and Outer-Loop Variables, Controlled Element Transfer Functions, Performance (Error) Requirements	2 2 8
2. Prepare a Prospectus of Control Loops by Numerator Inspection	Selected Loop Candidates	4
3. Assume Stability Margin Requirements		4
4. Analyze Loops Using Adaptive Feedback Selection Hypothesis	Selected Automatic and Displayed Feedbacks (Constituent Signals, Reference Systems, and "Quickening" Equalization for Displays), Piloting Techniques, and Describing Functions in Each Loop Pilot Opinion Ratings Closed-Loop Responses	5 5 7
5. Compute Effective Display Scanning Behavior which Minimizes Total Error Vector	Effective Dwell Interval, Dwell Fraction, Scanning Frequency for Each Display	6, 9
6. Compute Coherence Determinant and Test for Reasonability	Error Coherence (Relative Remnant)	8
7. Compute Input-Correlated Root-Sum-Squared Error Vector	Coherent System Error	8
8. Compute Total Root-Sum-Squared Error Vector and Test Against Performance Requirements	Total System Error	13
9. Compute Foveal Scanning Behavior	Foveal Dwell and Look Fractions for Rec. Display	10
10. Test Cumulative Scanning Workload for Saturation or Over-Saturation	Potentially Saturated and Oversaturated Scanning Requirements	11
11. Compute Fixation Probabilities and Link Values	Distribution of Scanning Workload Among Displays	12
12. Arrange Separate or Combined Displays.		
13. Establish Display Scaling and Resolution for the Task.	Resulting Preliminary Display Design	

Sometimes the sum of the effective dwell fractions will exceed unity in the scanning workload constraint. This is called oversaturation. More often the total sum will exceed $(1-M_0)$, where M_0 is a margin of scanning workload for monitoring, communication, navigation, search, identification, fuel management, and supervisory tasks. Effective dwell fractions, the sum of which apparently exceeds the scanning workload constraint, can be achieved with lower foveal dwell fractions if parafoveal perception of the appropriately displayed signals is not inhibited. Reduced foveal dwell fractions and look fractions in step 9 are based on the relative number, type, contrast, and separation of symbolic elements in the displayed field of view.

If the sum of foveal dwell fractions in step 10 still remains oversaturated, it may be necessary to combine displays, allocate more work to automatic loops, or, in some cases, assign tasks to another crew member.

In step 11, the computation of probabilities of fixation and eye movement link values follows the same procedure as is already documented in Tables 19 and 20, p. 134-135 of Ref. 10.

In step 12, one should be guided by logical display-control associations and the Display Arrangement Hypothesis in Ref. 10, p. 62.

Finally, in step 13 one may establish the display scaling and resolution by following the rationale set forth on p. 60 of Ref. 2.

This concludes a summary of the procedure for determining average multi-axis scanning behavior on a preliminary display design. In view of the experience which we have with its application to five different aircraft to date, we have high confidence of its value in display problem-solving as well as preliminary design. Let us now finally discuss some models for quantifying pilot workload in control tasks.

PILOT WORKLOAD MODELS

Someone has observed that one of the prerequisites for conducting research in any discipline should be a set of accepted definitions. For example, in the "hardware world" such terms as reliability, failure, MTBF, and performance measurement have acquired disciplined meaning. Yet no such established glossary of terms exists for analysis of human reliability, workload, or performance. In practice many measurements of system error in human factors studies fail to distinguish adaptive properties of human behavior, because even a simple measure of workload such as mean-square control activity, which is sensitive to adaptive behavior, is not included. In the spirit of offering a more general definition of workload which can be measured and predicted, we suggest that the ability (or capacity) to accomplish additional (expected or unexpected) tasks is a suitable definition of workload. For example, the pilot opinion rating scale satisfies this definition up to its "uncontrollable" limit point. The fractional scanning workload also satisfies this definition as long as there exists a margin which can be reliably traded for additional tasks. Furthermore, a number of auxiliary tasks, the decrements in scores on which, from the unloaded state, give an index of the demand of the primary task, will also satisfy this definition of workload. However, one particular measure has, at the moment, very great promise in integrating many of the measures into one basic context. This is excess control capacity, the major connector with pilot rating and main task effective time delay. From this, we shall then develop the further connections with scanning workload, physiological measures of neuromuscular tension, and the effects of additional modalities.

Pilot Rating and Excess Control Capacity

Several scales for use in handling quality ratings exist; the most widely used, the Cooper Scale, contains ten probably unequal divisions. In spite of its ten subdivisions, it is probably fair to say that the Cooper Scale deliberately emphasizes three categories of increasing workload. The category boundaries are between satisfactory for normal operation and acceptable for emergency operation (a numerical 3.5), and between the emergency operation category and unacceptable (a numerical 6.5). Its limit point of 10 implies that the pilot had no excess control capacity--even for survival! The considerable pilot rating data available in Ref. 21 for the estimation of handling qualities indicate that, where closed-loop compensatory tracking is the task, the pilot's increments in rating are indeed based on the relative difficulty with which he obtains and maintains the specified performance.

The notion that among the causal factors of pilot rating are the pilot's attempts to maintain performance by working to control in spite of the increasing difficulty was further supported by an experiment which measured a parameter uniquely related to excess control capacity (Ref. 21). A secondary subcritical tracking task was used to "load" the pilot so that his performance on the primary task began to deteriorate. A block diagram of these tasks is shown in Fig. 4. The difficulty of the secondary task was made proportional to primary task performance. Thus when the pilot was keeping primary task error performance less than a criterion value, the secondary task difficulty was automatically increased by increasing the rate of divergence of the secondary instability. Conversely, when the pilot was so busy with the secondary task that primary error was larger than the criterion value, the secondary task difficulty automatically decreased. The final stationary level of secondary difficulty was determined by the sensitivity of the primary task performance to loading. The final "score" is λ_0 , the stationary value of the secondary unstable pole (λ) in rad/sec. The scores obtained from this cross-coupled secondary task represent its degree of difficulty; consequently, they also represent the "degree of ease" of the primary task or the excess control capacity available with respect to the primary task.

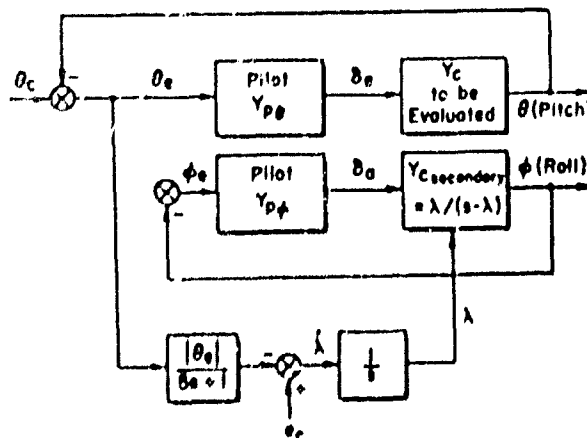


Figure 4. Single-Loop Primary Task with Secondary Cross-Coupled Loading Task

The achievement of the critical limiting score in the cross-coupled secondary task indicates a condition of maximum available excess control capacity. We speak of the secondary task as a "critical" task in this limiting case. The critical task provides a divergent controlled element of a form that tightly constrains the allowable pilot equalization near the region of gain crossover. This property of the critical task leaves

The achievement of the critical limiting score in the cross-coupled secondary task indicates a condition of maximum available excess control capacity. We speak of the secondary task as a "critical" task in this limiting case. The critical task provides a divergent controlled element of a form that tightly constrains the allowable pilot equalization near the region of gain crossover. This property of the critical task leaves

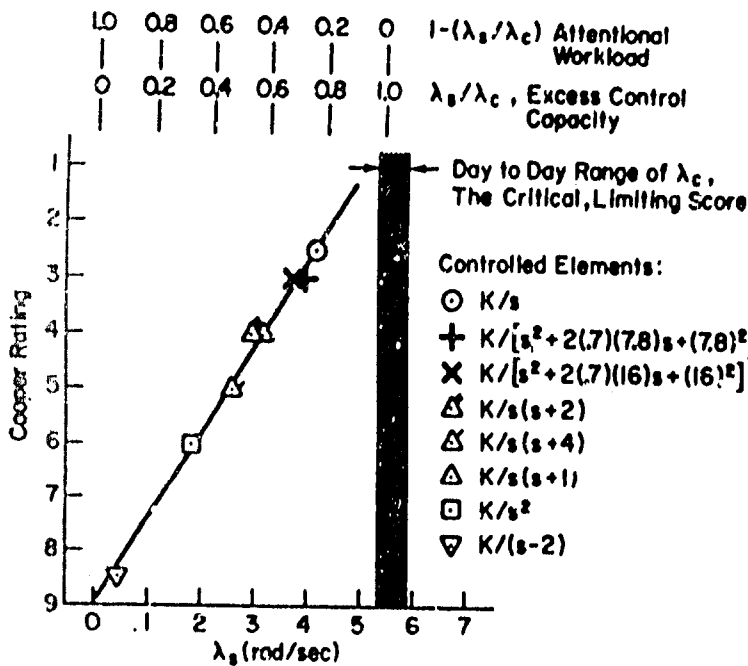


Figure 5. Subjective Pilot Rating Versus First-Order Cross-Coupled Instability Score

In our first application of the cross-coupled secondary subcritical task for display evaluation, secondary scores have been recently obtained for JANAIR (Ref. 22) using several integrated display configurations shown in Fig. 6. The primary task was longitudinal station-keeping with simulated helicopter dynamics in a formation approach using a cathode ray display. The primary controlled element remained the same throughout the tests. In addition the pilot subjects were required to maintain the assigned altitude by regulating against disturbances with the collective lift control using the altitude and vertical speed displays. The secondary subcritical task was employed as the controlled element for motions in roll attitude presented on the artificial horizon and was cross-coupled to longitudinal separation error on the primary task. The pilot subjects were asked to maintain as level a roll attitude as possible while trying to maintain the assigned altitude and to minimize their longitudinal separation error in following the quasi-random velocity fluctuations of the leader of the formation.

The secondary scores so obtained are shown in Fig. 7 as a function of the primary display format. Notice the tendency of measured excess control capacity to increase, if explicit rate information (S + R) is combined with a display of the "state" (S) of altitude and the task error. Both eye-point-of-regard measurements and pilot comments confirmed that in using the "state-and-rate" (S + R) format the subjects were not monitoring the airspeed indicator as much as with the "state" (S) format. Hence, we may infer that this measured

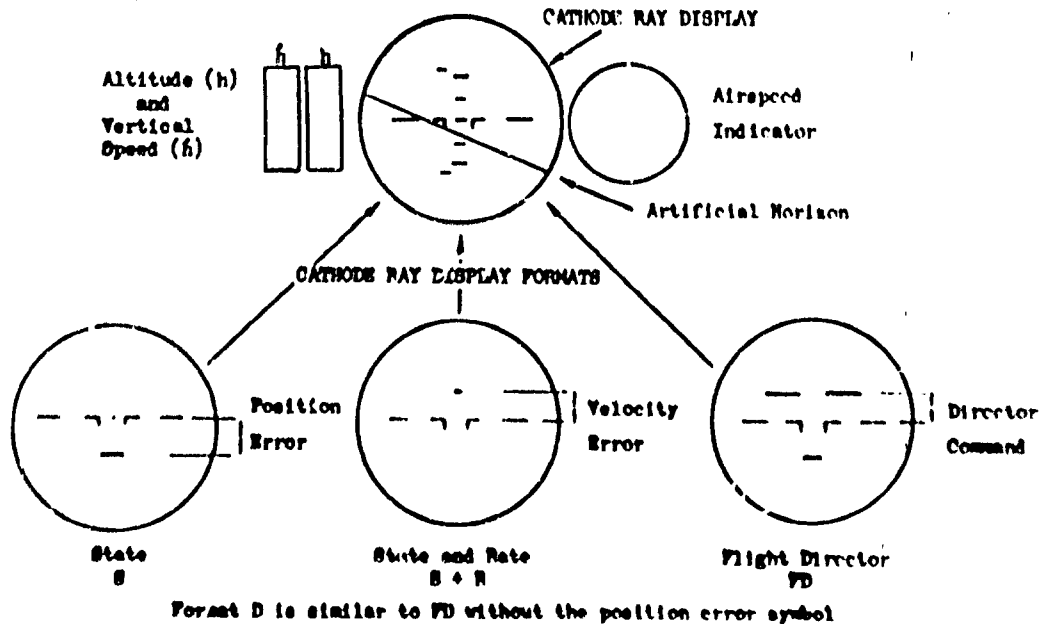
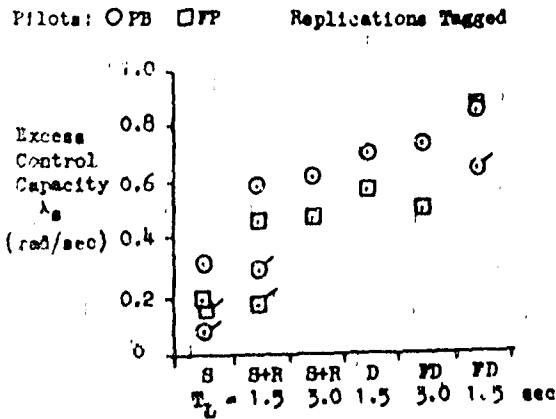


Figure 6. Integrated Display Arrangement with Examples of Format Tested for Excess Control Capacity

the pilot's effective time delay, τ_e , as the sole determinant of system stability. When the divergence is gradually increased until control is lost on the divergence, this "critical" divergence time constant is a measure of τ_e . (Ref. 22) Thus any activity by the pilot which demands an increase in τ_e on the whole task can be expected to prevent him from achieving his critical limiting score on the cross-coupled secondary task. We shall return to partition τ_e for the whole task after illustrating some results which we have obtained with the cross-coupled, subcritical task.

Secondary scores obtained for a variety of primary controlled elements are presented in Ref. 21. Figure 5 shows how the scores for the best gain configurations of each controlled element compare with the Cooper ratings. The agreement is extremely good. Even the subcritical task itself in the role of the primary task, which has been a notable culprit in other correlations, seems to be correlated linearly with the other data. In Fig. 5 a score $\lambda_s = 0$ corresponds to 100 percent of the pilot's attention being devoted to the primary task or no excess control capacity, whereas a limiting score ($\lambda_s = 5.5$) means that no attention is required to maintain primary task performance or that 100 percent excess control capacity is available.



Display Configuration and Displayed Lead Time Constant, T_l (sec). (See Text For Definition of Configurations)

Figure 7. Cross Adaptive Task Measure of Excess Control Capacity

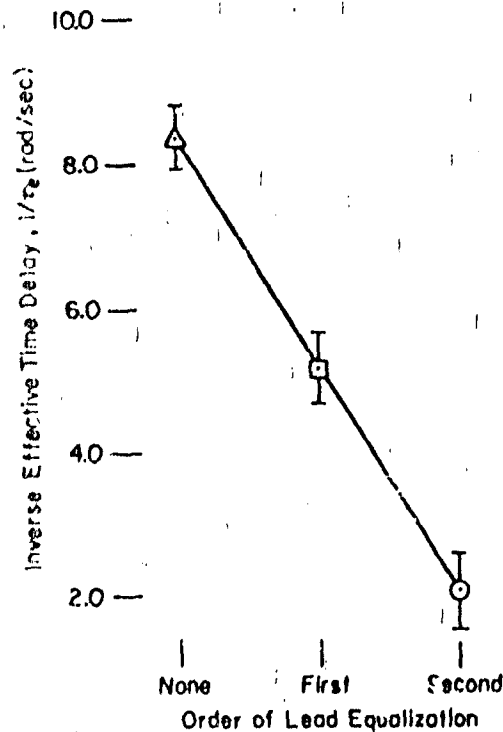


Figure 8. Inverse Effective Time Delay as a Function of the Order of Lead Equalization Required of the Pilot

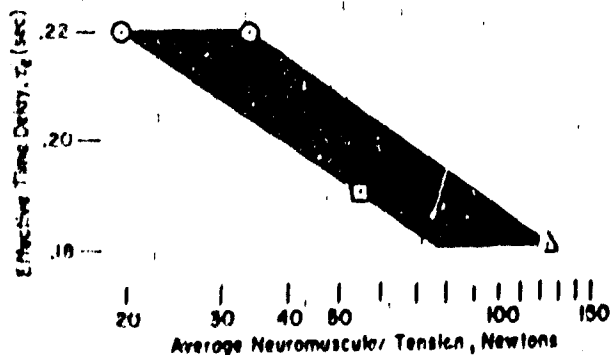


Figure 9. Effective Time Delay as a Function of Average Neuromuscular Tension

increase in excess control capacity is attributable to a decrease in the monitoring workload margin, because the subjects' effective time delays did not decrease in using the B + R format. The excess control capacity measurement in Fig. 7 exhibits a further increment, if only a director command (D) having the proper lead equalization time constant ($T_l = 1.5$ sec) is displayed with attitude information. This measured increase in excess control capacity may be attributed to a decrease in the whole-task effective time delay. When the confidence-inspiring task error display is integrated with the flight director display (FD) having the proper lead equalization ($T_l = 1.5$ sec), the measured excess control capacity tends to increase even more. This application of a secondary task has an excellent potential of becoming an objective measure of workload in multi-axis display control tasks by using a weighted quadratic sum of primary task errors to regulate the secondary instability.

Excess Control Capacity and Whole Task Effective Time Delay

The effective time delay for continuous attention on any task can be partitioned as follows:

$$\tau_e = \tau_0 \left(\begin{array}{l} \text{proportional} \\ \text{control} \end{array} \right) + \Delta\tau_f \left(\begin{array}{l} \text{low-frequency} \\ \text{lead generation} \end{array} \right) + \Delta\tau_n \left(\begin{array}{l} \text{neuromuscular} \\ \text{tension} \end{array} \right)$$

These are the principal components for effective time delay in a fixed-base single-axis situation. Each of the incremental components, $\Delta\tau_f$ and $\Delta\tau_n$, can themselves be considered as demanding an incremental workload change. The $\Delta\tau_f$ has in the past been considered a cause of perceptual workload. A plot of $1/\tau_e$ versus the order of lead equalization is shown in Fig. 8. The $\Delta\tau_n$ component which is related principally to neuromuscular tension is accordingly itself one of the best workload associations with physiological measures. Figure 9 shows that the average effective time delay decreases as average neuromuscular tension increases.

Multiaxis scanning can also induce significant additions to the effective time delays needed to accomplish the entire task. To the extent that the net time delay increment due to scan is a predominant scanning effect, the scanning workload can itself be considered as an increment in τ_e for the whole task. It can then be measured, in principle, as a change in the excess control capacity because the attainable score, λ_s , on a side task will decrease as τ_e increases. For instance, our multiple-loop results for both lateral and longitudinal aircraft control with integrated displays, i.e., altitude and pitch attitude for elevator and bank angle and yaw rate for lateral control, had outer-loop pilot describing functions which were substantially the same as those for single-axis equivalent tasks (Refs. 24 and 25). However, with separation of the variables about the panel and with the scanning then needed, the excess control workload measured on a cross-coupled side task would presumably increase. The difference between the separated and integrated display excess control capacities would then be an indication of the scanning workload.

When other modalities are available, such as rotary motion cues from a moving base simulator or actual aircraft, certain of the visual workload requirements can be reduced. In the case of rotary motions greater than semicircular canal threshold levels, the low-frequency lead generation requirements are reduced (Ref. 26). In essence, the rotary motion cues permit the pilot to close an inner loop akin to that of a rate gyro. The net effect is to reduce the effective whole-task time delay by about 0.15 sec (which also happens to be the $\Delta\tau_f$ increment required to develop a first-order low-frequency lead). Thus the total visual workload will have been reduced by the addition of motion. One could say that the total workload has not been changed because what had previously been done with the visual channel was now accomplished by the visual plus motion channels acting together. However, the motion loops are

essentially automatic--nearly reflexive in nature--so the presence of the additional modality really reduces the conscious workload as reflected by pilot ratings. The reinforcing use of aural and other modalities also has a qualitatively similar effect.

CONCLUDING REMARKS

We believe that many of the complexities which devolve from the human pilot's presence are now a proper and useful subject of engineering analysis in guidance and control display design. The closed-loop theory for manual control display systems provides a rational basis for orienting this engineering analysis toward a predictable practical measure of pilot workload. This measure is excess control capacity. Pilot workload increments due to load generation, scanning, alternate modalities, and that component of physiological stress exhibited in neuromuscular system tension can all be subsumed under a whole-task effective time delay, τ_e , and the cross-adaptive side task as a measure of excess control capacity is, in principle, a convenient indication of pilot workload. Comprehensive measures of workload in this context can then be the components and/or totality of τ_e and the associated side task scores.

To the aeronautical display designer unfamiliar with or unpracticed in using the mathematics of feedback control theory, the use of verbal-analytical models of pilot dynamics still seems to be a cumbersome and difficult "art" to learn. However, these "difficulties" are gradually disappearing as more rapid computational aids appear to reduce the artistry in application. The biggest challenge for the practitioners remains--to attract more users by simplifying the application of the theory without compromising its scope or validity and the physical insight for problem-solving provided thereby.

REFERENCES

1. McRuer, D. T., and H. R. Jex, "A Systems Analysis Theory of Manual Control Displays," Third Annual NASA-University Conference on Manual Control, NASA SP-144, 1967, p. 9-28.
2. Clement, W. F., and L. O. Hofmann, A Systems Analysis of Manual Control Techniques and Display Arrangements for Instrument Landing Approaches in Helicopters, Vol. I: Speed and Height Regulation, JANAI Rept. 690718, Systems Technology, Inc. Tech. Rept. 183-1, July 1969.
3. McRuer, D. T., D. Graham, E. Krendel, and W. Reiserer, Jr., Human Pilot Dynamics in Compensatory Systems, Theory, Models, and Experiments with Controlled Element and Forcing Function Variations, AFFDL-TR-65-15, July 1965.
4. McRuer, D. T., and D. H. Weir, "Theory of Manual Vehicular Control," Ergonomics, Vol. 12, No. 4, 1969, pp. 599-633.
5. Klein, R. H., R. B. Archer, and D. W. Lev, Supersonic Transport Handling Characteristics During Approach and Landing Flight Regimes, AFFDL-TR-65-227, December 1965.
6. Weir, David H., and Richard H. Klein, The Measurement and Analysis of Pilot Scanning and Control Behavior During Simulated Instrument Approaches, NASA CR-1535, June 1970.
7. Vreuls, D., S. R. Barnebey, J. E. Brown, and D. E. Nichols, Evaluation of Flight Director Elements--Rising Runway, Expanded Localizer, and Rollout Steering--During Simulated Category II-C Manual and Split-Axis Landings, Federal Aviation Administration SBDS Rept. No. RD 68-10, February 1968.
8. Brown, I. D., S. D. Moleqvist, and M. C. Woodhouse, "A Laboratory Comparison of Tracking with Four Flight-Director Displays," Ergonomics, Vol. 4, No. 3, July 1961, pp. 229-251.
9. Weir, D. H., R. H. Klein, and D. T. McRuer, Principles for the Design of Advanced Flight Director Systems Based on the Theory of Manual Control Displays, NASA CR-1748, March 1971.
10. McRuer, D. T., H. R. Jex, W. F. Clement, and D. Graham, Development of a Systems Analysis Theory of Manual Control Displays, JANAI-Systems Technology, Inc. Tech. Rept. 163-1, October 1967.
11. Levison, W. H., and J. I. Elkind, Studies of Multivariable Manual Control Systems, Two-Axis Compensatory Systems with Separated Displays and Controls, NASA CR-875, October 1967.
12. Hopkin, V. D., "Peripheral Vision and Flight Information," Human Problems of Supersonic and Hypersonic Flight, Proceedings of the Fifth European Congress of Aviation Medicine, London, 29 August - 2 September 1960.
13. Winblade, R. L., Current Research on Advanced Cockpit Display Systems, NATO, AGARD Rept. 491, October 1964.
14. Beniers, J. W., "The Estimation of Pilot Workload," AGARD Ad Hoc Panel in Guidance and Control Symposium on "The Human Operator and Aircraft and Missile Control", Paris, September 3-6, 1966.
15. Clement, W. F., H. R. Jex, and D. Graham, "A Manual Control-Display Theory Applied to Instrument Landings of a Jet Transport," IEEE Trans., Vol. MMB-9, No. 4, December 1968, pp. 93-110. Also, "Flight Application of a Theory for Manual Control Display Systems," Problems of the Cockpit Environment, AGARD CP-55, March 1970, pp. 5-0 to 5-23.
16. Allen, P. W., and H. R. Jex, An Experimental Investigation of Compensatory and Pursuit Tracking Displays with Rate and Acceleration Control Dynamics and a Disturbance Input, NASA CR-1082, June 1968.
17. Allen, P. W., W. F. Clement, and H. R. Jex, Research on Display Scanning, Sampling, and Reconstruction Using Separate Main and Secondary Tracking Tasks, NASA CR-1569, July 1970.
18. McRuer, D. T., and H. R. Jex, "A Review of Quasi-Linear Pilot Models," IEEE Trans., Vol. MFF-8, No. 3, September 1967, pp. 231-249.
19. Ringland, R. F., R. L. Stapleford, R. E. Magdaleno, Motion Effects on an IFR Hovering Task--Analytical Predictions and Experimental Results, Systems Technology, Inc. Tech. Rept. 188-1, October 1970.
20. Baron, B., D. L. Kleinman, D. C. Miller, V. H. Levison, and J. I. Elkind, Application of Optimal Control Theory to the Prediction of Human Performance in a Complex Task, AFFDL-TR-69-81, March 1970.
21. McInnell, J. D., Pilot Rating Techniques for the Estimation and Evaluation of Handling Qualities, AFFDL-TR-68-76, December 1968.
22. Clement, W. F., P. W. Allen, D. Graham, Experiments for a Theory of Integrated Display Format, JANAI-Systems Technology, Inc. Tech. Rept. 183-2, August 1971.

23. McDonnell, J. D., and H. R. Jex, A Critical Tracking Task for Man-Machine Research Related to the Operator's Effective Delay Time: Part II. Experimental Effects of System Input Spectra, Control Stick Stiffness, and Controlled Element Order, NASA CR-674, January 1967.

24. Stapleford, R. L., D. T. McRuer, and R. E. Magdaleno, "Pilot Describing Function Measurements in a Multiloop Task," IEEE Trans., Vol. NPE-8, No. 2, June 1967, pp. 115-124.

25. Stapleford, R. L., and D. J. Craig, Measurement of Pilot Describing Functions in Single-Controller Multiloop Tasks, NASA CR-1238, January 1969.

26. Stapleford, R. L., Richard A. Peters and Fred R. Alex, Experiments and a Model for Pilot Dynamics with Visual and Motion Inputs, NASA CR-1322, May 1969.

ACKNOWLEDGEMENT

This paper includes the results of work performed under the Joint Army Navy Aircraft Instrumentation Research (JANAIR) Program, a research and exploratory development program directed by the United States Navy, Office of Naval Research, and work sponsored by the Biotechnology Division of NASA-Ames Research Center.

The theory for manual control displays is quite naturally founded on the research by a number of interdisciplinary scientists and engineers, many of whom we have acknowledged by reference. However, the authors especially wish to recognize here the significant contributions by their colleagues, Dunstan Graham, Henry R. Jex, John D. McDonnell and R. Wade Allen. An exposition such as this must inevitably include some of their unidentified contributions for which the authors are most grateful.

APPENDIX B

SUMMARY OF PREDICTED PILOT LOOP CLOSURES FOR THE MULTIAxis EXPERIMENT WITH CH-53 AIRFRAME DYNAMICS

Contributions by Richard E. Blodgett

A. LONGITUDINAL SEPARATION CONTROL CLOSURE ANALYSIS

A general block diagram for the loops being closed through the human pilot is shown in Fig. B-1. The block indicated "augmented CH-53 airframe dynamics" is obtained as shown in Fig. B-2 by adding the effects of rotor and actuator lags, and AFCS feedback to the bare airframe dynamics. The resulting numerators and denominator for the various closed-loop transfer functions have been obtained from Table IX of Ref. 2 and are listed here in Table B-I.

The order in which the loops in Fig. B-1 will be closed is: first, $\theta \rightarrow \delta_b$, and then, $u \rightarrow \theta_c$ and $x \rightarrow u_c$ simultaneously. The augmented airframe transfer function * θ/δ_b is

$$\frac{\theta}{\delta_b} = \frac{4.41 (0.0)(0.668)(-10.3)}{(0.0284)(0.717)(6.48)[0.509; 2.275]} \quad (1)$$

The first loop $\theta \rightarrow \delta_b$ is a low gain manual loop with effective time delay $\tau_\theta = .33$ sec. Although this manual closure may seem redundant and deleterious because of the pitch AFCS, the purpose in making this closure is to investigate the effects of transfer of training in adopting a $\theta \rightarrow \delta_b$ loop by helicopter pilots who may not be accustomed to the augmented airframe "short period" dynamic properties provided by the pitch AFCS. In terms of the block diagram in Fig. B-1, $G_\theta = e^{-.33s}$ and $F_\theta = K_\theta$. The objective is to choose K_θ such as to reduce the damping ratio of the "short period" complex pair $[0.509; 2.275]$ to not less than about 0.3. For the purpose of analysis, the exponential will be represented by a first order Padé approximation.

*Abbreviated notation is used throughout this Appendix for polynomial factors of each transfer function in root locus form. Numbers enclosed in parentheses are first order factors, viz., $(s + a) = (a)$. Quadratic factors are enclosed in brackets, viz., $[s^2 + 2\zeta\omega_n s + \omega_n^2] = [\zeta; \omega]$. Prefixed numbers not enclosed are the high frequency gains of the transfer functions.

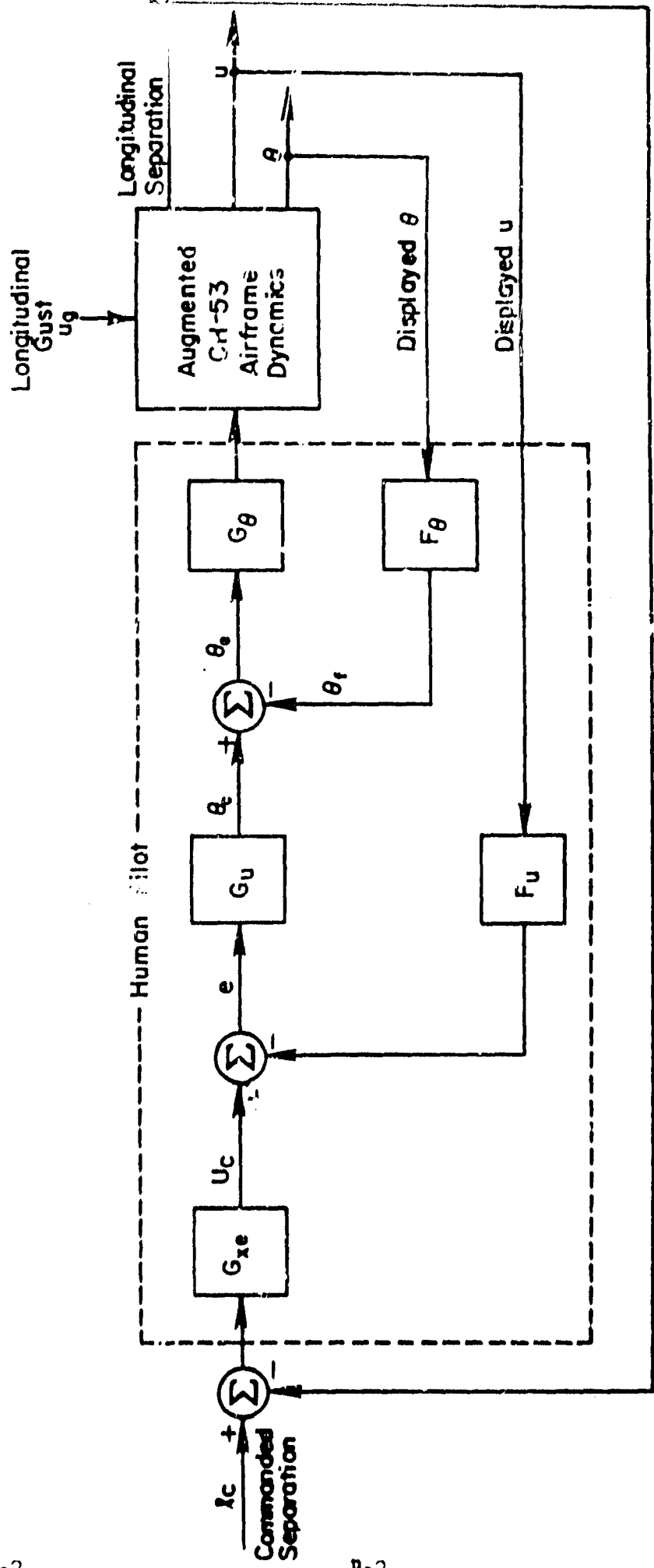


Figure B-1. Human Pilot Loop Closure Configuration

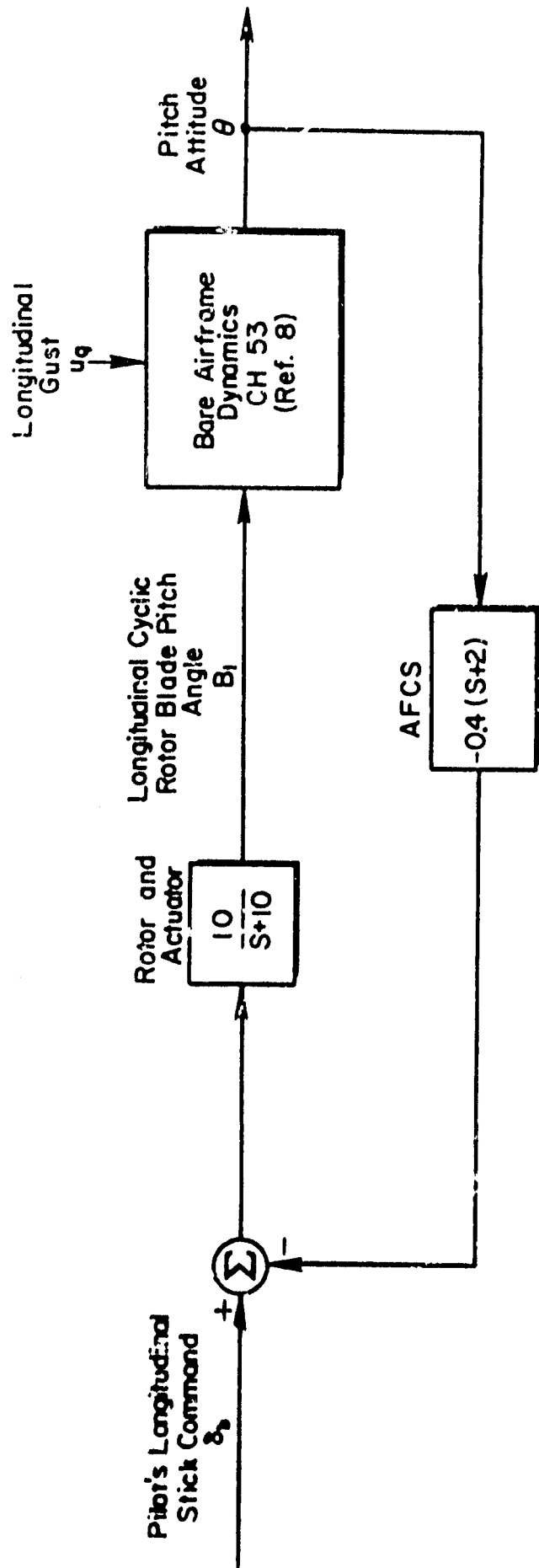


Figure B-2. Detailed Implementation of Augmented Airframe Dynamics

TABLE B-1

AUGMENTED LONGITUDINAL TRANSFER FUNCTIONS RESULTING
FROM AFCS IMPLEMENTATION IN FIG. B-2 (Ref. 2)

Denominator

$$\Delta = (0.0284)(0.717)(6.48)(10.0)[0.509; 2.275]$$

Selected Control Input Numerators

$$N_{\delta_b}^{\theta} = 4.41(0.00056)(0.668)(10.0)(-10.314)$$

$$N_{\delta_b}^u = -16.9(0.693)(10.0)(-19.112)[0.034; 2.09] \frac{\text{ft/sec}}{\text{rad}} \quad (\text{see footnote})$$

$$N_{\delta_c}^{-sh} = -3110.0(0.0267)(6.77)[0.449; 2.279] \frac{\text{ft/sec}}{\text{rad}}$$

$$N_{\delta_c}^u = -32.1(0.477)(15.2)[-0.663; 2.312] \frac{\text{ft/sec}}{\text{rad}}$$

$$N_{\delta_c}^{-sd} = N_{\delta_c}^{-sh} - 0.1N_{\delta_c}^u \quad \text{for a 1:10 glideslope}$$

Selected Gust Input Numerators

$$N_{u_g}^{\theta} = -0.00324(0.0)(0.643)(10.0)^2 \frac{\text{rad}}{\text{ft/sec}}$$

$$N_{u_g}^u = 0.0227(0.681)(9.4)(10.0)[0.0351; 2.168]$$

*The numerator $N_{\delta_b}^u$ is approximated as

$N_{\delta_b}^u = -16.9 \{-19.112(0.693)(10.0)[0.034; 2.09]\}$ for use in the
loop closure calculations.

$$e^{-\tau_\theta s} = -\frac{s - \frac{2}{\tau_\theta}}{s + \frac{2}{\tau_\theta}} \quad (2)$$

The effective time delay τ_θ includes the effect of higher frequency neuromuscular lags and visual delays in the human pilot. A detailed explanation of the components of this effective delay is given in Ref. 1. Since the longitudinal gust forcing function bandwidth is so low (0.2 rad/sec), we expect virtually no reduction in time delay from prefiltering by increased neuromuscular tension.

Combining equations (2) and (1) gives the approximate open-loop expression

$$\frac{\theta_r}{\theta_e} = K_\theta \frac{-4.41(0.0)(-6.0)(0.668)(-10.3)}{(0.0284)(0.717)(6.0)(6.48) | 0.509; 2.275 |}$$

Closing this loop with a gain $K_\theta = -0.2$ gives the closed-loop denominator

$$\Delta' = (0.0255)(0.700) | 0.316; 2.29 | | 0.949; 7.041 | / (6.0) \quad (3)$$

where the damping ratio of the short period oscillation has been reduced to not less than about 0.3.

The next loops to be closed are for perturbed position and velocity. The column for the "state" display format in Table B-II indicates the predicted appropriate block values for the diagram in Fig. B-1. The open-loop transfer function for this loop closure is

$$\frac{x}{x_e} = \frac{323.0 K_x T_{Lx} e^{-(0.33 + \Delta\tau_{LEAD})s} (1/T_{Lx})(0.693)(6.0) | 0.034; 2.09 |}{(0.0)(0.0225)(0.700) | 0.316; 2.29 | | 0.949; 7.041 |} \quad (4)$$

The additional increment of time delay $\Delta\tau_{LEAD}$ will be taken as 0.2 sec. (Ref. 3). This results from the pilot having to generate first order lead as indicated in the transfer function G_{x_e} in Table B-II. The required lead time constant T_{Lx} typically ranges from two to five sec with five sec being about the measured human upper limit. The location of the zero at $-1/T_{Lx}$ is very critical with respect to closed-loop system stability margin. Larger values of T_{Lx} lead to more heavily damped dominant closed-loop roots. The cases to be considered are listed

TABLE B-II

Predicted forms for the human pilot describing functions in Fig. B-1 with changes in Display Format.

BLOCK DIAGRAM	DISPLAY FORMAT		
	STATE	STATE-AND-RATE	DIRECTOR
G_θ	$e^{-\tau_\theta s}$	$e^{-\tau_\theta s}$	$e^{-\tau_\theta s}$
F_θ	K_θ	K_θ	K_θ
G_u	1	1	1
F_u	0	$K_u *$	$K_u *$
G_{xe}	$K_x(T_{L_x}s + 1)e^{-\Delta\tau_{LEADS}}$	$K_x *$	$K_x *$

*The last two entries in the State and Rate and Director columns are equivalent to $G_{xe} = K_x(T_{L_x}s + 1)$, where $T_{L_x} = K_u/K_x$, if F_u is changed to zero and command input x_c is changed to $\frac{x_c}{(T_{L_x}s + 1)}$ in Fig. B-1.

below with their corresponding open-loop transfer functions.

$$T_{Lx} = 5.0 \text{ sec } (\Delta\tau_{LEAD} = 0.2 \text{ sec})$$

$$\frac{x}{x_e} = K_x \frac{-1615.0 (-3.77)(0.2)(0.693)(6.0)[0.034; 2.09]}{(0.09)(0.0225)(0.700)(3.77)[0.316; 2.29][0.949; 7.041]} \quad (5)$$

$$T_{Lx} = 3.33 \text{ sec } (\Delta\tau_{LEAD} = 0.2 \text{ sec})$$

$$\frac{x}{x_e} = K_x \frac{-1075.59 (-3.77)(0.3)(0.693)(6.0)[0.034; 2.09]}{(0.0)(0.0225)(0.700)(3.77)[0.316; 2.29][0.949; 7.041]} \quad (6)$$

The resulting root loci are shown in Figs. B-3a and B-3b. From the corresponding open-loop frequency response in Tables B-IIIa and B-IIIb, values of K_x can be chosen to yield the gain crossover frequency for maximum phase margin. The results are given in Table B-IV. They represent the predicted loop closure characteristics for the pilot with the state display format.

The final case to be considered is for the pilot to be given a display of rate as well as position. This is indicated by either the state-and-rate column or the director column in Table B-II. It may be noted that $\Delta\tau_{LEAD} = 0$ for the reasons that the pilot does not have to generate his own lead information and no incremental scanning delay is predicted on the integrated display. The open-loop transfer functions are

$$T_{Lx} = 5.0 \text{ sec } (\Delta\tau_{LEAD} = 0)$$

$$\frac{x}{x_e} = K_x \frac{-1615.0(-6.0)(0.2)(0.693)[0.034; 2.09]}{(0.0)(0.0225)(0.700) [0.316; 2.29][0.949; 7.041]} \quad (7)$$

$$T_{Lx} = 2.5 \text{ sec } (\Delta\tau_{LEAD} = 0)$$

$$\frac{x}{x_e} = K_x \frac{-807.5 (-6.0)(0.4)(0.693)[0.034; 2.09]}{(0.0)(0.0225)(0.700) [0.316; 2.29][0.949; 7.041]} \quad (8)$$

Table B-IV again gives the values of K_x which yield the gain crossover frequency for maximum phase margin from the corresponding open-loop frequency responses in Tables B-IIIc and B-IIIi. These results in

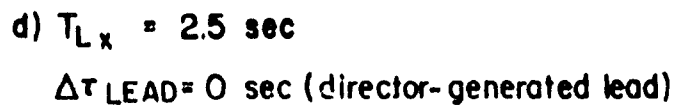
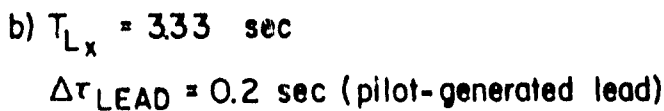
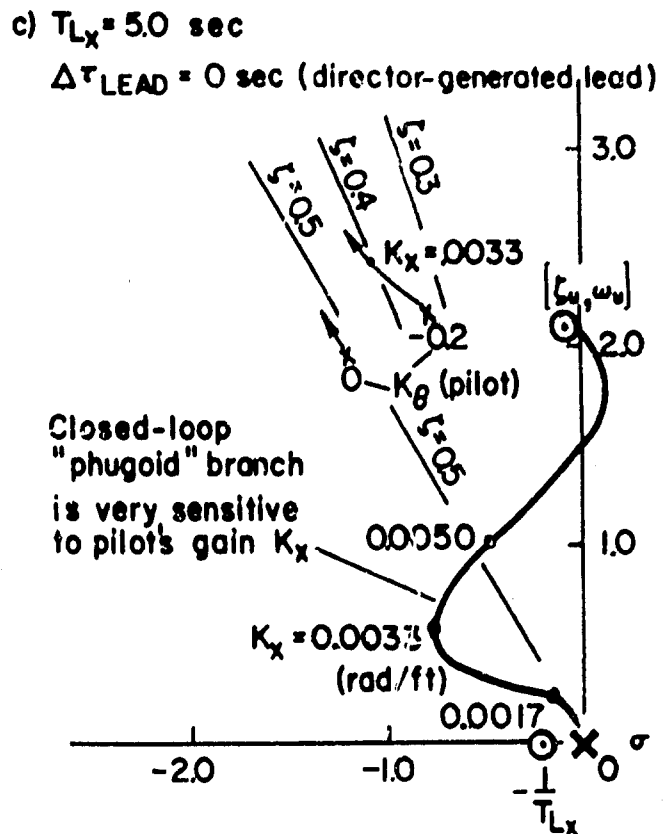
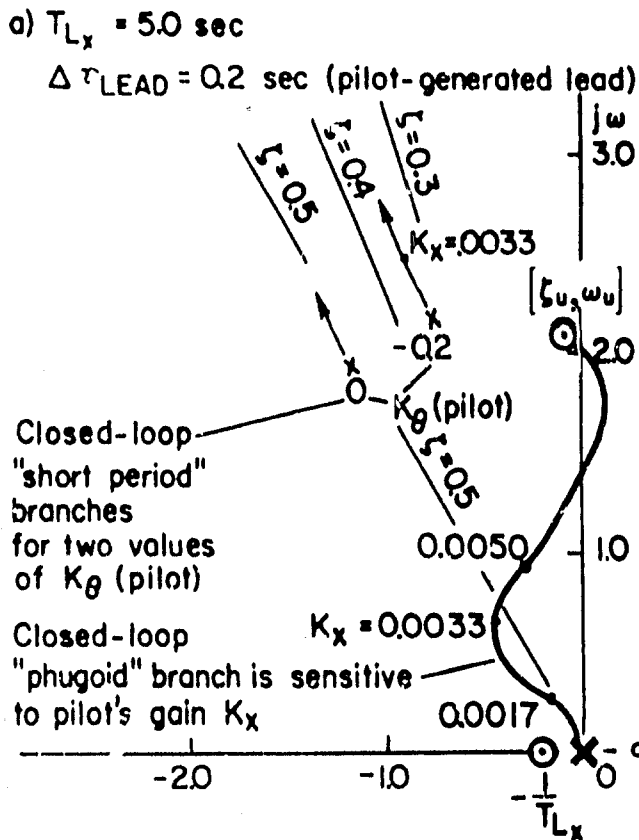


Figure B-3. Root Loci for $x \rightarrow \theta_c$ Loop Closure with K_x as the Variable Gain and the Effective Time Delay $\tau_{\theta} = 0.33$ sec

TABLE B-III (a)

Open-loop frequency response $|x/x_e|$ for $T_{Lx} = 5.0$, $\Delta\tau_{LEAD} = 0.2$ sec

ω rad/sec	$ x/x_e $ dB	$\angle x/x_e$ deg	
.100	71.03	-145.4	
.200	61.18	-138.3	
.300	56.24	-134.2] Probable Crossover Range
.400	53.09	-133.2	
.500	50.77	-134.2	
.600	48.92	-136.4	
.700	47.37	-139.4	
.800	46.00	-143.1	
.900	44.76	-147.2	
1.000	43.60	-151.6	
1.100	42.48	-156.4	
1.200	41.37	-161.5	
1.300	40.24	-167.0	
1.400	39.04	-172.7	
1.500	37.71	-178.6	
1.600	36.19	-184.8	
1.700	34.54	-190.8	

Reproduced from
best available copy.

TABLE B-III (b)

Open-loop frequency response $|x/x_e|$ for $T_{Lx} = 3.33$, $\Delta\tau_{LEAD} = 0.2 \text{ sec}$

ω rad/sec	$ x/x_e $ dB	$\angle x/x_e$ deg	
.100	70.50	-153.6	
.200	59.75	-149.7	
.300	54.13	-145.5	
.400	50.53	-143.5] Probable Crossover Range
.500	47.93	-143.3	
.600	45.90	-144.5	
.700	44.23	-146.7	
.800	42.70	-149.6	
.900	41.45	-153.1	
1.000	40.27	-157.0	
1.100	39.12	-161.4	
1.200	37.99	-166.1	
1.300	36.83	-171.2	
1.400	35.62	-176.6	
1.500	34.28	-182.4	
1.600	32.74	-188.3	
1.700	30.88	-194.1	

Reproduced from
best available copy.

TABLE B-III (c)

Open-loop frequency response $|x/x_e|$ for $T_{Lx} = 5.0$, $\Delta\tau_{LEAD} = 0.0$ sec

ω rad/sec	$ x/x_e $ dB	$\angle x/x_e$ deg	
.100	71.53	-144.3	
.200	61.18	-136.1	
.300	56.24	-130.8] Probable Crossover Range
.400	53.09	-128.7	
.500	50.77	-128.0	
.600	48.92	-127.7	
.700	47.57	-131.7	
.800	46.00	-134.3	
.900	44.76	-137.4	
1.000	43.60	-140.0	
1.100	42.48	-144.7	
1.200	41.37	-148.9	
1.300	40.24	-153.4	
1.400	39.04	-158.2	
1.500	37.71	-163.3	
1.600	36.19	-168.6	
1.700	34.34	-173.9	
1.800	31.98	-178.5	
1.900	28.75	-180.4	

Reproduced from
best available copy.

TABLE B-III (d)

Open-loop frequency response $|x/x_e|$ for $T_{Lx} = 2.5$, $\Delta\tau_{LEAD} = 0.0$ sec

ω rad/sec	$ x/x_e $ dB	$\angle x/x_e$ deg	
.100	70.32	-156.8	
.200	59.14	-154.5	
.300	53.06	-150.3	
.400	49.11	-147.1] Probable Crossover Range
.500	46.25	-145.5	
.600	44.04	-145.0	
.700	42.23	-145.5	
.800	40.66	-146.8	
.900	39.31	-148.8	
1.000	38.05	-151.3	
1.100	36.86	-154.4	
1.200	35.69	-157.8	
1.300	34.51	-161.7	
1.400	33.27	-166.0	
1.500	31.92	-170.7	
1.600	30.36	-175.5	

Reproduced from
best available copy.

TABLE B-IV

Summary of parameter choices for maximum phase margin in the outer longitudinal separation loop closure.

LEAD TIME CONSTANT T_{L_x} , sec	$\Delta\tau_{LEAD}$, sec	Gain K_x rad/ft	CROSSOVER FREQUENCY ω_c rad/sec	APPROXIMATE PHASE MARGIN deg	APPROXIMATE GAIN MARGIN dB
5.0	0.2	0.0022	0.4	47	16
3.33	0.2	0.0032	0.4	36	15
5.0	0	0.0022	0.4	51	24
2.5	0	0.0050	0.5	35	17

Table B-IV can be used to predict the best displayed scaling ratio between state-and-rate signal content and to establish the best feedback gains for the director command "law", so as to relieve the pilot of generating the necessary lead equalization solely from a state display of longitudinal separation error x_e .

Since the lead equalization time constant T_{Lx} , equals K_u/K_x , the proper displayed scaling ratio between rate \dot{x}_e ($\dot{x}_e = u$, if $x_c = 0$) and state x_e is given explicitly by T_{Lx} . In other words, the gain of the u-display should be T_{Lx} times the gain of the x_e display. Then by controlling longitudinal cyclic pitch so as to match the u and x_e symbols in the state-and-rate format or to null the director command in the director format, the pilot will be assured that the proper lead equalization is being provided to null x_e . The results in Table B-IV show that $2.5 < T_{Lx} < 5$ sec, depending on the adopted phase margin (or damping ratio of the closed-loop phugoid shown in Fig. B-3). Comparison of the corresponding root loci in Fig. B-3c and B-3d shows that a value of $T_{Lx} = 3.3$ sec should provide adequate phase margin in excess of 30 deg. (Table B-IV) and a closed-loop phugoid damping ratio in excess of 0.4 which is less sensitive to the pilot's gain variation than if a larger value of T_{Lx} were selected. A separation error loop gain on the order of $K_x=0.0032$ rad/ft will provide a crossover frequency in excess of 0.4 rad/sec to regulate against the longitudinal gust forcing function bandwidth of about 0.2 rad/sec at 60 knots true air speed.

The root loci in Fig. B-3 also show the effects of the pilot's adopting a low gain ($K_\theta = -0.2$) pitch attitude closure through his longitudinal cyclic pitch control stick in addition to the loop closure for the pitch AFCS described in Fig. B-2. The root loci show that the pilot will reduce the damping ratio of the "short period" characteristic oscillation to between 0.3 and 0.4 with the recommended AFCS in Ref. 10 and depicted in Fig. B-2, viz.,

$$B_1(s) = \frac{\overbrace{10}^{\text{Rotor and Actuator Lag}}}{s + 10} \left[\overbrace{\theta_b(s) - 0.4(s + 2)\theta(s)}^{\text{AFCS}} \right] \quad (9)$$

where B_1 is the longitudinal cyclic (rotor blade) pitch angle. Further

increase in K_θ by the pilot will reduce the short period damping ratio unfavorably. However, the second order lead equalization provided by the complex zeros, $[\zeta_u; \omega_u]$, in the speed response will tend to reduce the sensitivity of the decreasing short period damping ratio to further increase in the pilot's pitch attitude gain, K_θ .

The flight director command equation can be implemented with the aid of Table B-II by forming a linear combination of all of the human pilot's feedback and feedforward transfer functions which contribute to the signal labelled θ_e in Fig. B-1, viz.,

$$\begin{aligned}\theta_e &= -K_\theta\theta - K_u u - K_x x, & \text{if } x_c &= 0 \\ &= -K_\theta\theta - K_x(T_{Lx}s + 1)x\end{aligned}\quad (10)$$

where $-0.2 \leq K_\theta \leq 0$ for command consistency with mid-frequency pitch attitude motion, $K_x = 0.0032 \frac{\text{rad}}{\text{ft}}$ for adequate gust upset suppression bandwidth, and $T_{Lx} = 3.3$ sec for adequate closed-loop phugoid damping ratio ($0.4 \leq \zeta \leq 0.5$). The relative gains of the various contributions to the flight director are now established. The actual flight director command signal on the display is given by

$$\delta_x = \frac{\theta_e}{K_{\text{PILOT}} K_{\text{STICK}} K_{\text{DISPLAY}}}\quad (11)$$

where the values for gains K_{DISPLAY} and K_{STICK} must be partitioned in the experiment to the personal satisfaction of each subject following the procedure outlined in Ref. 5.

This completes the analysis of predicted pilot loop closures for a longitudinal separation control task in landing approach with CH-53 dynamics. The following section in this Appendix presents a simplified approximate analysis of a decoupled altitude deviation control task.

B. ALTITUDE CONTROL CLOSURE ANALYSIS

The simplified transfer function to be used for simulating the airframe altitude deviation (h) response to collective lift control (δ_c) can be approximated from Table B-I as

$$\frac{h}{\delta_c} = \frac{-3055.0}{(0.0)(0.717)(10.0)} \frac{\text{ft}}{\text{rad}}\quad (12)$$

The pure integration in the altitude deviation response to collective lift control will be approximated as a slow divergence, $(-\mu)$, where $\mu \doteq 0.1$ rad/sec, so that the only forcing function necessary for this task will be the pilot's remnant. Therefore, the simulated controlled element transfer function for the altitude regulation task will be

$$\frac{h}{\delta_c} = \frac{-3055.0}{(-0.1)(0.717)(10.0)} \frac{ft}{rad} \quad (13)$$

Block diagrams of the altitude deviation feedback to the display and of the pilot's loop closure through the collective control to regulate altitude deviation are presented in Figs. IV-2 and IV-4 in the text, Section IV. Although it will be displayed, the altitude rate (or instantaneous vertical speed) feedback will probably not be needed by the pilot for equalization, as the closure analysis will show subsequently. Instead the altitude rate (or instantaneous vertical speed) display will probably be required only for monitoring rates of change of the state of vertical error.

The bandwidth of the vertical gust forcing function which would normally upset altitude deviation at a speed of 60 knots true air speed is about $1/3$ rad/sec. This is only about one-half the bandwidth of the helicopter's heaving subsidence at 60 knots and suggests that adequate altitude regulation can be achieved with a pure gain closure or perhaps a closure with only high frequency lead to reduce the pilot's time delay. In the actual experiment, of course, the much broader bandwidth of the pilot's remnant will serve as a forcing function. In order to try to predict the gain crossover frequency and equalization which the pilot may adopt in performing the simulated altitude regulation task, we have examined the sensitivity of the closure to several values of gain and high frequency lead equalization.

The pilot's effective time delay (τ_e) for this closure can be estimated with sufficient precision by partitioning the delay in two parts: (1) the pure latency, $\tau \doteq 0.1$ sec, and (2) the effective low frequency lag of the neuromuscular system coupled with a free collective stick, $T_H \doteq 0.2$ sec.

Root loci for two illustrative closures are shown in Fig. A-4. Corresponding open-loop frequency responses including the probable gain

Effective Time delay $\tau_e = \tau + T_N$

$$= 0.1 + 0.2 = 0.3 \text{ sec.}$$

Subscript "N" Neuromuscular System

a)

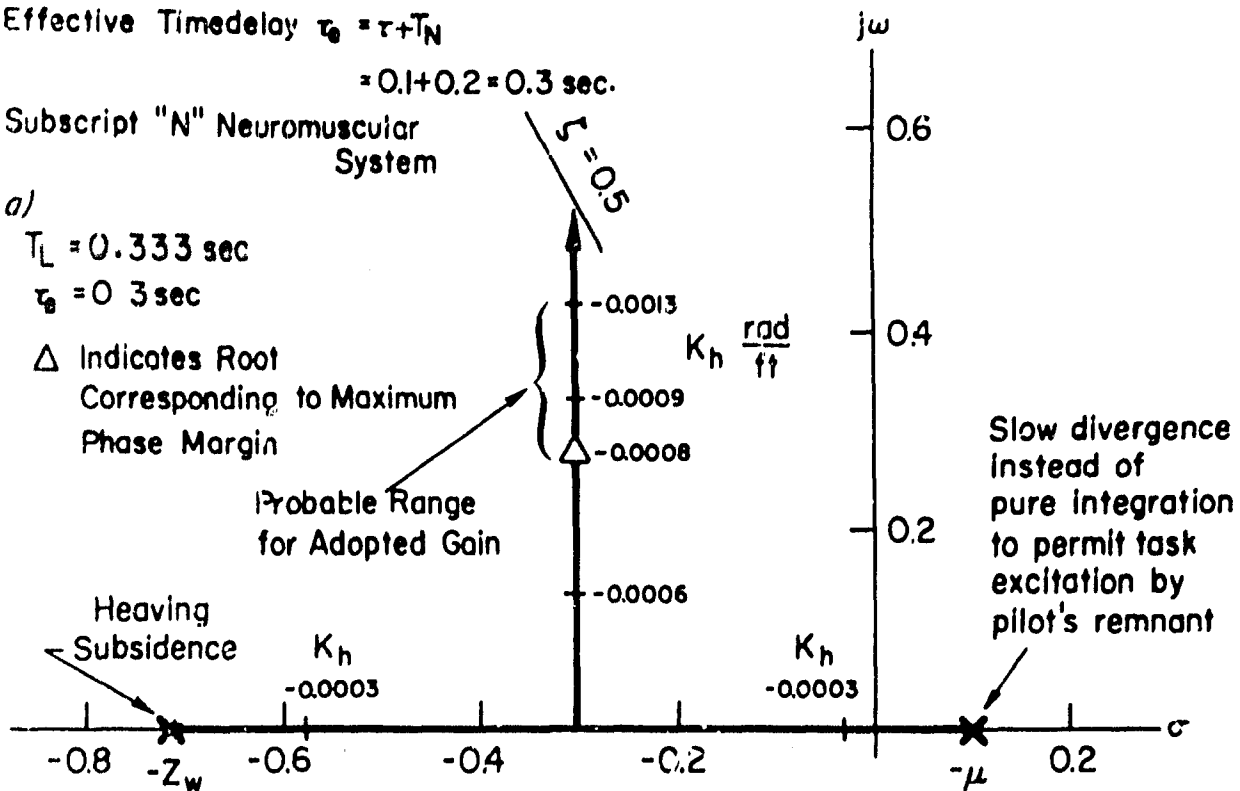
$$T_L = 0.333 \text{ sec}$$

$$\tau_e = 0.3 \text{ sec}$$

Δ Indicates Root Corresponding to Maximum Phase Margin

Probable Range for Adopted Gain

Heaving Subsidence



Slow divergence instead of pure integration to permit task excitation by pilot's remnant

b)

$$T_L = 0.1 \text{ sec}$$

$$\tau_e = (0.3 \text{ sec} - T_L) = 0.2 \text{ sec}$$

Probable Range for Adopted Gain

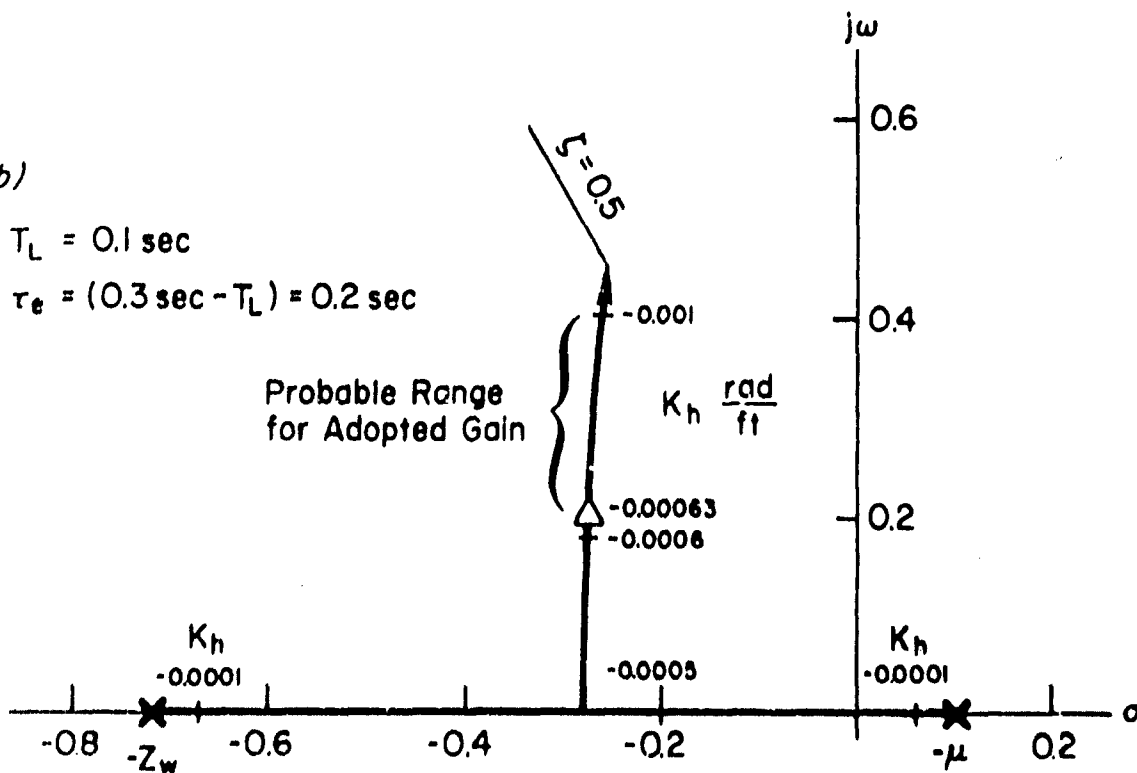


Figure B-4. Root Loci for $h - b_c$ Loop Closure with K_h as the Parameter and Using a Free Collective Stick

crossover frequency range are listed in Table B-V. The probable crossover frequency ranges are bounded from below by the gains for maximum phase margin listed in Table B-VI.

The effect of high frequency lead equalization ($0.1 \leq T_L \leq 0.333$ sec) is presented in Fig. B-4a and B-4b and Tables B-Va and B-Vb. The estimated crossover frequency range is from 0.3 to 0.4 rad/sec, if the pilot should adopt lead equalization such that $T_L = 0.333$ sec. Otherwise, in all cases examined, the estimated crossover frequency range is from 0.2 to 0.3 rad/sec. Closures without lead and with 0.1 sec additional effective time delay, presumed due to an additional scanning delay or neuromuscular lag, exhibit slightly smaller stability margins (and damping ratio) as shown in Table B-VI.

Since we do not expect the pilot to adopt lead equalization below 2 rad/sec and requiring significant perceptual motor workload in the simulated altitude regulation task, the displayed signal gain for the instantaneous vertical speed display need be only one-half that for the altitude deviation display.

C. EXCESS CONTROL CAPACITY (ATTENTIONAL WORKLOAD) ANALYSIS

The results obtained in Ref. 5 with a secondary cross-coupled subcritical roll tracking task as a function of various single-axis controlled elements will form a basis for predicting excess control capacity for the present pilot experiment. The score obtained from the cross-coupled secondary task is the steady-state value of its unstable pole, which represents its rate of divergence or degree of difficulty; consequently, the same score also represents the "degree of ease" of the primary task. The abscissa in Fig. A-5 illustrates the secondary task scores obtained from Ref. 5 as a function of several forms of controlled element denoted by the symbols along the ordinate. The secondary task scores also correlated well with the subjective pilot opinion rating of the primary tasks.

Two interpretations can be given to the secondary task score by normalizing the score with respect to the critical or limiting score which the subject can achieve if the secondary task is the only task. These two interpretations of the normalized score are shown on scales at the top of Fig. A-5. The normalized score itself can be interpreted

TABLE B-V (a)

Open-loop frequency response $|h/\delta_c|$ for $T_L = 0.333$, $\tau_e = 0.3$ sec
 $\tau_e = \tau + T_N$, where the latency, $\tau = 0.1$ sec and the effective low
 frequency neuromuscular lag, $T_N = 2.0$ sec. The lead equalization is
 represented by the first order factor, $(1 + j\omega T_L)$

ω rad/sec	$ h/\delta_c $ dB	$\angle h/\delta_c$ deg
.100	69.50	-143.3
.200	65.29	-132.9
.300	61.93	-132.3
.400	59.18	-134.8
.500	56.83	-138.2
.600	54.76	-141.8
.700	52.90	-145.3
.800	51.22	-148.6
.900	49.68	-151.6
1.000	48.27	-154.4
1.100	46.97	-157.0

Probable
Crossover
Range

Reproduced from
best available copy.

TABLE B-V (b)

Open-loop frequency response $|h/s_c|$ for $T_L = 0.1$, $\tau_e = (0.3 - T_L)$ sec
 $\tau_e = \tau + T_N - T_L$, where the latency, $\tau = 0.1$ sec and the effective low
 frequency neuromuscular lag, $T_N = 2.0$ sec. The lead equalization is
 included in the effective time delay.

ω rad/sec	$ h/s_c $ dB	$\angle h/s_c$ deg	
.100	69.50	-144.7] Probable Crossover Range
.200	65.27	-135.6	
.300	61.89	-136.3	
.400	59.10	-140.1	
.500	56.71	-144.8	
.600	54.59	-149.7	
.700	52.67	-154.5	
.800	50.92	-159.0	
.900	49.31	-163.2	
1.000	47.81	-167.2	
1.100	46.42	-170.9	

TABLE B-VI

Summary of parameter choices for maximum phase margin
in the altitude regulation closure

Pilot Effective Time Delay τ_e , sec	Lead Time Constant T_L , sec	Gain K_h (rad/ft)	Crossover Frequency ω_c , rad/sec	Approx. Phase Margin deg	Approx. Gain Margin dB
0.3	0.333	-0.0008	0.3	48	25
(0.3 - T_L)	0.1	-0.00063	0.2	44	22
0.3	0.0	-0.00063	0.2	43	19
0.4	0.0	-0.00063	0.2	42	17

as the excess control capacity which the pilot has available for performing other tasks while maintaining performance on the primary task(s). If the normalized score is subtracted from unity, the resulting scale can be interpreted as a measure of the pilot's fractional attentional workload required for performing the primary task.

At the present state of our understanding, the "best" partition of controlled element and display gains ("control gains", for short) required to produce the results in Fig. A-5 must still be empirically determined. Over a wide range of control gains, however, research in handling qualities has shown that the average absolute tracking error is nearly constant, whereas the pilot's gain varies inversely with the control gain. The subjective rating of the task and the secondary task score show a distinct optimum, which is not revealed by either the error score or the pilot's gain. (Refs. 4 and 5.)

The principal cause of the trends shown in Fig. A-5 is due to the increasing attentional workload which accompanies the generation of low frequency lead equalization by the pilot as the controlled element form progresses from K/s to K/s^2 . However, the extremely high attentional workload (low excess control capacity) associated with the unstable primary controlled element $K/(s - 2)$ in Fig. A-5 is probably associated with a different cause. This cause is thought to be the increasing neuromuscular tension which accompanies the consistently reduced effective pilot's time delay measured with this type of controlled element for which low frequency lead equalization is not required.

Since the present experiment involves two simultaneous piloting tasks for which we wish to predict the excess control capacity, we shall adopt a technique from Ref. 6 for predicting pilot ratings for multi-axis control tasks using single-axis rating data. This technique is based on an empirical relationship between measured excess control capacity and the pilot's generated lead time constant, T_L . The single-axis prediction technique is illustrated graphically in Fig. B-5 using results extrapolated from Ref. 5. The upper portion of Fig. B-5 is entered at the ordinate corresponding to the estimated pilot's lead time constant predicted from display-pilot-vehicle closed-loop analysis. Then by following the indicated arrows, one can estimate either the attentional workload fraction or the excess control capacity for the

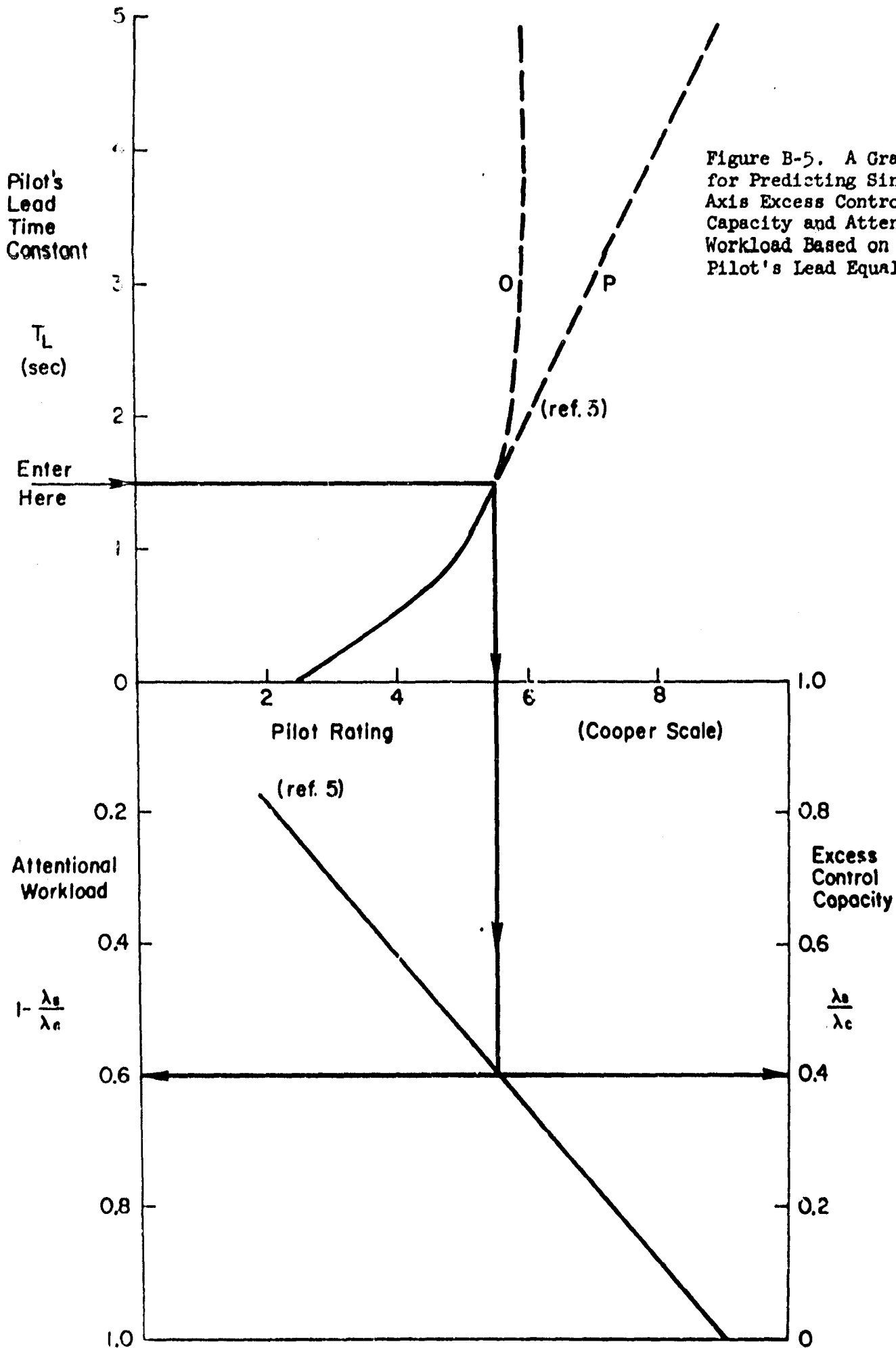


Figure B-5. A Graph for Predicting Single-Axis Excess Control Capacity and Attentional Workload Based on the Pilot's Lead Equalization

single-axis task.

Reference 6 predicted multiaxis pilot ratings of handling quantities using a method proposed by BTTI in Ref. 7. The predictions were then compared in Ref. 6 with two-axis pilot ratings obtained experimentally and the average correlation was shown to be excellent. When the same method (Ref. 7) is extended for predicting excess control capacity with the aid of the lower portion of Fig. B-5 for each axis, multiaxis excess control capacity, $(x_{scc})_m$, is obtained from the equation

$$(x_{scc})_m = f \left\{ T_{L_{BASE}} + \sum_{i=2}^N \left[f^{-1}(\lambda_{s_i}/\lambda_c) - T_{L_{BASE}} \right] \right\} \quad (14)$$

where $\lambda_s/\lambda_c = f(T_L)$ is defined by Fig. B-5.

$$T_{L_{BASE}} = f^{-1}(\lambda_{s_{MAX}}/\lambda_c)$$

$\lambda_{s_{MAX}}/\lambda_c =$ maximum excess control capacity among the single axes comprising the multi-axis situation.

We shall illustrate the use of Eq. 14 by predicting a multiaxis excess control capacity for the experiment. The estimated pilot's lead time constant for the longitudinal control axis is $T_L = 3.3$ sec from topic A in this Appendix. (The effective controlled element is K/s^2 .) By entering the ordinate of the upper portion of Fig. B-5 at $T_L = 3.3$ sec, we can use the optimistic extrapolation of Ref. 5 denoted by the broken line labelled "O", to estimate an upper bound of 0.35 on the excess control capacity for the longitudinal axis. We can also use the pessimistic extrapolation of Ref. 5 denoted by the broken line labelled "P", to estimate a lower bound of 0.19 on the longitudinal excess control capacity.

The estimated pilot's lead time constant for the vertical control axis is $T_L < 0.5$ sec from topic B in this Appendix. A glance at Fig. B-5 shows that, if $T_L < 0.5$ sec, the predicted single-axis control capacity would be $\lambda_B/\lambda_c > 0.58$ for the vertical axis from the data of

Ref. 5. However, the effective controlled element for the vertical axis is $K/s(s + 0.7)$, which is approximately like the controlled element $K/s(s + 1)$, for which a measurement of excess control capacity is plotted in Fig. A-5 as $\lambda_B/\lambda_C = 0.46$. This measurement corresponds to an inferred pilot lead time constant, $T_L = 1$ sec.

Since either task could be performed with an effective director display-and-controlled element K/s , we shall adopt the excess control capacity of 0.75, corresponding to K/s in Fig. A-5, as λ_{BMAX}/λ_C for use in Eq. 14. Reference to Fig. B-5 will show that $\lambda_{BMAX}/\lambda_C = 0.75$ corresponds to $T_{LBASE} = 0$ in Eq. 14. Hence the indicated summation in Eq. 14 becomes simply a sum of two single-axis values for T_L , corresponding to the longitudinal and vertical axes in the experiment. The estimated range for this sum is

$$4.3 \geq \sum_{i=2}^2 T_{L_i} > 5.3 \text{ sec} \quad (15)$$

The corresponding optimistic range for the predicted multiaxis excess control capacity in this experiment is

$$0.08 \leq (x_{scc})_m < 0.35 \quad (16)$$

and the corresponding pessimistic range is

$$0.08 \leq (x_{scc})_m \leq 0.19 \quad (17)$$

There is a much simpler empirical way to make these multiaxis estimates from the single-axis estimates of excess control capacity, viz., to multiply the single-axis estimates, if they are different, and to use the single-axis maximum estimate itself when the estimates for each axis are equal to the maximum estimate for display-and-controlled element K/s . To illustrate how closely this rule approximates the pessimistic range in Eq. 17, we shall form the indicated products in Eq. 18.

$$\begin{aligned} (0.46)(0.19) &\leq (x_{scc})_m < (0.58)(0.35) \\ 0.09 &\leq (x_{scc})_m < 0.2 \end{aligned} \quad (18)$$

Although Ref. 6 presents none of the single-axis experimental data by which the accuracy of this "product rule" could be tested, it also works quite well on the data cited in Ref. 7 on the basis of which Eq. 14 was derived. In the form of an equation, the product rule for

multiaxis excess control capacity is

$$(x_{scc})_M = \begin{cases} \prod_{i=2}^N (\lambda_{B_i} / \lambda_c) & ; \quad \lambda_{B_i} < \lambda_{B_{MAX}} \\ \lambda_{B_{MAX}} & ; \quad \lambda_{B_i} = \lambda_{B_{MAX}} \\ & i=1, 2, \dots, N \end{cases} \quad (19)$$

The optimistic estimate of multiaxis excess control capacity is less than 0.35 for the longitudinal and vertical control tasks. This optimistic prediction corresponds to a Cooper Scale Rating of less than 6. The pessimistic estimate of multiaxis excess control capacity is between 0.1 and 0.2 for the same tasks. This pessimistic prediction corresponds to a Cooper Scale Rating between 7 and 8. The corresponding subjective rating of multiaxis controllability and precision based on the scale proposed in Table IV-3 is estimated to be about C3: "Controlable, with less than adequate precision." The corresponding subjective rating of multiaxis attentional demand based on the scale proposed in Table IV-3 is estimated to be about D4: "Quite demanding."

Estimates of excess control capacity and subjective rating with the director format are expected to be more favorable and less demanding of attention. The multiaxis excess control capacity is predicted to be about 0.5 ± 0.1 ; the subjective controllability, about C2, "Easy to control, with fair precision"; and the subjective attentional demand, about D3, "Mildly demanding."

Measurements of excess control capacity and subjective rating with the state-and-rate format are expected to be between those for the state format and those for the director format.

D. Multiaxis Scanning Behavior

The general principles and analytical techniques for predicting multi-axis scanning behavior and performance on a preliminary control display design are described and applied in Refs. 8 and 9. Four points of fixation will be hypothesized in the pilot experiment: two for the purpose of control and two for the purpose of monitoring. The two fixation points for control will be the integrated display and the pair of vertical scale displays; the two points for monitoring will be the airspeed indicator and altimeter.

The effective dwell fraction (η_e) and the scanning frequency (ω_B) for the integrated display will be estimated by hypothesizing three conditions, viz., (1) the look fraction on the integrated display will approach its limiting value, 0.5; (2) the average scanning frequency (and look fraction) on the integrated display will be approximately the same as that on the pair of vertical scale displays for height control, because these are the only two points of fixation for the purpose of control; and, (3) sampling remnant power for the integrated display will be suppressed to the same order of magnitude as equalization remnant power for the longitudinal position (x) display.

The third hypothesis enables a lower bound to be estimated for the effective sampling-to-crossover frequency ratio, S, defined by Eq. 20.

$$S = \omega_B / \omega_C (1 - \eta_e) \quad (20)$$

Experimental results in Ref. 11 suggested the following ranges of values for S:

- 4 < S ≤ 6 for separate displays among which parafoveal perception is inhibited
- 6 < S < 10 for combined displays among which parafoveal perception may be significant.

However, recent measurements in Ref. 12 suggest that S > 15 for the outer (position) loop and that 6 < S < 15 for the inner (attitude) loop under simulated instrument flight conditions.

A physical interpretation of the ratio S can be gained by converting the circular frequencies ω_C and ω_B in Eq. 20 into their respective periods, P_C and T_B , through the substitutions: $\omega_C = 2\pi/P_C$ and $\omega_B = 2\pi/T_B$. Then by using the definition of effective dwell interval (T_{d_e}) from Eq. 26 below, the ratio S can be expressed as the ratio of the crossover period (P_C) relative to the effective fixation interrupt interval ($T_B - T_{d_e}$) or time-away from a display. The ratio S should be large to minimize effects of scanning remnant. An integrated display should help the pilot to adopt a large ratio S.

In order to suppress sampling remnant power to the same order of magnitude as equalization remnant power in the x-display, the third hypothesis can be expressed by the inequality

$$\frac{1}{S_x \omega_{c_x}} < \frac{\sigma_{T_{S1}} (1-\eta_e)_1 \left(1 + T_{L_x}^2 \frac{\sigma_u^2}{\sigma_x^2} \right)}{\pi} \quad (21)$$

where $\sigma_{T_{S1}}$ and $(1-\eta_e)_1$ are internal values for processing remnant adapted from Table II-3 in the text. $\sigma_{T_{S1}}$ will be taken as 0.1 sec and $(1-\eta_e)_1$ as 0.9 for making this estimate of S_x . The value for ω_{c_x} , 0.1 rad/sec, and the value for T_{L_x} , 3.3 sec, are from Topic A in this Appendix. The value for the longitudinal variance ratio (σ_u^2/σ_x^2) will be estimated from the performance calculations which follow subsequently in Topic E of this Appendix. The longitudinal variance ratio lies in the range

$$0.061 < \sigma_u^2/\sigma_x^2 < 0.214.$$

The lower bound is the u_g -gust-correlated value; the upper bound is the uncorrelated variance ratio governed by remnant. After substituting numerical values in Eq. 21, we obtain a range for S_x : $25.9 < S_x < 52.3$. Since this range exceeds the measured values for S obtained to date, we shall adopt a value $S_x = 39$ near the mid-point for making predictions of the effective dwell fraction and the scanning frequency on the integrated display. The predictions are summarized in Table B-VII. There it is also shown that a value of $S_\theta = 8$ in the range of Ref. 12 for the inner (attitude) loop (which is also presented on the integrated display), when multiplied by the inner loop crossover frequency, $\omega_{c_\theta} = 2$ rad/sec, satisfies the equality $\omega_{c_x} S_x = \omega_{c_\theta} S_\theta = \omega_B/(1-\eta_e)$ required by Eq. 20 for the integrated display.

Now the adopted foveal scanning behavior is still unknown. It depends, for example, on satisfying performance requirements and the physical upper bound on cumulative visual foveal fixation dwell fraction (scanning workload) expressed in the following equation of constraint.

$$M_B + \sum_{i=1}^M \eta_i = 1 ; \quad \begin{array}{l} M \text{ separate displays; with an optional} \\ \text{scanning workload margin } M_B \text{ for} \\ \text{non-control tasks} \end{array} \quad (22)$$

TABLE B-VII

Predicted Average Display Scanning Statistics for the Pilot Experiment

Predicted	Cross over Frequency ω_c rad/sec	Frequency Ratio S	Effective Interrupt Fraction $1-\eta_e$	Effective Dwell Fraction η_e	Parafoveal Gain Ratio to Foveal	Foveal Dwell Fraction η_f	Scanning Frequency		Effective Dwell Interval T_{de} sec	Foveal Dwell Interval T_{df} sec	Look Fraction $\frac{v}{f_{s1}}$	
							ω_s rad/sec	f_s Hz				
b) Vertical Scales	0.3	17	0.49	0.51	0.22	0.37	2.5	0.4	2.5	1.3	0.9	0.42
c) Integrated g	0.4	35 8	0.16	0.84	0.63	0.57	2.5	0.4	2.5	2.1	1.4	0.42
	2.0											
Airspeed Altitude		Monitored Monitored				0.03		0.075	13.3		0.4	0.08
				0.03		0.075	13.3		0.4	0.08		
Totals						1.00		0.95				1.00

This equation is called the "scanning workload constraint." It is applied in Table B-VII by summing the foveal dwell fraction column, η_f .

The sum of the effective dwell fractions will exceed unity in the scanning workload constraint. This is called oversaturation. Effective dwell fractions, the sum of which apparently exceeds the scanning workload constraint, can be achieved with lower foveal dwell fractions if parafoveal perception of the appropriately displayed signals is not inhibited. A reduced foveal dwell fraction is estimated in Table B-VII from Eq. 23.

$$\eta_f = \frac{\eta_e - \Omega}{1 - \Omega} \quad (0 \leq \Omega \leq 1) \quad (23)$$

where $\Omega = \omega_{c_p}/\omega_{c_f}$, the average parafoveal-to-foveal gain crossover frequency ratio.

Ω is largest on a combined display with two signals and homogeneous equalization. Increasing display separation reduces Ω and increasing the number of displays also reduces Ω . A predicted parafoveal-to-foveal gain ratio, $\Omega = 0.63$, makes it possible to achieve a high effective dwell fraction, $\eta_e = 0.84$, on the integrated display with a smaller foveal dwell fraction, $\eta_f = 0.57$, listed in Table B-VII.

Predictions for the two monitored displays, airspeed and altitude, in Table B-VII are based on two different hypotheses, viz. (1) a foveal dwell fraction (η_f) of 0.03 for each; and a foveal dwell interval, $T_d = 0.4$ sec for each.

Predictions for the pair of vertical scale displays, h , \dot{h} , are based on the remaining foveal dwell fraction ($\eta_e = 0.37$) required to occupy fully the pilot's time with less weight given to parafoveal perception. Since $\Omega = 0.22$ by hypothesis, a lower value of the sampling-to-crossover frequency ratio, $\beta = 17$, is assumed for the height display-control task.

The average scanning frequency, (f_B), scanning interval (T_B), and effective dwell interval (T_{d_e}) follow from their definitions.

$$f_B = \omega_B/2\pi \text{ (Hz)} \quad (24)$$

$$T_B = 1/f_B \text{ (sec)} \quad (25)$$

$$T_{d_e} = \eta_e T_B \text{ (sec)} \quad (26)$$

The predicted probabilities of fixation are identical to the foveal dwell fractions whose sum is unity in the central column of Table B-VII. The sum of the dwell fractions is unity because all of the pilot-subjects' time will be occupied by the controlling and monitoring tasks.

Likewise the sum of look fractions in the extreme right column of Table B-VII is unity, because all of the pilot-subjects' fixations are predicted to be on the experimental displays. The look fraction on the integrated display, 0.42 is estimated to approach its limiting value, one-half. The greatest proportion of fixation transitions will be between the integrated display and the pair of vertical scale displays. The transition "link value" for these two displays can be estimated as 0.79 from the predicted probabilities of fixation by the following relationship from Ref. 13.

$$\frac{2\phi_1\phi_1}{1-\sum_k\phi_k^2} = \frac{2(0.57)(0.37)}{1-0.464} = 0.79 \quad (27)$$

Other lesser link values between the control displays and the monitored displays can be estimated in analogous fashion as shown in Fig. B-6.

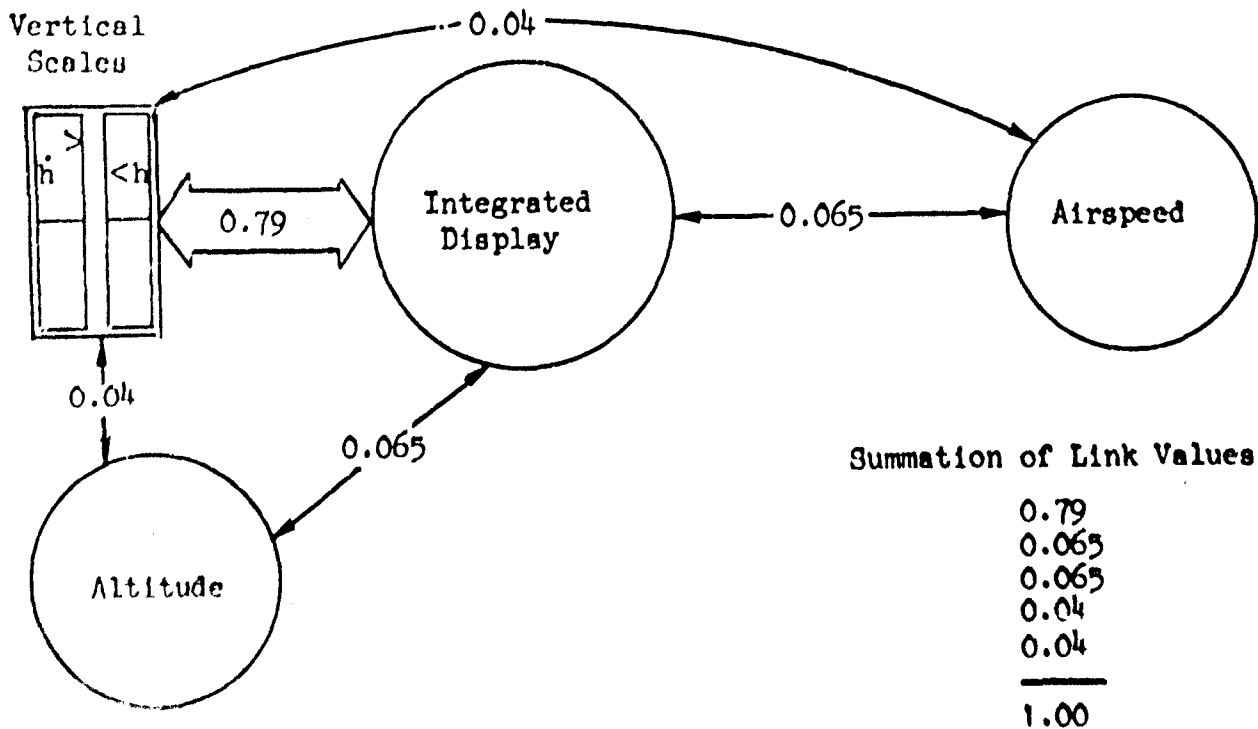


Fig. B-6. Predicted Link Values for the Multiaxis Experiment.

E. Multiaxis Performance

The total error variance vector $\{\overline{\epsilon^2}\}$ is related to the coherent variance vector $\{\epsilon_l^2\}$ by the equation

$$[\Delta_B] \{\overline{\epsilon^2}\} = \{\epsilon_l^2\} \quad (28)$$

where $[\Delta_B]$ is a square coherence matrix containing elements of the form

$$\Delta_{B\epsilon_1\epsilon_j} = \left[\delta_{1j} - \frac{0.09}{\pi} \left(1 + T_L^2 \frac{\sigma_{\epsilon_1}^2}{\sigma_{\epsilon_j}^2} \right) \int_0^\infty \left| \frac{\epsilon_1}{n\epsilon_j} \right|^2 \frac{d\omega}{(1 + T_L^2 \omega^2)} \right] \quad (29)$$

with i states in the variance vector and j displayed variables and

$\delta_{ij} = \begin{cases} 1; & i = j \\ 0; & i \neq j \end{cases}$ is the Kronecker delta.

Equation 28 incorporates from Table II-3 in the text that portion of processing remnant power spectral density which is identified with the lead equalization time constant T_L and which is expected to predominate over other types of remnant in the multiaxis task with the integrated display. The determinant of $[\Delta_B] = \Delta_B$ is called the characteristic determinant of stability in the mean-square sense, or the coherence determinant. Each component of the coherent variance vector has the form

$$\overline{\epsilon_l^2} = \sum_{j=1}^N \int_0^\infty \left| \frac{\epsilon_l}{\epsilon_j} \right|^2 \phi_{lj} d\omega \quad (30)$$

where $l_k = x_c, u_g, w_g$, for example, for $N = 3$ independent longitudinal inputs such as separation measurement noise, and longitudinal and normal gust velocities. Thus the vector $\{\overline{\epsilon_l^2}\}$ will, in general, be a column matrix of linear combinations of input-correlated mean-squared errors. The formal result for the total variance vector is

$$\left\{ \overline{\epsilon_l^2} \right\} = \frac{\text{adj}[\Delta_B]}{\Delta_B} \left\{ \overline{\epsilon_l^2} \right\} \quad (31)$$

The coherence determinant governs multiloop stability in the mean-square sense; therefore, it must be greater than zero. A value for the determinant which is much less than unity means that incoherent error power due to processing remnant will be much greater than the coherent error power due to inputs and disturbances. If the coherence determinant approaches unity (its upper bound), the error power will become increasingly coherent.

We shall illustrate the estimation of the coherent variance vector, $\{\overline{\epsilon_l^2}\}$, for two forms of a longitudinal (u_g) gust velocity input, viz., (1) a random input having a continuous power spectrum and (2) a quasi-random sum-of-sine waves. Both spectra will have the same root-mean-square (rms) gust velocity, $\sigma_{u_g} = 5.1$ ft/sec. The required open-loop transfer functions and closed-loop roots, power spectra, signal variances and rms values are listed in Table B-VIII. Bode diagrams of the required open-loop transfer functions are illustrated in Fig. B-7 for typical values of the pilot's pitch attitude and longitudinal separation loop gains selected from Topic A in the Appendix. Ratios of the correlated rate-to-displacement signal variance ratios, σ_u^2/σ_x^2 , and $\sigma_q^2/\sigma_\theta^2$, can be estimated from the variances at the end of Table B-VIII. The coherent variance vector for this example with the indicated u_g -sum-of-sine waves input is

$$\left\{ \overline{\epsilon_l^2} \right\} = \begin{bmatrix} \overline{x_l^2} \\ \overline{\theta_l^2} \\ \overline{\delta_{B_l}^2} \end{bmatrix} = \begin{bmatrix} 3.26 \text{ ft}^2 \\ 0.341\text{E-}04 \text{ rad}^2 \\ 0.417\text{E-}04 \text{ rad}^2 \end{bmatrix} \quad (32)$$

Obviously, the manually-controlled separation-keeping task is not

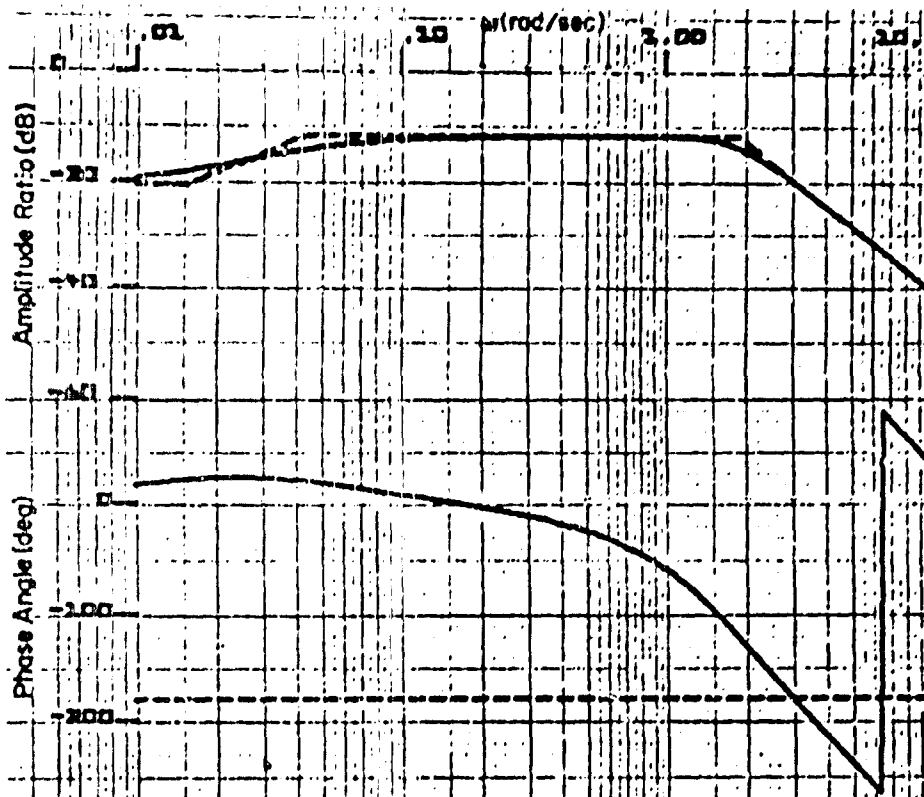


Figure B-7(a). Open-Loop Bode Diagram for
a Manually Controlled Inner Loop
with $K_{\theta} = -0.02$

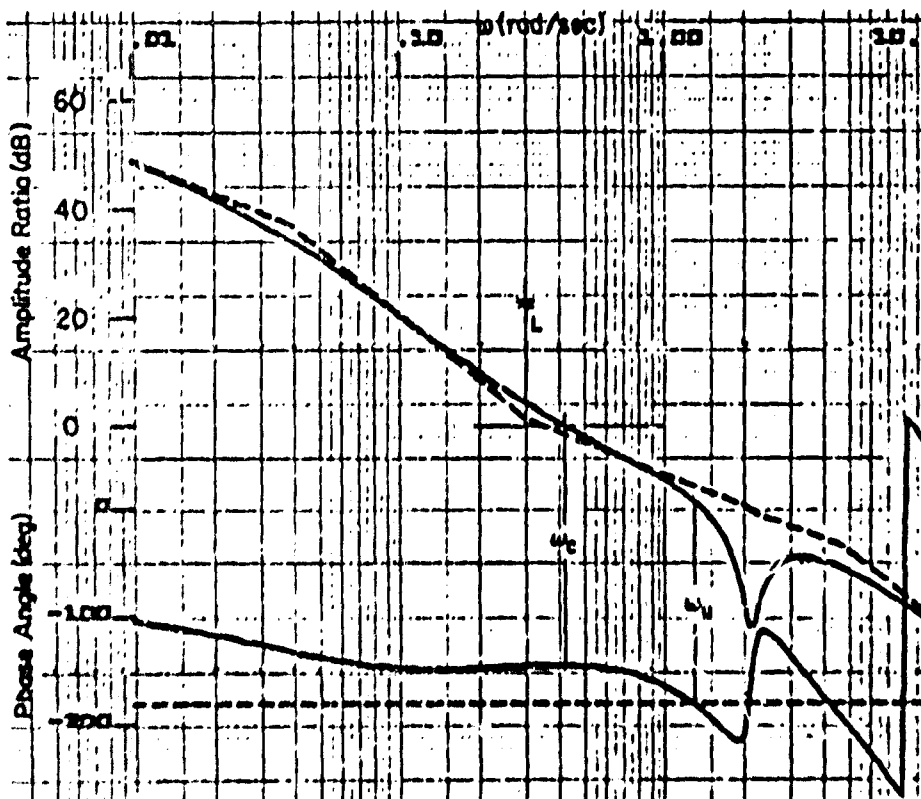


Figure B-7(b). Open-Loop Bode Diagram for
a Manually Controlled Outer Loop with
 $K_x = 0.00317$ Rad/Ft; $T_L = 3.33$ Sec

TABLE B-VIII

Open-Loop Transfer Functions and Closed-Loop Roots, Spectra and Variances for Manually Controlled Inner Pitch Attitude and Outer Longitudinal Separation Loops with a State Display and Longitudinal Gust Disturbances

INNER LOOP $\theta \rightarrow \delta_p$ with $K_p = -0.2$

TRANS. FUNC. ON OUTPUT FILE

NUMERATOR

High Frequency Gain
 .91000E 0 ←
 (.15703E- 1) (.10000E 1) (-.12121E 2) (-.12121E 2)
 (1/T_{θ1}) (-Z_w) (-4/T_θ) (-4/T_θ)

DENOMINATOR

High Frequency Gain
 .10000E 1 ←
 (.42999E- 1) (.10000E 1) (.12121E 2) (.12121E 2)
 (1/T_{p1}) (-Z_w) (4/T_θ) (4/T_θ)
 .62799E 0 .18918E 1
 ζ ω

N.S. FREQ GAIN MARGIN
 RAD/SEC DB
 2.941 19.575

NO WC

CLOSED LOOP ROOTS (NUM+DENOM)

.10000E 1
 (.37300E- 1) (.10000E 1)
 .48277E 0 .20614E 1
 .98651E 0 .12485E 2



OUTER LOOP $u \rightarrow \delta_p$ with $K_x = 0.00317$ rad/ft with inner loop closed

TRANS. FUNC. ON OUTPUT FILE

NUMERATOR

High Frequency Gain
 .17048E 1 ←
 (.30030E 0) (.10000E 1) (-.12121E 2) (-.12121E 2)
 (1/T_x) (-Z_w) (-4/T_θ) (-4/T_θ)
 .38525E- 1 .21311E 1
 ζ ω

DENOMINATOR (from closed-loop roots for inner loop above)

.10000E 1
 (.00000E 0) (.37300E- 1) (.10000E 1) (.50000E 1)
 (1/ΔT_{LEAD})
 .48277E 0 .20614E 1
 .98651E 0 .12485E 2

TABLE B-VIII

Open-Loop Transfer Functions and Closed-Loop Roots, Spectra and Variances
for Manually Controlled Inner Pitch Attitude and Outer Longitudinal
Separation Loops with a State Display and Longitudinal Gust Disturbances
(Continued)

N.S. FREQ RAD/SEC	GAIN MARGIN DB
1.285	14.093
2.103	38.197
4.211	26.193

WC RAD/SEC	PHASE MARGIN DEG
.414	36.263

CLOSED LOOP ROOTS (NUM+DENOM)

.10000E 1			
(.10000E 1)	(.25857E 1)		
.47914E 0	.39387E 0	0	
.65033E 0	.21609E 1	1	
.96085E 0	.13467E 2	2	

UG-SUM OF SINE WAVES INPUT RMS= .5100E 1

$5.1^2 = 26 \frac{1}{2}$

X /UG TRANS. FUNC.

FREQ	MAGNITUDE	PHASE	REAL	IMAGINARY
.19	-7.98	-36.56	.3207E 0	-.2378E 0
.50	-12.13	-133.05	-.1688E 0	-.1808E 0
1.26	-32.34	-197.63	-.2301E- 1	.7313E- 2
3.02	-50.80	-157.39	-.2662E- 2	-.1108E- 2
6.28	-61.14	-170.31	-.8647E- 3	-.1476E- 3

	VARIANCE	RMS
X (FT)	.32509E 1	.18055E 1
U (FT/SEC)	.20065E 0	.44794E 0
THETA (RAD)	.34122E- 4	.58414E- 2
Q (RAD/SEC)	.83898E- 5	.20965E- 2
DB (IN)	.41678E- 4	.64549E- 2

TABLE B-VIII

Open-Loop Transfer Functions and Closed-Loop Roots, Spectra and Variances
for Manually Controlled Inner Pitch Attitude and Outer Longitudinal
Separation Loops with a State Display and Longitudinal Gust Disturbances
(Concluded)

UG RANDOM INPUT RMS= .510 E 1 1/TCR= .3142E 0

C.L. SPECTRA ON OUTPUT FILE

↑
Half-Power Frequency (rad/sec) of first
Order Spectrum.

DENOMINATOR

.10000E 1
(.31417E 0)(.10000E 1)(.25857E 1)

.47914E 0 .39387E 0
.65033E 0 .21669E 1
.96085E 0 .13467E 2

X NUMERATOR

.84391E - 1
(.10000E 1)(.50000E 1)

.22908E 0 .21085E 1
.99459E 0 .12256E 2

Reproduced from
best available copy.

THETA NUMERATOR

-.68125E - 2
(.18144E 0)(-.37324E 0)(.10000E 1)(.14623E 2)

.98956E 0 .74838E 1

DB NUMERATOR

-.58227E - 2
(.34365E 0)(.10000E 1)(-.12121E 2)(-.12121E 2)

.57170E 0 .16674E 1

UG RANDOM INPUT RMS= .5100E 1 1/TCR= .3142E 0

	VARIANCE	RMS
X (FT)	.25175E 1	.15867E 1
U (FT/SEC)	.16519E 0	.40644E 0
THETA (RAD)	.32779E - 4	.57253E - 2
Q (RAD/SEC)	.14765E - 4	.38425E - 2
DB (RAD)	.33647E - 4	.58006E - 2

upset significantly by the longitudinal gust rms velocity of 5.1 ft/sec.

We shall illustrate the estimation of the total variance vector, $\{\epsilon^2\}$, for the same longitudinal gust rms velocity of 5.1 ft/sec with three sources of processing remnant n_x , n_θ , n_{δ_b} , depicted in Fig. B-1 or page B-2. The injected remnant n_x will include the contribution from n_u which is appropriate for the state display format wherein the pilot must supply lead equalization in the outer-loop. Table B-IX presents estimated closed-loop spectra and variances for each source of processing remnant having a unit rms value and first order input noise spectrum with the indicated half power frequency, $1/T_L = 1/TCR$. The results in Table B-IX provide the values for the nine integrals required in Eq. 29 to estimate the elements of the 3 x 3 coherence matrix:

$$[\Delta_B] = \begin{bmatrix} 0.741 & -35.2 & -38.27 \\ -1.91E-05 & 0.9987 & -3.02E-03 \\ -3.85E-05 & -4.28E-03 & 0.980 \end{bmatrix} \quad (33)$$

The coherence determinant $|\Delta_B| = \Delta_B = 0.732$, therefore, we expect that at least the outer-loop error power will be primarily coherent, i.e., due to the gust disturbance.

The coherent variance vector for $\sigma_{u_g} = 5.1$ ft/sec in Table B-VIII is

$$\{\overline{\epsilon^2}\} = \begin{bmatrix} 3.26 \text{ ft}^2 \\ 0.341E-04 \text{ rad}^2 \\ 0.417E-04 \text{ rad}^2 \end{bmatrix} \quad (34)$$

After the operations required by Eq. 31 are performed, the resulting total variance vector is

$$\{\overline{\epsilon^2}\} = \begin{bmatrix} \overline{x^2} \\ \overline{\theta^2} \\ \overline{\delta_b^2} \end{bmatrix} = \begin{bmatrix} 4.40 \text{ ft}^2 \\ 1.19E-04 \text{ rad}^2 \\ 2.14E-04 \text{ rad}^2 \end{bmatrix} \quad (35)$$

The coherence vector then becomes

$$\{\rho^2\} = \begin{bmatrix} \rho_x^2 \\ \rho_\theta^2 \\ \rho_{\delta_b^2} \end{bmatrix} = \begin{bmatrix} 0.74 \\ 0.286 \\ 0.195 \end{bmatrix} \quad (36)$$

TABLE B-IX

Closed-Loop Spectra and Variances for Manually Controlled Inner
Pitch Attitude and Outer Longitudinal Separation
Loops with a State Display and Remnant Disturbances

NDB RANDOM INPUT RMS= .1000E 1 1/TCR= .1000E 2

C.L. SPECTRA ON OUTPUT FILE

DENOMINATOR

.10000E 1
(.10000E 1)(.25857E 1)(.10000E 2)

.47914E 0 .39387E 0
.65033E 0 .21669E 1
.96085E 0 .13467E 2

X NUMERATOR

.81497E 2
(.10000E 1)(.50000E 1)

.38325E- 1 .21311E 1
.10000E 1 .12121E 2

THETA NUMERATOR

-.11480 2
(.00000E 0)(.15703E- 1)(.10000E 1)(.50000E 1)(.12121E 2)
(.12121E 2)

DB NUMERATOR

.25231E 1
(.00000E 0)(.42999E- 1)(.10000E 1)(.50000E 1)

.62799E 0 .18918E 1
.10000E 1 .12121E 2

NDB RANDOM INPUT RMS= .1000E 1 1/TCR= .1000E 2

	VARIANCE		RMS	
X (FT)	.38271E 4		.61863E 2	2
U (FT/SEC)	.44597E 3		.21118E 2	2
THETA (RAD)	.30184E 0		.54960E 0	0
Q (RAD/SEC)	.87526E 0		.93510E 0	0
DB (RAD)	.10780E 1		.10360E 1	1

Reproduced from
best available copy.

TABLE B-IX

Closed-Loop Spectra and Variances for Manually Controlled Inner
Pitch Attitude and Outer Longitudinal Separation
Loops with a State Display and Remnant Disturbances
(Continued)

NTHETA RANDOM INPUT RMS= .1000E 1 1/TCR= .4000E 1

C.L. SPECTRA ON OUTPUT FILE

DENOMINATOR

.10000E 1
(.10000E 1)(.25857E 1)(.40000E 1)

.47914E 0 .39387E 0
.65033E 0 .21669E 1
.96085E 0 .13467E 2

X NUMERATOR

-.10309E 2
(.10000E 1)(.50000E 1)(-.12120E 2)(-.12122E 2)

.38325E- 1 .21311E 1

THETA NUMERATOR

.1412E 1
(.0000E 0)(.15703E- 1)(.10000E 1)(.50000E 1)(-.12121E 2)
(-.12121E 2)

DB NUMERATOR

-.31915E 0
(.00000E 0)(.42999E- 1)(.10000E 1)(.50000E 1)

.62799E 0 .18918E 1
-.10000E 1 .12121E 2

NTHETA RANDOM INPUT RMS= .1000E 1 1/TCR= .4000E 1

	VARIANCE	RMS
X (FT)	.38045E 3	.19505E 2
U (FT/SEC)	.43327E 2	.65823E 1
THETA (RAD)	.27110E- 1	.16465E 0
O (RAD/SEC)	.63180E- 1	.25137E 0
DB (RAD)	.46305E- 1	.21519E 0

TABLE B-IX

Closed-Loop Spectra and Variances for Manually Controlled Inner
Pitch Attitude and Outer Longitudinal Separation
Loops with a State Display and Remnant Disturbances
(Concluded)

NX RANDOM INPUT RMS= .1000E 1 1/TCR= .3003E 0

C.L. SPECTRA ON OUTPUT FILE

DENOMINATOR

.10000E 1
(.30030E 0)(.10000E 1)(.25857E 1)

.47914E 0 .39387E 0
.65033E 0 .21669E 1
.96085E 0 .13467E 2

X NUMERATOR

.74541E 1
(.30030E 0)(.10000E 1)(-.12121E 2)(-.12121E 2)

.38325E- 1 .21311E 1

THETA NUMERATOR

-.10500E
(.00000E 0)(.15703E- 1)(.30030E 0)(.10000E 1)(-.12121E 2)
(-.12121E 2)

DB NUMERATOR

.23078E- 1
(.00000E 0)(.42999E- 1)(.30030E 0)(.10000E 1)(-.12121E 2)
(-.12121E 2)

.62790E 0 .18918E 1

NX RANDOM INPUT RMS= .1000E 1 1/TCR= .3003E 0

	VARIANCE	RMS
X (FT)	.12763E 1	.11297E 1
U (FT/SEC)	.14644E 0	.38268E 0
THETA (RAD)	.94506E- 4	.97214E- 2
Q (RAD/SEC)	.23570E- 3	.15353E- 1
DB (RAD)	.19041E- 3	.13799E- 1

The predicted gust-correlated and total rms values of the five variables listed in Table B-VIII are summarized below for $\delta_{ug} = 5.1$ ft/sec and including contributions from processing remnant as described above.

	Gust-Correlated rms Value for $\sigma_{ug} = 5.1$ ft/sec	Total rms Value with Processing Remnant	Relative Coherence ρ^2
x (ft)	.18055E 1	.210 E 1	0.74
u (ft/sec)	.44794E 0	.970 E 0	0.21
θ (rad)	.58414E- 2	1.090 E- 2	0.29
q (rad/sec)	.28965E- 2	3.520 E- 2	0.007
δ_b (in)	.64559E- 2	1.460 E- 2	0.2

APPENDIX B
REFERENCES

1. McRuer, D., D. Graham, E. Krendel, W. Reisener, Jr., Human Pilot Dynamics in Compensatory Systems; Theory, Models, and Experiments with Controlled Element and Forcing Function Variations, AFFDL-TR-65-15, July 1965.
2. Shah, K. V., Two Automatic Flight Control System Designs for CH-53A Longitudinal Approach Control, Systems Technology, Inc., Working Paper 198-2, Sept. 1970.
3. Jex, H. R., R. W. Allen,, NASA Ames Project Review: Reference Experiment Summary, Conclusions and Recommendations, Systems Technology, Inc., Working Paper 175-16, Jan. 1970, Fig. 13, p. 23.
4. McRuer, D. T., and H. R. Jex, "A Review of Quasi-Linear Pilot Models", Trans. IEEE, Vol. HFE-8, No. 3, Sept. 1967, pp. 231-249.
5. McDonnell, J. D., Pilot Rating Techniques for the Estimation and Evaluation of Handling Qualities, AFFDL TR 68-76, Dec. 1968.
6. Dander, V. A., "Predicting Pilot Ratings of Multiaxis Control Tasks from Single-Axis Data", Trans. IEEE, Vol. HFE-4, No. 1, Sept. 1963, pp. 15-17.
7. Anonymous, Proposal for a Theoretical Investigation of Handling Qualities for Multiloop, Constant Coefficient Control Situations, Systems Technology, Inc., Technical Proposal No. 34, 30 Nov. 1960.
8. Clement, W. F., and L. G. Hofmann, A Systems Analysis of Manual Control Techniques and Display Arrangements for Instrument Landing Approaches in Helicopters Vol. I: Speed and Height Regulation, Systems Technology, Inc., Technical Report 183-1, July 1969.
9. Ringland, R. F., R. L. Stapleford, R. E. Magdaleno, Motion Effects on an IFR Hovering Task--Analytical Predictions and Experimental Results, Systems Technology, Inc., Technical Rept. 188-1, Oct. 1970.
10. Carter, E. S., Simulation Information for CH-53A JANAIR Study, letter from Sikorsky Aircraft Division to Systems Technology, Inc., Reference SE-2915, 14 Nov. 1968.
11. Allen, R. W., W. F. Clement and H. R. Jex, Research on Display Scanning, Sampling, and Reconstruction Using Separate Main and Secondary Tracking Tasks, NASA CR 1569, July 1970.
12. Weir, D. H., and D. T. McRuer, Analysis and Interpretation of Pilot Response and Performance Data for Simulated Instrument Approach Tasks, Systems Technology, Inc., Tech. Rept. 193-2, 1971, (Forthcoming NASA CR-).

REFERENCES (Concluded)

13. McRuer, D., H. R. Jex, W. F. Clement and D. Graham, A Systems Analysis Theory for Displays in Manual Control, Systems Technology, Inc., Tech. Rept. 163-1, June 1968.

APPENDIX C

DERIVATION OF RATING SCALES FOR DISPLAY EVALUATION

by Henry R. Jex

The purpose of this appendix is to derive an appropriate set of rating scales for subjective evaluation of the control task difficulty and the attentional demands of the display in simulation programs involving display/pilot/vehicle interactions.

A. BACKGROUND AND RATIONALE

The technical approach employed here derives from the well established art of aircraft handling qualities assessment; pioneered by Cooper (Ref. 1), refined by Harper (Ref. 2), put on a rational basis by Ashkenas (Ref. 3), and connected to the equally complex art of psychophysical scaling by McDonnell (Ref. 4).

Our rationale for selecting the scales and scheme was based on the following criteria:

1. It is necessary to separate out the difficulty of the task (situation, criteria, forcing functions, control and vehicle dynamics) from the attentional workload of the display, per se (related to its perceptual properties, dynamics, viewing conditions, etc.).
2. The problem is less "global" (more specialized) than overall handling-qualities ratings, and the scales should reflect these constraints.
3. It is desirable to have a scale known to be of "interval" type, to permit simple arithmetic averaging and classical statistical analyses.

The first two criteria result from the realization that, whereas overall handling qualities evaluations lump all of the system characteristics under one evaluation, display quality evaluations must be able to isolate display defects from (say) controlled-element defects. Consequently, an independent subjective evaluation of the latter is required. For the majority of foreseeable situations, the primary task-related traits will

be the "controllability and adequacy of precision" obtainable under the ideal display conditions, as well as the "attentional workload" of the display itself.

The third criterion (interval-type scales) is based on practical considerations. "Ranking" scales require nonparametric statistical analyses, which are less well developed and less available as computer subroutines than classical parametric statistical methods (e.g., analysis of variance, linear regression analysis, etc.). Interval-type scales permit all these efficient subroutines to be used. Ratio-type subjective scales have been evolved and used successfully, notably by Vercace (Ref. 5) and Nordström (Ref. 6). However, ratio-type scales are needlessly complex for the intended experiments, because each evaluation requires return to the reference configuration. In our experiments, which would involve resetting a large number of parameters for each data point, this technique would consume too much time.

The research in Ref. 4 showed that an interval-type semantic scaling of specific evaluation phrases could be derived via the "Method of Successive Intervals," basing these intervals on the "discriminal dispersion," σ_{ψ} (standard deviation of subjective numerical ratings for a given phrase among a large population of pilots). The resulting semantic scale is called a " ψ -scale" and has the properties of an interval-type scale with roughly homogeneous rating variances (σ_{ψ}^2) across the scale. In light of the foregoing considerations, the display rating scales were based on the phrases and ψ -scale data in Ref. 4.

B. SELECTION OF THE SCALES

The array of 64 handling qualities evaluation phrases in Ref. 4 included gradations within several "trait" groups, such as: overall handling qualities, controllability and precision, vehicle response characteristics, demands on the pilot, etc. Most of the vehicle-specific trait groups are not of interest here, but the (task) Controllability and Precision and Demands on Pilot groups are directly applicable to display rating. Within each group a selection of five phrases was made, according to the following criteria:

1. Roughly uniform intervals across the total range of ψ from 1 to 10.
2. Roughly equal discriminial dispersions.
3. Context relevant to the display task situation.
4. Simple terms with consistent adjectives.

Five evaluation levels are considered quite adequate for the simple traits being rated (9 or 10 are required for global handling qualities to provide more contextual degrees of freedom). The selected phrases are shown in Table C-I, arranged in their semantic relationship ($\bar{\psi}$) as determined from Table B-I (Col. 5) of Ref. 4. Also shown in Table C-I are the corresponding discriminial dispersions, σ_{ψ} . It is clearly apparent that the goals of uniform coverage and variance are met. Furthermore, there is an approximately $2\sigma_{\psi}$ separation between phrases, implying clear semantic distinctions.

The five levels in each category are given rating scale numbers from 1 to 5 from best-to-worst, in line with established handling qualities rating practice. Task Controllability and precision ratings are coded as C1-C5, while Display attentional demand ratings are coded as D1-D5, as shown in Table IV-3 in the text.

C. USE OF SCALES

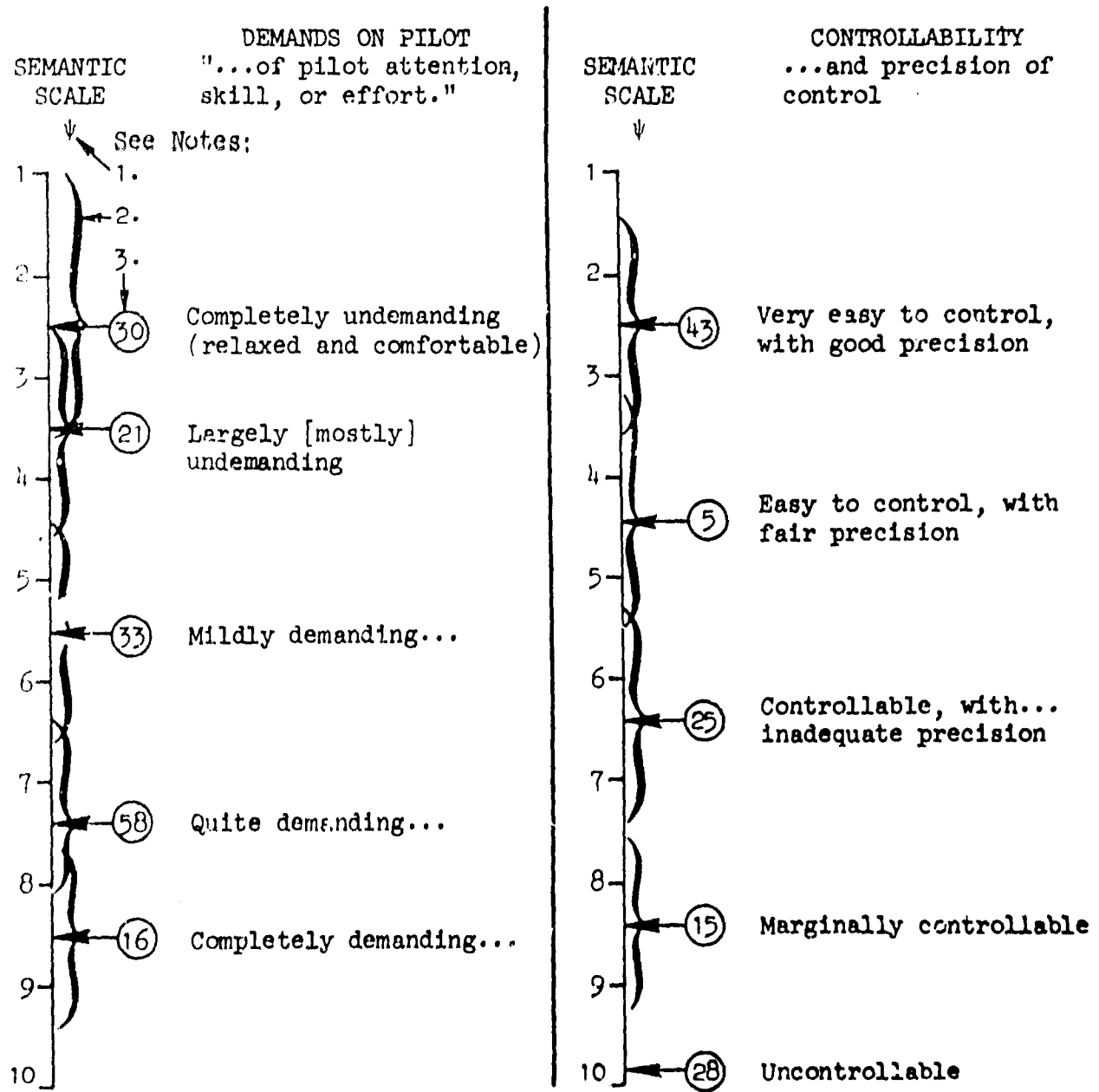
For proper evaluation of a display, it should be tested in the context of the intended operational situation. Practically speaking, this means specifying a realistic "scenario" for the simulation and using similar mission criteria, commands, disturbances and controlled elements. All subjects must be told the same scenario and criteria.

Both the task controllability and display workload must be rated, to be able to separate out the demands due to controllability (of task and vehicle origin) from those of the display itself. A specific formula for this separation is not yet available and will be one object of pending experiments.

To guide the controllability and precision rating, a three-stage decision process has been indicated in Table IV-3 in the text:

TABLE C-1

SEMANTIC RELATIONSHIP OF DISPLAY RATING PHRASES



Notes: (Data are from AFFDL-TR-68-76; Ref. 4)

1. ψ denotes semantic scale obtained by method of Successive Intervals.
2. $\{$ denotes the "semantic discriminational dispersion" (standard deviation of ψ scores).
3. \bigcirc denotes code number of phrase in Ref. 4.

1. "Is it controllable?" Separates C1-C4 from C5.
2. "Is the control precise enough for the mission criteria?" Separates C1-C2 from C3-C4.
3. "What remaining phrase best describes the evaluation?" Selects the specific phrase and rating.

A corresponding decision tree is not useful for the display workload rating, because the 5 levels are simply gradations along the continuum of demands on the operator's attention, skill or effort in using the display for the task at hand.

In use, experience has shown that at least two replications per configuration should be made with two or more experienced operators to provide a measure of intrinsic variance and remove learning and chance artifacts. A typical comparison between objective (performance) measures and subjective display rankings among four pilots is given in Ref. 7.

CONCLUSIONS

A pair of simple rating scales for use in research on manual control displays has been derived (Table IV-3), based on the extensive foundation provided in Ref. 4. These scales are of interval-scale quality and will permit averaging and other standard parametric statistical analyses. Use of two trait categories: "task controllability-and-precision" and "display attentional workload," should permit separation of these often-confounded effects.

It is recommended that these rating scales be used in all display-related simulations to provide the data base needed to refine them and to provide a formula for separating the controllability and display workload factors.

**APPENDIX C
REFERENCES**

1. Cooper, G. E., "Understanding and Interpreting Pilot Opinion," Aeron. Eng. Rev., Vol. 16, No. 3, Mar. 1957, pp. 47-52.
2. Harper, R. P., Jr., and George E. Cooper, A Revised Pilot Rating Scale for the Evaluation of Handling Qualities, Cornell Aerc. Labs. Rept. 153, Sept. 1966.
3. Ashkenas, I. L., and D. T. McRuer, "A Theory of Handling Qualities Derived from Pilot-Vehicle System Considerations," Aero. Eng., Vol. 21, No. 2, Feb. 1962, pp. 60, 61, 83-102.
4. McDonnell, John D., Pilot Rating Techniques for the Estimation and Evaluation of Handling Qualities, AFFDL-TR-68-76, Dec. 1968.
5. Vergace, J., Measurement of Ride Comfort, SAE Paper 638A, Jan. 1963.
6. Nordström, Lennart, and Håkan Arne, "A Simulator Comparison Between Two Methods of Computing and Displaying the Velocity in a Head-Up Display for Low Speed Flight Path Control," ICAS Paper No. 66-16, Sept. 1966.
7. Allen, R. W., and H. R. Jex, An Experimental Investigation of Compensatory and Pursuit Tracking Displays with Rate and Accelerating Control Dynamics and a Disturbance Input, NASA CR-1082, June 1968.